Identification and characterization of novel telomere binding proteins in *Caenorhabditis elegans*

Dissertation

Zur Erlangung des Grades

„Doktor der Naturwissenschaften“

am Fachbereich Biologie

der Johannes Gutenberg-Universität Mainz

Sabrina Franziska Dietz

geb. am 02.05.1988 in Rüsselsheim/Main

Mainz, 2020

Dekan:

1. Berichterstatter:

2. Berichterstatter:

Tag der mündlichen Prüfung:

Table of contents

Table of contents i
Summary 2
Zusammenfassung 3
Abbreviations 4
Introduction 7
Telomeres – structured ends 7
Structure and associated proteins of mammalian and yeast telomeres 7
Telomeres and the end-protection problem 9
Telomeres and the end-replication problem 12
Telomere replication and the telomere replication problem 13
Telomere length maintenance 14
Telomerase-mediated maintenance 14
Alternative lengthening of telomeres (ALT) 16
Non-canonical ALT 17
Telomere chromatin and telomere transcription 18
Telomere position effect and chromatin modification 18
TERRA 18
Telomeres and senescence 19
Telomeres and disease 20
Telomeres and meiosis/fertility 21
Caenorhabditis elegans – a multifunctional model organism 22
Telomeres in *C. elegans* 22
End protection in *C. elegans* 23
Telomere length maintenance in *C. elegans* 24
Telomeres and longevity 25
Telomeres and fertility 26
Rationale 26
Results 27
Identification of novel telomere associated factors in *C. elegans* 27
Screening for interactors with quantitative proteomics 27
R06A4.2 and T12E12.3 are paralog genes in *C. elegans* 28
Interaction with the telomeric sequence *in vitro* 28
Study of R06A4.2 and T12E12.3 on organismal level in *C. elegans* 31
Creation of CRISPR mutants and tagged strains 31
R06A4.2 and T12E12.3 are expressed throughout development 31
R06A4.2 and T12E12.3 localize to telomeric DNA in vitro and to telomeres in vivo 31
R06A4.2 and T12E12.3 show opposite telomere phenotypes when mutated 34
Double mutation of R06A4.2 and T12E12.3 leads to synthetic sterility 35
Mutations of R06A4.2 and T12E12.3 influence transgenerational fertility but not lifespan 40
R06A4.2 and T12E12.3 are part of a telomeric complex in *C. elegans* 41

R06A4.2 and T12E12.3 interact with each other 41
R06A4.2 and T12E12.3 interact with single-strand binding proteins 41
R06A4.2 and T12E12.3 are conserved in other *Caenorhabditis* species 45
Telomere association in *Caenorhabditis briggsae* 45
Discussion 47
Identification of novel telomere binders in *C. elegans in vitro* 47
Detection of novel factors at *C. elegans* telomeres 47
R06A4.2 and T12E12.3 interact with the telomeric sequence *in vitro* 49
R06A4.2 and T12E12.3 bind to telomeres *in vivo* 50
R06A4.2 and T12E12.3 are functionally relevant at telomeres 50
R06A4.2 and T12E12.3 are required for fertility and germline health but not longevity 51
R06A4.2 and T12E12.3 form a telomeric complex 55
Interaction of R06A4.2 and T12E12.3 in dividing tissues 55
Interaction of R06A4.2 and T12E12.3 with other telomeric proteins 56
Telomere binding is conserved in at least one other *Caenorhabditis* species 57
Conclusions 58
Appendix 59
Materials and Methods 61
Materials 61
Methods 84
References 103

Summary

Telomeres are nucleoprotein structures at the ends of linear eukaryotic chromosomes. The specific DNA structures are exposed to the so-called end-replication and end-protection problems. Proteins that bind specifically to the unique sequences of telomeres aid in solving these problems. In vertebrates, the core protective complex is called shelterin and supports telomere maintenance and protection with its several subunits. Similar complexes guarding and maintaining telomeric DNA have been described in many other species such as *Saccharomyces cerevisiae*, *Schizosaccharomyces pombe*, *Arabidopsis thaliana* or *Drosophila melanogaster*.

In this study, we aimed at identifying and characterizing previously unknown telomeric factors in the model organism *Caenorhabditis elegans*. Utilizing quantitative proteomics coupled to a DNA pulldown experiment performed with nuclear extract of *C. elegans*, we identified a set of proteins associating with telomeres. In this set of proteins, we detected previously described telomere binders, proteins that were described in other functions and proteins that had no reported functions. This suggests more potential interactors at *C. elegans* telomeres then previously reported.

Among the set of identified proteins, we focused on the paralog proteins R06A4.2 and T12E12.3 and further characterized their function at *C. elegans* telomeres. A validation of binding *in vivo* and *in vitro* showed association of the proteins to the double-stranded telomere in a nanomolar range and colocalization with a known telomere binder, POT-1. Interestingly, despite sharing a high percentage of amino acid and nucleotide sequence identity, animals with a mutation in either gene show divergent phenotypes. While deletion of R06A4.2 leads to telomere elongation, deletion of T12E12.3 leads to shorter telomeres and a mortal germline phenotype. We show that a double mutant of both proteins leads to immediate synthetic sterility in the first homozygous generation, with an obvious underdevelopment of the germline. Furthermore, we show with different biochemical approaches that R06A4.2 and T12E12.3 interact not only with each other at specific times in *C. elegans* development, but additionally interact with the previously reported single-strand telomere binders POT-1, POT-2 and MRT-1. In addition, we could demonstrate that a homolog of the candidate proteins in *C. briggsae* is also interacting with telomeres, giving the proteins a potential conserved function throughout the *Caenorhabditis* genus. Altogether, our data provides indication for the first described complex of telomere binding proteins in *C. elegans*, involving the first reliably described telomere double-strand binders R06A4.2 and T12E12.3.

Zusammenfassung

Telomere sind Nukleoprotein-Strukturen an den Enden linearer, eukaryotischer Chromosomen. Die spezifischen DNS Strukturen sind den sogenannten End-Replikation und End-Schutz Problemen ausgesetzt. Proteine, die spezifisch an die einzigartigen Sequenzen von Telomeren binden, helfen bei der Bewältigung dieser Probleme. Der Kern-Schutz Komplex in Vertebraten wird shelterin genannt und unterstützt mit seinen verschiedenen Untereinheiten sowohl Telomer-Instandhaltung als auch -Schutz. Ähnliche Komplexe, die telomerische DNS abschirmen und erhalten wurden in vielen verschiedenen Spezies beschrieben, z.B in *Saccharomyces cerevisiae*, *Schizosaccharomyces pombe*, *Arabidopsis thaliana* oder *Drosophila melanogaster*.

Das Ziel dieser Studie war die Identifikation und Charakterisierung bisher unbekannter telomerischer Faktoren im Modellorganismus *Caenorhabditis elegans*. Durch die Verwendung von quantitativer Proteomik in Verbindung mit einer DNS Pulldown Strategie, die mit nuklearem Extrakt von *C. elegans* durchgeführt wurde, identifizierten wir eine Reihe von Proteinen, die mit Telomeren assoziieren. Wir entdeckten bereits im Vorfeld bekannte Telomer-Binder, sowie Proteine, die in anderen Funktionen beschrieben wurden. Zusätzlich enthielt unser Set Proteine ohne bisher beschriebene Funktion. Dies legt nahe, dass *C. elegans* Telomere mehr potentielle Interaktionspartner besitzen, als bisher bekannt.

Innerhalb der identifizierten Proteine fokussierten wir uns auf die paralogen Proteine R06A4.2 und T12E12.3 und charakterisierten ihre Funktion an den Telomeren von *C. elegans*. Eine Bestätigung des Bindens *in vivo* und *in vitro* zeigte eine Assoziation der Proteine mit doppelsträngigen Telomeren im nanomolaren Bereich, sowie eine Co-Lokalisation mit POT-1, einem bekannten Telomer-Binder. Interessanterweise zeigen Tiere mit einer Mutation in je einem der Gene divergente Phänotypen, obwohl die Aminosäure- und Nukleotidsequenzen der Proteine zu einem hohen Prozentsatz identisch sind. Während Deletion von R06A4.2 zu einer Verlängerung von Telomeren führt, hat Deletion von T12E12.3 zu verkürzte Telomere und eine sterbliche Keimbahn zur Folge. Wir zeigen, dass eine Doppelmutante beider Proteine zu direkter synthetischer Sterilität in der ersten homozygoten Generation führt, und dass diese eine offensichtlich unterentwickelte Keimbahn besitzt. Weiterhin zeigen wir mit verschiedenen biochemischen Ansätzen, dass R06A4.2 und T12E12.3 nicht nur zu spezifischen Zeitpunkten der Entwicklung von *C. elegans* miteinander interagieren, sondern zusätzlich mit den vorher beschriebenen Einzelstrang Telomer-Bindern POT-1, POT-2 und MRT-1 assoziieren. Zusätzlich konnten wir zeigen, dass ein Homolog der Kandidaten-Proteine in *C. briggsae* ebenfalls mit Telomeren interagiert, was den Proteinen eine potenziell konservierte Funktion innerhalb des Genus *Caenorhabditis* zuspricht. Zusammenfassend weisen unsere Daten auf den ersten beschriebenen Komplex Telomer-bindender Proteine in *C. elegans* hin, der ebenfalls die ersten zuverlässig beschriebenen Telomer-Doppelstrang-Binder R06A4.2 und T12E12.3 umfasst.

Abbreviations

°C	degrees celsius
µl	microliter
µm	micrometer
9-1-1	RAD9/RAD1/HUS1 DNA damage response checkpoint
A	adenine
AGE-1	ageing alteration 1
ALT	alternative lengthening of telomeres
alt-NHEJ	alternative non-homologous end joining
APB	ALT-associated promyelocytic leukemia body
ARIA	telomeric RNA in fission yeast S. pombe, consists of C-rich repeats
ARRET	antiparallel telomeric RNA species
ATM	Ataxia telangiectasia mutated
ATP	adenosine tri-phosphate
ATR	ATM and RAD3-related
ATRX	Transcriptional regulator ATRX
BIR	Break induced replication
BLM	Bloom syndrome RecQ-like helicase
bp	base pairs
BQT	bouquet
C	cytosine
C. briggsae	*Caenorhabditis briggsae*
C. elegans	*Caenorhabditis elegans*
C-circle	extrachromosomal circular DNA
CDC13	cell division control protein 13
CEH-37	*C. elegans* homeobox 37
CLK-2	clock abnormality 2
CoIP	Co-immunoprecipitation
CR	calorie restriction
CRISPR/Cas9	Clustered regularly interspaced short palindromic repeats/ CRISPR-associated protein 9
CSM4	chromosome segregation in meiosis 4
CST	CDC1, STN1, TEN1 complex
C-strand	telomeric cytosine-rich strand
D. melanogaster	*Drosophila melanogaster*, fruit fly
DAF	abnormal dauer formation
DAPI	4′,6-Diamidin-2-phenylindol
dATP	deoxyadenosine tri-phosphate
DCP-66	deacetylase complex protein 66
DDR	DNA damage response
DIC	Differential interference contrast (microscopy)
DML	dimethyl labeling
DNA	deoxyribonucleic acid
DNA2	DNA replication ATP-dependent helicase/nuclease 2
DNase	unspecific DNA cleaving endonuclease
DNMT	DNA methyl transferase
ds	double-strand
DSB	double-strand break
E. coli	*Escherichia coli*
ECTR	extrachromosomal telomeric repeats
EMSA	electrophoretic mobility shift assay
EST	ever shorter telomeres
EXO1	exonuclease 1
f.c.	final concentration
FITC	fluorescin isothiocyanate
FP	fluorescence polarization
FPC	fork protection complex
G	guanine
g	grams
G4	G (guanine) quadruplex
GAL4	galactose metabolism 4
GFP	green fluorescent protein
G-strand	telomeric guanine-rich strand
HATTI	heterochromatin amplification dependent and telomerase independent survivors (*S. pombe*)
HDAC	histone deacetylase
HDR	Homology directed repair
Him	high incidence of males (phenotype)
HMG-5	High-Mobility-Group-Protein 5
HMT	histone methyl transferase
hnRNP	Heterogeneous nuclear ribonucleoprotein
HOT1/HMBOX1	Homeobox 1
HR	homologous recombination
HSP	heat shock protein

HTT	D. melanogaster telomeric transposons (Het-A, TART, Tahre)
ICL	interstrand crosslink
IGF	Insulin-like-growth-factor
INM	inner nuclear membrane
IP	immunoprecipitation
IP-qMS	IP followed by quantitative mass spectrometry
KASH	KASH (Klarsicht, ANC-1, Syne Homology) domain-containing protein
kb	kilobase pairs
Kd	equilibrium dissociation constant
kDa	kilodalton
L	liters
LFQ	label-free quantitation
LIG-4	ligase 4
LIN-40	abnormal cell lineage 40
LINC	linker of nucleoskeleton and cytoskeleton
M	molar
MAJIN	Membrane-anchored junction protein
mCherry	red fluorescent protein derivate
mg	milligrams
miDAS	mitotic DNA synthesis
ml	milliliters
mM	millimolar
mP	millipolarization
MPS3	mono-polar spindle 3
MRN	MRE11, RAD50, NBS1 complex
Mrt	mortal germline (phenotype)
MRT-1	mortal germline 1
MRT-2	mortal germline 2
MRX	MRE11, RAD50, XRS2 complex
MS	mass spectrometry
Myb	Myeloblastosis gene
NDJ1	non-disjunction 1
NGM	nematode growth medium
NHEJ	non-homologous end joining
nM	nanomolar
NR2C2	nuclear receptor subfamily 2, group C, member 2
nt	nucleotides
NuRD	nucleosome remodeling and histone deacetylase
OB-fold	oligonucleotide binding-fold
PARP1	poly(ADP-ribose) polymerase 1
PC	pairing center
PCNA	Proliferating-Cell-Nuclear-Antigen
PD	population doubling
PFH1	PIF1 helicase homolog 1
PGL-1	P-granule abnormality 1
P-granule	perinuclear granule
PIF1	Petite Integration Frequency
PLP-1	Pur alpha-like protein 1
PNK	polynucleotid kinase
POL	polymerase
POT1	protection of telomeres 1
POT-1	protection of telomeres 1 (*C. elegans*)
POT-2	protection of telomeres 2 (*C. elegans*)
POT-3	protection of telomeres 3 (*C. elegans*)
pRB	p16 retinoblastoma protein
qFISH	quantitative fluorescence in-situ hybridization
RAD	Radiation sensitive
RAP1	Repressor/Activator protein 1
RFP	red fluorescent protein
RIF	Replication Timing Regulatory Factor
R-loop	RNA:DNA hybrid structure
RNA	ribonucleic acid
RNAi	RNA interference
RPA	Replication factor A
RPM	rapid meiotic prophase chromosome movement
rpm	rounds per minute
RRM3	rDNA Recombination Mutation
RTEL	Regulator Of Telomere length
RT	room temperature
S	DNA synthesis phase of cell cycle (between G1 and G2)
S. cerevisiae	*Saccharomyces cerevisiae*, budding yeast
S. pombe	*Schizosaccharomyces pombe*, fission yeast
SATB2	Special AT-rich sequence-binding protein 2
SET	set domain-containing
sgRNA	single-guide RNA
SH	subtelomeric homologous (subtelomere of fission yeast)
SIR	silent information regulator
SLX	Synthetic Lethal of unknown (X) function
Sm nuclease	*Serratia marcescens* nuclease
SNM1	Ribonuclease MRP protein subunit SNM1

ss	single-strand
STN1	suppressor of CDC13
SUN	SUN (Sad1p, UNC-84) domain-containing protein
T	thymine
T. thermophila	*Tetrahymena thermophila*
TALT	template for ALT (*C. elegans)*
TANK-1	tankyrase related 1
TAS	telomere-associated sequences
T-circles	telomeric circles
TEBP	Telomere binding protein
TEL1	telomere maintenance 1
TEN1	Telomeric pathways with STN1
TER1	telomerase RNA
TERB	Telomere Repeat Binding Bouquet Formation Protein
TERC	Telomerase RNA component
TERRA	telomeric repeat-containing RNA
TERT	Telomerase reverse transcriptase
TIF	telomere dyfunction induced foci
TIN2	TINF2, TRF-interacting nuclear factor 2
TLC1	telomerase component
t-loop	telomeric loop
TOR	target of rapamycin
TPE	telomere position effect
TPP1	TINT1, PTOP, PIP1, interactor of POT1 and TIN2
TRF1/2	Telomere repeat binding factor 1/2
TRT	Telomerase reverse transcriptase
T-SCE	telomeric sister-chromatid exchange
UPF1	up-frameshift 1
UPR mt	mitochondrial unfolded protein response
v/v	volume per volume
w/v	weight per volume
WRN	Werner Syndrome RecQ-like helicase
WT	wild-type
xg	times gravity
Y2H	yeast two-hybrid
ZBTB	zinc-finger and BTB-domain containing protein
ZNF	zinc-finger protein

Introduction

Telomeres – structured ends

Telomeres, the ends of linear eukaryotic chromosomes, were discovered in laboratories working with *Drosophila melanogaster* and *Zea mays* (Creighton and McClintock 1935; Muller 1938) nearly a century ago. Barbara McClintock went on to describe that these newly identified chromosome ends behaved differently than usual broken DNA ends and were important for chromosome stability (McClintock 1941). Further interest in telomeres arose with the discussion of the Hayflick limit, describing the limited lifespan of primary cells in cell culture (Hayflick 1965), and the definition of the end-replication problem by Watson (Watson 1972). The end-replication problem describes the shortening of linear DNA fragments due to incomplete synthesis by the DNA replication machinery (Olovnikov 1973), thereby leading to chromosome shortening and finally, limited lifespan. With the discovery of the telomerase enzyme and its RNA template in *Tetrahymena thermophila* (*T. thermophila*) (Greider and Blackburn 1985; Greider and Blackburn 1987; Greider and Blackburn 1989), telomere biology became an even more expanding field. Today, telomere structures and sequences of many model and non-model organisms are partially known and are being studied. In addition, telomeres have been implicated in important discoveries in human aging, health, and disease (Armanios and Blackburn 2012; Opresko and Shay 2017).

In this thesis, we aimed to study telomere biology in the model organism *Caenorhabditis elegans* (*C. elegans*). In the following sections, an overview about general telomere biology in different exemplary organisms as well as in *C. elegans* will be provided.

Structure and associated proteins of mammalian and yeast telomeres

As described above, telomeres are the ends of linear eukaryotic chromosomes, capping them for protection. To be able to fulfill this function properly, the majority of telomeres consists of repetitive DNA sequences associated with specific proteins.

After the detection of the first telomeric sequence in *T. thermophila* (Blackburn and Gall 1978), a hexameric repeat sequence of $(TTGGGG)_n$, telomeric sequences started to be investigated in other organisms as well. In humans, a related $(TTAGGG)_n$ sequence was reported (Moyzis et al. 1988) and found to be conserved among more than 90 vertebrate species including all mammals (Meyne et al. 1989; Gomes et al. 2011). The length of human telomeres varies between 5 and 15 kb in the double-stranded region and 35 to 600 nt in the single-stranded overhang (Samassekou et al., 2010), depending on the cell type but also on the individual (Takubo et al. 2002). Additionally, the so-called subtelomeric region of human chromosomes contains non-random distributions of variant repeats consisting of one basepair substitutions to the canonical telomere sequence (for example TCAGGG, TGAGGG, TTGGGG) (Allshire et al. 1989; Conomos et al. 2012).

Shelterin is the main complex at mammalian telomeres and consists of six proteins (Palm and de Lange 2008). Telomeric repeat binding factor 1 (TRF1) was the first protein to be described at human telomeres due to its specificity for the TTAGGG repeat (Zhong et al. 1992; Chong et al. 1995). Searching for homologs in the human genome, TRF2 was identified (Bilaud et al. 1997; Broccoli et al. 1997), followed by TIN2 and RAP1, which were identified by yeast 2 hybrid screens using TRF1/2 as bait (Kim et al. 1999; Li et al. 2000). POT1 was found together with its *S. pombe* counterpart by sequence similarity to the *Oxytricha nova* telomere binding protein TEBP (Gottschling and Zakian 1986; Baumann and Cech 2001). When looking for interaction partners of TIN2, the last member of the shelterin complex, TPP1, could be confirmed (Liu, Safari, et al. 2004). Together these proteins form a complex on telomeric DNA (de Lange 2005). TRF1, TRF2 and POT1 are the three members of the complex that directly interact with telomeric DNA – TRF1/2 as homodimers in the double-stranded regions, POT1 on the single-stranded overhang (de Lange 2005). Bridged by TIN2, it brings together the POT1/TPP1 and TRF1/TRF2/RAP1 complexes to form a fully functional shelterin (Fig. I1A) (Liu, O'Connor, et al. 2004).

The recruitment of shelterin to the telomeric DNA is essential for telomere length maintenance and protection (de Lange 2018). Outside of shelterin, there have been additional telomere-binding proteins reported, supporting telomere maintenance. HOT1/HMBOX1, ZBTB48/TZAP, ZNF827, NR2C2 and ZBTB10 have been experimentally confirmed at the telomeres or subtelomeres and are aiding in telomere length maintenance or interacting with shelterin members (Déjardin and Kingston, 2009; Kappei *et al.*, 2013; Conomos, Reddel and Pickett, 2014; Jahn *et al.*, 2017; Li *et al.*, 2017; Bluhm *et al.*, 2019). In addition, a specific telomere complex has been described at mammalian telomeres during meiosis (Wang et al. 2019). These observations place additional importance on proteins outside the canonical shelterin.

The telomeres of fission yeast *Schizosaccharomyces pombe* (*S. pombe*) and budding yeast *Saccharomyces cerevisiae* (*S. cerevisiae*) have been shown to consist of a more non-canonical telomeric repeat with high variability (Szostak and Blackburn 1982). For *S. cerevisiae* a double-stranded TG-rich sequence ($C_{1-3}A/TG_{1-3}$) of about 300 bp with a single-stranded 3' overhang that varies in size between 12 and 100 nt depending on the cell cycle phase was reported (Wellinger and Zakian 2012). The telomeric repeat in *S. pombe* contains an around 300 bp heterogeneous repeat of $G_{2-6}TTAC[A]$ (Dehé and Cooper 2010) with a single-stranded 3' overhang. Similar to human telomeres there are subtelomeric regions found in the chromosomes of *S. pombe* and *S. cerevisiae*. In the fission yeast these sequences are the subtelomeric homologous (SH) region close to the telomere, containing multiple homologous sequence segments, and the telomere-distal region containing unique sequences (Tashiro et al. 2017). The SH regions on the *S. pombe* chromosomes facilitate chromosome homeostasis and gene expression by working as buffer regions in case of telomere loss (Tashiro et al. 2017). In *S. cerevisiae* there are two types of subtelomeric regions described, the Y' and the X elements. Whereas the X elements are present in all budding yeast telomeres in various lengths, the Y' elements are only located in a subset of telomeres, containing tandem sequences (Chan et al. 1983; Louis and Haber 1992; Wellinger and Zakian 2012).

At *S. pombe* telomeres, a shelterin-like complex was described. TAZ1 is the *S. pombe* homolog to mammalian TRF1/TRF2, and binds to the double-stranded telomere. Similar to shelterin, TAZ1 is interacting with RAP1 as well as with RIF1 reminiscent of *S. cerevisiae* (Cooper et al. 1997; Chikashige and Hiraoka 2001). POT1 is binding to the single-stranded 3' overhang and is interacting with TPZ1 (the TPP1 homolog of *S. pombe*), which in turn can bind POZ1 and CCQ1 (Miyoshi et al. 2008). Additionally, POZ1 bridges the POT1/TPZ1 complex on the single-strand with the TAZ1/RAP1 complex on the double-strand, connecting different telomeric regions (Fig. I1C) (Miyoshi et al. 2008). In *S. cerevisiae*, RAP1 was the first described telomeric protein (Buchman et al. 1988). Contrary to mammals and *S. pombe*, this protein is binding directly to the double-stranded telomere, affecting telomere structure and length regulation (Conrad et al. 1990; Lustig et al. 1990). RAP1 is interacting with RIF and SIR proteins to mediate telomeric hetrochromatin and regulate telomere length (Moretti et al. 1994; Levy and Blackburn 2004; Wellinger and Zakian 2012). On the single-stranded telomeric overhang, another complex independent of the RAP1 complexes was detected. This complex is comprised of the DNA-binding protein CDC13 and its interactors STN1 and TEN1 (CST complex), and it functions in telomere end protection as well as in telomere length regulation (Fig. I1B) (Grandin et al. 1997; Grandin et al. 2001). Additionally, CDC13 has been published to interact with EST1 and EST3 to facilitate telomerase recruitment (Qi and Zakian 2000).Taken together, *S. pombe* and *S. cerevisiae* telomeric DNA is also bound by complexes, consisting of single- and double-strand binding proteins and their interactors, which are necessary for proper telomere protection and maintenance.

These variable complexes of single- and double-strand binding proteins are found not only in the here described organisms, but also in other species such as *Neurospora crassa* (Casas-Vila et al. 2015), *Tetrahymena thermophila* (Linger et al. 2011) or *Drosophila melanogaster* (Raffa et al. 2013). This indicates that telomere structure and proteins are variable between organisms, but protection and maintenance are fulfilled in a similar manner despite the differences.

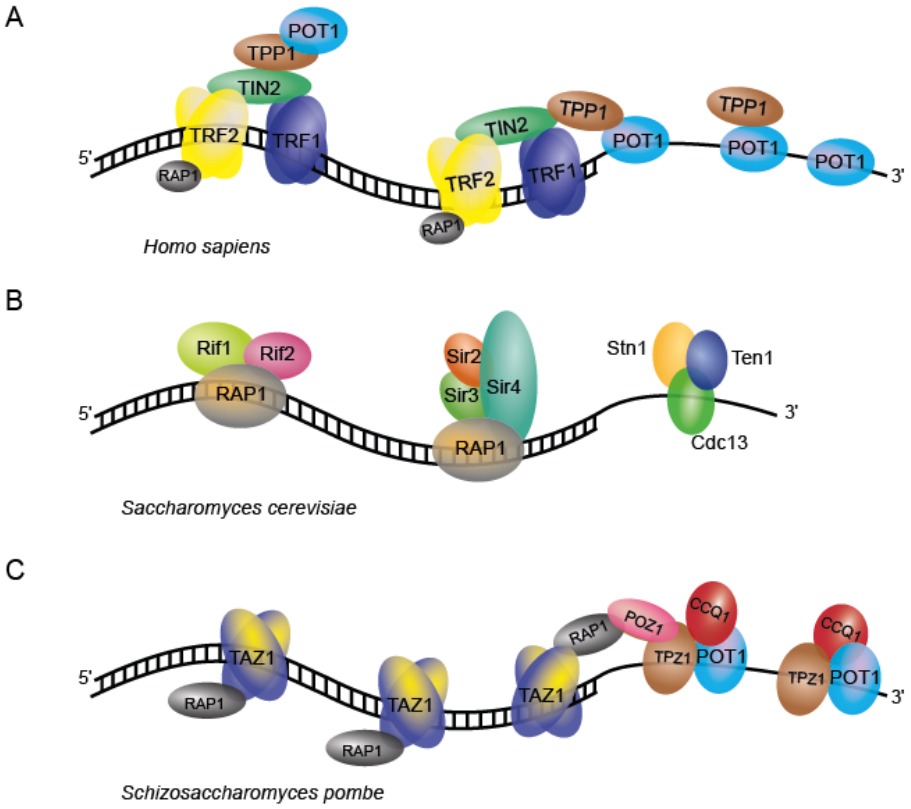

Figure I1: Schematic telomere structure of exemplary organisms. (A) Human telomeres containing TRF1 and TRF2 homodimers binding the ds telomere, interacting proteins RAP1, TIN2 and TPP1 as well as single-strand binder POT1. Double- and single-stranded telomere binders are bridged by interaction between TPP1 and TIN2. (B) *S. cerevisiae* telomeres contain two sets of RAP1 complexes (including RIF or SIR proteins) at the ds telomeric sequence and the CST complex at the ss telomeric sequence. (C) *S. pombe* telomeres contain TRF1/2 homolog TAZ1 at the double-stranded telomere with interactor RAP1, as well as POT1/TPZ1/CCQ1 complex at the single-stranded telomere. Both complexes are bridged by interaction of POZ1 between RAP1 and TPZ1. Proteins with homology between the organisms are colored in the same colors.

Telomeres and the end-protection problem

The structure of telomeric DNA, a double-strand ending in a single-stranded overhang, resembles DNA double-strand breaks (DSBs). When unprotected, telomeres can trigger DNA damage surveillance and thereby DNA repair mechanisms (de Lange 2009), leading to genome instability. DNA repair pathways such as non-homologous end-joining (NHEJ) or homology directed repair (HDR) are recruited to repair the potential damage, resulting in chromosome fusions (NHEJ) or chromosome loss (HDR) (de Lange 2009). Detection of DNA damage in general activates checkpoints within the cell that stop proliferation to maintain chromosome integrity and stability (Weinert and Hartwell 1988; Callegari and Kelly 2007). Accumulation of DNA damage factors at unprotected or dysfunctional telomeres can be visualized by immunofluorescence staining in so-called telomere dysfunction induced foci (TIF) (Takai et al. 2003).

In mammalian cells, there are six pathways that define the end-protection problem (Sfeir and de Lange 2012). Next to the previously mentioned NHEJ and HDR, these pathways include the activation of the checkpoint kinases Ataxia-telangiectasia-mutated (ATM) and Ataxia telangiectasia and Rad3-related (ATR), as well as an alternative NHEJ mediated by PARP1 (alt-NHEJ) and unmitigated 5' end resection (Fig. I2A) (Sfeir and de Lange 2012). Each member of the shelterin, as well as the full complex, play a role in the prevention of these pathways. Even though ATM and ATR are required for the regulation of the DNA damage response (DDR) both also work in the maintenance of overall genomic integrity including telomeres (Awasthi et al. 2015), regulating for example the maintenance of telomere length by

telomerase (Lee et al. 2015; Tong et al. 2015). The DDR signaling of both these kinases is facilitated by recognizing DNA ends (ATM) or single-stranded overhangs (ATR) (de Lange 2009). To ensure end-protection and genome integrity at the telomeres, the shelterin members control the damage signaling of these kinase pathways. TRF1 inhibits ATR activation during replication of telomeres in the S phase of the cell cycle (Sfeir et al. 2009), whereas TRF2 and POT1 inhibit ATM or ATR signaling throughout the cell cycle (Karlseder et al. 2004; Denchi and De Lange 2007). Loss of TRF1 results in elongated, fragile telomeres, growth arrest and senescence, while loss of TRF2 leads to 3' overhang shortening and finally NHEJ mediated chromosome fusions (van Steensel and de Lange 1997; Celli and de Lange 2005; Hockemeyer et al. 2006; Sfeir et al. 2009; Kibe et al. 2010). Interaction of POT1 with the single-stranded telomere and the rest of shelterin is mediated by TPP1, and loss of these proteins leads to ATR activation and an excessive single-stranded 3' overhang due to 5' end resection (Kibe et al. 2010). Loss of the bridging protein TIN2 results in reduced association of the other shelterin members at telomeres and DDR activation (Takai et al. 2011). Additional protection of the telomere structure and integrity is provided by binding of proteins that are not members of the canonical shelterin. The KU heterodimer, for example, forms an interaction with TRF1, thus preventing fusions of telomeres (Hsu et al. 2000). Additionally, KU proteins redundantly inhibit alt-NHEJ and HDR at telomeres (Sfeir and de Lange 2012). Helicases and exonucleases such as RTEL and Apollo also have been described as essential for protection against DDR (van Overbeek and de Lange 2006; Barber et al. 2008) and even interaction of shelterin with DDR members aids in telomere protection (Okamoto et al. 2013; de Lange 2018).

In addition to protein binding, overall structure of telomeres plays an important role in protection from DDR. In this regard, telomeric DNA undergoes a structural change for its protection (Griffith et al. 1999). To form the so-called telomeric loop (t-loop), the single-stranded 3' overhang invades the double-stranded region, thereby displacing one strand of the double-stranded telomere (Fig. I2B). This structure is facilitated by TRF2, as it has been shown, that formation of t-loops is impaired upon its loss (Griffith et al. 1999; Doksani et al. 2013). T-loop formation is a means of protection against ATM, NHEJ and nucleolytic activity as the telomeric 3' overhang is hidden (de Lange 2009; de Lange 2018).

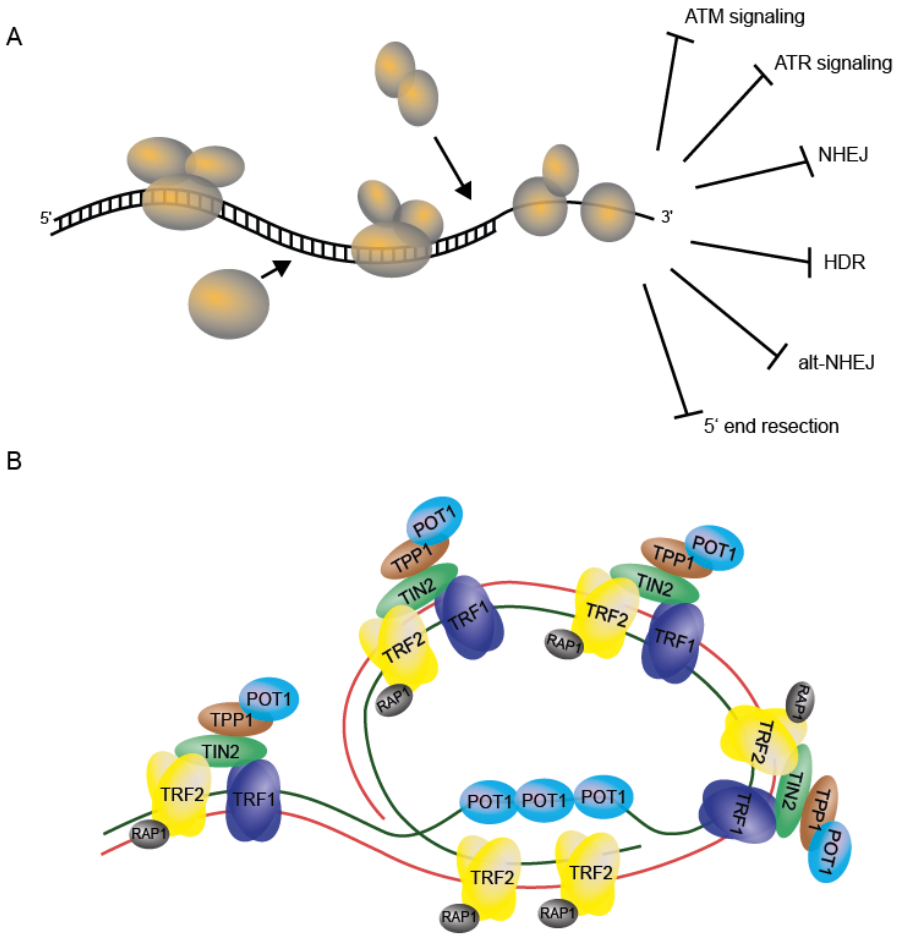

Figure I2: Telomere protection is carried out by interacting proteins and telomeric structure. (A) Proteins binding to and interacting with the telomeric DNA are protecting the integrity of chromosome ends by inhibition of DNA damage signaling and DNA damage repair pathways. Bound proteins are attached at the DNA structure; interacting proteins are marked with an arrow. (B) T-loop structure at mammalian telomeres. TRF2 binding promotes t-loop formation. The ss 3' overhang invades the ds region and displaces one strand for homologous pairing. The resulting single-strand is potentially bound by POT1 for protection. (reviewed in de Lange, 2018 and Sfeir and de Lange, 2012) ATM: Ataxia-telangiectasia-mutated, ATR: Ataxia telangiectasia and Rad3-related, NHEJ: non-homologous end joining, HDR: homology directed repair, alt-NHEJ: alternative non-homologous end joining.

The telomere binding proteins in fission and budding yeast aid in the inhibition of DDR as well. In *S. pombe*, the deletion of *taz1* or *rap1* causes elongated telomeres as well as chromosome fusions. This indicates a role for these proteins in length maintenance and the protection from NHEJ (Ferreira and Cooper 2001; Miller et al. 2005). Deletions of the single-strand binding protein POT1 and its interactor TPZ1 on the other hand lead to loss of telomeres, implicating them in telomere maintenance (Baumann and Cech 2001; Miyoshi et al. 2008). Loss of telomeres in these mutants leads to self-circularized chromosomes, which are considered a hallmark of deprotected telomeres in *S. pombe* (Miyoshi et al. 2008). This phenotype was described when mutating the *rad3* gene, the ATR homolog in *S. pombe*, whose deletion causes a telomere defect in addition to a checkpoint defect (Dahlén et al. 1998). Both NHEJ and single-strand annealing (SSA) are responsible to form circularized chromosomes but depending on length and structure of the respective telomeres. SSA has been shown to be the pathway used to fuse short telomeres (Wang and Baumann 2008). Interestingly, the DNA damage checkpoint plays an important role in the maintenance of these circular chromosomes, to ensure survival of the cells (Shamim et al. 2017). As in mammalian cells, the checkpoint genes also play an important role for telomere maintenance in *S pombe*. Both ATM/ATR homologs TEL1 and RAD3 promote telomere protection and proper telomere maintenance by stabilizing the TPZ1-CCQ1 binding to telomeres and recruitment of telomerase (Moser et al. 2009). The conserved KU heterodimer (spKU) prevents recombination and nucleolytic activity (Baumann and Cech 2000). Similar to mammalian cells, telomeres

of *S. pombe* potentially fold into a t-loop structure and thereby support telomere protection (Tomaska et al. 2004). Here, the loop structure is mediated by TAZ1, the TRF homolog of fission yeast.

In *S. cerevisiae*, both single- and double-strand telomere binders support telomere protection, though at different stages of the cell cycle (Vodenicharov and Wellinger 2006; Vodenicharov et al. 2010). The single-stranded overhang of budding yeast telomeres is protected by the CST complex during late S and G2 phase of the cell cycle by hiding it through its binding (Vodenicharov and Wellinger 2006). In the other phases of the cell cycle RAP1 and its interacting partners at the double-stranded telomere are essential for capping (Bonetti et al. 2010; Vodenicharov et al. 2010), inhibiting NHEJ and over-elongation of telomeres (Marcand et al. 1997; Levy and Blackburn 2004; Marcand et al. 2008). RIF2 prevents checkpoint activation by reducing the association of the DNA damage repair complex MRX to the telomeres (Bonetti et al. 2010). The scKU heterodimeric complex (scKU70/scKU80), which through binding to the telomeres prevents nucleolytic activity and recombination, provides additional protection in *S. cerevisiae* (Gravel et al. 1998; Polotnianka et al. 1998; Bertuch and Lundblad 2003). Unlike in mammalian cells the 3' overhangs of budding yeast telomeres are short throughout the majority of the cell cycle, so there is no evidence for a t-loop like structure at budding yeast telomeres (Cooper 2000). Nevertheless, it has been reported, that *S. cerevisiae* telomeres engage in a fold-back loop structure for gene expression regulation (de Bruin et al. 2000; de Bruin et al. 2001; Poschke et al. 2012). Furthermore, it has been shown that normal yeast telomeres engage in a fold back structure that is mediated by histone modifiers SIR2, SIR3 and SET2, as well as the HR proteins RAD51, RAD52, and the checkpoint kinase RAD53. This suggests that strand invasion, as seen in the mammalian t-loop, and chromatin environment play a role in the establishment of the fold (Wagner et al. 2020). Interestingly, this structure is retained when telomeres are short, but not when cells undergo replicative senescence. In addition to the fold back structures, potential capping of telomeres by G-quadruplex (G4) structures has been suggested to prevent end-resection, as G4 binding proteins rescue a CST-capping defect (Smith et al. 2011).

Telomeres and the end-replication problem

The end-replication problem arises because linear chromosomes and their ends are replicated in a semi-conservative manner (Watson 1972; Olovnikov 1973). As the polymerases used for DNA replication can only polymerize in 5' to 3' direction, telomeres cannot be replicated fully and shorten with every replication cycle (Lingner et al. 1995). The leading and lagging strand telomeres are thereby replicated with a different outcome. While the lagging strand telomere is replicated with a 3' overhang due to primer removal after replication, the leading strand telomere is generated with a blunt end (Lingner et al. 1995), leading to subsequent shortening in consecutive replications (Fig. I3) (Gilson and Géli 2007). The reverse transcriptase enzyme telomerase counteracts the end-replication problem and the following loss of telomeric sequence (Greider and Blackburn 1985; Greider and Blackburn 1987; Greider and Blackburn 1989). Utilizing a RNA template (TERC in mammals, TER1 in *S. pombe*, TLC1 in *S. cerevisiae*), telomerase is able to elongate the 3' G-strand of telomeres and restore telomere length.

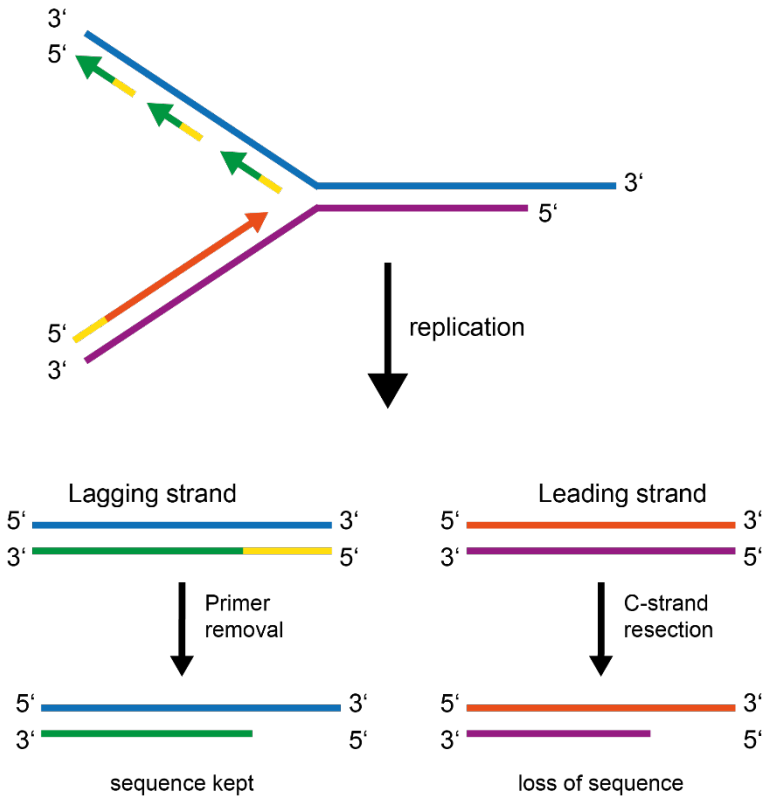

Figure I3: Schematic depiction of the end-protection problem. During DNA replication the leading and lagging strand are differentially replicated. While replication of the leading strand results in a blunt ended product with no overhang, replication of the lagging strand keeps an overhang due to RNA primer removal after replication. Therefore, lagging strand telomeres do not lose telomeric sequence, whereas C-strand resection for the creation of overhangs on the leading strand leads to loss of sequence. Blue and purple lines depict lagging and leading strand, respectively. Orange and green lines show the newly synthetized DNA, yellow lines represent RNA primers for initiation of DNA synthesis.

Since the 3’ overhang is the template for telomerase and it plays a role in telomere protection (t-loops, binding of single-strand telomere proteins), it has to be reconstituted after replication is finished. For this, mammalian and yeast cells use controlled C-strand resection (Wellinger et al. 1996; Wu et al. 2010). In mammalian cells, this mechanism is initiated by TRF2-mediated recruitment of the exonuclease Apollo to the leading-strand telomere (van Overbeek and de Lange 2006; Wu et al. 2010). Apollo resects the leading-strand telomere in 5’ to 3’ direction, leaving a 3’ single-stranded overhang (Lam et al. 2010). Overhangs on both lagging- and leading-strand telomeres are further processed by the exonuclease EXO1 and the mammalian CST complex to derive functional telomere structure (Miyake et al. 2009; Wu et al. 2012). In *S. pombe* the pathway for C-strand resection is less investigated. However, it has been demonstrated, that resection is performed by the DDR RAD50/MRN complex (RAD50/RAD32/NBS1) recruiting the 5’-to-3’ nuclease DNA2 (Tomita et al. 2004; Ueno 2010). In *S. cerevisiae* the C-strand of the leading strand is resected in a TEL1 dependent pathway to create an overhang (Soudet et al. 2014). Additionally, other factors like the MRX complex, EXO1, and DNA2 are participating in overhang production (Bonetti et al. 2009; Longhese et al. 2010; Budd and Campbell 2013). This overhang is afterwards further filled in to generate the common short 3’ overhang of about 10 nt (Soudet et al. 2014).

Telomere replication and the telomere replication problem

Telomere replication is a coordinated mechanism in all cells and thereby temporally regulated. While telomeres in *S. cerevisiae* and *S. pombe* are replicated in late S phase, mammalian telomeres are replicated throughout S phase (Wright et al. 1999; Kim and Huberman 2001; Raghuraman et al. 2001). Replication of human telomeres was described to be a two-stage process in S and late S/G2 phase

(Verdun and Karlseder 2006). Both phases involve a DNA damage response, phase I to restart stalled replication forks, and phase II to generate a 3' overhang for t-loop formation (Verdun and Karlseder 2006). As previously mentioned, DNA damage factors are widely involved in telomere protection and maintenance in mammalian cells and yeast.

Given the sequence and structure of telomeres, replication through chromosome ends is a difficult process. The telomere replication problem describes the difficulties of semi-conservative replication to properly replicate through chromosome ends, leading to replication fork stalling (Maestroni et al. 2017). Fork stalling at telomeres can be caused by their heterochromatin structure, tight association of telomere binding proteins, G-quadruplexes formed by the sequence, DNA-RNA hybrids resulting from transcription, and t-loops (Maestroni et al. 2017). Once stalled, the replication fork needs restarting, as collapse of the replication fork would lead to a DDR and subsequent DNA repair with potential loss of telomeric sequences (Gilson and Géli 2007). For *S. pombe* and mammalian cells it has been established that TAZ1 and TRF1/TRF2 respectively aid in resolving stalled replication forks and prevent fork stalling (Miller et al. 2006; Sfeir et al. 2009). In human cells it has been shown, that TRF1 and TRF2 are interacting with different proteins to prevent fork stalling. In addition, interaction with the fork protection complex (FPC) has been described (Leman et al. 2012; Leman and Noguchi 2012). Depending on the impeding structure, different nucleases or helicases are recruited to the telomeres. Helicases such as Werner syndrome RecQ like helicase (WRN) and Bloom syndrome RecQ like helicase (BLM), as well as RTEL1 (regulator of telomere length 1) are implicated in G4 and t-loop processing (Opresko et al. 2005; Vannier et al. 2012). Improper t-loop resolution by SLX1-SLX4 nucleases in case of RTEL1 loss leads to t-circle formation and rapid telomere loss (Vannier et al. 2012). Additionally, binding of POT1 and RPA is able to prevent formation of G4 structures at telomeres (Salas et al. 2006). Mammalian helicase UPF1 (Up-frameshift 1) on the other hand has been implicated in the displacement of telomeric transcripts prior to replication fork passage (Azzalin et al. 2007; Chawla et al. 2011). Additional factors have been described to aid in telomere replication, and together with the before mentioned proteins they facilitate proper leading- and lagging-strand synthesis. In *S. cerevisiae*, unwinding of G4 structures requires the helicases such as RRM3 and PIF1 (Azvolinsky et al. 2006; Paeschke et al. 2011). The main acting helicase at telomeres was decribed to be RRM3, which is traveling with the replisome (Azvolinsky et al. 2006). The PIF1 homolog in *S. pombe*, PFH1, has as well been implicated in telomeric G4 structure resolution and thereby promotion of telomere replication (McDonald et al. 2014; Wallgren et al. 2016).

Telomere length maintenance

As maintaining the length of telomeres is essential to the protection of chromosomes in replicating cells, different strategies evolved to aid in the resolution of the end-replication problem. The first one is the maintenance pathway involving the reverse transcriptase telomerase; others involve homologous recombination as a means of telomere maintenance.

Telomerase-mediated maintenance

Telomerase is a reverse transcriptase enzyme, first described in *Tetrahymena thermophila*, which counteracts telomere shortening by addition of telomeric repeats to the 3' overhang (Greider and Blackburn 1985; Greider and Blackburn 1987; Greider and Blackburn 1989). Shortly after its discovery, it was also described in human cancer cells and yeast (Morin 1989; Cohn and Blackburn 1995). Telomerase consists of a catalytically active subunit and an RNA template used for addition of nucleotides to the 3' overhang (Greider and Blackburn 1987). The catalytically active subunits are TRT1/TERT in human cells, TRT1 in *S. pombe* and EST2 in *S. cerevisiae* (Lendvay et al. 1996; Nakamura et al. 1997), the RNA subunits TR/TERC, TER1 and TLC1, respectively (Singer and Gottschling 1994; Feng et al. 1995; Webb and Zakian 2008). In *S. cerevisiae* two more protein subunits next to the catalytically active EST2 have been described, EST1 and EST3 (Lundblad and Szostak 1989; Lendvay et al. 1996), but only EST2 and TLC1 are needed for telomerase activity (Lingner et al.

1997). EST1 has also been identified as a telomerase associate in *S. pombe* and humans (Beernink et al. 2003; Reichenbach et al. 2003; Snow et al. 2003). These and additional protein subunits work in recruitment of telomerase to the telomeres as for example EST1 of *S. cerevisiae*, which interacts with CDC13 at the telomere (Wu and Zakian 2011; Maciejowski and De Lange 2017). In short, repeat addition via telomerase is induced via base pairing of the template region of the telomerase RNA with the overhang to be elongated. Once the active site of the catalytic subunit closes, elongation proceeds until the end of the template region. When the 5' end of the template is reached, the 3' end of the template dissociates and leads to active site opening and duplex unpairing, followed by template translocation and product dissociation (Wu et al. 2017).

Telomerase activity is a tightly regulated mechanism, dependent on the cell type, tissue or organism. While telomerase-mediated lengthening of telomeres in the unicellular yeasts *S. cerevisiae* or *S. pombe* supports cell division and organismal propagation, its activity is downregulated in most cells of multicellular long-lived organisms as a suppression measure against tumor development (Maciejowski and De Lange 2017). For this reason, telomere regulation by telomerase plays an important role in the studies of cancer, as in 85-90% of cancers telomerase activity is upregulated (Fig I4) (Kim et al. 1994). In dividing tissues such as germ cells, telomerase is active (Fujisawa et al. 1998; Wright et al. 2000) to ensure inheritance of full-length chromosomes.

Telomerase-mediated maintenance of telomeres is set in S-phase of the cell cycle in yeast and human cells (Marcand et al. 2000; Tomlinson et al. 2006; Dehé et al. 2012). Recruitment of telomerase to the telomeres involves interaction of the holoenzyme with telomere binding proteins. In *S. cerevisiae* and *S. pombe* the telomerase subunit EST1 interacts with CDC13 and CCQ1 respectively (Taggart et al. 2002; Tomita and Cooper 2008; Webb and Zakian 2012; Armstrong et al. 2018). In addition, an interaction with replication protein A (RPA) facilitates telomerase loading to the telomeres by EST1 and thereby telomerase activity (Taggart et al. 2002; Schramke et al. 2004; Luciano et al. 2012). In mammalian cells, telomerase is recruited by TPP1, the interactor of POT-1 and TIN2 (Wang et al. 2007; Abreu et al. 2010; Zhong et al. 2012). The activation of telomerase is dependent on further protein-protein interactions after recruitment to the telomeres (Armstrong et al. 2014). It has been shown that the preferred substrate of telomerase are short telomeres (Teixeira et al. 2004; Bianchi and Shore 2007). In *S. cerevisiae* the MRX complex and TEL1 accumulate at short telomeres to recruit telomerase for elongation (Bianchi and Shore 2007; Hector et al. 2007; Sabourin et al. 2007; McGee et al. 2010). Mammalian cells facilitate telomerase activity by the binding of hnRNP proteins (Zhang et al. 2006). In addition, both yeasts and mammalian cells utilize telomeric transcripts for telomerase regulation (Cusanelli et al. 2013; Redon et al. 2013; Moravec et al. 2016). An additional DNA damage checkpoint complex is described to facilitate the repeat addition via telomerase. The so-called 9-1-1 (RAD9/RAD1/HUS1) PCNA-like complex including its clamp loader RAD17 has been implicated in facilitation of telomerase activity as deficiency for complex members leads to telomere shortening (Longhese et al. 2000; Francia et al. 2006; Verdun and Karlseder 2006). Mammalian cells deficient for the 9-1-1 complex are inviable and show a reduction in telomere length (Francia et al. 2006).

There are two models as to how telomerase is regulated at telomeres of different length. The so-called "protein-counting model" was established in *S. cerevisiae* where it was proposed, that the amount of bound RAP1 is used as counting mechanism for telomere length (Krauskopf and Blackburn 1996) as RAP1 was described as a negative regulator of telomere length (Conrad et al. 1990; Lustig et al. 1990). Additionally, other telomere-associated proteins have been described to act as negative regulators of telomerase. In *S. cerevisiae*, RIF proteins act as regulators of telomere length, whereas in *S. pombe* TAZ1 and CCQ1 have been shown to have regulatory effect (Cooper et al. 1997; Teng et al. 2000; McGee et al. 2010; Armstrong et al. 2018). TRF1 is the negative regulator of telomerase in human cells (van Steensel and de Lange 1997; Smogorzewska et al. 2000). According to the model, a decreased number of negative regulators at telomeres accounts for shorter telomere length, which leads to telomerase recruitment. The other proposed mechanism is the "replication fork model", in which telomerase travels with the replication fork. Depending on the amount of associated proteins at the telomeres telomerase dissociates from the replication fork at long telomeres and stays on at short telomeres to elongate them (Greider 2016). Telomere homeostasis is therefore a layered pathway,

implicating telomere length and accessibility, as well as telomerase levels and activity in its regulation (Cristofari and Lingner 2006; Hug and Lingner 2006).

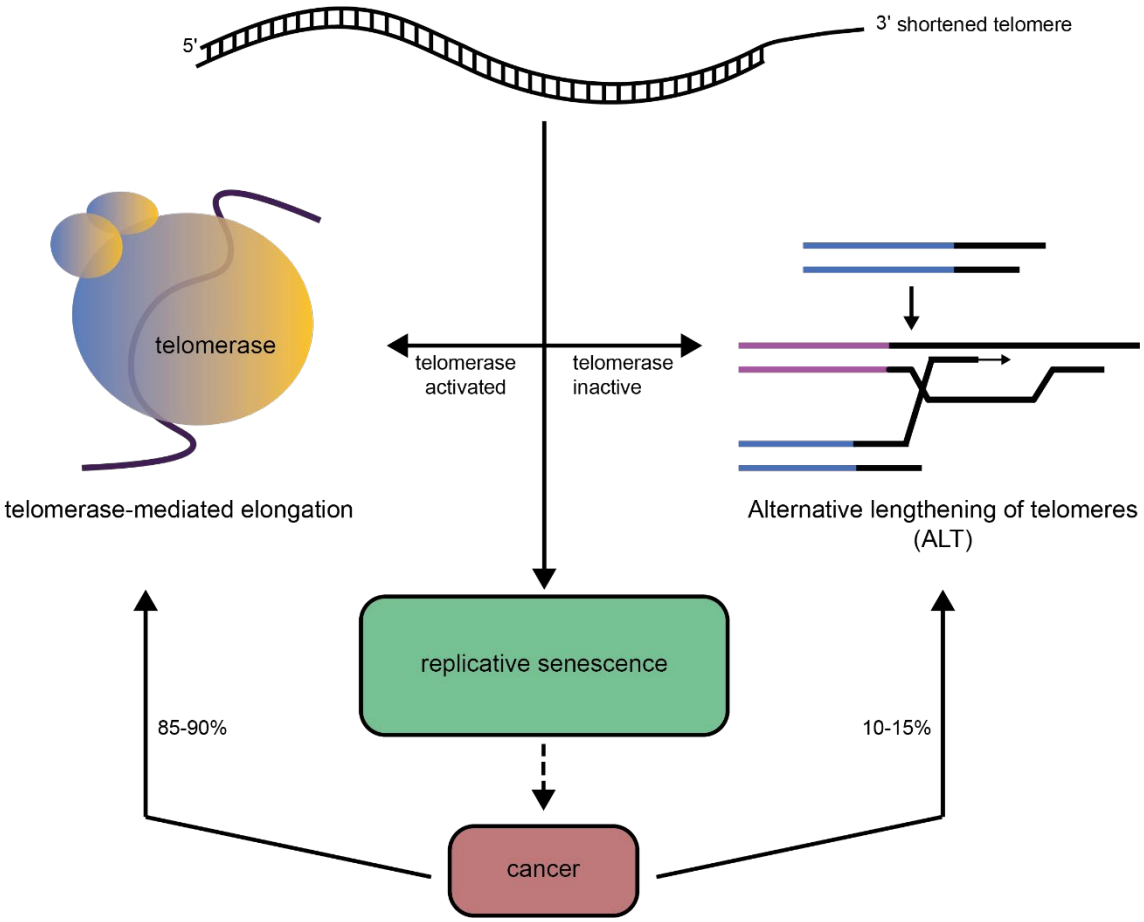

Figure I4: Canonical telomere maintenance mechanisms. Shortened telomeres, here depicted by a black DNA scheme, result in cell cycle arrest and replicative senescence if not properly re-elongated. One option for elongation is activation of telomerase. The other option in telomerase-negative cells is alternative lengthening of telomeres (ALT). Here, telomeres are re-elongated by an HR-mediated pathway utilizing homologous sequences on other chromosomes. In developing cancer cells telomeres must be re-elongated as well to gain immortality. This is achieved either through re-activation of telomerase or utilizing ALT. Telomerase and associated factors are depicted as colored circles, the RNA template as purple line within the protein. For ALT, different chromosomes are colored in blue and purple respectively, telomeres as homologous sequences are colored black.

Alternative lengthening of telomeres (ALT)

A number of cells are able to maintain their telomere length and thereby their proliferative potential also in the absence of a functioning telomerase pathway. This way of telomere maintenance is called alternative lengthening of telomeres (ALT) and was first described in *S. cerevisiae* (Lundblad and Blackburn 1993). Next to upregulation of telomerase activity, ALT is a secondary way for immortalization and is active in 10-15% of human cancers (Bryan et al. 1997; Bryan and Reddel 1997). Maintenance of telomeres by this pathway relies on homologous recombination (Fig. I4) (Lundblad and Blackburn 1993).

Human cells that rely on ALT for telomere elongation possess several features making them distinguishable from cells employing the telomerase pathway. As telomeres are elongated in a HR fashion, a sister telomere can be used as a template for the reaction by strand invasion (Teng and Zakian 1999; Cesare and Reddel 2010). This leads to a higher probability of sister chromatid exchanges (t-SECs) between the telomere to be elongated and its template (Londoño-Vallejo et al. 2004). ALT cells show very heterogeneous telomere lengths ranging from 2 to 20 kb (Murnane et al. 1994). In addition,

abundant extrachromosomal DNA made up of telomeric repeats (ECTR) such as C-circles (Henson et al. 2009), as well as specialized nuclear structures containing telomere DNA, termed ALT-associated promyelocytic leukemia (PML) bodies (APBs) were described in ALT cells (Yeager et al. 1999; Cesare and Griffith 2004; Nabetani and Ishikawa 2009). Next to telomeric DNA, several other factors, such as DNA repair proteins (RAD51, RAD52) and helicases (BLM, WRN), can be found in APBs (Apte and Cooper 2017), making them very specialized structures that are promoting ALT (Zhang et al. 2019; Loe et al. 2020). Indeed, APB factors such as BLM and RAD52 have been shown to facilitate ALT by triggering break-induced replication (BIR) and mitotic DNA synthesis (miDAS) to elongate telomeres (Min et al. 2019; Zhang et al. 2019). Interestingly, not only canonical telomeric sequences, but also variant repeats can be found in ALT cells, potentially facilitating recruitment of ALT factors (Conomos et al. 2012). TERRA the telomeric transcript (see Telomere chromatin and telomere transcription - TERRA) is involved at ALT telomeres as well, proposed to facilitate HR by DNA-RNA hybrid (R-loop) formation without challenging telomere stability (Arora et al. 2014).

As *S. cerevisiae* cells depend on telomere length maintenance for survival and propagation, a progressive loss of telomere length and decreased viability up to senescence can be observed upon the loss of telomerase (Lundblad and Blackburn 1993). Interestingly, during senescence, budding yeast is able to develop viable cells, so-called “survivors”. Two types of survivors have been described, both depending on HR-mediated telomere length maintenance (Lundblad and Blackburn 1993; Teng and Zakian 1999). Type I survivors elongate their telomeres by amplification of the Y’ elements in their subtelomeric region in a RAD51 dependent manner, while type II survivors amplify long telomeric repeats with the help of MRX and RAD59 (Lundblad and Blackburn 1993; Le et al. 1999; Chen et al. 2001). Continuous maintenance of both survivors is dependent on RAD52, as no survivors emerge upon RAD52 loss in telomerase-negative cells (Lundblad and Blackburn 1993; Le et al. 1999; Teng and Zakian 1999). Involvement of POL32 indicates BIR-mediated telomere maintenance as in human ALT cells (Lydeard et al. 2007). Similar to human ALT the telomeric RNA TERRA is also present at short *S. cerevisiae* telomeres, implicated in the prevention of replicative senescence by activation of HR-mediated telomere elongation (Graf et al. 2017).

Non-canonical ALT

Formation of survivors in telomerase-negative cells has also been described in *S. pombe* (Nakamura et al. 1998). Interestingly, fission yeast does not employ a canonical ALT pathway to maintain its telomeres. One type of survivors shows circularization of the three *S. pombe* chromosomes by end fusion instead of recombination (Nakamura et al. 1998; Apte and Cooper 2017). Survival with circularized chromosomes depends on DNA damage factors and the RecQ helicase RQH1 (Nanbu et al. 2013; Shamim et al. 2017). A second mode of survival that maintains linear chromosomes is the amplification of telomere-associated sequences (TAS) by recombination, which results in re-elongated telomeres (Nakamura et al. 1998). Later studies have shown that the TAS themselves, as well as factors of the DNA damage pathways such as the TEL1-MRN complex and RAD51/Rad52, as well as TERRA act in the promotion of the telomere recombination pathway (Subramanian et al. 2008; Khair et al. 2010; van Emden et al. 2019; Hu et al. 2019). A third form of telomerase-independent survival in *S. pombe* is the replacement of telomeric repeats by heterochromatin repeats through recombination. These heterochromatin amplification-mediated and telomerase-independent survivors (HAATI) utilize POT1 and CCQ1 to maintain linear chromosomes and replace their telomeres by heterochromatic repeats such as rDNAs and sub-telomeric elements (STEs) (Jain et al. 2010).

Other organisms harboring non-canonical telomeres evolved additional, non-canonical ways of telomere maintenance. Telomeres in the model organism *Drosophila melanogaster* have a different sequence than the conserved TTAGGG and its genome does not encode for a telomerase enzyme (Mason and Biessmann 1995). *Drosophila* telomeres contain three retrotransposon elements named Het-A, TART, and Tahre (HTT), whose transcripts (GAG-like proteins and reverse transcriptases) target chromosome ends (Abad et al. 2004; Capkova Frydrychova et al. 2009). The interaction of the transposon products with the chromosome end leads to sequence addition in a reverse transcription reaction, integrating the

retrotransposons into the chromosome end (Pardue and Debaryshe 2008). Similar to mammalian and yeast telomeres, the retrotransposon telomeres of *D. melanogaster* are bound by proteins providing a telomere protection (Cenci et al. 2005). These proteins include HP1 and HOAP as the cap, as well as ATM and the MRN complex for protection and were named terminin (Cenci et al. 2005; Raffa et al. 2013).

Telomere chromatin and telomere transcription

Telomere position effect and chromatin modification

Telomeres have been shown to have influence on transcription of neighboring genes. This is called the telomere positon effect (TPE) and is due the heterochromatin formation and epigenetic modification (Gottschling et al. 1990; Baur et al. 2001; Dehé and Cooper 2010). In mammalian cells, it has been in line with the appearance of tri-methylation marks at nucleosomes and low levels of acetylation on histones H3 and H4, which correspond to transcriptional silencing marks (Blasco 2007). For both yeast and mammalian cells TPE increases with telomere length (Gottschling et al. 1990; Baur et al. 2001) suggesting TPE to be a regulatory pathway. Indeed, TPE in *S. cerevisiae* regulates expression of metabolic and stress response genes (Ai et al. 2002), while TPE in mammalian cells regulates several genes, including the expression of the telomerase catalytic subunit TERT (Robin et al. 2014; Kim and Shay 2018). In *S. pombe*, telomere-adjacent heterochromatin is mediated by the telomere binder TAZ1 at subtelomeres and plays an important role in proper meiotic chromosome segregation (Nimmo et al. 1998; Kanoh et al. 2005; Matsuda et al. 2015).

The heterochromatin landscape of telomeres contributes to their function as well as overall genome integrity. The human telomeres for example contain nucleosomes with respective posttranslational modifications (methylation, acetylation), as well as methylation of DNA in the subtelomeric region (Blasco 2007), while in *S. cerevisiae* only the subtelomeric regions contain nucleosomes (Wright et al. 1992). Histone modifications and DNA methylation have been shown to influence telomere length in mammalian cells and vice versa (Benetti et al. 2007; Schoeftner and Blasco 2010). Factors such as histone methyltransferases (HMTs), histone deacetylases (HDACs), and DNA methyltransferases (DNMTs) directly influence telomere length by promoting a more accessible or inaccessible telomere (García-Cao et al. 2004; Benetti et al. 2007; Schoeftner and Blasco 2010). This way, elongation of the telomeres can be supported or inhibited. At this point, there is still discussion whether compaction or decompaction of telomeric DNA is responsible for promotion of the ALT mechanism (Episkopou et al. 2014; Gauchier et al. 2019). In *S. cerevisiae,* it has been reported that subtelomeres also accumulate epigenetic marks at histones. SIR complex-mediated histone deacetylation, as well as histone methylation and ubiquitylation by other factors were described to influence telomere silencing, replication and elongation (Maicher et al. 2012; Rhie et al. 2013; Wu et al. 2018).

TERRA

For a time, telomeres were considered transcriptionally silent. The first report of transcription of telomeres came from mammalian cells in 2007 when probing a Northern Blot of total RNA from HeLa cells with a telomeric probe (Azzalin et al. 2007). The obtained signal ranged between a few hundred nucleotides to about 9 kb and was abolished upon RNase treatment (Azzalin et al. 2007). Further studies confirmed transcription of these telomeric repeat containing RNAs (TERRA) in other cell types and organisms from different mammalian systems and plants to yeast (Azzalin et al. 2007; Luke et al. 2008; Schoeftner and Blasco 2008). In mammalian cells and *S. cerevisiae* the C-rich strand is transcribed into TERRA and subtelomeric regions can be integrated in the transcript, potentially due to start of transcription in the subtelomeric regions (Azzalin et al. 2007; Luke et al. 2008; Schoeftner and Blasco 2008). In addition, a subtelomeric species of RNA named ARRET is transcribed in opposing direction to TERRA in *S. cerevisiae* (Luke et al. 2008). *S. pombe* on the other hand transcribes both its C- and G-rich strands into TERRA and ARIA transcripts respectively, as well as its subtelomeric regions into

ARRET and α-ARRET transcripts (Bah et al. 2012; Greenwood and Cooper 2012). Transcription of telomeric RNAs is carried out by RNA polymerase II, yielding molecules of different lengths (Luke et al. 2008; Schoeftner and Blasco 2008; Bah et al. 2012).

As mentioned above, chromatin formation and epigenetic marks play a role in telomere biology. Transcription of TERRA is as well mediated by the modification on telomeric DNA. DNA methylation in the subtelomeres of human cells represses transcription, whereas cohesin binding can have an activating effect through recruitment of RNA polymerase II (Ng et al. 2009; Deng et al. 2012; Rippe and Luke 2015). In addition, there is evidence that epigenetic modifications of nucleosomes at telomeres regulate TERRA expression, potentially by a negative feedback loop involving the transcript itself (Azzalin and Lingner 2008; Arnoult et al. 2012; Cusanelli and Chartrand 2014; Rippe and Luke 2015; Montero et al. 2018). In *S. cerevisiae* TERRA transcription is determined by the subtelomeric Y' and X elements involving RAP1 interaction with either SIR proteins or RIF proteins (Iglesias et al. 2011). TERRA levels in both human and budding yeast are cell cycle dependent and regulated not only by transcription levels but also by RNA degradation (Porro et al. 2010; Graf et al. 2017).

Studies in different systems show that TERRA can mediate telomere elongation in the absence of telomerase, as TERRA levels increase in ALT cells and yeast survivors, thereby promoting HR (Balk et al. 2013; Arora and Azzalin 2015; Hu et al. 2019). Interestingly, it has been shown that TERRA in mammalian cells is an inhibitor of telomerase activity, while it is promoting telomerase activity in *S. cerevisiae* and *S. pombe* (Schoeftner and Blasco 2008; Redon et al. 2010; Cusanelli et al. 2013; Moravec et al. 2016). Additional studies implicate TERRA in regulation of telomere replication and the DNA damage response (Deng et al. 2009; Flynn et al. 2011; Beishline et al. 2017; Chu et al. 2017). However, unbalanced accumulation of TERRA and its associated RNA-DNA hybrids (R-loops) can lead to telomere dysfunction and genome instability (Azzalin et al. 2007; Luke et al. 2008; Sagie et al. 2017; Crossley et al. 2019).

Telomeres and senescence

Leonard Hayflick marked the term replicative senescence with his experiments to limited lifespan of cultured primary cells in the 1960's (Hayflick and Moorhead 1961; Hayflick 1965). Also known as the "Hayflick Limit", he described a concept after which normal cells divide a specific number of times before entering replicative senescence and thereby lose the ability to divide. In later studies by Watson and Olovnikov, it was determined that the telomere length of cells plays an important role in this pathway. Due to incomplete DNA replication by the canonical pathway, telomeres shorten in every replication cycle – also known as the end-replication problem (Watson 1972; Olovnikov 1973). In cells that do not counteract this telomere shortening by telomerase activity or ALT, this will lead to a stop in mitotic cell division, so-called replicative senescence (Harley et al. 1990). The DNA damage response due to critically short telomeres triggers a cell cycle arrest, which, if not resolved, leads to apoptosis or senescence (Kuilman et al. 2010). Senescent cells are still metabolically active, but retain the DNA damage signals that have accumulated as can be visualized by the senescence-associated DNA damage foci (SDF) (Holmes et al. 1992; Galbiati et al. 2017). Telomere shortening, followed by DNA damage signaling, and activation of the p53 pathway is not the only way of inducing senescence (Herbig et al. 2004). In addition, exposure to oxidants, γ-irradiation, UVB light, and DNA damaging chemotherapies can activate the DDR and lead to telomere-independent senescence (Childs et al. 2015). Stress and resulting p16 expression engages the p16–retinoblastoma protein (pRB) pathway, which in turn leads to replicative senescence as well (Brenner et al. 1998; Kuilman et al. 2010). Characteristics of senescent cells include, next to the retention of DNA damage, permanent growth arrest, apoptosis resistance, altered gene expression, and display of other senescence markers such as senescence-associated heterochromatin foci (SAHF) and senescence-associated β-galactosidase (SA-Bgal) staining (Dimri et al. 1995; Campisi and D'Adda Di Fagagna 2007). Taken together, DDR that is activated by different factors such as telomere state, stress, or oncogene expression, is the main driver of senescence (D'Adda Di Fagagna 2008).

Replicative senescence in multicellular organisms limits the proliferation of cells as a means to counteract the development of cancer (Campisi and D'Adda Di Fagagna 2007). As most human cells, except for germ cells and stem cells, have very little telomerase activity, telomeres shorten over time, leading to replicative senescence (Hayflick 1965; Kim et al. 1994; Bodnar et al. 1998). This counteracts proliferation of cells with accumulated damages and acts as a tumor suppressor mechanism (Campisi and D'Adda Di Fagagna 2007).

Due to short lifespan and availability of molecular techniques, *S. cerevisiae* has become a prime model organism to study replicative senescence (Fabrizio and Longo 2003). Loss of telomerase components leads to telomere shortening and the onset of senescence after a certain amount of population doublings (PD) due to DNA damage signaling by the shortest telomere (Teixeira 2013). In addition, yeast survivors maintain their telomeres in a HR-mediated pathway similar to ALT cells (Lundblad and Blackburn 1993; Teng and Zakian 1999). In the following, *S. cerevisiae* has been used to study the molecular bases of senescence and potential countermeasures to increase lifespan in telomerase negative cells such as calorie restriction (CR) (Kenyon 2001; Dilova et al. 2007; Longo et al. 2012; Teixeira 2013; Lin and Austriaco 2014). The fission yeast *S. pombe* is used in senescence studies, as some cellular processes are conserved between mammals and fission yeast but not in *S. cerevisiae* (Roux et al. 2010; Lin and Austriaco 2014). On the other hand, many identified longevity factors exist in both yeasts, making *S. pombe* a complementary model (Lin and Austriaco 2014).

Aging in the sense of organismal senescence is defined as a deteriorative process involving the progressive loss of physical integrity, impaired function, and increased vulnerability (López-Otín et al. 2013). In particular, the accumulation of different cellular damages over time is considered the cause of aging. In 2013, nine hallmarks of aging were proposed which are common between most organisms (López-Otín et al. 2013). Next to cellular senescence they include: Stem cell exhaustion, altered intercellular communication, genomic instability, telomere attrition, epigenetic alterations, loss of proteostasis, deregulated nutrient sensing, and mitochondrial dysfunction (Blasco 2007; Collado et al. 2007; Powers et al. 2009; Green et al. 2011; Barzilai et al. 2012; Talens et al. 2012; López-Otín et al. 2013; Moskalev et al. 2013). Interestingly, the nutrient sensing mechanism including the insulin/IGF-1 and target of rapamycin (TOR) pathways have been shown to potentially mediate the effect of CR on senescence and are conserved across different model organisms like mouse, *D. melanogaster* and *C. elegans* (Gems and Partridge 2013).

Telomeres and disease

In addition to contributing to cellular and organismal senescence, telomeres have been implicated in a variety of human diseases such as cancer. Cancer cells have overcome their replicative senescence by either re-activating telomerase or by maintaining their telomeres by HR via ALT (Kim et al. 1994; Bryan et al. 1997; Shay and Bacchetti 1997).

Telomere shortening is a double-edged sword that plays a role in cancer development. On one hand telomere shortening acts as a tumor suppressor mechanism, on the other hand short and unprotected telomeres can induce a state called telomere crisis, which in turn is a promoter of cancer progression (Maciejowski and De Lange 2017; Cleal and Baird 2020). Telomere crisis induces genomic rearrangements like chromothripsis and chromosome tetraploidization (Artandi et al. 2000; Maciejowski et al. 2015). One of the ways to exit telomere crisis is to reactivate telomerase, potentially by a TERT promoter mutation or genomic rearrangement, and regain proliferative potential (Maciejowski and De Lange 2017). However, further studies have to be conducted to gain insight in the specifics of how different types of cancer reactivate telomerase. In some cancer types, telomeres are re-elongated by ALT (Bryan et al. 1997). This coincides with a mutation in the chromatin remodeler ATRX in some cancers (Lovejoy et al. 2012). Interestingly, ATRX and TERT promoter mutations seem to be mutually exclusive, implicating two separate pathways in the escape of telomere crisis (Maciejowski and De Lange 2017).

In addition to cancer, several other disorders that stem from direct or indirect telomere involvement have been described. These conditions are called telomere maintenance spectrum disorders or telomeropathies and are mostly premature aging syndromes with exceptionally shortened telomeres (Armanios and Blackburn 2012; Opresko and Shay 2017). Telomeropathies are divided into two groups: the primary telomeropathies, direct mutations in genes involved in the telomerase maintenance pathway, and secondary telomeropathies, mutations in DNA repair or structural proteins that indirectly affect telomeres. Primary telomeropathies include dyskeratosis congenita and idiopathic pulmonary fibrosis with mutations in for example TIN2, RTEL1, or TERT/TERC. Secondary telomeropathies on the other hand include Ataxia telangiectasia, Bloom syndrome as well as Werner syndrome with mutations in ATM, BLM, and WRN respectively (Holohan et al. 2014; Opresko and Shay 2017). The majority of these telomere associated diseases increase the chance of developing cancer as a secondary pathology (Armanios and Blackburn 2012).

Telomeres and meiosis/fertility

Somatic stem cells, such as germ cells or hematopoietic stem cells, have higher proliferative potential than normal somatic cells. Therefore, telomere length maintenance by telomerase and protection of telomeres by associated proteins is important in these cell types as they give rise to new cells (Blasco 2005; Behrens et al. 2014). Interestingly, stem cell exhaustion by accumulation of DNA damage over time has been named as one of the hallmarks of aging (López-Otín et al. 2013; Behrens et al. 2014).

Indeed, telomere length has also been implicated in fertility in human (Kalmbach et al. 2013; Lopes et al. 2019; Vasilopoulos et al. 2019). Maintenance of telomere length is therefore important in the germline. Telomerase activity is measured in adult ovaries and testes but not in mature oocytes or sperm (Wright et al. 1996). Next to their length and maintenance, it has been established that telomeres are an essential part in meiosis in the germline, as they promote homology search of chromosomes (Scherthan 2007). Telomeres facilitate rapid meiotic prophase chromosome movements (RPM) by attachment to the inner nuclear membrane (INM) during meiotic prophase and cluster together, forming the so-called “bouquet” (Lee et al. 2012). The shelterin complex facilitates the attachment to the nuclear membrane in mammals by interaction with the TERB1-TERB2-MAJIN complex (Wang et al. 2019). TERB1 (telomere repeat binding bouquet formation protein 1) interacts with TRF1 in a TIN2-like manner to facilitate a “cap exchange” (Shibuya et al. 2015; Pendlebury et al. 2017). This exchange promotes the interaction of telomeres with the transmembrane linker of nucleoskeleton and cytoskeleton (LINC)-complex comprised of SUN and KASH domain proteins (Hiraoka and Dernburg 2009; Link et al. 2015). The KASH domain proteins of the LINC complex interact with cytoskeletal elements and thereby promote telomere movements and bouquet formation, while the SUN domain proteins present the inner nuclear link (Hiraoka and Dernburg 2009; Shibuya et al. 2014). It has been shown that the TRF1-TERB1 interaction is important for fertility in male and female mice (Long et al. 2017; Wang et al. 2019) and that the disruption of TERB2 abolishes telomere association to the INM and leads to disordered synapsis, underlining the importance of telomeres and associated proteins for proper meiosis.

In *S. cerevisiae* and *S. pombe* telomeres also cluster to the nuclear membrane during meiosis by interaction with specific proteins. Here, this is not facilitated by a cap exchange but by telomere binding proteins interacting with linker proteins to attach to the yeast specific LINC (Hiraoka and Dernburg 2009). Chromosome movements during meiosis were first described in *S. pombe* (Chikashige et al. 1994). During meiosis in fission yeast telomeres are attached to the INM at the position of the spindle-pole body (SPB) (Chikashige et al. 1994). The proteins BQT1 and BQT2 (“bouquet”1 and 2) facilitate this attachment by interaction with the telomere protein RAP1, as well as the SUN-domain protein SAD1 (Chikashige et al. 2006). The bouquet formation in *S. pombe* has been shown to facilitate SPB activation and thereby promote prophase exit and meiosis progression (Moiseeva et al. 2017). Homologous pairing of meiotic chromosomes is as well facilitated by telomeres in *S. cerevisiae* but telomeres do not attach to the SPB (Rockmill and Roeder 1998). Telomeres interact with the nuclear membrane by the proteins NDJ1, MPS3 (SUN domain protein), and CSM4 (Conrad et al. 1997; Conrad et al. 2007; Wanat et al. 2008).

Caenorhabditis elegans – a multifunctional model organism

C. elegans is a widely used model organism throughout molecular biology, developmental biology, and several other biological and medical fields. It is a small (~1 mm) and transparent nematode that was initially isolated from soil. The majority of *C. elegans* are self-fertilizing hermaphrodites with a low percentage of naturally occurring males (Kenyon 1988). Initial work on *C. elegans* started in the beginning of the 20th century after its initial isolation (Maupas 1900). Sydney Brenner proposed *C. elegans* as a model organism for neuronal development in the 1960's and started working on its molecular and developmental biology soon after (Brenner 1974). Due to its easy cultivation, short life cycle, and easy genetic manipulation, *C. elegans* has become a popular organism to study biological questions (Schafer 2005). It became the first metazoan organism to have its cell lineage fully traced (Sulston and Horvitz 1977; Kimble and Hirsh 1979; Sulston et al. 1983), meaning the developmental fate of all embryonic cells is known (Kretzschmar and Watt 2012). *C. elegans* was also the first multicellular organism to have its neuronal network fully mapped out (White et al. 1986; Cook et al. 2019) and its genome fully sequenced (The C. elegans Sequencing Consortium 1998).

In addition, some of the most important biological findings of the last century have been made using this model organism. One example are the genes that are responsible for apoptosis. They have been identified in *C. elegans* (Hedgecock et al. 1983; Ellis and Horvitz 1986; Yuan and Horvitz 1992; Yuan 1993) and were shown to be conserved in mammals (Adams 2003; Danial and Korsmeyer 2004). The discovery of RNA interference (RNAi), a widely conserved mechanism of transcript silencing, was made in *C. elegans* as well (Fire et al. 1991; Fire et al. 1998). Today, *C. elegans* is a widely used model organism, as several pathways in the nematode are conserved also in higher mammals (Kaletta and Hengartner 2006; Markaki and Tavernarakis 2010). Even medical studies such as nicotine dependence and identification of Alzheimer's related genes have been made using this model organism (Feng et al. 2006; Ewald and Li 2010).

Telomeres in *C. elegans*

In comparison to the mammalian, yeast, or *Drosophila* system, there is less known about telomeres and telomere biology in the nematode. The telomeric DNA structure in *C. elegans* is comparable to mammalian telomeres, and its repeat is a similar hexameric sequence with a one-basepair substitution, namely TTAGGC$_n$ (Wicky et al. 1996). As in other organisms, *C. elegans* telomeres contain a double-stranded region followed by a single-stranded 3' G-rich overhang (Raices et al. 2008). In addition, a 5' C-rich overhang similar to ALT like cells in mammals has been described (Raices et al. 2008; Oganesian and Karlseder 2011). Telomere length in *C. elegans* varies on average between 2 and 9 kb in the wild type strain N2 Bristol (Wicky et al. 1996; Raices et al. 2005). Nonetheless, it was reported that telomere length differs, sometimes extensively, between different isolates and even between different clonal lines and generations of the same strain (Cheung 2004; Raices et al. 2005; Lowden et al. 2008; Cook et al. 2016).

Regarding telomere binding proteins, no complex reminiscent of shelterin in mammals and *S. pombe* or the CST/RAP1 complexes in *S. cerevisiae* has been described to date, as all shelterin components lack obvious homologs in *C. elegans* (Raices et al. 2008). Bioinformatical structure search has revealed four proteins in the *C. elegans* genome that show structural homology to the DNA-binding OB-folds of human POT1 and *Oxytricha nova* TEBPα (Raices et al. 2008). Interestingly, all four proteins only harbor one instead of two OB-folds used for DNA binding in hPOT1 (Raices et al. 2008; Meier et al. 2009). Of the four proteins, named POT-1 (or CeOB2), POT-2 (or CeOB1), POT-3, and MRT-1 (MoRTal germline-1), only POT-1/-2 and MRT-1 have been shown to interact with the telomeric sequence of the nematode (Raices et al. 2008; Meier et al. 2009). POT-3 is not interacting with telomeric DNA or shown to have a telomeric effect when lost (Shtessel et al. 2013). POT-1, POT-2, and MRT-1 have been shown to bind to the telomeric sequence of *C. elegans in vitro*. POT-1 and POT-2 additionally were shown to bind

telomeres *in vivo* (Raices et al. 2008; Meier et al. 2009; Shtessel et al. 2013). All three proteins bind to the single-stranded telomeric overhangs (Fig. I5). Interestingly, POT-1 and POT-2 have a proposed strand specificity for either the 3' G-rich overhang (POT-2) or the 5' C-rich overhang (POT-1) (Raices et al. 2008; Meier et al. 2009). MRT-1 on the other hand was shown to bind both the single-stranded overhangs with equal preference and additionally general binding to single-stranded repeat DNA of other sequences has been observed (Meier et al. 2009). In addition to the single-strand binders, three potential double-strand telomere binders have been described. CEH-37, PLP-1 and HMG-5 were detected by immunoprecipitation experiments and to bind telomeric double-stranded DNA *in vitro* (Im and Lee 2003; Kim et al. 2003; Im and Lee 2005). Furthermore, HMG-5 and CEH-37 GFP fusion proteins localize to chromosome ends, CEH-37 in a cell cycle dependent manner, HMG-5 in a developmental manner (Im and Lee 2003; Kim et al. 2003). If this localization coincides with telomeres has not been further investigated, as no colocalization experiments were done. In contrast to telomere binders in mammalian cells and yeast, no interaction between the telomere binding proteins of *C. elegans* has been described so far.

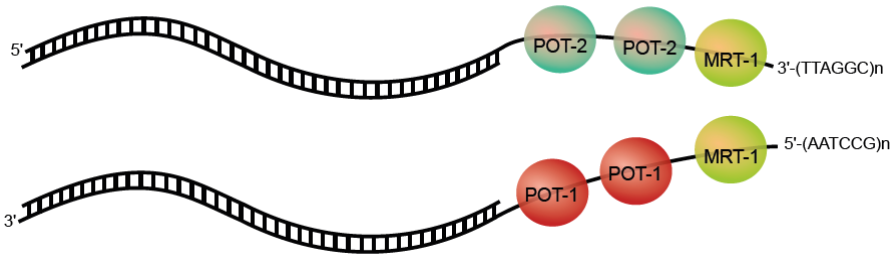

Figure I5: Schematic overview of the telosome in *C. elegans*. POT-1, POT-2, and MRT-1 have been shown to interact with the single-stranded telomeric sequence of the nematode. POT-1 and POT-2 interact with the C-rich or the G-rich strand, respectively. MRT-1 shows no strand preference (Raices et al., 2008, Meier et al., 2009). Telomeric DNA is depicted in black, proteins at their respective single-stranded overhang in different colored circles.

End protection in *C. elegans*

As described in the previous chapter, protection of telomeres by their structure and bound proteins is crucial for genome integrity. Interestingly, the somatic cells of a fully developed *C. elegans* are postmitotic, which means terminally differentiated and not dividing anymore. The DNA damage response in somatic cells is downregulated due to transcriptional repression and somatic cells do not activate ATM or ATR upon DNA damage (Vermezovic et al. 2012). Germline cells on the other hand are heavily dividing, as *C. elegans* possesses even more germ cells than somatic cells, divided in mitotic and meiotic regions (Hubbard and Greenstein 2005). In these cells protection of telomeres from DNA damage signaling and following repair is essential for propagation.

In contrast to mammals and yeasts, the implication of telomere binding proteins in the end protection of telomeres has not been as extensively studied in *C. elegans*. Loss of POT-1 or POT-2 does not lead to an activation of a DNA damage response in *C. elegans*. Mutants for one or both the homologs are viable and show an elongated telomere phenotype implicating them in telomere length maintenance. In addition, no change in fertility, implicating genome instability in the germline, could be determined (Raices et al. 2008; Cheng et al. 2012; Shtessel et al. 2013).

Loss of MRT-1 on the other hand leads to progressive telomere shortening and sterility over the course of several generations (Meier et al. 2009). This potentially implicates MRT-1 in telomere end-protection as its depletion leads to genome instability. Chromosome fusions are mainly mediated by HR in the germline of *C.elegans*, whereas NHEJ is more active in the soma (Lowden et al. 2008). An SNM1-like nuclease domain in MRT-1 shows relation to the SNM1 nucleases Apollo and Artemis, though nuclease activity of MRT-1 was only tested *in vitro* (Meier et al. 2009). Both Apollo and Artemis play a role in

telomere protection and maintenance in mammalian cells but in addition are a checkpoint for interstrand cross-links (ICLs) and DSBs (van Overbeek and de Lange 2006; Lam et al. 2010; Yasaei and Slijepcevic 2010). MRT-1 was not required for NHEJ or HR mediated DSB repair but facilitates interstrand-crosslink (ICL) repair together with the 9-1-1 complex of *C. elegans* (Meier et al. 2009).

Additional factors like the KU heterodimer and the WRN helicase have been implicated in end protection in mammals and yeast (Baumann and Cech 2000; Bertuch and Lundblad 2003; Rossi et al. 2010; Sfeir and de Lange 2012). Interestingly, mutants for both KU subunits did not lead to a telomere related phenotype such as a change in length or occurrence of chromosome fusions (Lowden et al. 2008). Mutation of the WRN-1 protein in *C. elegans* led to an accumulation of RPA and RAD-51 DNA damage markers (Ryu and Koo 2017). Telomere implication was not investigated in this study but a conserved role for WRN-1 in DNA damage response could also indicate an association with end-protection in *C. elegans*. So far, no shelterin-like proteins working in telomere end-protection have been identified in *C. elegans*.

Similar to mammalian cells, a potential second layer of telomere protection is telomeric DNA structure. The telomeres of *C. elegans* have been shown to form a t-loop structure with POT-1 and POT-2 binding at its base (Raices et al. 2008). In addition to looping, the single-stranded overhangs of *C. elegans* telomeres engage in specific fold back structures (Školáková et al. 2015).

Telomere length maintenance in *C. elegans*

Elongation of telomeres in *C. elegans* is carried out by telomerase. To date, only TRT-1, the catalytic subunit of telomerase has been identified (Malik et al. 2000; Meier et al. 2006). Interestingly, in comparison to telomerase catalytic subunits of other species, TRT-1 of *C. elegans* is shorter and lacks several motifs that are conserved in other telomerases (Malik et al. 2000). In agreement with the somatic cells of the organism being postmitotic, telomerase activity is only detected in isolated oocytes, reproductive-stage adults (germline), and during embryogenesis, as these are the only dividing cells that need telomere length maintenance (Hill et al. 2000; Baugh et al. 2003). As the RNA template and other components of *C. elegans* telomerase are not known, there is no knowledge about the exact mechanism of telomere repeat addition and procession in this organism. Due to its structurally different catalytic subunit the mechanism could differ from what is known in mammalian cells and yeast.

Telomere length in dividing cells of telomerase-negative worms shortens in a range that is more similar to *S. cerevisiae* than to mammals (Cheung 2006). In addition, the general fitness of *trt-1* mutants is decreased, and they become sterile after propagation for several generations (Cheung 2006; Meier et al. 2006). The sterility is due to progressive telomere shortening and subsequent chromosome fusions in the germline, which lead to genome instability and a decrease in viable offspring (Cheung 2006; Meier et al. 2006; Lackner et al. 2012). Similar phenotypes have been described for the mutants of the telomere protein MRT-1 and the 9-1-1 DNA damage checkpoint proteins MRT-2, HUS-1 and HRP-17 (Ahmed and Hodgkin 2000; Hofmann et al. 2002; Boerckel et al. 2007; Meier et al. 2009). The 9-1-1 complex and its clamp loader (HRP-17 in *C. elegans*) have been described to interact with telomeres in mammals and yeast and their loss leads to short telomeres and in mammals additionally to inviability (Francia et al. 2006; Verdun and Karlseder 2006; Holstein et al. 2017). Therefore, it seems that in *C. elegans* the 9-1-1 complex and MRT-1 work together to facilitate telomerase-mediated repeat addition. POT-1 and POT-2 on the other hand work in repression of telomerase, as mutants for both proteins show an elongated telomere phenotype (Raices et al. 2008; Shtessel et al. 2013). As there was no additive effect detected in a double mutant, both proteins are thought to share a common function in telomerease inhibition (Shtessel et al. 2013).

Though telomerase seems to be the default mechanism for telomere length maintenance in *C. elegans*, other maintenance pathways have been described. These other pathways resemble the previously described ALT pathway, elongation of telomeres by recombination. Mutation of the telomere binding protein POT-1 for example leads to much more heterogeneous telomere lengths as mutation of its

paralog POT-2, and is therefore proposed to inhibit recombination events at telomeres in the wild-type state (Raices et al. 2008). In addition to long, heterogeneous telomeres, an increase in telomeric C-circles, a marker of ALT, has been described in POT-1 mutants. Interestingly, C-circles have also been detected in wild-type *C. elegans* without mutation in POT-1 (Lackner et al. 2012). POT-2 on the other hand has been implicated in the inhibition of a specific ALT pathway that maintains shorter telomeres in the absence of telomerase or the 9-1-1 complex (Cheng et al. 2012). A proposed ALT pathway in *C. elegans* utilizes a subtelomeric sequence as template for ALT (TALT) (Seo et al. 2015). This TALT contains a unique sequence flanked by canonical and variant telomeric repeats that is duplicated in cis from a chromosomal location to one specific subtelomeric region. From this subtelomeric region, TALT is duplicated to the ends of other chromosomes by an HR mediated mechanism. It is proposed that inclusion of TALT and thereby variant repeats in telomeres could lead to recruitment of different telomere binders to stabilize chromosomes (Seo et al. 2015). This is in line with the knowledge that the variant repeats at telomeres in mammalian ALT cells recruit factors that suppress NHEJ to prevent chromosome fusions but promote HR to maintain telomeres via ALT (O'Sullivan and Almouzni 2014).

Telomeres and longevity

The first gene mutation to enhance lifespan of a multicellular organism was detected in *C. elegans*, the gene *age-1* (Klass 1983; Johnson and Friedman 1988). *C. elegans* is used in several aging studies, for example the involvement of nutrient restriction on lifespan, as the insulin/IGF-1 pathway is conserved up to mammals (Gems and Partridge 2013). It is known that several factors such as temperature, oxygenation, and food can have effects on the worm lifespan (Klass 1977; Honda et al. 1993). In addition, mutations in single genes as for example members of the insulin/IGF-1 pathway (*daf-2*, *daf-16*), the clock family (*clk-1*, *clk-2, clk-3, gro-1*), or ATL-1 (*C. elegans* ATR), have been shown to influence lifespan as well (Lakowski and Hekimi 1996; Bénard and Hekimi 2002; Raices et al. 2005; Suetomi et al. 2013).

Telomeres are one factor implicated in organismal senescence or aging (López-Otín et al. 2013). Lifespan of a wild-type N2 Bristol worm fluctuates between 12 and 18 days at 20°C (Klass 1977). As the somatic cells of the worm are postmitotic, there is no shortening of telomeres due to cell divisions, which would result in senescent cells. Contrary, the germline has mitotic and meiotic cell divisions, and damage signals induced by telomere dysfunction could influence the aging process. If the telomeres of *C. elegans* have an impact on organismal lifespan is a topic of controversy. In a study where HRP-1, the *C. elegans* sequence homolog of hnRNP A1 in humans or GBP2 in *S. cerevisiae*, was overexpressed, an elongation of telomeres as well as an increase in lifespan was detected (Joeng et al. 2004). The authors attributed the increased lifespan to the elongation of telomeres, as the worms had no other phenotypes and lifespan was assessed after the worms had lost the extrachromosomal array used for overexpression (Joeng et al. 2004). On the other hand, there are several studies stating no apparent correlation between telomere length and lifespan. Lim et al. investigated telomere length in *clk-2* mutants. CLK-2 is the homolog of yeast TEL2, a regulator of telomere length. Mutants for CLK-2 exhibit longer lifespan than wild-type worms but were found to have shorter telomeres (Lakowski and Hekimi 1996; Lim et al. 2001). In addition, mutations of DAF-2 or DAF-16 of the insulin/IGF-1 pathway increase or decrease lifespan respectively but show no difference in telomere length (Raices et al. 2005). Mutants with impairments in telomere maintenance and therefore short telomeres like *mrt-1*, *mrt-2*, and *trt-1* show no decreased lifespan, compared to the wild-type (Ahmed and Hodgkin 2000; Meier et al. 2006; Meier et al. 2009). The majority of these studies indicate thereby that there is no correlation between telomere length and organismal aging/lifespan in *C. elegans* (Bénard and Hekimi 2002; Raices et al. 2005).

Telomeres and fertility

As described above, telomeres seem to not have an influence on organismal lifespan in *C. elegans*. The transgenerational lifespan on the other hand is influenced by telomere length. Mutants that show shortening of telomeres due to telomere maintenance difficulties have been shown to become sterile after several generations with a decrease in progeny numbers along the way (Ahmed and Hodgkin 2000; Meier et al. 2006; Meier et al. 2009). This has been attributed to the accumulation of DNA damage in the germline, such as for example chromosome fusions (Ahmed and Hodgkin 2000). HR, the primary DSB repair pathway in the germline (Lowden et al. 2008), mediates these chromosome fusions. Interestingly, the holocentric nature of *C. elegans* chromosomes makes it possible that some chromosome fusions can be maintained and animals carrying fusions can kept as stable lines (Lowden et al. 2008).

In mammalian cells and yeast, telomeres are attached to the nuclear membrane during meiosis prophase to facilitate chromosome movement and homologous pairing (Chikashige et al. 1994; Rockmill and Roeder 1998; Hiraoka and Dernburg 2009). This is not the case in *C. elegans*, where specific sequences close to chromosome ends, the so-called pairing centers (PCs), are recruited to the nuclear membrane to aid in homologous pairing (MacQueen et al. 2005). Though they are close to telomeres on the chromosomes, this proximity is not essential for proper chromosome segregation (MacQueen et al. 2005). For this reason, meiotic pairing in *C. elegans* does not share the classical “telomere bouquet” formation. The PCs are interacting with zinc finger proteins that are specific for one or two chromosomes and anchor them to the INM by the SUN domain protein SUN-1 (Phillips and Dernburg 2006; Penkner et al. 2007). Interestingly, telomeres have been found to be tethered to the nuclear membrane by SUN-1 during embryogenesis and development. POT-1 interaction with SUN-1 mediates this attachment during embryogenesis but is not needed in postmitotic cells (Ferreira *et al.*, 2013). As telomeric proximity to the nuclear membrane has been observed in many organisms, this mechanism of nuclear organization is conserved over a broad range of organisms.

Rationale

As described in this introduction, telomeres are essential for genome stability and integrity in many different ways. Importantly, proteins that bind the telomeric sequence are indispensable for protection and maintenance of telomeres. Therefore, a thorough understanding of telomere biology, including structures, proteins, interacting factors, and their pathways is fundamental. Model organisms give a good overview of telomeric pathways and given the conserved nature of some of the interactions between telomeric factors of single-cell and multi-cellular organisms. We can use model organisms to search for and investigate telomere-associated factors. Some newly detected factors could potentially be implicated in human disease or aging in the future.

In this work, we aimed to investigate the telomere interactome (telosome) of *C. elegans*. Not many telomere binding proteins in this organism are known and no shelterin-like complex aiding in protection from DNA damage has been described. For this reason, we wanted to identify new factors at *C. elegans* telomeres and characterize their function in telomere biology. To do so, we used quantitative proteomics, which has proven to be a powerful tool in identification of telomeric factors in different model organisms and biological conditions (Scheibe et al. 2013; Jahn, Rane, Paszkowski-Rogacz, Sayols, Bluhm, Chung-Ting Han, et al. 2017; Li et al. 2017; Pérez-Martínez et al. 2020). Identification and characterization of novel telomere factors may provide further insight into telomere biology in *C. elegans*, especially in the context of postmitotic versus dividing tissue. In addition, we may be able to describe interactions between telomeric factors in this organism that have not been uncovered before.

Results

Identification of novel telomere associated factors in *C. elegans*

Screening for interactors with quantitative proteomics

To investigate the telosome of *C. elegans*, we performed DNA pulldowns coupled to quantitative proteomics approaches to identify novel proteins binding to the telomeric sequence. Similar experiments have been successfully used before to identify telomere-associated proteins in other species (Casas-Vila et al. 2015; Kappei et al. 2017). In brief, biotinylated and concatenated oligonucleotides carrying the *C. elegans* telomeric sequence or a scrambled control sequence were incubated with nuclear extract from gravid adult worms and enrichment of proteins determined with two different quantitative proteomics approaches: label-free quantitation (LFQ) (Cox et al. 2014) and reductive dimethyl labeling (DML) (Hsu et al. 2003). Following mass spectrometry (MS) measurement and bioinformatic analysis, we were able to identify 13 and 12 significantly enriched proteins at the telomeric sequence in LFQ and DML (Fig. 1 A/B), respectively.

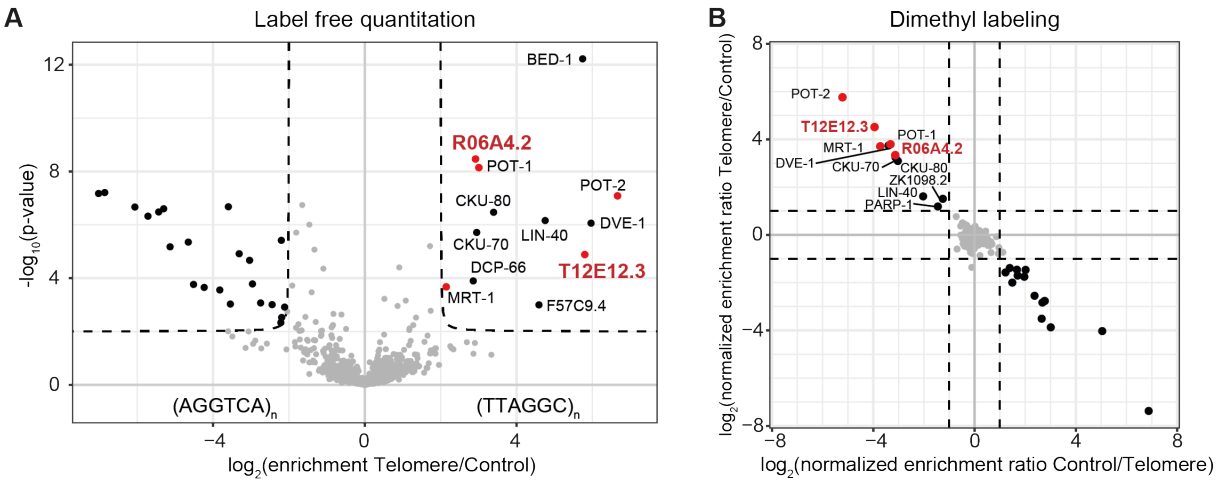

Figure 1: Quantitative proteomics screen for novel telomere binders in *C. elegans*. (A) Volcano plot depicting result of the LFQ experiment. Identified proteins are marked as individual dots in accordance to their respective $\log_2$ enrichment fold-change (x-axis) and $-\log_{10}$ p-value (y-axis). Grey dots are background binders, black dots are proteins enriched above the set threshold (4-fold enrichment, p-value ≤ 0.05), and red dots depict proteins of interest. (B) Scatterplot showing the result of the DML experiment. Identified proteins are marked as individual dots according to their calculated intensity ratio in the forward (y-axis) and reverse experiment (x-axis), respectively. Color of dots according to (A) with a threshold at 2-fold enrichment for both forward and reverse experiment.

Both approaches overlap in nine proteins, three of which are the previously described single strand telomere binders of *C. elegans*, POT-1, POT-2 and MRT-1 (Raices et al. 2008; Meier et al. 2009). We took detection of these proteins as validation of our experimental approaches. In addition to the known single-strand binders, the DNA repair heterodimer CKU-70/CKU-80 was enriched in both screens (Lowden et al. 2008). Furthermore, four additional proteins not previously implicated in telomere biology were significantly enriched on the telomeric sequence in both screens. From these proteins, we chose to characterize R06A4.2 and T12E12.3 in this study.

R06A4.2 and T12E12.3 are paralog genes in *C. elegans*

We picked R06A4.2 and T12E12.3 to continue in this study because these proteins were previously not characterized and therefore had no implication in *C. elegans* telomere biology. Interestingly, pairwise global alignment with EMBOSS Needle (Madeira et al. 2019) showed that they share 74.3% nucleotide sequence identity (Fig. 2 A) and 65.4% amino acid sequence identity. This suggests that these proteins are potentially paralogs in the *C. elegans* genome. Since no domain predictions were available for either of the proteins, we utilized bioinformatic homology structure prediction by HHPred (Zimmermann et al. 2018). The software predicted similarity to known protein structures close to the N-terminus in both proteins. Structural similarities were predicted to a homeodomain, as found for the DNA binding motif of *S. cerevisiae* RAP1, as well as Myb-domain Helix-turn-helix motifs found in human RAP1, the TRF2-interacting protein (Fig 2 B). This suggested that R06A4.2 and T12E12.3 could be able to bind to telomeric DNA directly.

A

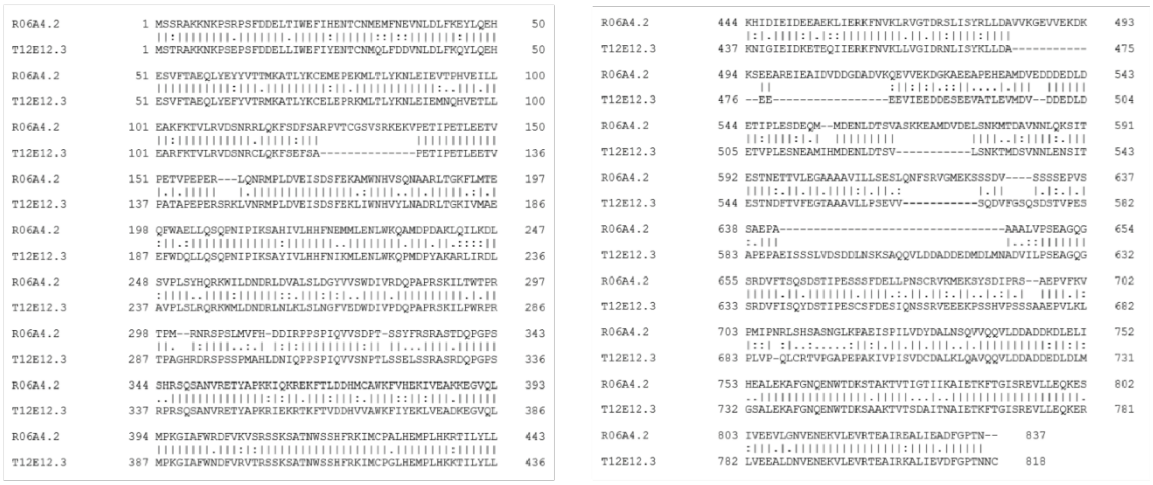

B

Protein	Structure	Probability	E-value	p-value	location (aa)
R06A4.2	helix-turn-helix hRAP1	96.8%	0.0028	5.5E-08	364-427
	helix-turn-helix hRAP1	94.1%	0.22	4.2E-06	10-69
	homeodomain scRAP1	93.8%	1.9	3.8E-05	3-229
	helix-turn-helix hRAP1	93.6%	0.3	5.9E-06	166-228
	homeodomain scRAP1	89.9%	7	0.00014	163-428
T12E12.3	helix-turn-helix hRAP1	96.8%	0.0039	7.6E-08	357-420
	helix-turn-helix hRAP1	95.03%	0.11	2.2E-06	9-69
	helix-turn-helix hRAP1	92.95%	0.36	7.1E-06	158-217
	homeodomain scRAP1	91.05%	5.7	0.00011	4-218
	homeodomain scRAP1	90%	7.7	0.00015	150-421

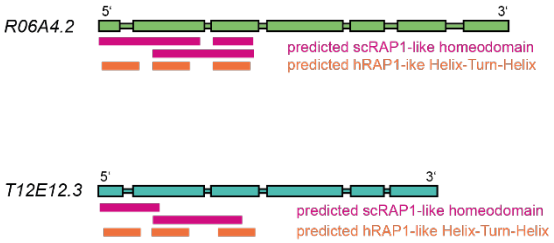

Figure 2: Protein alignment and domain search for R06A4.2 and T12E12.3 (A) Pairwise alignment of aminoacid sequences for both proteins via EMBOSS Needle. (|) identical residue (.) conserved change, similar residue (:) part of residue is similar but not strongly conserved. (B) HHPred results for structure similarity search in protein sequence of R06A4.2 and T12E12.3. Predicted similar structures are presented in the table along probability, E-value, p-value and respective location in the template proteins, respectively. Scheme of the respective gene is given with the location of the predicted structures indicated. hRAP1 – human RAP1 protein; scRAP1 – *S. cerevisiae* RAP1 protein.

Interaction with the telomeric sequence *in vitro*

We cannot exclude that proteins identified and enriched in our MS approaches are enriched because of protein-protein interactions and are thereby not actually binding to the telomeric sequence. Therefore we asked if our candidate proteins are indeed directly interacting with DNA, as their N-termini showed structural similarities to a known DNA binder, scRAP1. To determine the interaction with telomeric DNA, we cloned our candidate proteins into bacterial expression vectors and expressed them recombinantly

in *E. coli*. In addition to R06A4.2 and T12E12.3, we expressed POT-2 as control, as it is known to bind telomeric DNA (Raices et al. 2008). With the *E. coli* lysate, we repeated the previously mentioned DNA pulldown experiments (see Fig. 1 A/B), this time followed by western blot to determine enrichment on the telomere or the control sequence. Interestingly, with an N-terminal His_6-tag, R06A4.2 did bind both DNA templates equally well, while T12E12.3 did not bind to telomeric or control DNA (Fig. 3 A). We thought that the N-terminal tags might interfere with the predicted DNA-binding sites, so we re-cloned the expression plasmids to obtain C-terminally tagged proteins. With these proteins, we could detect binding of both proteins preferentially to the telomeric DNA (Fig. 3 B). This observation indicates the potential interference with the predicted DNA-binding domains at the N-terminus of both proteins (Fig. 2 B).

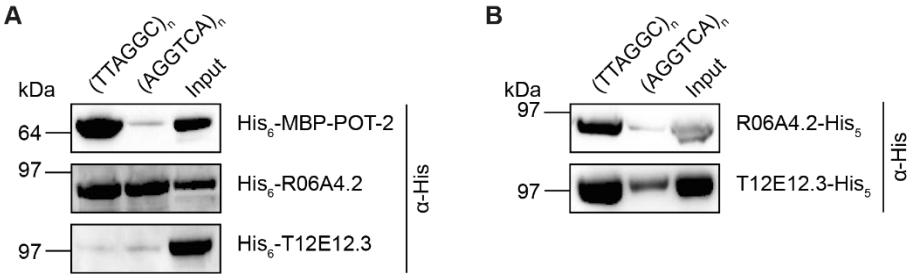

Figure 3: R06A4.2 and T12E12.3 interact with telomeric DNA. (A) Pulldown with recombinantly expressed, N-terminally tagged R06A4.2 and T12E12.3. DNA as experiment for Fig. 1. Western blot signal after incubation with anti-His-antibody. His_6-MBP-POT-2 was used as positive control for binding. (B) Repeat of pulldown experiment with C-terminally tagged R06A4.2 and T12E12.3. Western blot like (A).

For the calculation of binding affinity by equilibrium dissociation constants (K_d) and investigating the preference for single- or double-stranded DNA, we wanted to establish Electrophoretic Mobility Shift Assay (EMSA) with purified protein. As an initial test, we used the single strand binder POT-2 which is known to bind the G-rich single strand of *C. elegans* telomeres (Raices et al. 2008). In this trial experiment, we could determine a shift of protein with the supplied single-stranded $TTAGGC_3$ oligonucleotide (Fig 4 A). When we repeated this experiment with purified R06A4.2-His_5, we could not determine a shift in either single- or double-stranded conditions (Fig 4 B). Several repetitions of the assay under different conditions did not produce a positive result.

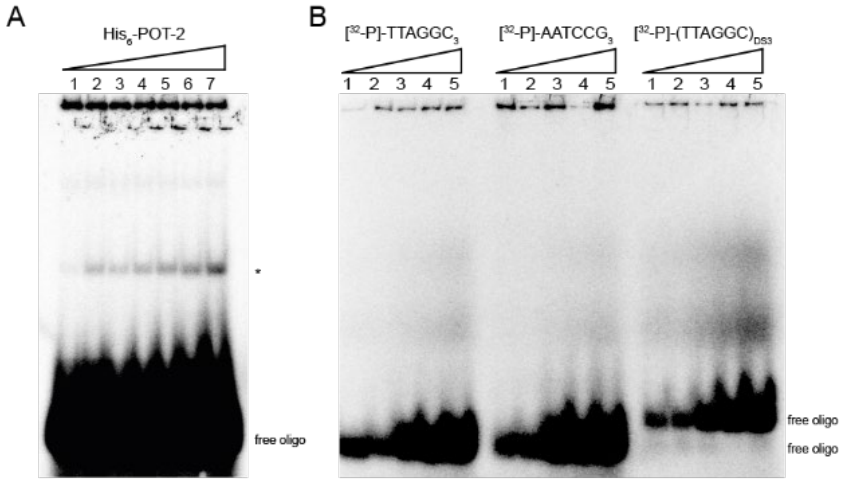

Figure 4: Interaction of candidate proteins with DNA. (A) EMSA with His_6-POT-2 in increasing concentrations of protein and constant 1.25 pmol [^{32}P]-labeled $TTAGGC_3$ oligonucleotide. Shift of protein with oligonucleotide marked with asterisk, free oligonucleotide indicated. Concentrations of protein: (1) 0.5 pmol, (2) 1 pmol, (3) 2 pmol, (4) 2.5 pmol, (5) 5 pmol, (6) 7.6 pmol, (7) 10 pmol. (B) EMSA with R06A4.2- His_5 with increasing concentrations of [^{32}P]-labeled oligonucleotides of single-stranded $TTAGGC_3$ or $AATCCG_3$ as well as double stranded $TTAGGC_3$ and constant protein concentration of 5 pmol. Free oligonucleotide is indicated. Concentrations of oligonucleotide for all three sets: (1) 125 fmol, no protein, (2) 125 fmol, (3) 250 fmol, (4) 375 fmol, (5) 500 fmol.

When we attempted to purify higher amounts of the C-terminally tagged constructs, it became apparent that R06A4.2 and T12E12.3 were aggregating in solution in our previously used purification conditions. After further improving protein expression and purification to gain more soluble protein, we were able to use fluorescence polarization (FP) to determine K_d values for our proteins. For this, either R06A4.2-His_5 or T12E12.3-His_5 were incubated with oligonucleotides carrying a fluorescein isothiocyanate (FITC) fluorescent label. Measurements were performed with double-stranded as well as single-stranded telomeric and control DNA containing a 2.5x repeat and varying concentrations of protein. Both R06A4.2 and T12E12.3 showed preferential interaction with the double-stranded telomere sequence over the other provided sequences (Fig. 5 A/B). Calculation of K_d values showed an affinity to the telomeric double-strand in the nanomolar range for both the proteins. Comparing both proteins, T12E12.3 displayed an even higher affinity for the double-stranded telomeric sequence with a K_d of 37.84 nM, over R06A4.2 with a K_d of 128.7 nM. Therefore, we conclude that we were able to identify two novel proteins associating with the *C. elegans* telomeric sequence directly *in vitro*.

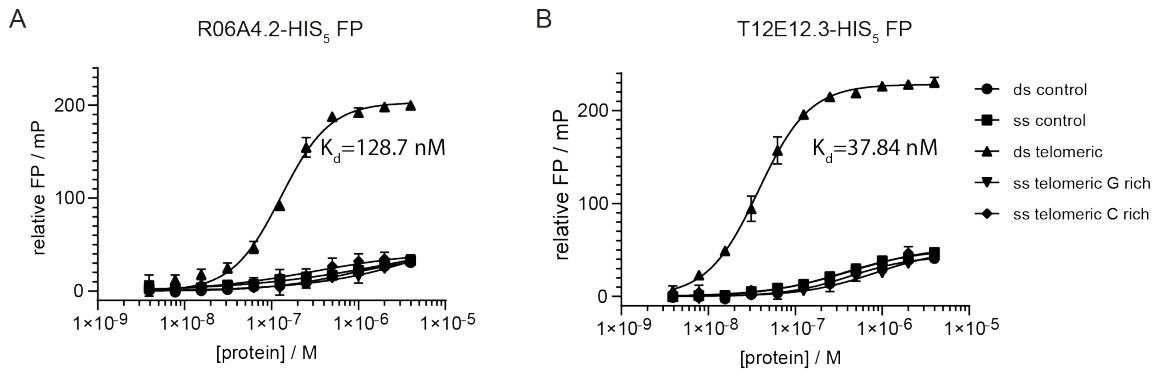

Figure 5: Fluorescence polarization assays to determine single- or double-strand binding preference. (A) FP assay for R06A4.2-His_5 using 2.5x repeat oligonucleotides as indicated in the legend. 20 nM f.c FITC-labeled oligonucleotides were incubated with protein in two-fold serial dilution from 4 µM to 4 nM. K_d calculated by Hill Slope fitting. (B) FP assay as in (A) but with T12E12.3-His_5. mP: millipolarization.

Study of R06A4.2 and T12E12.3 on organismal level in *C. elegans*

Creation of CRISPR mutants and tagged strains

To be able to characterize the candidate proteins on an organismal level, we created mutants and endogenously tagged versions of R06A4.2 and T12E12.3 via CRISPR/Cas9 genome editing. The endogenous genes were either disrupted using two guide RNAs creating an out-of-frame deletion with premature stop codons or endogenously tagged by insertion of a C-terminal GFP- and/or 3xFLAG-tag (Fig. 6).

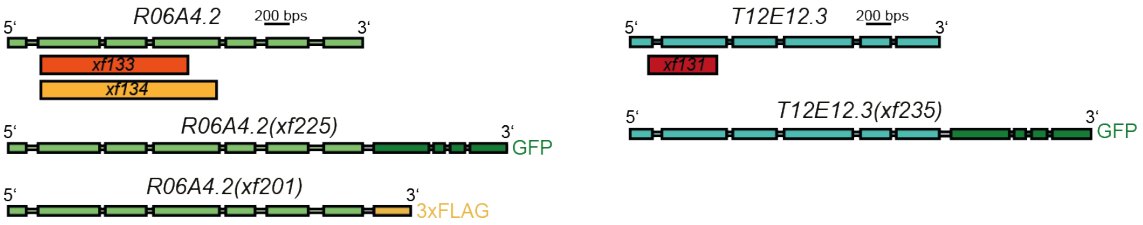

Figure 6: Gene overview schemes for deletion mutants and endogenous tags of R06A4.2 and T12E12.3. Sizes of the CRISPR deletions as well as location of the tag is indicated for both proteins. (CRISPR/Cas9 genome editing done by Dr. Miguel Almeida, previously Ketting and Butter lab, IMB, for the deletions and Jan Schreier, Ketting lab, IMB for the endogenous tags)

R06A4.2 and T12E12.3 are expressed throughout development

To examine expression of R06A4.2 and T12E12.3 throughout the development of *C. elegans*, we prepared extracts of each developmental stage of a double-transgenic strain expressing both R06A4.2::3xFLAG and T12E12.3::GFP. Detection by western blot showed presence of both the proteins throughout *C. elegans* development. Highest protein levels were detected in young adult worms, embryos, and L1/L2 stages, with a drop in the larval stages L3 and L4 (Fig. 7).

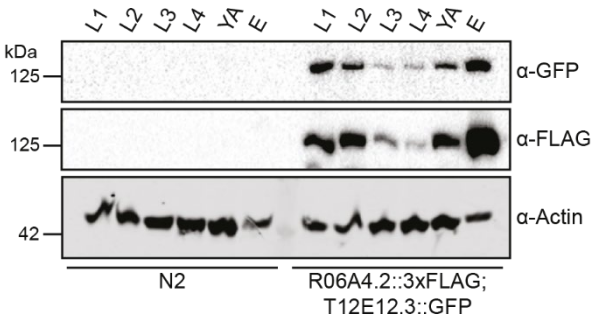

Figure 7: Expression of tagged R06A4.2 and T12E12.3 during development of *C. elegans*. 35 µg complete extract of developmental stages of wild-type (N2) and double transgenic strain were loaded as indicated. Western blot signal shown after incubation with α-GFP and α-FLAG antibodies, respectively. Actin was used as loading control. kDa: kilodalton

R06A4.2 and T12E12.3 localize to telomeric DNA in vitro and to telomeres in vivo

We asked, whether the interaction of R06A4.2 and T12E12.3 with telomeric DNA could be confirmed with endogenous proteins from *C. elegans*. Therefore, we repeated the aforementioned *in vitro* DNA pulldown with embryonic extract from the GFP- and FLAG-tagged strains. The western blot readouts of these experiments confirmed the interaction of the endogenous *C. elegans* proteins with the telomeric sequence (Fig. 8 A/B). Additionally, when providing single- or double-stranded 5x repeat telomere or control DNA, both proteins showed enrichment on the double-stranded telomere repeat (Fig. 8 C/D).

Thus, we were able to confirm *in vitro* association to the telomeric double-stranded DNA with endogenous *C. elegans* proteins.

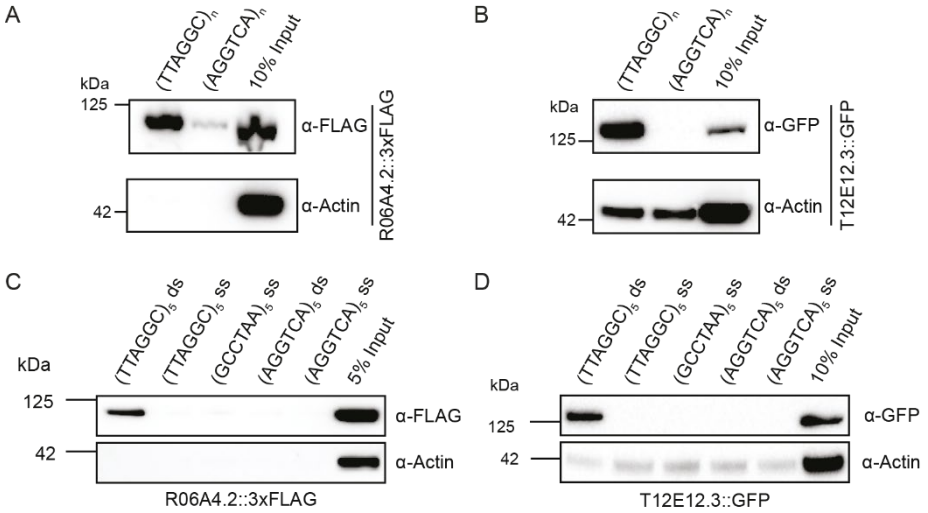

Figure 8: Interaction of tagged R06A4.2 and T12E12.3 with telomeric DNA. (A) DNA pulldown as in Fig. 3 with complete extract from embryos of R06A4.2::3xFLAG strain. Western blot after incubation with α-FLAG antibody. Actin was used as loading control. (B) DNA pulldown as in (A) with embryonic extract from T12E12.3::GFP strain and incubation with α-GFP antibody. (C) DNA pulldown with single- and double-stranded oligonucleotides with 5x telomeric or control repeats as indicated and embryonic extract from R06A4.2::3xFLAG strain. Western blot signal after incubation with α-FLAG antibody. Actin was used as loading control. (D) DNA pulldown as in (C) but with extract from T12E12.3::GFP strain and incubation with α-GFP antibody. ds: double-strand, ss: single-strand, kDa: kilodalton

To localize the tagged proteins to telomeres *in vivo* we employed fluorescence microscopy. Fixation and DAPI staining of worms carrying either R06A4.2::GFP or T12E12.3::GFP demonstrated that both proteins were localizing to nuclear foci (Fig. 9 A/B). These nuclear foci could be determined in several cell types of the worm, though signal in the excised germline and embryos was primarily better to image due to auto-fluorescence of the animals. To confirm telomere localization *in vivo*, we performed a cross of both GFP-tagged strains with a POT-1::mCherry transgenic strain. This transgenic strain had previously been used for telomere detection and quantification (Shtessel et al. 2013). Using double homozygous strains expressing both tagged proteins, we were able to colocalize R06A4.2::GFP or T12E12.3::GFP with POT-1::mCherry, respectively (Fig. 9 C-F). Due to the germline specific expression of the POT-1::mCherry transgene we could not colocalize R06A4.2 and T12E12.3 with telomeres in cell types other than proliferating germline cells and embryos. In conclusion, both R06A4.2 and T12E12.3 are associated to the telomere *in vivo* and *in vitro* as confirmed by DNA pulldowns and localization microscopy.

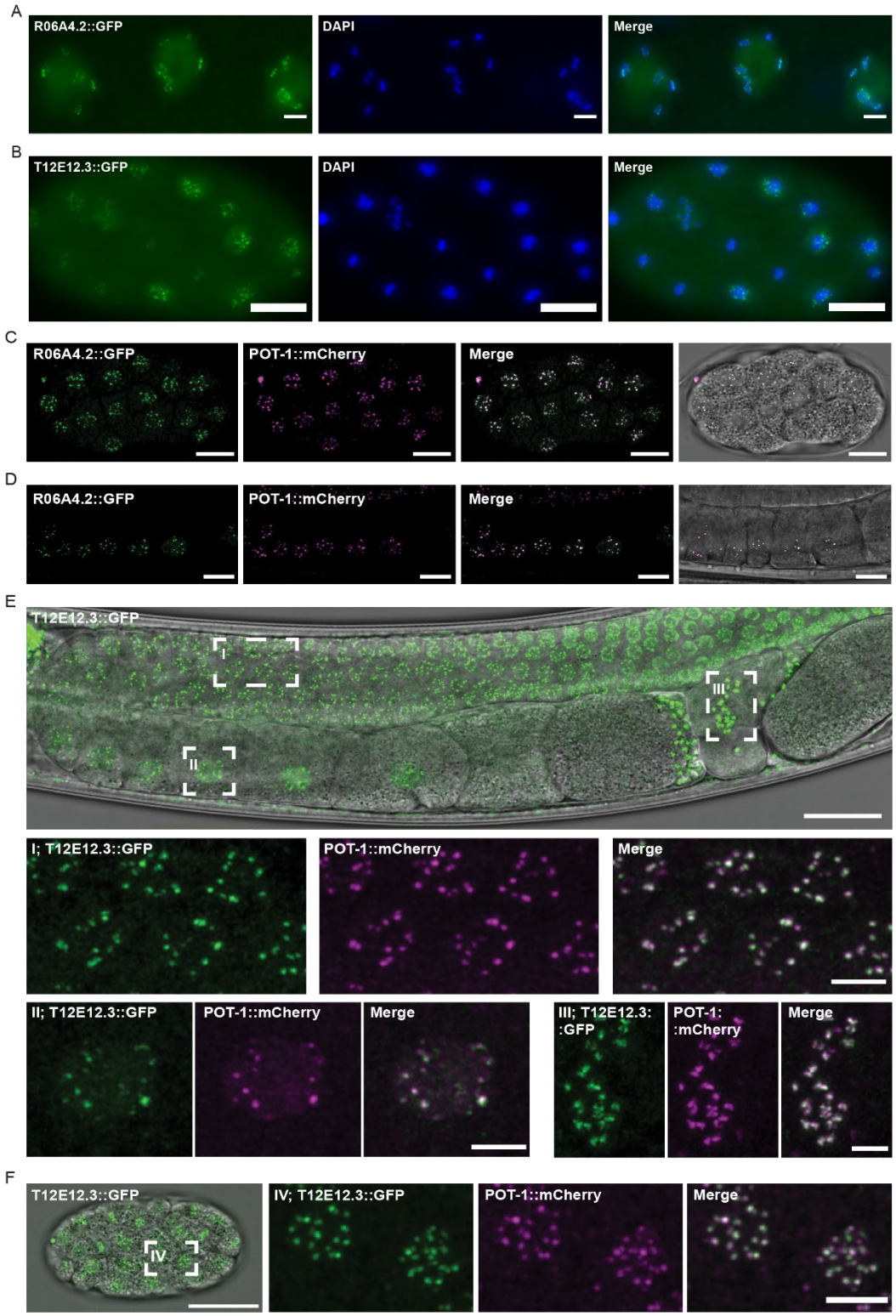

Figure 9: Localization of R06A4.2::GFP and T12E12.3::GFP using microscopy. (A) Maximum intensity projection of widefield z-stacks of oocytes from a fixed gravid adult worm expressing R06A4.2::GFP. DNA is stained with DAPI. Scale bar, 5 µm. (B) As in (A) but image of fixed embyro expressing T12E12.3::GFP. Scale bar, 10 µm. (C) Maximum intensity projection of confocal z-stacks of embryo expressing R06A4.2::GFP and POT-1::mCherry. Scale bar, 10 µm. (D) As in (C) but image of oocytes in an adult germline. Scale bar, 10 µm. (E) Maximum intensity projection of confocal z-stacks of adult germline expressing T12E12.3::GFP and POT-1::mCherry. Scale bar, 20 µm. Insets: (I) meiotic germ cell nuclei, (II) oocyte, (III) spermatozoa, scale bar, 4 µm. (F) As in (E) but image of an embryo. Scale bar, 20 µm. Inset: (IV) embryonic cells, scale bar, 4 µm. Confocal images were deconvoluted with Huygens.

R06A4.2 and T12E12.3 show opposite telomere phenotypes when mutated

Upon first examination, both T12E12.3 and R06A4.2 mutants did not show an immediate defect or visible phenotype. We compared brood size between the mutants and the *C. elegans* wild-type (N2) at 20°C and 25°C to determine potential differences in fertility. In both setups, we could not determine a significant difference in progeny numbers between the strains (Fig. 10A/B). Additionally, a created MosSCI rescue strain carrying a T12E12.3::GFP transgene in the *T12E12.3(xf131)* background did not affect fertility positively or negatively as well. This indicates that depletion of R06A4.2 or T12E12.3 does not have an immediate effect on fertility in the animals.

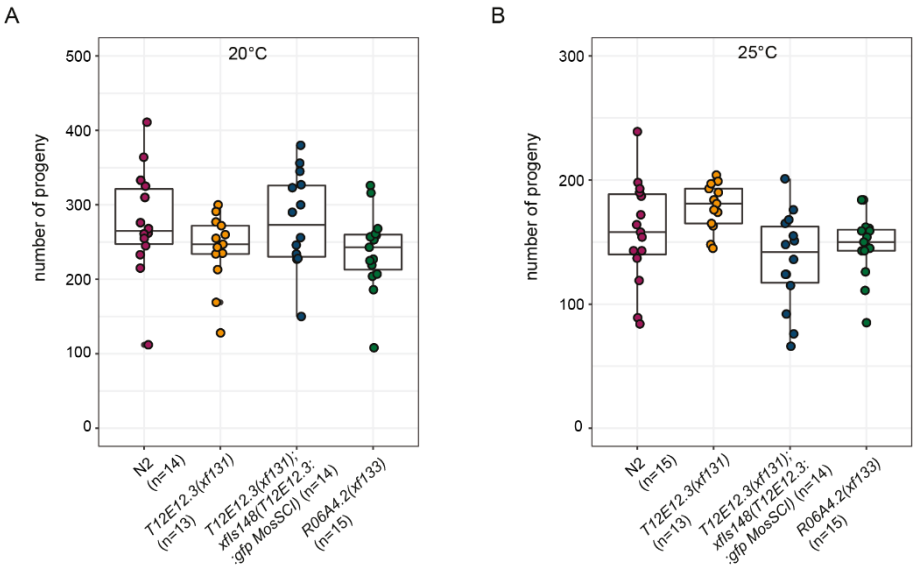

Figure 10: Single mutants of R06A4.2 and T12E12.3 do not show fertility defect. (A) Boxplot depicting brood sizes of the indicated strains at 20°C. The middle horizontal line of each box represents the median, while bottom and top lines represent the 25th or 75th percentile. n is indicated on the x-axis with the respective strain. (B) As in (A) but brood size assay was performed at 25°C. No significant difference to wild-type N2 could be determined with Wilcoxon and Mann-Whitney tests, p-values > 0.05.

Next, we wanted to address whether the mutants had a potential telomere length phenotype as it is known from mutants of the single-strand binders POT-1, POT-2, and MRT-1 (Raices et al. 2008; Meier et al. 2009). Telomere Southern blot from genomic DNA of mixed stage worms strikingly revealed an opposing telomere length phenotype for *R06A4.2(xf133)* and *T12E12.3(xf131)*. While the R06A4.2 mutant displayed an elongated telomere phenotype, the T12E12.3 mutant showed shortened telomeres when compared to wild-type (Fig. 11 A). This initial observation was confirmed by quantitative fluorescence in-situ hybridization (qFISH) with a telomeric PNA probe in dissected adult germlines and embryos (Fig. 11 B-K). In addition, we wanted to follow the progression of the telomere length phenotype over two separate time points to see potential changes in the phenotype. For this we compared qFISH signals from mutants propagated for one (generations F118/F126) or two years (generations F280/F288) to a wild-type set. Here we saw an additional increase in telomere length for *R06A4.2(xf133)*, while the length for *T12E12.3(xf131)* mutants became closer to the length of the used wild-type control (Fig. 11 F/K). Taken together, these proteins may share high similarity in sequence, but they seem to be involved in separate telomere length regulation pathways, whose disruption causes the observed opposite phenotypes. Interestingly, mutations of the previously described single-strand binders leads to opposing phenotypes as well. While mutation of POT-1 or POT-2 results in an elongated telomere phenotype, mutation of MRT-1 leads to shortened telomeres and a mortal germline phenotype caused by genome instability (Raices et al. 2008; Meier et al. 2009).

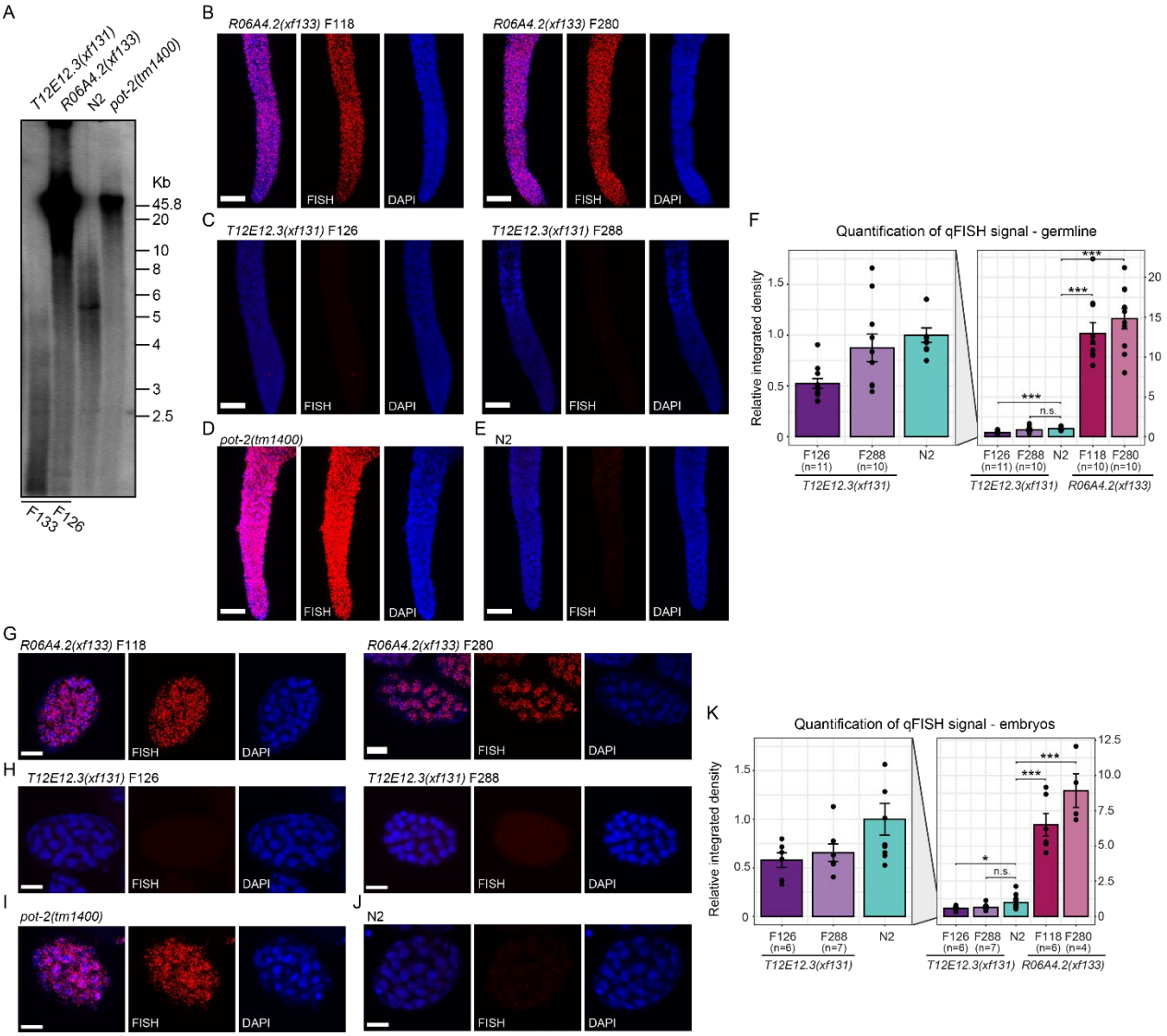

Figure 11: *R06A4.2(xf133)* and *T12E12.3(xf131)* show a telomere length phenotype. (A) Telomere restriction fragment Southern blot of mutant strains as indicated. N2 and *pot-2(tm1400)* were used as controls. Membrane signal detected after incubation with radiolabeled $GCCTAA_3$ probe. Marker lanes as well as approximate generation times for *R06A4.2(xf133)* and *T12E12.3(xf131)* are indicated next to and below the blot, respectively. (B-E) qFISH assay for telomere length determination in adult germlines. Strains used as indicated: *R06A4.2(xf133)*, *T12E12.3(xf131)*, pot-2(tm1400), and N2. Representative maximum projection z-stacks of all strains are depicted. Dissected germlines were incubated with telomeric PNA-FISH probe and DNA stained with DAPI. For R06A4.2(xf133) and T12E12.3(xf131) two generation snapshots were analysed. Approximate generation times and strains indicated above the pictures. Scale bars, 15 µm. (F) Analysis of qFISH images depicted in a bar plot. Strains used as in (B-E) with exception of *pot-2(tm1400)*. Relative integrated density is used as arbitrary unit to show average telomere length on the y-axis. Wild-type N2 is set to 1. Left-hand plot is a zoom in on the T12E12.3 values compared to wild-type. Generation times, n, and strains are indicated on the x-axis. Significant differences calculated by two-sided t-test are indicated by asterisks where * = p-value ≤0.05, *** = p-value ≤ 0.001, n.s. = not significant. (G-J) Maximum projections of qFISH assay as in (B-E) but for embryos of the respective strains. Scale bars, 10 µm. (K) Analysis of qFISH images as in (F) for embryos.

Double mutation of R06A4.2 and T12E12.3 leads to synthetic sterility

The opposite telomeric phenotypes of the candidate proteins made us curious to see the effect of a double mutant. Therefore, we wanted to create a strain carrying both the mutations for R06A4.2 and T12E12.3 by crossing. Interestingly, when crossing *R06A4.2(xf133)* and *T12E12.3(xf131)*, a double homozygous strain could not be established due to an immediate synthetic sterility phenotype. From the 127 isolated F2 worms of the first cross, eight were homozygous for both mutations. Out of these eight worms, seven were sterile, while one was semi-fertile, siring 13 progeny. From these 13 progeny we obtained eight sterile F3 worms, the rest were subfertile (Fig. 12 A). Repetition of the cross with another mutant allele for R06A4.2, *R06A4.2(xf134)*, resulted in the same observation. Here, from 115 isolated

F2 worms six worms had the desired double homozygous genotype. Of these six worms, all but one were sterile and the one subfertile worm produced a reduced number of 15 progeny (Fig. 12 B). Synthetic sterility in the crosses could be rescued with the introduction of a *T12E12.3::gfp* single copy transgene created by MosSCI, thereby confirming the double mutation of R06A4.2 and T12E12.3 as cause for the sterility. When investigating the brood size of single, homo-/heterozygous, and double homozygous mutants at 20°C and 25°C, reduction of progeny numbers compared to *T12E12.3(xf131)* alone was detected. In the homo-/heterozygous intermediate worms at 20°C the difference in offspring was already significant (Fig. 12 C), while the reduction in brood size was very evident in the double homozygous mutants at both temperatures (Fig. 12 C/D). This indicates that the loss of both proteins is indeed responsible for the phenotype. A reciprocal cross carried out with *T12E12.3(xf131)* males resulted in the same synthetic sterility phenotype. Interestingly, when crossing *R06A4.2(xf133)* or *T12E12.3(xf131)* with mutants of other telomeric binders (*pot-2(tm1400), mrt-1(tm1354)*) or telomerase (*trt-1(ok410)*) in a short versus long telomere manner, no synthetic sterility phenotype could be observed, implying this as a specific phenotype for our candidate proteins.

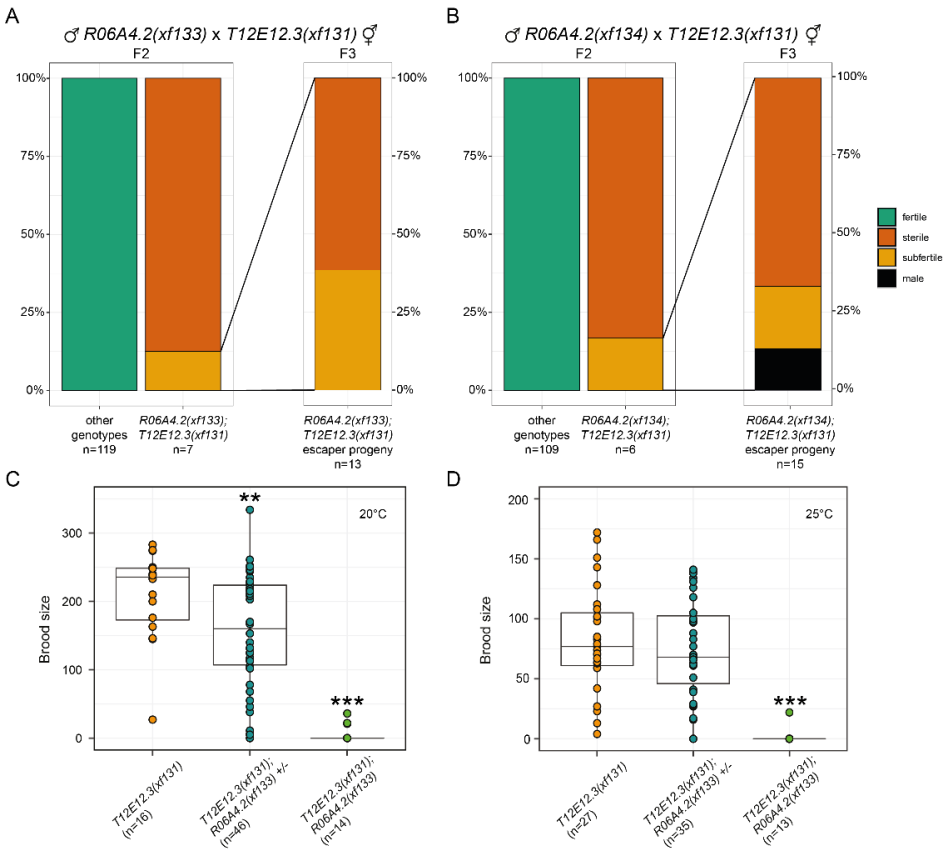

Figure 12: Both R06A4.2 and T12E12.3 are needed for fertility. (A) Quantification of fertility of the indicated *R06A4.2(xf133)*x *T12E12.3(xf131)* cross. Bar plots depict the quantification of each fertility subtype as percentage on the y-axis. Right hand bar depicts fertility subtypes of the F3 progeny of subfertile F2. Genotypes are indicated on the x-axis along with n for every genotype. Green depicts fertile progeny, yellow subfertile progeny, and orange sterile progeny. (B) as in (A) but for a cross with the second R06A4.2 allele, *R06A4.2(xf134)*. In addition, male progeny is indicated in black. (C) Broodsize assay of F3 worms from a *R06A4.2(xf133)*x *T12E123(xf131)* cross at 20°C. Isolated were F3 progeny carrying homozygous *T12E12.3(xf131)* and heterozygous *R06A4.2(xf133)*. Worms were genotyped after all embryos were laid and divided into their respective genotype, as indicated on the x-axis together with the n. Central lines of the boxes represent the median of progeny number, while top and bottom lines represent the 75th and 25th percentile, respectively. Asterisks represent Mann-Whitney and Wilcoxon test p-values of ** = 0.0096 and *** = 2.5E-06. (D) Broodsize assay as in (C) but carried out at 25°C. Asterisks indicate p-value of *** = 4.1E-07 calculated as in (C).

To investigate the sterility of the double homozygous mutants further, we looked at their germlines using microscopy. The sterile worms displayed a variety of germline states, from completely underdeveloped or “empty” germlines to an accumulation of unfertilized oocytes due to lack of a spermatheca (Fig. 13 A/B). In addition, we stained the DNA of escaper animals with DAPI to be able to count the chromosomes

in their oocytes, as oocytes arrest in metaphase and therefore can be used to visualize chromosome numbers (Meier et al. 2006). Intriguingly, when we compared chromosome numbers of double homozygous escapers to chromosome numbers of wild-type and single mutants, we could determine a reduction or an increase in the number of bivalents in some oocytes of the escapers (Fig. 13 C). As we did not have the numbers of escapers at that point, we could not quantify further, but chromosome aberrations could explain the sterility and the subfertility of the escapers. Following the escaper progeny into F3 and further, not only sterile and semi-fertile worms were detected, but also an increasing number of male worms (Fig. 12 B). One reason for the observed Him phenotype could be missegregation of chromosomes during meiosis in the *C. elegans* germline (Hodgkin et al. 1979). The observed difference in number of visible chromosomes could indicate fusions or missegregation. Curious if the sterility and Him phenotype are caused by NHEJ fusions of chromosomes, we created a triple mutant strain by crossing homozygous *R06A4.2(xf133);lig-4(ok716)* with *T12E12.3(xf131)*. The loss-of-function mutant *lig-4(ok716)* carries a deletion in the gene for Ligase-4 (LIG-4), the main ligase in NHEJ (Martin et al. 2005). Four out of eight F2 progeny homozygous for *T12E12.3(xf131);R06A4.2(xf133)* but heterozygous for *lig-4(ok716)* were sterile, reiterating the observation of the previous crosses. Triple homozygous mutants in the F3 generation already showed signs of synthetic sterility. All 26 obtained triple mutants had severely decreased progeny numbers, showing in addition dead embryos or unfertilized oocytes. In five of these mutants a Him phenotype could be established as well. Looking at chromosome numbers in oocytes of these triple mutants, fusions of chromosomes and reduction of chromosome number could be detected (Fig. 13 D). This indicates that depletion of NHEJ does not rescue the synthetic sterility effect and potential chromosome fusions are caused by another DNA repair pathway.

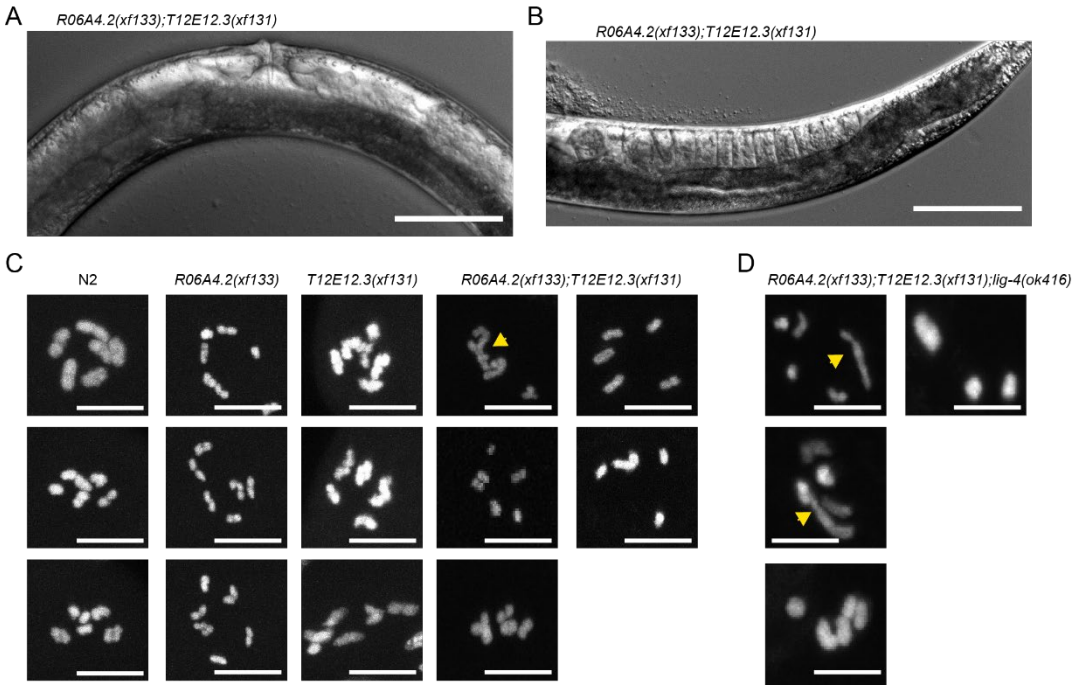

Figure 13: Double mutants are synthetically sterile and show chromosome aberrations. (A-B) Exemplary widefield DIC pictures of synthetic sterile double mutants with empty germlines (A) or stacked, unfertilized oocytes (B). Scale bar, 100 µm. (C) Maximum projection of oocytes from the indicated strains. DNA was stained with DAPI, greyscale is used for better visualization. Scale bars, 8 µm. Chromosome abnormalities are marked with a yellow arrowhead. (D) as in (C) but for triple mutants with *lig-4(ok716)*. DIC: differential interference contrast. DIC images were processed with Fiji to enhance brightness and contrast.

We further quantified and visualized the morphological defect of the germline by creating *R06A4.2* and *T12E12.3* mutant strains in combination with *pgl-1::mTagRfp-T* (Schreier et al., in submission). PGL-1 is an essential part of perinuclear (P-) granules in the germline. These granules are important for germline development and take part in gene regulation (Kawasaki et al. 1998; Strome and Updike 2015). By crossing *R06A4.2(xf133)* and *T12E12.3(xf131)* with *pgl-1::mTagRfp-T* in the background we were

able to visualize the germline. We isolated progeny from the indicated genotypes starting generation F2 (Fig. 14 A). When grown to day two of adulthood, we scored the germline health of the isolated animals into one of three categories and genotyped them. This was repeated until generation F5 to obtain sufficient numbers per genotype for each category. The categories for germline health were divided into 1) wild-type or wild-type like gonad, 2) one of the gonad arms atrophied, and 3) atrophy in both gonad arms. Overall analysis of the categories revealed that over 85% of homozygous *R06A4.2(xf133);T12E12.3(xf131)* mutants showed a germline of category 3, while the rest showed germlines of category 2 (Fig. 14 B). No wild-type like germline of category 1 could be observed for double homozygous mutants. Looking at the other genotypes, the majority of worms displayed germlines of category 1. Category 3 worms were detected when the mutation for T12E12.3 was hetero- or homozygously present, while R06A4.2 single mutants showed no category 3 germlines (Fig. 14 B). Figure 15 C-E shows exemplary images of each category taken prior to genotyping. Under-developed germlines rarely showed cells progressing into meiosis, and problems with proliferation in the mitotic zone, indicating defects in cell division. Looking at escapers from this cross, we could again determine a Him phenotype, as 17 out of 114 animals (15%) were male. This time we used these males for a cross with N2 wild-type hermaphrodites. The resulting F1 progeny showed a ~50% distribution of males/hermaphrodites, suggesting chromosomal missegregation as reason for the Him phenotype. In addition to the Him phenotype, some escaper progeny showed growth defects. Around 8% of the cross progeny grew to adulthood but remained physically smaller or arrested in larval stages prior to reaching adulthood (Fig. 14 F).

Taken together, we have found that both R06A4.2 and T12E12.3 were required for overall fertility as mutation of both proteins caused an immediate synthetic sterility effect. This effect was not observed when combining either one mutation with a mutation of another telomere associated protein, making it specific for these two proteins. In addition, sterility may be caused by defects in cell division, as animals with atrophied germlines showed a significant decrease of meiotic cells. The observed Him phenotype is potentially caused by chromosomal missegregation and chromosome loss, as a cross with N2 hermaphrodites shows normal distribution of males in the F1 generation.

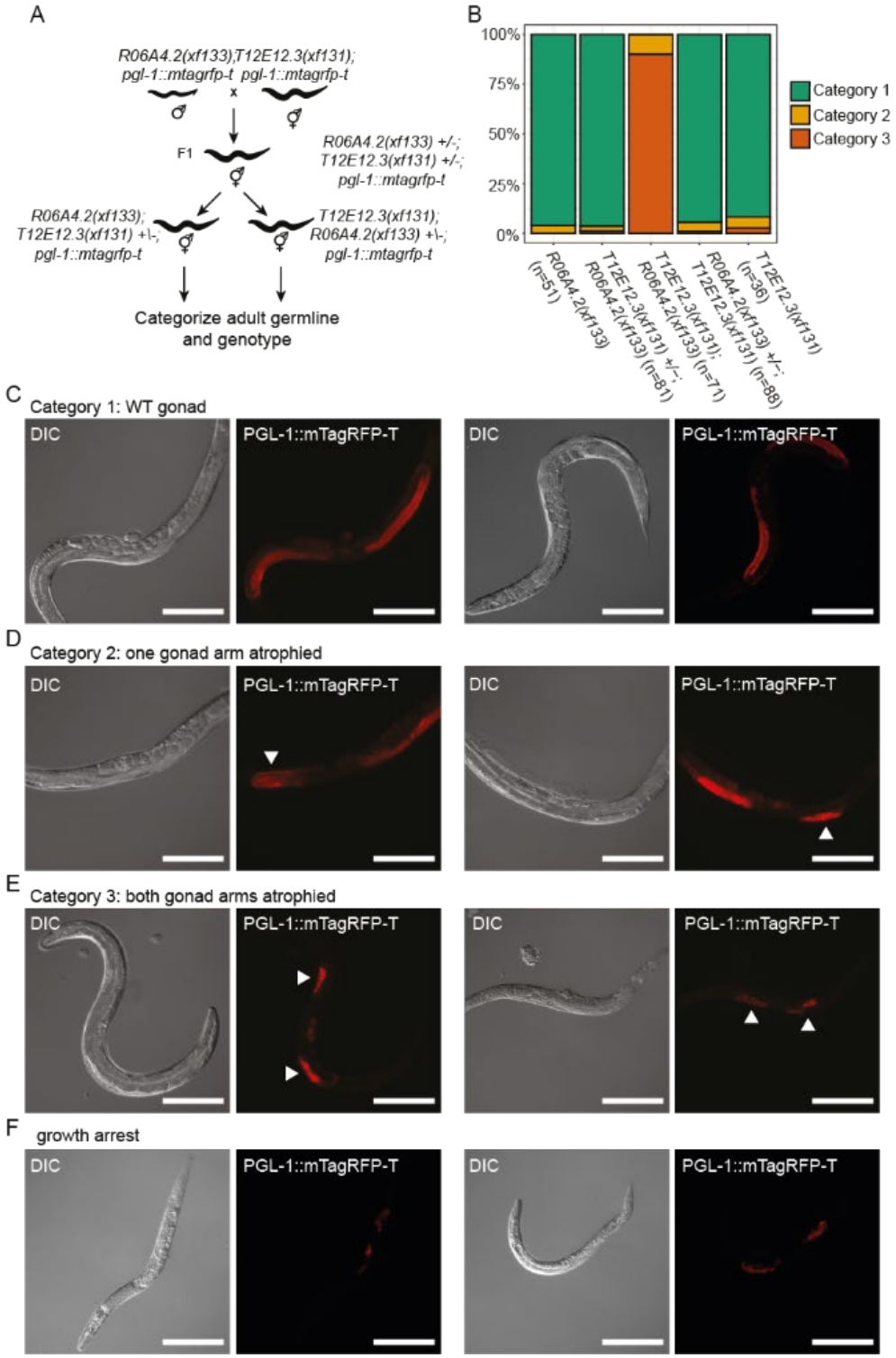

Figure 14: *R06A4.2;T12E12.3* double mutants show germline defects. (A) Cross scheme of *R06A4.2(xf133)* and *T12E12.3(xf131)* cross with expression of PGL-1::mTagRFP-T in the background. Starting F2, worms homozygous for one mutation and heterozygous for the respective other mutation were singled and the germline health category assessed on day two of adulthood via microscopy of the PGL-1::mTagRFP-T expression. After categorization and potential imaging worms were genotyped. (B) Quantification of the categories assessed over three consecutive generations. Genotypes and n indicated on the x-axis. Category distribution per genotype in percent on the y-axis. (C-E) Representative images of the assessed germline categories. Images taken with a widefield microscope in DIC and red fluorescence. Scale bars, 200 µm. White arrowheads mark the atrophied gonad arms in categories 2 and 3. (F) As in (D-E) but for worms that showed growth arrest prior to adulthood. DIC: differential interference contrast. DIC images were processed with Fiji to enhance brightness and contrast.

Mutations of R06A4.2 and T12E12.3 influence transgenerational fertility but not lifespan

We wondered if in addition to their telomere length phenotype, transgenerational fertility, or longevity were affected in the *R06A4.2* and *T12E12.3* mutants. To answer the question about transgenerational fertility, we conducted a mortal germline assay, comparing both our mutants to wild-type and mutants of POT-2, MRT-1, and TRT-1. It has been shown that MRT-1 and TRT-1 mutants in addition to telomere shortening display a mortal germline phenotype after being bottlenecked for several generations due to accumulation of genomic defects in the germline, finally leading to sterility (Meier et al. 2006; Meier et al. 2009). In our experiment we could determine the same mortal germline phenotype for *T12E12.3(xf131)*. Although the onset of the mortal germline phenotype was later than that of the MRT-1 or TRT-1 mutant, reaching generation 30, all worms were sterile (Fig. 15 A). This suggests a slower decline in germline health over the course of generations compared to *mrt-1(tm1354)* or *trt-1(ok410)*. On the opposite side, *R06A4.2(xf133)* did not show any mortal germline effect, just as the wild-type and *pot-2(tm1400)*. Interestingly, the T12E12.3::GFP MosSCI transgene in the background of a *R06A4.2(xf133);T12E12.3(xf131)* double mutant rescued the immediate synthetic sterility effect (see Fig. 12) but did not rescue the mortal germline phenotype, when transferring limited numbers of worms (Fig.15 A).

While shortening of telomeres leads to cellular senescence in the mammalian and yeast system (Watson 1972; Olovnikov 1973; Lundblad and Szostak 1989), there is discussion in the *C. elegans* telomere, whether disruption of telomere length homeostasis leads to an increase or decrease of life span (Joeng et al. 2004) or does not have any effect (Raices et al. 2005). To address this, we examined the lifespan of our mutants in comparison to wild-type and mutants for the other telomeric factors. As proposed by Raices *et al.* 2005, no significant difference in lifespan of the worms in comparison to their telomere length phenotype could be determined. Strikingly, the mutant that lived the longest was the *mrt-1(tm1354)* mutant that shows a telomere shortening phenotype (Bonferroni corrected p-value>0.03 compared to wild-type worms; Fig. 15 B).

Overall, our results indicate that T12E12.3, but not R06A4.2, is required for transgenerational fertility while both are needed for immediate fertility. In addition, telomere length did not influence lifespan in our experimental setup but rather influenced transgenerational fertility as mutants with shorter telomeres did exhibit a mortal germline phenotype.

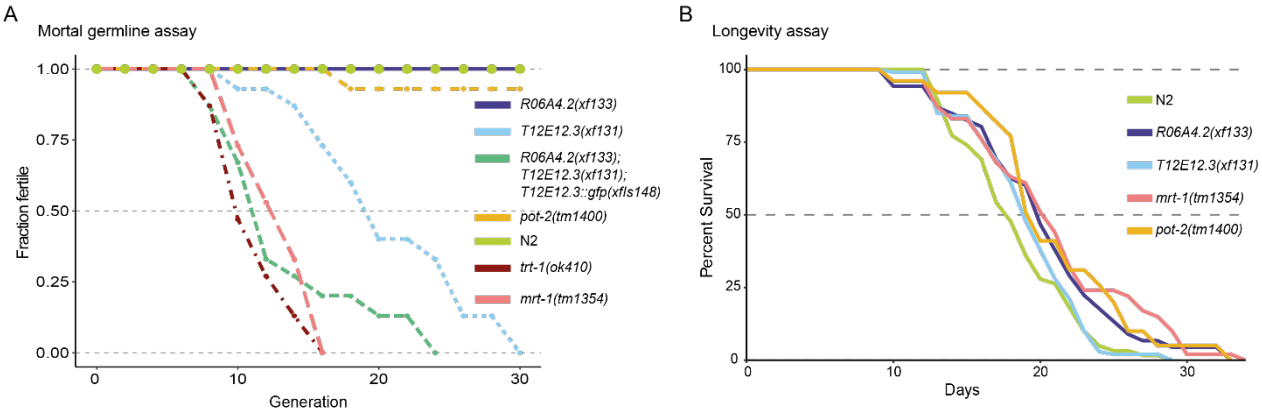

Figure 15: T12E12.3 mutation has additional implications on transgenerational fertility but not on lifespan. (A) Mortal germline assay plot. Individual lines indicate transgenerational fertility of different strains according to the strain legend on the right. The fraction of fertile population is indicated on the y-axis, while the generation number is indicated on the x-axis. n=15 populations grown across successive generations at 25°C. Mutants of known telomere binders as well as telomerase mutant *trt-1(ok410)* serve as controls next to the wild-type. (B) Longevity assay plot. Individual lines depict lifespan of respective strain as indicated in the legend. Starting at L4 100 worms per strain were transferred every day or every two days until death. Worms dying early due to wall climbing or bagging were censored. Final n per strain: N2 – n=62, *R06A4.2(xf133)* – n=47, *T12E12.3(xf131)* – n=62, *pot-2(tm1400)* – n=21, *mrt-1(tm1354)* – n=42.

R06A4.2 and T12E12.3 are part of a telomeric complex in *C. elegans*

R06A4.2 and T12E12.3 interact with each other

To interrogate, whether R06A4.2 and T12E12.3 interact with each other, or if they show differential binding partners, we performed Co-immunoprecipitation (CoIP) experiments with the double-transgenic *R06A4.2::3xFLAG;T12E12.3::GFP* strain. Pulling on either R06A4.2::3xFLAG or T12E12.3::GFP in embryos or young adults, we were able to detect the respective other protein, indicating interaction between the two (Fig. 16 A-D). Throughout development, we could only determine interaction in embryos and young adult worms in this experimental setup (Fig. 16 E/F). This suggests a potential need for the interaction of R06A4.2 and T12E12.3 in proliferating cells of embryos and the functional germline of young adult worms.

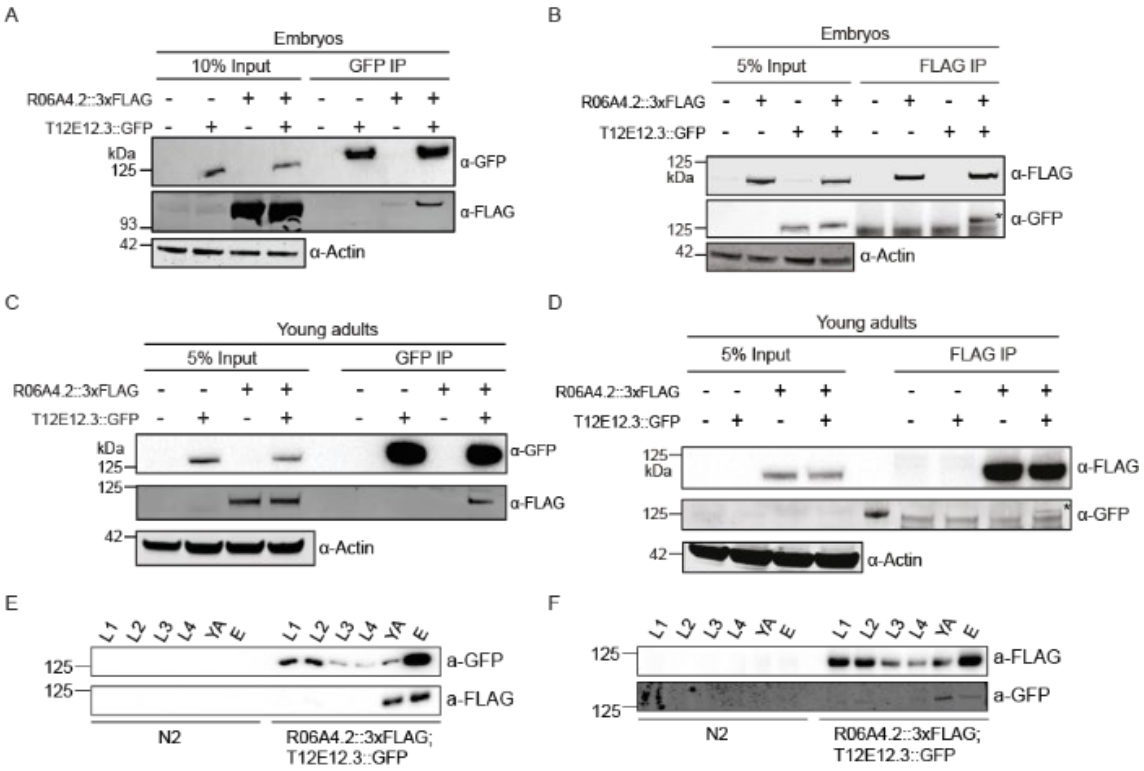

Figure 16: R06A4.2 and T12E12.3 interact with each other at certain developmental stages. (A) CoIP experiment in embryos. Strains as indicated above the western blots contain either one or both of the tagged proteins. -/- indicates N2 wild-type samples. IP was performed with a GFP-trap, western blots subsequently incubated with α-GFP and α-FLAG antibodies. Actin was used as loading control. (B) As in (A) but for FLAG-IP. (C-D) Like (A-B) but with extract from young adult worms. (E-F) GFP and FLAG CoIPs as in (A-B) but throughout developmental stages. Compared are wild-type and double transgenic strain R06A4.2::3xFLAG;T12E12.3::GFP. Developmental stages are indicated above the western blot.

R06A4.2 and T12E12.3 interact with single-strand binding proteins

To discover other potential interactors of R06A4.2 and T12E12.3 we performed immunoprecipitation experiments followed by quantitative mass spectrometry (IP-qMS). In comparison to wild-type, we could confirm that R06A4.2 and T12E12.3 show indeed enrichment when using the respective other as bait. Interestingly, we were able to detect the three known single-strand binding proteins POT-1, POT-2, and MRT-1 significantly enriched as potential interactors in both YA and embryos. In a follow up experiment, we repeated these IPs including Sm nuclease in the buffers to digest RNA and DNA potentially facilitating the interaction. The single-strand binders were still significantly enriched, suggesting a direct

association independent of DNA, even though we cannot exclude protection of the DNA by the bound proteins and therefore insufficient digest.

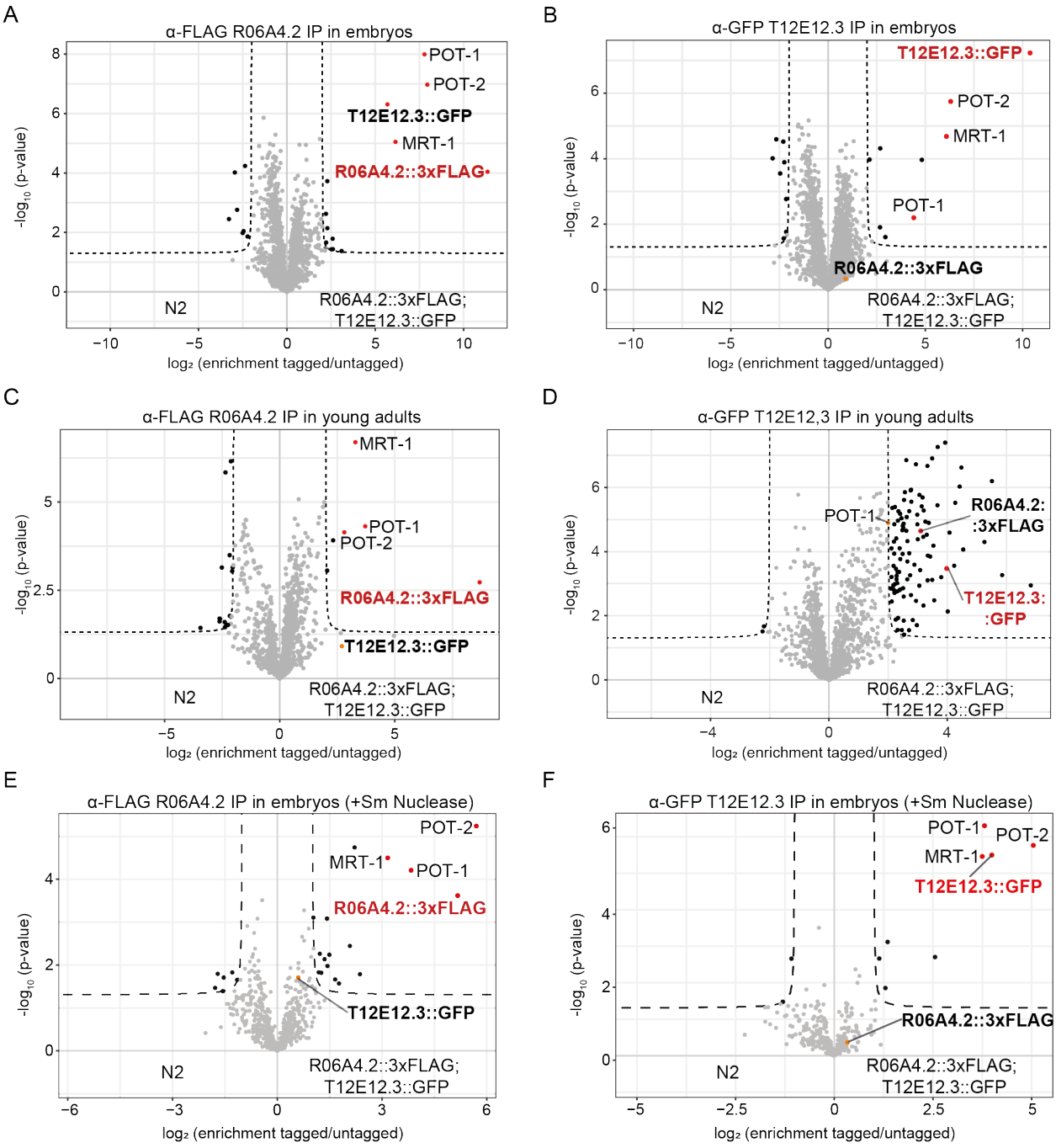

Figure 17: R06A4.2 and T12E12.3 interact with the telomeric single-strand binders. (A-B) Volcano plots of α-FLAG and α-GFP IP-qMS in embryos, respectively. Extract from the double transgenic strain was used for IP and samples were prepared in quadruplicates per condition. X-axis shows log_2 enrichment fold change, y-axis shows $-log_{10}$ transformed p-value. Background proteins are depicted as grey dots, enriched proteins (threshold: enrichment ≥ 2-fold, p-value ≤ 0.05) are depicted as black dots. Proteins of interest are depicted as red or orange dots depending on their enrichment. (C-D) As in (A-B) but for IPs conducted with YA extract. (E-F) Embryonic extract IP as in (A-B) with addition of Sm nuclease to the IP buffer.

In addition, we wanted to investigate, whether the interaction with the single-strand binders was dependent on the presence of the respective paralog protein or if there is a potential competition for the interactors. For this, we created strains carrying the GFP-tagged version of one protein in the mutant background of the other protein. When performing IP-qMS with embryo extracts of these strains versus

a GFP-strain with a wild-type background as control, we could detect the single-strand binders enriched in the strain with the mutant background. This implies that R06A4.2 and T12E12.3 may be redundant in their interaction with POT-1, POT-2, and MRT-1. Importantly, the higher enrichment in the mutant background was not observed because of higher expression levels of GFP-tagged protein in the mutant background. Comparison of expression levels in both conditions by western blot showed a slight stabilization of R06A4.2::GFP in the *T12E12.3(xf131)* background but a destabilization of T12E12.3::GFP in the *R06A4.2(xf133)* background.

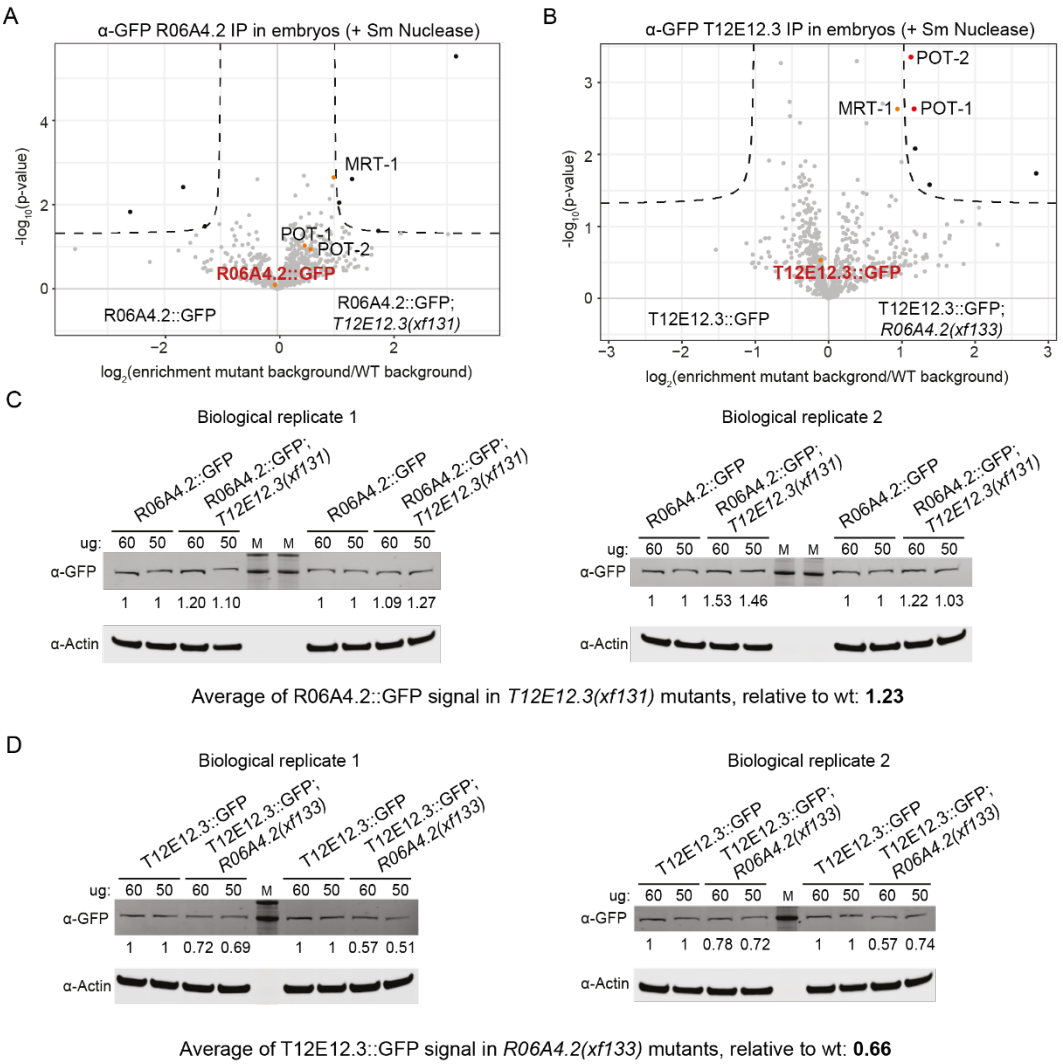

Figure 18: Interaction of R06A4.2 or T12E12.3 with the single-stranded binders does not depend on the other protein. (A-B) Volcano plots of α-FLAG and α-GFP IP-qMS in embryos, respectively. Extracts from a GFP-expressing strain with and without mutation of the respective other protein in the background were compared. X-axis shows $\log_2$ enrichment fold change, y.axis shows $-\log_{10}$ transformed p-value. Background proteins are depicted as grey dots, enriched proteins (threshold: enrichment ≥ 2-fold, p-value ≤ 0.05) are depicted as black dots. Proteins of interest are depicted as red or orange dots depending on their enrichment. (C) Analytical western blot for assessment of protein stability. Embryonic extract of R06A4.2::GFP strains was loaded as indicated and signal was analyzed with Image studio after incubation with LI-COR compatible secondary antibody. Expression in the wild-type background strain was set to 1 and the technical and biological replicates compared. Average expression signal is indicated below the western blot. Actin was used as loading control. (D) As in (C) but for T12E12.3::GFP strains.

To investigate the interactions between the telomeric proteins further, we performed a yeast two-hybrid (Y2H) assay with full-length proteins. T12E12.3 fused to the GAL4-DNA-binding domain self-activated the reporter, but we were still able to identify direct interactions between POT-1, T12E12.3, and R06A4.2 under stringent growth conditions (Fig. 19 A; middle and right panel). No interactions between these three proteins and POT-2 or MRT-1 were apparent (Fig. 19 A; middle and right panel). This confirms the previous CoIP-western blot and IP-qMS experiments showing direct interaction between R06A4.2

and T12E12.3. In addition, a direct interaction of both proteins with POT-1 could be observed. Non-detectable interactions were not due to a lack of expression of fusion proteins, as we could corroborate by western blot (Fig. 19 B/C). All fusion proteins that did not show interaction were detected in the assay. Expression of DBD-R06A4.2 and AD-POT-1 was not detected which could imply expression below the western blot detection threshold, as growth for the combination of these proteins could be observed in the stringent conditions of the Y2H assay.

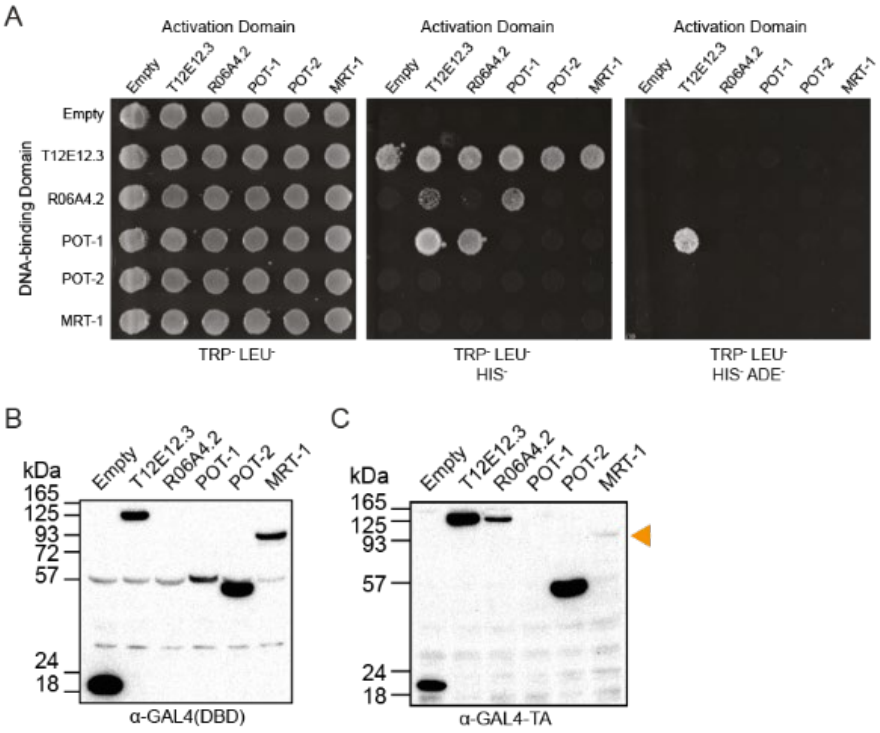

Figure 19: R06A4.2 and T12E12.3 interact with POT-1 in Y2H assay. (A) Grid of the spotted Y2H colonies. Combination of full length proteins fused to scGAL4 activation or DNA-binding domain as indicated above and on the left. Left panel: Growth control on non-restrictive medium, middle panel: Growth on restrictive medium indicating interaction, right panel: Growth on highly restrictive medium indicating a strong interaction. (B-C) Western blots to assess expression of the DNA-binding domain constructs (B) and the activation domain constructs (C). Samples for western blot were taken diagonally across the grid of (A; left panel) and membranes incubated with the respective antibodies as indicated. Very low expression signal of MRT-1-AD (C) is marked with an orange arrowhead. kDa: kilodalton, TRP: tryptophan, LEU: leucine, HIS: histidine, ADE: adenine

As determined by the Y2H assay and various IP-MS experiments, both R06A4.2 and T12E12.3 are interacting with each other and at least one of the single-strand binders. To investigate a potential complex we performed size-exclusion chromatography (SEC) to see a distribution of the proteins across size separation. The assay was performed with embryonic extract of the *R06A4.2::3xFLAG,T12E12.3::GFP* transgenic line. Western blot of elution fractions along the gradient showed very similar distribution for both proteins, with the highest signal detectable at a size corresponding to around 1.1 MDa (Fig. 20 A). Performing a second round of SEC, with and without Sm nuclease treated extract did not shift the elution peak (Fig. 20 B/C). A reason for not observing a shift could be the protection of DNA from degradation by the Sm nuclease due to an associated complex or several associated complexes. To investigate if the single-strand binders were present in the fractions containing the R06A4.2 and T12E12.3 elution peaks we performed qMS on the gel filtration samples from Fig. 20 A/B, treating them as replicates in an LFQ measurement. Interestingly, POT-2 and MRT-1 were detected in only one of the elution fractions at around 1.1 MDa with low measured intensity. The main peaks for both these proteins were found at a lower molecular weight (Fig. 20 D). POT-1 on the other hand was not detected in the measurements at all.

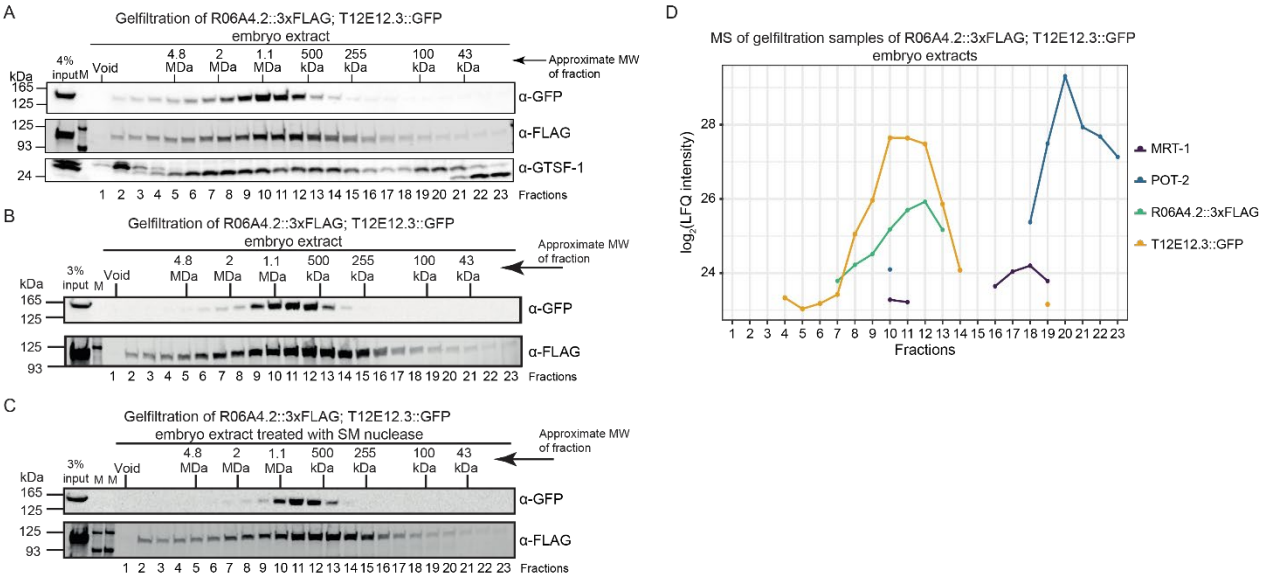

Figure 20: R06A4.2 and T12E12.3 interact in high molecular weight complexes. (A) Western blot analysis of elution fractions from size-exclusion chromatography of R06A4.2::3xFLAG;T12E12.3::GFP embryo extract. Membrane was probed with α-FLAG and α-GFP antibodies to determine elution profiles of the proteins. Fraction numbers and estimated molecular weight (MW) are indicated below and above the blots, respectively. GTSF-1 was used as control due to its known elution pattern in these experiments (Almeida et al., 2018). (B-C) Size-exclusion chromatography as in (A) but without (B) or with Sm nuclease treatment (C) of the embryo extract. (D) MS measurement of fractions from (A) and (B) treated as replicates in an LFQ measurement. Fractions are indicated on the x-axis, $\log_2$ transformed LFQ intensities are indicated on the y-axis. Respective intensities of the proteins of interest over the fractions are depicted.

Taken together, we have shown that R06A4.2 and T12E12.3 interact with each other at certain developmental time points, that they are interacting with the single-strand binder POT-1, and potentially also with POT-2 and MRT-1. This may indicate that R06A4.2 and T12E12.3 are part of one or several complexes present at telomeres in *C. elegans*.

R06A4.2 and T12E12.3 are conserved in other *Caenorhabditis* species

When searching for homologous genes in other species via BlastP search, it became apparent that R06A4.2 and T12E12.3 are conserved in the *Caenorhabditis* genus. While some species like *C. remanei* and *C. brenneri* showed two orthologs of the proteins as well, only one ortholog was detected in *C. briggsae*. We thus thought of investigating the telomere association of the single *C. briggsae* ortholog CBG11106 as well.

Telomere association in *Caenorhabditis briggsae*

We wanted to interrogate, whether the single ortholog of *C. briggsae* is able to bind to telomeres like its *C. elegans* counterparts. For this, we repeated the initial DNA pulldown with concatenated telomeric or control DNA, using nuclear extract from *C. briggsae* gravid adults. As can be seen in Figure 21, CBG11106, the ortholog of R06A4.2 and T12E12.3 was significantly enriched on the telomeric DNA. As validation for our pulldown we found one of the two *C. briggsae* MRT-1 orthologs enriched and the POT-1 ortholog CBG16601 just below the set threshold. This indicates a potential role for CBG11106 at *C. briggsae* telomeres in accordance to its orthologs in *C. elegans*, which were generated by a gene duplication with potential separation of functions.

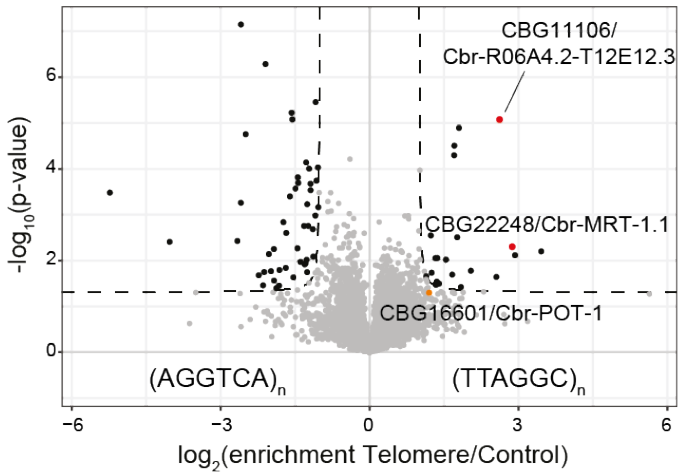

Figure 21: The single *C.briggsae* ortholog of R06A4.2 and T12E12.3 interacts with telomeric DNA. Volcano plot depicting result of DNA pulldown with telomeric DNA and nuclear extraxt from *C. briggsae* gravid adults. X-axis indicates $\log_2$ fold enrichment, while y-axis indicates $-\log_{10}$ transformed p-values. Threshold is set at 2-fold enrichment and p-value ≤ 0.05. Grey dots indicate background proteins; proteins above the threshold are black. Proteins of interest are depicted as red or orange dots depending on their enrichment.

Taken together, we have shown here the potential first telomeric complex in *C. elegans*. We have identified two previously uncharacterized proteins, R06A4.2 and T12E12.3, in our quantitative MS screens and shown that they interact with telomeric DNA *in vitro* and *in vivo*. In addition, distinctly different phenotypes could be observed in single mutants of these proteins, with telomere elongation and shortening, as well as requirement for transgenerational fertility. This suggests different roles for these two proteins in telomere maintenance. Nonetheless, we have demonstrated that both R06A4.2 and T12E12.3 are required for immediate fertility and germline health. Several lines of experiments provided the indication that R06A4.2 and T12E12.3 interact with each other at certain time points of *C. elegans* development coinciding with high proliferation such as embryonic development and gametogenesis in young adult animals. Moreover, we have seen association between the proteins and the previously described single-strand binders in different assays, suggesting the existence of one or more distinct telomeric complexes in *C. elegans*. Lastly, we could show that the single ortholog of R06A4.2 and T12E12.3 in *C. briggsae* is able to bind to telomeric DNA as well, suggesting a conserved function at telomeres in a common ancestor.

Discussion

Identification of novel telomere binders in *C. elegans in vitro*

Telomere nucleoprotein structures are essential for the protection of genome integrity in eukaryotes. Their DNA structure and associated proteins ensure proper DNA replication at the chromosome end as well as protection from DNA damage. In the popular model organism *C. elegans*, not a lot of information about telomere associated proteins is known, as only single-strand binders have been identified reliably so far (Raices et al. 2008; Meier et al. 2009). In this study, we have employed quantitative proteomics to identify new proteins binding to *C. elegans* telomeres to characterize new factors. The used approach has been proven successful in previous studies aiming to identify telomere associated factors in vertebrates and yeasts (Casas-Vila et al. 2015; Kappei et al. 2017; Pérez-Martínez et al. 2020). We have identified a set of telomere associated proteins and continued to characterize two previously unstudied proteins for their role at *C. elegans* telomeres.

Detection of novel factors at *C. elegans* telomeres

In this project, we aimed to identify proteins not previously identified at *C. elegans* telomeres in an unbiased manner with a quantitative proteomics approach and two separate read-out methods. The employed DNA pulldown assay resulted in a set of 12 and 13 proteins respectively (Fig. 1), some of which have not been described in telomere biology before. The high overlap between the two experiments accounts for the technical reproducibility of the DNA pulldown experiment. Furthermore, our screen has been validated by the detection of the previously identified single-strand binding proteins POT-1, POT-2 and MRT-1. As these proteins have been shown to bind to the *C. elegans* telomeric sequence *in vivo* and *in vitro*, their detection is an additional sign of the value of our screen (Raices et al. 2008; Meier et al. 2009; Cheng et al. 2012; Shtessel et al. 2013). In addition to the single-strand binders, we enriched for the *C. elegans* homologs of the KU heterodimer, CKU-70 and CKU-80 (Fig. 1). This heterodimer is a part of the NHEJ pathway and has been implicated in telomere length regulation and protection in other organisms, such as *S. cerevisiae*, *D. melanogaster* and *H. sapiens* (Fisher and Zakian 2005; Riha et al. 2006), while in *C. elegans*, no regulatory functions could be determined (Lowden et al. 2008). While depletion of the KU heterodimer in *S. cerevisiae* or *S. pombe* leads to shortened telomeres and in mammals to telomere loss and chromosome fusions (Gravel et al. 1998; Baumann and Cech 2000; Celli et al. 2006; Wang et al. 2009), a depletion in *C. elegans* was found to have no effect on life span, telomere length or chromosome fusions (Lowden et al. 2008). Therefore, enrichment of the KU heterodimer in our screen might be independent of a telomeric function. The fourth hPOT1 homolog POT-3 was identified among the background proteins in the LFQ screen, and not at all in the DML screen (Appendix, Table 1). This supports the previously described lack of telomeric phenotypes in *pot-3* mutants (Raices et al. 2008). Though POT-3 shows structural homology to hPOT1 in its OB-fold, the lack of telomeric phenotypes suggests other functions in *C. elegans*.

Next to R06A4.2 and T12E12.3 that we chose to characterize further, the screens resulted in additional significantly enriched proteins at the *C. elegans* telomeres (Appendix, table 1). Three other, previously uncharacterized proteins ZK1098.2, F57C9.4 and BED-1 were found to be enriched. A potential function as a transcription factor has been suggested for BED-1 (Blazie et al. 2017) and potential functions in embryonic development for F57C9.4 (Kasap et al. 2018). The other enriched proteins, DVE-1, PARP-1, LIN-40 and DCP-66 have orthologous genes in human. DVE-1 is orthologous to human SATB2, which is involved in chromatin remodeling and transcriptional regulation as well as being a biomarker for cancers (Britanova et al. 2005; Szemes et al. 2006; Gyorgy et al. 2008; Ma et al. 2018; Zhang et al. 2018; Ma et al. 2019). In *C. elegans*, DVE-1 was described as transcription factor, involved in the mitochondrial unfolded-protein response (UPR^{mt}) by binding to promoters of mitochondrial chaperone genes HSP-6 and HSP-60. In addition, it has been shown to be important for mitochondrial integrity and

embryonic development (Haynes et al. 2007; Tian et al. 2016). PARP-1 (also known as PME-1) is a structural homolog of hPARP1 (Poly(ADP-ribosyl)ation polymerase 1). PARP proteins facilitate the post-transcriptional modification Poly(ADP-ribosyl)ation (PARylation) which is involved in the regulation of DNA damage repair, chromatin structure, apoptosis, and mitosis (D'Amours et al. 1999; Wei and Yu 2016). Another member of the PARP protein family, tankyrase1, has been described at vertebrate telomeres interacting with TRF1 and regulating its interaction with telomeric DNA via PARylation, thereby influencing telomere length (Smith et al. 1998; Smith and De Lange 2000). *C. elegans* PARP-1 has been shown to exhibit the same PARylation activity as its human counterparts but has not been implicated at telomeres thus far (Gagnon et al. 2002). The *C. elegans* tankyrase homolog TANK-1 (PME-5) has been localized to chromosomes but no telomere function has been described for this protein either (White et al. 2009). LIN-40 (also known as EGR-1) and DCP-66 are part of the *C. elegans* nucleosome remodeling and histone deacetylase (NuRD) complex (Passannante et al. 2010). Both proteins have orthologs in vertebrates; DCP-66 is the ortholog of p66, while LIN-40 is an ortholog of MTA1/2 proteins (Solari et al. 1999; Brackertz et al. 2002; Feng et al. 2002; Zhao et al. 2005; Sen et al. 2014). In vertebrates, the NuRD complex is involved in chromatin remodeling by hyperacetylation of histones for the initiation and maintenance of gene expression (Xue et al. 1998; Denslow and Wade 2007). Additionally, the NuRD complex plays a role in cancer, as its interaction with different transcription factors leads to positive, as well as negative regulation of cancer progression (Lai and Wade 2011). The human NuRD complex has been shown to act at telomeres in ALT cells where it promotes telomere elongation by HR through its chromatin decompaction activity and the recruitment of HR factors (Conomos et al. 2014). The *C. elegans* orthologs of the NuRD complex have been shown to regulate gene expression as well. LIN-40 and DCP-66 are members of the so-called synMuv (synthetic multivulva) genes that regulate vulval development (Ahringer 2000; Chen and Han 2001; Poulin et al. 2005; Passannante et al. 2010). In addition, LIN-40 is involved in the regulation of transcription factors that are responsible for embryonic patterning (Solari et al. 1999). Taken together, in addition to the previously described telomere binders and the KU-heterodimer, we identified several new genes with no previous telomere implication. Given that some of their vertebrate orthologs have been shown to have functions at telomeres, it would certainly be interesting to also characterize these proteins in further studies to see if some of these functions are conserved in *C. elegans*.

Next to the enriched proteins, there were several proteins missing in our screens that had previously been described to show telomeric association or telomeric phenotypes. One of these proteins is MRT-2, a homolog of the DNA damage checkpoint gene *S. cerevisiae* RAD17/*S. pombe* RAD1 which was identified in a screen for mortal germline phenotype mutants and shows a telomere shortening phenotype upon depletion (Ahmed and Hodgkin 2000). RAD17/RAD1 proteins function as part of their 9-1-1 checkpoint complexes in regulating the progression of the cell cycle in the presence of DNA damage or replication stress and are conserved in human (Boddy and Russell 1999; Volkmer and Karnitz 1999; Longhese et al. 2000). Like its yeast and mammalian counterparts, the 9-1-1 complex of *C. elegans* has been shown to be involved in telomere replication and length regulation, as telomeres shorten upon its depletion and chromosome fusions are apparent (Ahmed and Hodgkin 2000; Hofmann et al. 2002). Interestingly, MRT-2 has been proposed to work in a pathway with MRT-1 to promote telomere elongation by telomerase TRT-1 (Meier et al. 2009). Thus, MRT-2 potentially facilitates telomere lengthening in a context that could not be uncovered by our screen, as it might be independent of the proteins direct interaction with telomeric DNA. On the other hand we cannot exclude that its binding cannot be recapitulated in our experimental conditions, as the 9-1-1 complex interacts with DNA as assembled heterotrimeric clamp (Doré et al. 2009; Liu 2019) and is loaded onto DNA by a clamp loading complex including HPR-17 (Boerckel et al. 2007).

In addition to MRT-2, the previously described potential telomeric double-strand binders PLP-1, CEH-37, and HMG-5 were not enriched on the telomeres in our screen. Association with telomeric DNA was investigated for all three proteins *in vitro*. CEH-37 as well as HMG-5 were localized to chromosome ends by microscopy *in vivo* (Im and Lee 2003; Kim et al. 2003; Im and Lee 2005). Surprisingly, PLP-1 was the highest enriched protein found in our scrambled control sequence (Appendix, table 1). This suggests PLP-1 to be rather a general DNA double-strand binder, than a specific telomere binder. HMG-5 was

detected in the background of the MS experiments (Appendix, table 1), suggesting no preference for either of the provided DNA baits. Lastly, CEH-37 was not detected in any of the experiments of our screen. Therefore, our obtained results do not support these three proteins as telomeric double-strand binders. Nevertheless, PLP-1 and HMG-5 were described after IP-MS experiments as well (Im and Lee 2003; Im and Lee 2005). Given these circumstances, we cannot fully exclude that the specific conditions used in our screen versus the screen that identified these proteins might cause differing results.

R06A4.2 and T12E12.3 interact with the telomeric sequence *in vitro*

From all obtained candidate proteins in the screen, we chose to further characterize R06A4.2 and T12E12.3. A 65.4% amino acid sequence identity between the two proteins indicates a common origin and thereby a potential gene duplication event that gave rise to these paralogs in *C. elegans*. As no domain annotations were given for these two proteins, we analyzed their sequences with a structure homology prediction software (HHPred) (Zimmermann et al. 2018). Interestingly, both proteins showed structural similarity to motifs found in already described telomere associated proteins (Fig. 2). Similarity to the scRAP1 homeodomain motif indicated a potential for R06A4.2 and T12E12.3 to bind to telomeric DNA. Indeed, both proteins were found to not only interact preferentially with the telomeric DNA over our scrambled control sequence but to prefer the telomeric double-strand over the single-stranded baits as shown by western blot and FP (Fig. 3, 5). In addition, FP showed that a 2.5x repeat of telomeric sequence is enough for both proteins to bind, indicating that their binding motif can be found inside that sequence. Comparing the human double-strand binders TRF1/TRF2 and the *S. cerevisiae* double-strand binder RAP1, both show Myb-like domains that are utilized for DNA binding. As TRF1 and TRF2 each only possess one Myb-like domain in their structure (Broccoli et al. 1997), they need to dimerize to bind their 5'-TAGGGTT-3' target sequence (Fig. D1 A) (Court et al. 2005). RAP1 in *S. cerevisiae* on the other hand contains two Myb-like domains that are arranged tandemly within the protein, which makes it possible for RAP1 to bind double-stranded telomeric DNA (tandemly arranged repeat 5'-GGTGTGTGGGTGT-3') as a monomer (König et al. 1996). Looking at R06A4.2 and T12E12.3 we can suggest that the DNA binding domain is located in the N-terminal part of the proteins as shown by structure prediction and initial DNA pulldown data (Fig. 2 and 3). Still, the actual number of Myb-like domains in these proteins needs to be further investigated. By creating shorter constructs covering the N-terminal part of the protein, as well as constructs bearing only one of the predicted Myb-like domains it could be elucidated which part of the N-terminal end is involved in DNA binding. In addition, these results may be able to indicate whether R06A4.2 and T12E12.3 are binding as monomers or dimers. Nonetheless, we have identified never before characterized telomeric double-strand binders in *C. elegans*.

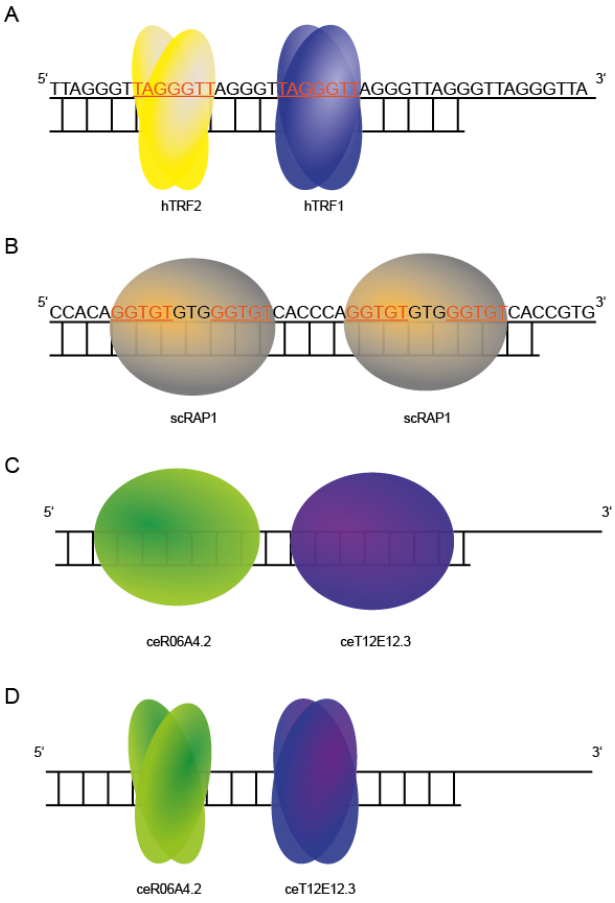

Figure D1: DNA-binding of telomere double-strand binders. (A) Binding of the human TRF homodimers to their TAGGGTT target sequence. (B) *S. cerevisiae* RAP1 monomer binding to tandemly arranged target sequences so both Myb-like domains aid in DNA binding. (C-D) Potential binding for *C. elegans* R06A4.2 and T12E12.3 to the telomere double-strand. Monomeric (C) or homodimeric (D) binding is possible.

R06A4.2 and T12E12.3 bind to telomeres *in vivo*

In addition to both of our candidate proteins binding to double-stranded telomeric DNA when expressed recombinantly, we were able to confirm this with endogenous proteins from tagged *C. elegans* strains (Fig. 8). *In vivo* association with telomeres could be confirmed by microscopy, showing overlap between nuclear foci of GFP-tagged versions of the candidate proteins with the known telomere binder POT-1 (Fig. 9). Thus, our candidate proteins localize to the telomeres *in vivo*. Due to the used transgene POT-1::mCherry (strain YA1197) (Shtessel et al. 2013), we could not colocalize our candidate proteins to telomeres in somatic cells. As the promoter used to create this transgene (*daz-1p*) is the promoter of a germline specific transcript, the transgene was not expressed in somatic cells. Creation of a CRISPR/Cas9 genome edited strain for either POT-1 or POT-2 with fluorescent tags could ease attempts to colocalize our candidate proteins to telomeres in non-germline settings. GFP microscopy of the R06A4.2 and T12E12.3 GFP-strains revealed expression also in somatic cells, though in a lesser intensity than in the germline or embryos. This correlates with the developmental expression profile of both proteins (Fig. 7), as both show a decrease in protein abundance during the larval stages and an increase in young adult and embryonic stages. This coincides with the progression of gametogenesis in YA and the proliferation of cells in the embryos. This indicates that both R06A4.2 and T12E12.3 are present at the telomeres during these stages, suggesting a role for them during cell proliferation.

R06A4.2 and T12E12.3 are functionally relevant at telomeres

Mutant alleles of our candidate proteins created by CRISPR/Cas9 genome editing showed no direct or obvious phenotypes and could be grown under standard conditions without detectable abnormalities. Though when looking at telomere length, we could see a striking difference in phenotypes between the two mutants. While *R06A4.2(xf133)* showed a significant increase in telomere length, *T12E12.3(xf131)* showed a decrease in telomere length when compared to wild-type by telomere Southern blot (Fig. 11 A). qFISH experiments with samples from two separate time points at approximately one and two years past creation of the mutants (Fig. 11 B-K) revealed an additional trend for both mutants in the germline and embryos. Telomere length in *R06A4.2(xf133)* mutants continued to extend, whereas telomere length for *T12E12.3(xf131)* mutants became more equal to wild-type length (Fig. 11 F/K).

We cannot say for sure if this elongation is due to a re-elongation of the telomeres in the *T12E12.3(xf131)* mutants, as telomere lengths in *C. elegans* are known to fluctuate between strains and even between generations of the same clonal line (Cheung 2004; Raices et al. 2005; Lowden et al. 2008; Cook et al. 2016). For this reason, the result of the qFISH can have two potential causes. First, *T12E12.3(xf131)* mutants re-elongated their telomeres over the course of time between the two time points by a mechanism that needs to be investigated. Elongation could involve both telomerase activity or ALT, as either pathway is present in *C. elegans* (Meier et al. 2006; Lackner et al. 2012; Seo et al. 2015). Second, *T12E12.3(xf131)* telomere length effects could be masked by the aforementioned fluctuation in telomere length. Telomere length for the mutant might have been fluctuating between the time points. In addition, telomere length of the wild-type qFISH control could have been different from wild-type control used for telomere Southern blot. It has been shown that telomere length in N2 wild-type animals can range from 2 to 9 kb in different clonal lines (Raices et al. 2005). To fully investigate and comprehend this shortening effect of *T12E12.3(xf131)*, the qFISH or Southern blot experiments would have to be repeated over several time points with a wild-type control growing along the timeline to account for the natural fluctuations in telomere length in *C. elegans*.

Overall, the two telomeric phenotypes of *R06A4.2(xf133)* and *T12E12.3(xf131)* represent previously described phenotypes of mutants of the single-strand telomere binders in *C. elegans*. Mutants of POT-1 and POT-2 have been shown to exhibit the same telomere elongation phenotype we have observed for *R06A4.2(xf133)* (Raices et al. 2008; Shtessel et al. 2013). It has been proposed that both of their elongation phenotypes result from a lack of inhibition of the telomerase enzyme in the mutants (Shtessel et al. 2013). Experiments where both POT mutants were independently crossed into a telomerase

mutant (*trt-1(ok410)*) showed a decrease of telomere length over consecutive generations, indicating telomerase as driving force behind the elongation (Shtessel et al. 2013). Further experiments in this direction have to be conducted with the *R06A4.2* mutant to investigate a potential telomerase involvement in its telomere length phenotype. Decrease in telomere length in that same cross setting as for POT-1 or POT-2 would indicate telomerase activity as a reason for the elongation of telomeres in this mutant. The telomere shortening effect as seen for *T12E12.3(xf131)* has been described for mutants of MRT-1 and MRT-2 (Ahmed and Hodgkin 2000; Meier et al. 2009). Both have been suggested to work in a pathway that facilitates telomere elongation by telomerase, as additional mutation of telomerase did not increase the rate of telomere shortening (Meier et al. 2009). After confirmation of the telomere shortening effect of the *T12E12.3* mutation, it would be interesting to investigate if T12E12.3 is an additional factor of that proposed telomere maintenance pathway, or acts independently of MRT-1 and MRT-2.

Mutation of double-strand telomere binders in mammals and yeasts results in telomere length phenotypes as well. Depletion of *S. cerevisae* RAP1 leads to telomere shortening until a certain point where telomeres are maintained in their short state (Conrad et al. 1990; Lustig et al. 1990). Mutation of TRF1/TRF2 in mammals on the other hand leads to telomere elongation without altering the expression level of telomerase itself (van Steensel and de Lange 1997; Smogorzewska et al. 2000). This indicates that both TRF1 and TRF2 are negative regulators of telomerase, as overexpression of either protein leads to the opposite phenotype, telomere shortening (Smogorzewska et al. 2000). Similar to its orthologs in vertebrates, mutation of TAZ1 in *S. pombe* leads to telomere elongation (Cooper et al. 1997). It was reported that this protein is a negative regulator of telomerase as the elongation phenotype is only detected in telomerase positive cells but not in cells depleted of telomerase (Nakamura et al. 1998). Additionally, it has been shown to be able to also positively regulate telomere length by interaction with either RAP1 or RIF1 (Miller et al. 2005). The results of our telomere length experiments suggest that R06A4.2 and T12E12.3 might also be regulators of telomerase. Interestingly, even though they are paralog proteins, they show a divergence in their telomere length phenotypes upon depletion. Thus, we propose that R06A4.2 is a negative regulator of telomere length as TRF1/TRF, and T12E12.3 a positive regulator of telomere length as scRAP1 (Fig. D2 B/C). This suggests that these proteins are not redundant in their respective function in regulation of telomere homeostasis. However, how this regulation is achieved, and if it involves participation of the single-strand binders as part of the pathway needs to be further investigated.

R06A4.2 and T12E12.3 are required for fertility and germline health but not longevity

Initially, no fertility defect could be detected for *R06A4.2(xf133)* and *T12E12.3(xf131)* when conducting a fertility assay to count brood sizes of the respective mutants under normal growth conditions at 20°C or 25°C (Fig. 10). However, when performing a mortal germline assay to evaluate transgenerational fertility, T12E12.3 was essential for fertility over a longer period of time but R06A4.2 was not (Fig. 15 A, Fig. D2 C). While depletion of R06A4.2 did not have an effect on transgenerational fertility, *T12E12.3(xf131)* mutants became fully sterile after being bottlenecked for 30 generations (Fig. 15 A). Again, though these proteins share a high sequence identity, experiments suggest that they have divergent functions. Mortal germline phenotypes have also been described for the proteins involved in the positive regulation of telomere length, the telomere binder MRT-1, the checkpoint protein MRT-2, and telomerase TRT-1 itself (Ahmed and Hodgkin 2000; Meier et al. 2006; Meier et al. 2009). Compared to *T12E12.3(xf131)*, these mutations reach the mortal germline phenotype at earlier time points, in our case at half the time (Fig. 15 A). The mortal germline phenotype arises in these mutants due to the accumulation of DNA damage in the germline over time, which leads to chromosome segregation defects (Meier et al. 2006). This suggests the same might be happening in *T12E12.3* mutants, just at a slower pace. To investigate this hypothesis, the mortal germline assay should be repeated and *T12E12.3* mutant animals checked for the additional phenotypes such as germline degeneration and chromosome fusions at time points where fertility starts to decline. Under normal growth conditions, no chromosome fusions were detectable in the R06A4.2 or T12E12.3 single mutants (Fig. 13 C),

suggesting a late onset phenotype for *T12E12.3(xf131)* which needs to be examined further. In addition, potential accumulation of DNA damage could be made visible by crossing in a fluorescently tagged protein of the DNA damage pathway such as RAD-51 or CEP-1 (p53 ortholog in *C. elegans*) to visualize DNA damage by microscopy (Levi-Ferber et al. 2014; Koury et al. 2018). Another option would be to stain for DNA damage using antibodies against the respective proteins (Schumacher et al. 2005; Garcia-Muse et al. 2019).

Strikingly, double mutants of R06A4.2 and T12E12.3 showed a highly penetrant synthetic sterility phenotype, already visible in the first homozygous generation (Fig. 12). This indicates that both proteins play a role in normal, immediate fertility (Fig. D2 D). Double mutant crosses between the described single-strand binders and the telomerase mutant have not displayed this direct sterility effect (Meier et al. 2006; Cheng et al. 2012; Shtessel et al. 2013). In addition, crosses between *R06A4.2(xf133)* and *mrt-1(tm1354)* or *trt-1(ok410)* as well as *T12E12.3(xf131)* and *pot-2(tm1400)* did not result in this immediate sterility phenotype as well. This indicates that the observed phenotype is specific to our paralog candidate proteins. Four independent crosses, including two mutant alleles of *R06A4.2* and a reciprocal cross, resulted in the same synthetic sterility phenotype (Fig. 12, 14), additionally underlining the importance of the discovered phenotype. Looking at germline health (Fig. 13), we could observe animals with germlines containing stacked oocytes and no spermatheca, as well as animals that did not show any germline development (“empty”). To further investigate the germlines of the double mutant animals, we used a PGL-1::mTagRFP-T transgene (Schreier *et al.*, in submission) to visualize the developmental state of the germlines by fluorescence microscopy. We chose to use PGL-1 as germline marker, as it is a part of perinuclear (P-) granules in the germline. P-granules are important for germline development and gene expression, and they can be found in all germ cells except mature sperm (Kawasaki et al. 1998; Strome and Updike 2015). Animals of the triple mutant cross were singled, categorized and genotyped as described. Strikingly, we could see that none of the *R06A4.2(xf133);T12E12.3(xf131)* double mutants showed a wild-type like germline (category 1, Fig. 14 B). All double homozygous mutants showed at least one gonad arm atrophied (category 2), while the majority had both gonad arms atrophied (~85%, category 3). In addition, all genotypes containing homozygous or heterozygous *T12E12.3(xf131)* showed a small number of category 3 germlines as well, while genotypes homozygous for *R06A4.2(xf133)* did not (Fig. 14 B). This suggests that even though both proteins are needed for immediate fertility, T12E12.3 might have a more distinct contribution to fertility, as mutation of this protein alone already results in decline in germline health. The observed mortal germline phenotype for *T12E12.3(xf131)* supports this hypothesis as well. Development of the germline was compromised in the double mutants due to under-proliferation of germ cells. This suggests that germ cells are likely failing to enter and progress through mitosis and meiosis properly. Interestingly, deletion of the telomerase catalytic subunit TRT-1 shows the same phenotypes as we have described here for our double mutants (Meier et al. 2006). Mutants for *trt-1* showed sterility, developmental defects such as body morphology defects and under-development of gonad arms. For *trt-1* mutants these phenotypes were proposed to arise from chromosome fusions that lead to mitotic and meiotic failure (Meier et al. 2006). Further experiments need to be conducted to determine if this is as well the case in our double mutants and if indeed chromosome segregation defects are the reason for the observed germline degeneration and sterility.

As mentioned, the sterility phenotype in *trt-1* mutants are likely the result of a chromosome segregation defect. We could as well detect chromosome number aberrations in the oocytes of escaper worms (Fig. 13 C). These escaper worms were double homozygous for both *R06A4.2(xf133)* and *T12E12.3(xf131)* but escaped sterility and gave rise to a very low number of progeny. This suggests that the germlines of these animals accumulated damage as well but not to an extent where it fully abolished their fertility. The imaged escapers showed different chromosome numbers when compared to the wild-type and the single mutants. Generally, six bivalents of highly condensed chromosomes are visible in the oocytes of the diakinesis stage (Hubbard and Greenstein 2005). In the escapers, between four and seven bivalents could be observed (Fig. 13 C). Furthermore, we observed chromosome fusions in some of the oocytes (yellow arrowheads, Fig. 13 C). Chromosome fusions are a common outcome in cells with destabilized telomeres due to disruption of telomere-binding factors. Depletion of TRF2, and thereby disruption of

the shelterin complex leads to growth arrests and chromosome end fusions facilitated by NHEJ in human cells (Van Steensel et al. 1998; Smogorzewska et al. 2002). In addition, depletion of the RAP1-TRF2 heterodimer can facilitate chromosome end fusions mediated by homologous recombination (Rai et al. 2016). In *S. pombe*, the TRF ortholog TAZ1 is needed to prevent chromosome fusions that are mediated by the KU heterodimer and NHEJ (Ferreira and Cooper 2001). Lastly, also mutation of the double-strand telomere binder RAP1 in *S. cerevisiae* leads to chromosome fusions through NHEJ (Pardo and Marcand 2005). In addition, chromosome fusions have been described for the late stage mutants of *trt-1, mrt-1* and *mrt-2*, after shortening of the telomeres has surpassed a certain threshold (Ahmed and Hodgkin 2000; Cheung 2006; Meier et al. 2006; Meier et al. 2009). Therefore, our results suggest potential de-protection of the telomeres through absence of both R06A4.2 and T12E12.3, which leads to an accumulation of DNA damage, chromosome fusions, and finally, sterility.

To determine if chromosome fusions in the double mutants were facilitated by NHEJ, we created a triple mutant of our candidates together with a mutant for Ligase-4 (LIG-4), the main ligase in NHEJ (Martin et al. 2005). Interestingly, we could still observe chromosome fusions in the triple mutants (yellow arrowheads, Fig. 13 D). This indicates that the observed chromosome fusions are not a result of NHEJ. However, though NHEJ is active in germ cells (Morton et al. 2006; Robert and Bessereau 2007), it has been shown that NHEJ is not the main acting DNA repair pathway in the *C. elegans* germline (Clejan et al. 2006; Lowden et al. 2008). This suggests the possibility that the detected chromosome fusions are likely the result of HR mediated DNA repair. Another explanation might be immediate telomere loss upon homozygosity of both mutants, as it has been shown in several organisms such as *S. pombe*, *S. ceverisiae* and mice that critically short telomeres are fused by other DNA repair pathways than NHEJ (Baumann and Cech 2000; Hackett et al. 2001; Maser et al. 2007; Lowden et al. 2008). Immediate telomere loss has been described in telomerase mutants of *C. elegans* before (Cheung 2006). To investigate these fusions and the potential involvement of HR further, it would therefore be important to repeat the double mutant cross with mutants of other DNA repair pathways such as *mre-11* and *rad-51* from HR (Takanami et al. 1998; Chin 2001), and in addition obtain data of more oocytes to quantify the fusion phenotype and investigate potential telomere loss. Telomere loss could be visualized by FISH, to compare signals between wild-type, sterile, and subfertile worms. In addition, FISH could indicate chromosome fusions, if telomere sequences are contained in the fusion points. The chromosome fusion phenotype might play a role in the development of the Him phenotype we have observed in three out of four crosses. Him phenotypes can be observed when X-chromosomes are not segregated properly due to translocations with autosomes. This nondisjunction of the X-chromosome leads to an increase in male progeny from the standard wild-type frequency of 0.2% (Herman et al. 1982). Due to its holocentric chromosomes, *C. elegans* is capable of maintaining fused chromosomes even through meiosis (Herman et al. 1982; Albertson and Thomson 1993). Him phenotypes are also observed in the mutants of *trt-1*, *mrt-1*, and *mrt-2* (Ahmed and Hodgkin 2000; Meier et al. 2006; Meier et al. 2009), indicating chromosome fusions in the *C. elegans* germline as a result of telomere shortening.

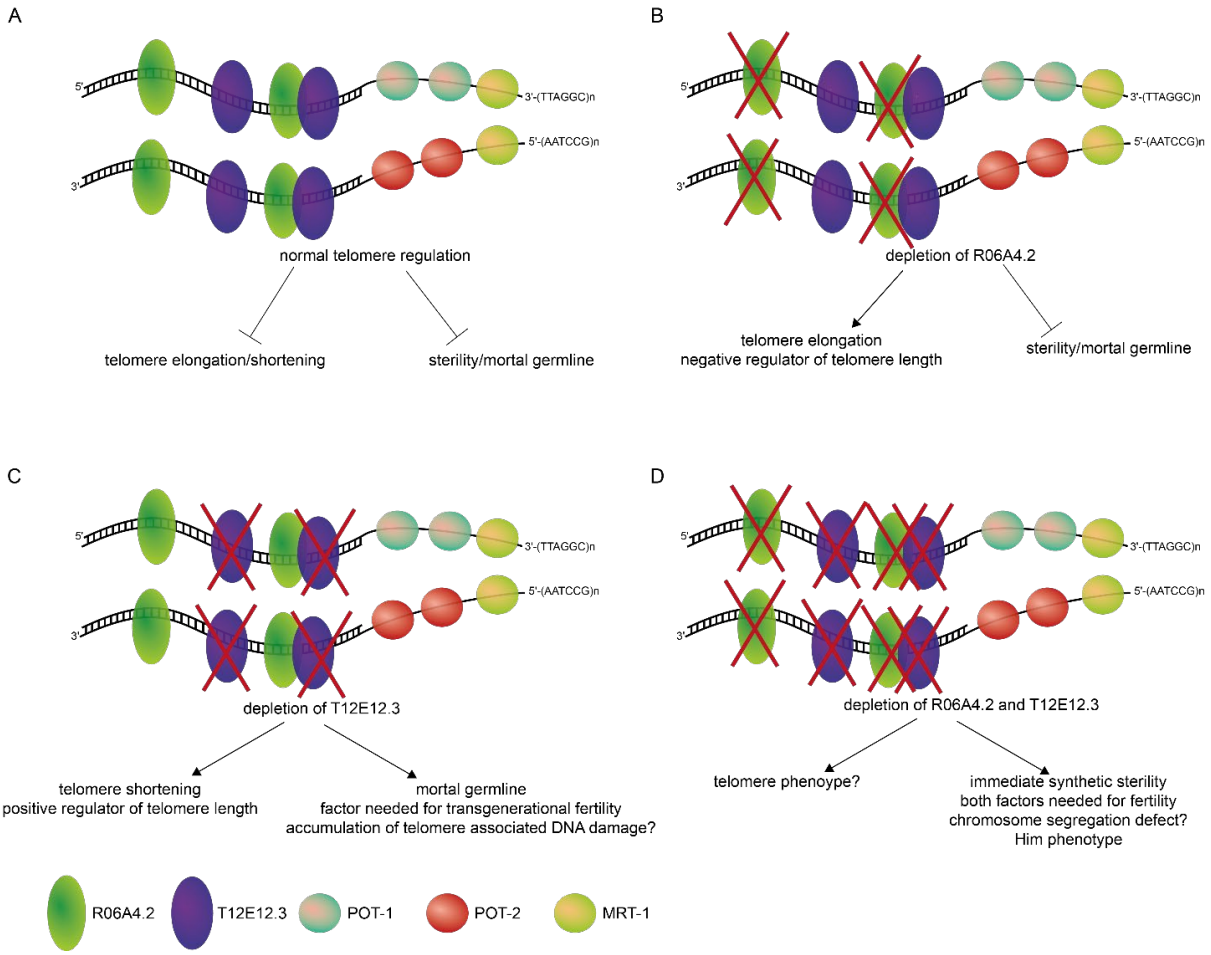

Figure D2: R06A4.2 and T12E12.3 function at *C. elegans* telomeres. (A) Steady state telomere with all factors present. Telomere maintenance is in homeostasis and animals are fertile. (B) Depletion of R06A4.2 leads to telomere elongation but has no other phenotypes. Telomere elongation hints at R06A4.2 being a negative regulator of telomerase. (C) Depletion of T12E12.3 leads to telomere shortening and a mortal germline phenotype. T12E12.3 could be a positive regulator of telomerase and is needed for transgenerational fertility. Sterility might be influenced by accumulation of telomere related DNA damage in the germline. (D) Mutation of both R06A4.2 and T12E12.3 leads to immediate synthetic sterility. Both factors are essential for fertility.

Telomere deprotection, telomere shortening, and chromosome fusions are triggers of the DNA damage response and lead to senescence in proliferating cells (Palm and de Lange 2008). We investigated if telomere length in *C. elegans* influences life span of the organism. The majority of studies argue that life span is not influenced by telomere length, as telomere mutants with short telomeres like *trt-1*, *mrt-1*, or *mrt-2* did not show significant reduction in life span as compared to telomere mutants with long telomeres like *pot-1* or *pot-2* (Ahmed and Hodgkin 2000; Raices et al. 2005; Meier et al. 2006; Meier et al. 2009; Shtessel et al. 2013). In our longevity assay, *R06A4.2(xf133)* and *T12E12.3(xf131)* did not show a significant increase or decrease in life span compared to the wild-type as well as short and long telomere mutants (Fig. 15 B). Therefore, our results are in line with previous publications stating no influence of telomere length on life span in *C. elegans*. However, the somatic cells of *C. elegans* are postmitotic and consequently do not undergo cell divisions anymore. Lack of cell divisions diminishes telomere shortening by DNA replication, as telomeres cease to be replicated. In addition, the DNA damage response is not active in somatic cells of the worm. While DNA repair itself is possible, it has been shown, that somatic cells do not react to DNA damage due to transcriptional silencing of key DDR proteins (Vermezovic et al. 2012). Thus, deprotection of telomeres or short telomeres would not trigger a DNA damage response in the soma. This would circumvent senescence or apoptosis reactions, and the life span of the organism remains unaltered. This suggests in addition, that telomere length and integrity in *C. elegans* are more important for fertility than life span, as the animals with short or deprotected telomeres become sterile but do not experience a decrease in life span if they have grown to adulthood.

R06A4.2 and T12E12.3 form a telomeric complex

Interaction of R06A4.2 and T12E12.3 in dividing tissues

R06A4.2 and T12E12.3 share a large portion of their nucleotide and amino acid sequence, but displayed different phenotypes in our telomere length and fertility assays. This suggests that both have distinct functions at *C. elegans* telomeres in regards to regulation, though they both are required for immediate fertility. Interestingly, we were able to show that R06A4.2 and T12E12.3 interact with each other in embryos and young adult *C. elegans* via Western Blot and IP-qMS (Fig. 16-19). The yeast two-hybrid assay confirmed that this interaction is a direct interaction between the two proteins (Fig. 20). Expression of both proteins was detected in all stages by western blot, but CoIP in the different life stages showed interaction only in embryos and young adults (Fig. 16). As the expression of the proteins in the larval stages L3 and L4 is much lower (Fig. 7, 16), we cannot exclude that interaction may be happening in these stages as well. Our readout in this experiment might have not been sensitive enough to detect interactions. As we have loaded equal amounts of extract of all the developmental stages, repeating this experiment with higher input for these specific stages might result in a different outcome. Though larval stages L1 and L2 show a similar expression pattern for both proteins when compared to young adults (Fig. 7, 16), we could not detect interaction between R06A4.2 and T12E12.3 in these stages.

Interaction of our candidate proteins in these specific developmental stages may indicate a need for their function in actively dividing tissues during embryogenesis and gametogenesis. More than half the somatic cell divisions has happened in embryogenesis before the L1 larvae hatches. By the time the animal hatches, 558 cells have been produced by mitosis (Sulston and Horvitz 1977; Koreth and Van Den Heuvel 2005). In the following larval stages, 55 of the somatic cells divide further and leave the adult hermaphrodite animal with 959 somatic cells (Sulston and Horvitz 1977; Kimble and Hirsh 1979; Lambie 2002). The gonad proliferates from four of the 558 cells that differentially divide to give rise to the somatic gonad and the reproductive gonad. The two germ cells comprising the initial reproductive gonad divide to around 1000 cells in the adult germline, starting in the mid-L1 stage (Kimble and White 1981; Lambie 2002). Germ cells that are not in the proliferative distal region enter meiosis as the germline develops after late L3 stage (Kimble and White 1981). The detected direct interaction of the candidate proteins in these highly proliferative stages indicates a potential need for telomere maintenance and protection involving R06A4.2 and T12E12.3. Telomere binding complexes in vertebrates, yeasts and other organisms such as *Arabidopsis thaliana* or *D. melanogaster* protect telomere integrity in proliferative tissues and ensure proper cell division (Moser and Nakamura 2009; Wellinger and Zakian 2012; Raffa et al. 2013; Procházková Schrumpfová et al. 2014; Schmutz and De Lange 2016). This suggests that our candidate proteins might have a similar function in *C. elegans*.

Interestingly, as described above, depletion of both R06A4.2 and T12E12.3 leads to an immediate synthetic sterility phenotype. Strikingly, the double homozygous worms develop mostly normal until adulthood, but show a germline that is not developed properly (Fig. 13, 14). This indicates that the expression and interaction between these two proteins may not be essential in the embryos, as otherwise we would expect to see an embryonic lethal phenotype and the animals would not have grown to adulthood. If interaction of R06A4.2 and T12E12.3 is not essential for proper mitotic divisions, the lack of interaction in L1 and L2 stage could be explained. On the other hand, meiotic divisions in the germline start in the late L3 stage (Kimble and White 1981). Interactions in the larval stages L3 and L4 could not be determined as mentioned above. Here it would be of interest to repeat the experiments to see if interaction in these stages is detectable. If so, it would suggest that interaction of R06A4.2 and T12E12.3 might be essential for meiotic progression, and therefore in addition explain the synthetic sterility phenotype of the double mutants.

In mouse, a germ cell specific complex has been described at the telomeres. The so-called TERB1-TERB2-MAJIN complex replaces shelterin at the telomeres during meiosis in the germ cells (Wang et al. 2019). TERB1 interacts with TRF1 and displaces the shelterin components from the telomeres (Shibuya et al. 2015; Pendlebury et al. 2017). TERB2 and MAJIN tether the TERB1-telomere interaction to the nuclear envelope where the complex interacts with the LINC complex, which in turn facilitates

telomere movements, bouquet formation and proper progression of meiosis. Disruption of the complex by depletion of TERB1 or TERB2 has been linked to infertility in both male and female mice (Long et al. 2017; Wang et al. 2019). The infertile mutant mice show no imminent somatic phenotype but their ovaries and testes were greatly underdeveloped (Wang et al. 2019). This phenotype resembles our observations and suggests that R06A4.2 and T12E12.3 are part of a telomeric complex that is needed for meiotic progression and fertility. The TERB1-TERB2-MAJIN complex was recently proposed to stem from a common metazoan ancestor, as homology search revealed orthologs in vertebrates, molluscs, annelids, and even the basal metazoan *Hydra vulgaris*. Strikingly, orthologs could not be detected in lineages leading to *C. elegans* and *D. melanogaster*, indicating a loss or divergence of this complex in these evolutionary branches (da Cruz et al. 2020). To investigate the possibility of R06A4.2 and T12E12.3 taking over TERB-like functions, mutant animals that do not develop a germline (e.g. thermo-sensitive *glp-4(bn2)*) could be crossed with our double-transgenic strain expressing R06A4.2::3xFLAG and T12E12.3::GFP. CoIP in these animals without germlines could determine if the interaction of the two proteins is limited to the germline or present in the post mitotic soma as well. Moreover, it would be of interest to investigate the role of the interaction in embryos.

Interaction of R06A4.2 and T12E12.3 with other telomeric proteins

In addition to the direct interaction between R06A4.2 and T12E12.3, we were able to detect association of both proteins with the single-strand telomere binders POT-1, POT-2, and MRT-1 in IP-qMS experiments (Fig. 17, 19, 20). Supplementing the IP buffers with Sm nuclease, to digest nucleic acids present in the extracts, did not change the enrichment of the single-strand binders in the IPs (Fig. 17 E/F). Though we cannot exclude that parts of telomeric DNA were inaccessible to degradation by the nuclease through bound proteins, we suggest the presence of one or more telomeric complexes. Interaction with the single-strand binders is not relying on the presence of the respective other protein as we could confirm by IP-qMS (Fig. 18). This indicates that both proteins have the ability to interact with POT-1, POT-2, and MRT-1 independently of the other. Western blot analysis of extracts revealed a slight destabilization of T12E12.3::GFP in the *R06A4.2(xf133)* mutant, indicating that R06A4.2 might stabilize T12E12.3 on protein level.

In the Y2H assay, we could confirm that both R06A4.2 and T12E12.3 are directly interacting with POT-1 (Fig. 19 A). Interactions with the other two single-strand binding proteins could not be determined. On the other hand, both POT-2 and MRT-1 co-eluted with R06A4.2 and T12E12.3 in one fraction of the size exclusion chromatography (Fig. 20 D). This fraction at about 1.1 MDa could indicate one or more complexes of double- and single-strand binders. Therefore, we propose the presence of protein complexes consisting of R06A4.2, T12E12.3, POT-1, POT-2, and MRT-1 at *C. elegans* telomeres (Fig. D3). As previously reported *in vitro* experiments have shown, POT-1 and POT-2 bind to the 5’ or 3’ single-stranded overhang, respectively (Raices et al. 2008). Considering this information, the presence of distinct telomeric subcomplexes that form *in vivo* and do not contain all the telomere-binding proteins simultaneously might be possible (Fig. D3). Interestingly, POT-1 has been described to be required for tethering telomeres to the nuclear envelope during embryogenesis (Ferreira *et al.*, 2013). Telomere association with the nuclear periphery is a conserved phenomenon in eukaryotes and has been described in yeasts (Funabiki et al. 1993; Palladino et al. 1993), *D. melanogaster* (Marshall et al. 1996), and human (Crabbe et al. 2012). Telomere anchoring has been suggested to aid in nuclear organization in mitotic and meiotic cells (Penkner et al. 2007; Starr 2009). Given the interaction of R06A4.2 and T12E12.3 in embryos (Fig. 16, 17) and the confirmed direct interaction with POT-1 (Fig. 19), the identified telomeric complex might be involved in this process. This would indicate a function for R06A4.2 and T12E12.3 during embryogenesis, which could be maintained also in the absence of the two proteins. This would explain why proper development of the embryos is not stalled in the double mutants.

Telomeric complexes counteract the DNA damage surveillance machinery by shielding the telomeres and inhibiting the DNA damage response (de Lange 2005; Vodenicharov and Wellinger 2006; Moser and Nakamura 2009; Vodenicharov et al. 2010). When subunits of these complexes are abrogated, the DNA damage response is activated and genome integrity endangered. The repair of falsely detected

DNA damage at telomeres leads to end-to-end chromosome fusions (Van Steensel et al. 1998; Ferreira and Cooper 2001; Pardo and Marcand 2005; He et al. 2006). Chromosome fusions have not been observed in mutants of *pot-1* or *pot-2* in *C. elegans* in previous studies (Cheng et al. 2012; Shtessel et al. 2013). Furthermore, we could not detect chromosome fusions in the single mutants for R06A4.2 and T12E12.3 (Fig. 13C). This suggests, that the here described *C. elegans* telomeric complex does probably not share the protective role seen in other organisms. However, we cannot exclude that the synthetic sterility, as well as the mortal germline phenotype observed in the *R06A4.2;T12E12.3* double mutant and the *T12E12.3* single mutant, respectively, are downstream effects of genome instability caused by DNA damage in the *C. elegans* germline.

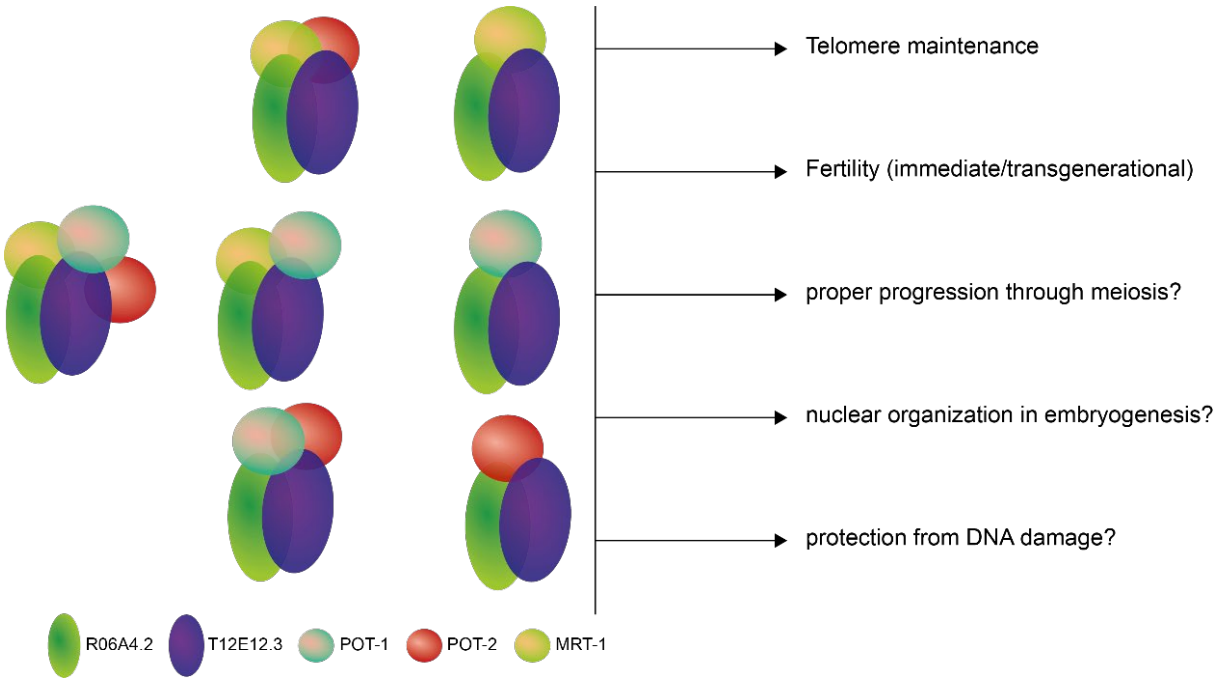

Figure D3: (Sub-)Complexes at *C. elegans* telomeres. Our data provides evidence that R06A4.2 and T12E12.3 interact with the known single-strand binders. Direct interaction with POT-1 was established by Y2H. Associations with POT-2 and MRT-1 were shown by IP-qMS and size exclusion chromatography. Exact complex composition is not known, therefore different (sub-)complexes of the telomeric binders in various combinations are depicted in this figure. The telomeric complex is needed for telomere maintenance and fertility. Involvement in meiosis, embryogenesis and protection from DNA damage need to be elucidated.

Telomere binding is conserved in at least one other *Caenorhabditis* species

Homology search revealed the conservation of R06A4.2 and T12E12.3 in the *Caenorhabditis* genus. We were able to provide results that the single ortholog in *C. briggsae* is interacting with telomeric DNA, suggesting telomeric functions as well (Fig. 21). This indicates that the homologs of our candidate proteins have the potential to bind to telomeric DNA at least since *C. elegans* and *C. briggsae* diverged from a common ancestor 80-100 million years ago (Coghlan and Wolfe 2002). Our candidate proteins could stem from a common ancestor that bound double-stranded telomeric DNA and was associated with fertility. The functions of the other ortholog proteins might be further investigated to determine if all homologs work in the same pathways. This could be done by DNA pulldowns in other *Caenorhabditis* species such as *C. japonica* or *C. inopinata* to confirm telomere association, followed by creation of deletion mutants or RNAi for knock-down to infer their influence on fertility. The common ancestor of R06A4.2 and T12E12.3 was duplicated along evolution after the divergence from *C. briggsae*. Three outcomes for gene duplications were suggested: 1) one copy is not used and becomes silenced (non-

functionalization), 2) one copy obtains a new function that is beneficial for the organism and will thereby be retained (neofunctionalization), 3) both copies accumulate mutations that separate their functions to a point where they together have the functions of the previous single gene (subfunctionalization) (Lynch and Conery 2000). Comparing *C. elegans* and *C. briggsae*, nonfunctionalization can be excluded, as both R06A4.2 and T12E12.3 were shown to have functions in telomere maintenance and fertility in *C. elegans*. However, with the current data, we cannot exclude the possibility for either neo- or subfunctionalization. Further experiments could give an indication, as for example mutation in *C. briggsae* might lead to the same fertility defect thereby indicating subfunctionalization of R06A4.2 and T12E12.3 in *C. elegans*. Investigation of the ortholog proteins in other species would bring an interesting evolutionary perspective to our reported telomere binders.

Conclusions

In this study, we have screened for yet unknown telomeric interactors of the nematode model organism *C. elegans*. In addition to already known telomere binding proteins, we have identified a set of novel factors that had not been implicated in *C. elegans* telomere biology. Characterization of these factors in respect to their function at telomeres might broaden our knowledge of *C. elegans* telomere organization and maintenance.

From the screen, we chose to characterize the paralog proteins R06A4.2 and T12E12.3 in relation to their function at *C. elegans* telomeres. We describe the first double-strand binding telomere proteins that show telomeric phenotypes and a fertility defect when depleted. In addition, these proteins are interacting with the previously characterized single-strand telomere binding proteins POT-1, POT-2, and MRT-1. This is the first described complex at telomeres in *C. elegans*. Further characterization of the proteins and the interactions will give more insights in telomere regulation in this model organism. Furthermore, this study shows the fluidity of telomere protection between different organisms. Even though *C. elegans* has a telomeric sequence close to vertebrates, the proteins interacting with the telomeric sequence are not direct orthologs of shelterin subunits. Despite their differences, these proteins likely fulfill the same or similar functions at telomeres.

C. elegans is an interesting model organism for telomere biology, as post-mitotic soma and actively dividing germline provide insights into telomere function in separate conditions. Our identification of a previously unknown telomeric complex allows further investigation of telomere regulation in this organism and between the different tissues.

Appendix

Table 1: Detection of previously described telomere proteins in *C. elegans* in quantitative MS runs

Values over 2 or -2 in the mean difference and over 2 in the $-\log_{10}$ p-value of the LFQ measurement determine significant enrichment on the telomeric (>2) or the control (<-2) DNA bait. For DML, ratios high in the forward experiment and low in the reverse experiment show enrichment on the telomeric DNA bait, whereas high ratios in the reverse experiment show enrichment on the control DNA bait.

Protein	LFQ		DML	
	-log10 p-value	Mean difference	Normalized ratio forward	Normalized ratio reverse
R06A4.2	8,466	2,919	10,130	0,114
T12E12.3	4,883	5,799	22,877	0,065
POT-1	8,143	3,008	13,871	0,100
POT-2	7,085	6,663	54,284	0,027
MRT-1	3,674	2,147	13,063	0,076
CKU-70	5,713	2,950	9,502	0,115
CKU-80	6,469	3,396	8,550	0,122
POT-3	0,717	0,719	Not detected in DML	
MRT-2	NA	NA	NA	NA
HMG-5	0,509	0,364	NA	0,362
PLP-1	7,173	-7,018	0,006	117,430
CEH-37	NA	NA	NA	NA

Table 2: Marker run of size exclusion chromatography.

Fractions collected from the NGC Quest system with indication of column elution volume, calculated MW of the respective fraction as well as position of the respective fractions on the 96-well plate used to recover elution fractions. Red square depicts the size coverage of the used superose 6 column, green square depicts fractions covered by the marker run with high fidelity.

Fraction	volume [ml]	log MW	calculated MW [kDa]	96 well
A1	1,0	8,982	960063,591	a1
A2	2,0	8,727	533212,105	a2
A3	3,0	8,472	296141,997	a3
A4	4,0	8,216	164475,040	a4
A5	5,0	7,961	91348,201	a5
A6	6,0	7,705	50734,105	a6
A7	6,5	7,578	37809,419	a7
A8	7,0	7,450	28177,340	**a8**
A9	7,5	7,322	20999,067	a9
A10	8,0	7,195	15649,483	**a10**
A11	8,5	7,067	11662,724	a11
A12	9,0	6,939	8691,605	**a12**
A13	9,5	6,811	6477,389	**b12**
A14	10,0	6,684	4827,252	**b11**
A15	10,5	6,556	3597,493	**b10**
A16	11,0	6,428	2681,020	**b9**
A17	11,5	6,301	1998,021	**b8**
A18	12,0	6,173	1489,018	**b7**
A19	12,5	6,045	1109,686	**b6**
A20	13,0	5,918	826,990	**b5**
A21	13,5	5,790	616,311	**b4**
A22	14,0	5,662	459,304	**b3**
A23	14,5	5,534	342,295	**b2**
A24	15,0	5,407	255,094	**b1**
A25	15,5	5,279	190,108	**c1**
A26	16,0	5,151	141,677	**c2**
A27	16,5	5,024	105,584	**c3**
A28	17,0	4,896	78,686	**c4**
A29	17,5	4,768	58,641	**c5**
A30	18,0	4,641	43,702	**c6**
A31	18,5	4,513	32,569	**c7**
A32	19,0	4,385	24,272	**c8**
A33	19,5	4,257	18,088	c9
A34	20,0	4,130	13,480	c10
A35	20,5	4,002	10,046	c11
A36	21,0	3,874	7,487	c12
A37	21,5	3,747	5,580	d12
A38	22,0	3,619	4,158	d11
A39	22,5	3,491	3,099	d10
A40	23,0	3,364	2,309	d9
A41	23,5	3,236	1,721	d8
A42	24,0	3,108	1,283	d7

Superose 6 5-5000 kDa

covered by marker run

Materials and Methods

Materials

C. elegans/*C. briggsae* strains

Strain Reference	Genotype	Source
N2	wild-type	CGC
YA1197	*ypIn2 [daz-1p::pot-1::mCherry::tbb-2 3'UTR + Cbr-unc-119(+)] II*	a kind gift from Shawn Ahmed
tm1400	*pot-2(tm1400) II*	National Bioresource Project for the nematode, Japan
YA1116	*mrt-1(tm1354) I*	CGC
YA1059	*trt-1(ok410) I*	CGC
RFK641	*T12E12.3(xf131) IV*	This study
RFK671	*R06A4.2(xf133) II*	This study
EG6699	*ttTi5605 II; unc-119(ed3) III; oxEx1578*	CGC
RFK659	*T12E12.3(xfIs148[t12e12.3(prm)::t12e12.3::GFP::t12e12.3(3'UTR)]) II; unc-119(ed9) III*	This study
RFK965	*R06A4.2(xf218[R06A4.2::d10]) II*	This study
RFK1048	*T12E12.3(xf234[T12E12.3::d10]) IV*	This study
RFK1096	*T12E12.3(xf235[T12E12.3::GFP]) IV*	This study
RFK1022	*R06A4.2(xf225[R06A4.2::GFP]) II*	This study
RFK958	*R06A4.2(xf201[R06A4.2::3xFLAG]) II*	This study
RFK1173	*T12E12.3(xf235[T12E12.3::GFP]) IV; R06A4.2(xf201[R06A4.2::3xFLAG]) II*	This study
RFK1174	*T12E12.3(xf235[T12E12.3::GFP]) IV; ypIn2[daz-1p::pot-1::mCherry::tbb-2 3'UTR + Cbr-unc-119(+)] II*	This study
RFK1067	*R06A4.2(xf225[R06A4.2::GFP]) II; ypIn2[daz-1p::pot-1::mCherry::tbb-2 3'UTR + Cbr-unc-119(+)] II*	This study
-	*T12E12.3(xf131) IV;pot-2(tm1400) II*	This study
-	*R06A4.2(xf133) II;mrt-1(tm1354) I*	This study
-	*R06A4.2(xf133) II;trt-1(ok410) I*	This study
RFK834	*lig-4(ok716) III*	CGC
-	*R06A4.2(xf133) II; lig-4(ok716) III*	This study
-	*T12E12.3(xf131) IV; lig-4(ok716) III*	This study
RFK1086	*pgl-1(xf233[pgl-1::mTagRfp-T]) IV.*	Jan Schreier, Ketting Lab, IMB
-	*T12E12.3(xf131) IV; pgl-1(xf233[pgl-1::mTagRfp-T]) IV*	This study

-	*R06A4.2(xf133) II; pgl-1(xf233[pgl-1::mTagRfp-T]) IV*	This study
AF16	*C. briggsae wild-type*	CGC

Yeast strains

Strain Reference	**Genotype**	**Source**
PJ69-4α	*MATα, trp1-901, leu2-3,112, ura3-52, his3-200, gal4Δ, gal80Δ, LYS2::GAL1-HIS3, GAL2-ADE2, met2::GAL7-lacZ*	Ulrich Lab, IMB

E. coli strains

Strain Reference	**Genotype**	**Source**
DH5alpha	*fhuA2, Δ(argF-lacZ)U169, phoA, glnV44, f80D(lacZ)M15, gyrA96, recA1, relA1, endA1, thi-1, hsdR17*	New England BioLabs, #C2987
OneShot ccdB Survival 2 T1^{R}	*F, $^{-}$mcrA, Δ(mrr-hsdRMS-mcrBC), Φ80lacZΔM15, ΔlacX74, recA1, araΔ139, Δ(ara-leu)7697, galU, galK, rpsL, (Str^{R}), endA1, nupG, fhuA::IS2*	Thermo Fisher Scientific, #A10460
Rosetta 2(DE3) pLysS	*F^{-}, ompT, hsdS$_{B}$(r$_{B}^{-}$ m$_{B}^{-}$), gal, dcm, (DE3,) pLysSRARE2 (Cam^{R})*	Novagen/Merck, #71401
BL21(DE3)-T1^{R}	*F^{-}, ompT, hsdS$_{B}$(r$_{B}^{-}$m$_{B}^{-}$)gal, dcm, λ(DE3), tonA*	Sigma-Aldrich, #B2935
Arctic Express (DE3)	*F$^{–}$, ompT, hsdS(rB– mB–), dcm+, Tet^{r}, gal, λ(DE3), endA, Hte, [cpn10 cpn60 Gent^{r}], [argU proL Str^{r}]*	Agilent, #230192

Plasmids

internal number	**Plasmid insert**	**backbone**	**description**
P683	*C. elegans* R06A4.2	pCoofy1	protein expression, N-terminal His$_{6}$ tag
P706	*C. elegans* pot-2	pCoofy4	protein expression, N-terminal His$_{6}$-MBP tag
P693	*C. elegans* T12E12.3	pCoofy1	protein expression, N-terminal His$_{6}$ tag
P1145	*C. elegans* T12E12.3	pCoofy1	protein expression, C-terminal His$_{5}$ tag
P855	*C. elegans* R06A4.2	pCoofy1	protein expression, C-terminal His$_{5}$ tag
P836	Pmyo-3:mCherry:unc-54 3'UTR	pCFJ104	co-injection plasmid Crispr & MosSCI
P837	GFP-tagged Y48G1C.1	pKBA99	plasmid used for PCR amplification of worm optimized GFP
P848	*C. elegans* T12E12.3 3' UTR	pDONR221 (P2r-P3)	3' UTR entry clone for MosSCI

P870	*C. elegans* T12E12.3 promoter	pDONR221 (P4-P1r)	promoter entry clone for MosSCI
P871	*C. elegans* T12E12.3 CDS + GFP	pDONR221 (P1-P2)	gene+tag fusion entry clone for MosSCI
P1174	*C. elegans* T12E12.3::GFP	pCFJ150	vector for MosSCI injection
P841	*C. elegans* R06A4.2-sgRNA1	pdd162	Crispr editing in *C. elegans*, contains sgRNA 1 for R06A4.2
P842	*C. elegans* R06A4.2-sgRNA2	p46169	Crispr editing in *C. elegans*, contains sgRNA 2 for R06A4.2
P843	*C. elegans* T12E12.3-sgRNA1	pdd162	Crispr editing in *C. elegans*, contains sgRNA 1 for T12E12.3
P844	*C. elegans* T12E12.3-sgRNA2	p46169	Crispr editing in *C. elegans*, contains sgRNA 2 for T12E12.3
pRFK2411	CeCas9 and sgRNA(F+E)	pDD162	Plasmids for CRISPR/Cas9 genome editing to tag R06A4.2 and T12E12.3 (made by Jan Schreier, Ketting Lab, IMB)
pRFK2412	sgRNA(F+E)	pJS012	
pRFK2568	CeCas9 and *dpy-10*_protospacer_1 sgRNA(F+E)	pJS012	
pRFK2588	CeCas9 and *unc-58*_protospacer_1 sgRNA(F+E)	pJS012	
pRFK3304	*R06A4.2*_protospacer_1 sgRNA(F+E)	pJS013	
pRFK3311	*T12E12.3*_protospacer_1 sgRNA(F+E)	pJS012	
P727	*C. elegans* pot-1	pCR8/GW/TOPO	holding vector for use in LR recombination for yeast 2 hybrid
P680	*C. elegans* pot-2	pCR8/GW/TOPO	holding vector for use in LR recombination for yeast 2 hybrid
P1151	*C. elegans* T12E12.3	pCR8/GW/TOPO	holding vector for use in LR recombination for yeast 2 hybrid
P1152	*C. elegans* R06A4.2	pCR8/GW/TOPO	holding vector for use in LR recombination for yeast 2 hybrid
P1153	*C. elegans* mrt-1	pCR8/GW/TOPO	holding vector for use in LR recombination for yeast 2 hybrid
P1147	*C. elegans* POT-1 yeast 2 hybrid DNA binding domain	pGBT9-GW	y2h assay vector
P1148	*C. elegans* POT-1 yeast 2 hybrid Activating domain	pGAD424-GW	y2h assay vector

P1149	*C. elegans* POT-2 yeast 2 hybrid DNA binding domain	pGBT9-GW	y2h assay vector
P1150	*C. elegans* POT-2 yeast 2 hybrid Activating domain	pGAD424-GW	y2h assay vector
P1162	*C. elegans* R06A4.2 yeast 2 hybrid DNA binding domain	pGBT9-GW	y2h assay vector
P1163	*C. elegans* R06A4.2 yeast 2 hybrid Activating domain	pGAD424-GW	y2h assay vector
P1164	*C. elegans* T12E12.3 yeast 2 hybrid DNA binding domain	pGBT9-GW	y2h assay vector
P1165	*C. elegans* T12E12.3 yeast 2 hybrid Activating domain	pGAD424-GW	y2h assay vector
P1166	*C. elegans* MRT-1 yeast 2 hybrid DNA binding domain	pGBT9-GW	y2h assay vector
P1167	*C. elegans* MRT-1 yeast 2 hybrid Activating domain	pGAD424-GW	y2h assay vector
P1172	ScUBC9	pGAD424-GW	positive control for y2h (pHU273, gift from Ulrich lab, IMB)
P1173	ScSMT3	pGBT9-GW	positive control for y2h (pHU620, gift from Ulrich lab, IMB)

Oligonucleotides

Number	**use**	**5'-3' sequence**
#1679	amplification of gene coding sequences for cloning	ATGTCCTCGTTCGACCGTCG
#1680		TTATTGTGGTGGATCTCTCGGTC
#1681		ATGCAATACACTTACCAGCA
#1682		TCAAATATTAATATTGTAGAAAAC
#1689		ATGTCAACGCGAGCAAAGAAGA
#1690		TCAACAGTTATTGGTTGGCCCAA
#2662		ATGTCATCTCGAGCAAAGAAGAACAAG
#2665		TTAATTGGTTGGCCCAAAATCAGC
#1829		ATGTCTACAATGCTTGAAAGACGAG
#1830		TTATAGTCCTGGATTTCTCGGCC

#1452	linearization of pCoofy plasmids	GGGCCCCTGGAACAGAACTTCCAG
#1453		CGCCATTAACCTGATGTTCTGGGG
#1642	amplification of gene coding sequences for SLIC cloning	AAGTTCTGTTCCAGGGGCCCATGTCCTCGTTCGACCGTCG
#1643		CCCCAGAACATCAGGTTAATGGCGTTATTGTGGTGGATCTCTCGGTC
#1654		AAGTTCTGTTCCAGGGGCCCATGTCATCTCGAGCAAAGAA
#1655		CCCCAGAACATCAGGTTAATGGCGTTAATTGGTTGGCCCAAAATCAG
#1656		AAGTTCTGTTCCAGGGGCCCATGTCAACGCGAGCAAAGAA
#1657		CCCCAGAACATCAGGTTAATGGCGTTAACAGTTATTGGTTGGCCCAA
#2023	EMSA and telo blot	TCGAACGATGGGTTAGGCTTAGGCTTAGGC
#2024		GCCTAAGCCTAAGCCTAAGCTTCGTACCC
#2025		GCCTAAGCCTAAGCCTAACCCATCGTTCGA
#2635	Fluorescence polarization	[FITC]-CTGTTAGGCTTAGGCTTAG
#2636		CTAAGCCTAAGCCTAACAG
#4185		[FITC]-CTGGCCTAAGCCTAAGCCT
#4186		[FITC]-CTGAGGTCAAGGTCAAGGT
#4187		ACCTTGACCTTGACCTCAG
#2894	single-/double-strand DNA pulldown	BIOTIN-TTCGTGACTCGAACGATGGGTTAGGCTTAGGCTTAGGCTTAGGCTTAGGCAGCCCTGGATTACGAACTGC
#2895		BIOTIN-GCAGTTCGTAATCCAGGGCTGCCTAAGCCTAAGCCTAAGCCTAAGCCTAACCCATCGTTCGAGTCACGAA
#2896		GCAGTTCGTAATCCAGGGCTGCCTAAGCCTAAGCCTAAGCCTAAGCCTAACCCATCGTTCGAGTCACGAA
#2897		TTCGTGACTCGAACGATGGGTTAGGCTTAGGCTTAGGCTTAGGCTTAGGCAGCCCTGGATTACGAACTGC
#3329		BIOTIN-TTCGTGACTCGAACGATGGGAGGTCAAGGTCAAGGTCAAGGTCAAGGTCAAGCCCTGGATTACGAACTGC
#3330		GCAGTTCGTAATCCAGGGCTTGACCTTGACCTTGACCTTGACCTTGACCTCCCATCGTTCGAGTCACGAA
#2290	inverse PCR for tag change	ATGTCATCTCGAGCAAAGAAGAACAAGCC
#2291		TTTCATGGTATATCTCCTTCTTAAAGTTAAACAAAATTATTTCTAGA
#2331		CATCACCATCACCATCACTAACGCCATTAACCTGATGTTCTGGGGAATATAAG
#2332		ATTGGTTGGCCCAAAATCAGCCT
#2349		ATGTCAACGCGAGCAAAGAAGAATAAGC
#2350		TTTCATGGTATATCTCCTTCTTAAAGTTAAACAAAATTATTTCTAGAGG
#2351		ACAGTTATTGGTTGGCCCAAAATCAACC

#2264	inverse PCR for sgRNA plasmid creation	ACATGAGTCTGTGTTTACGGGTTTTAGAGCTAGAAATAGCAAGTTAAAAT
#2265		ACGGCTCATAAGAGACTTGGGTTTTAGAGCTAGAAATAGCAAGTTAAAAT
#2266		GCATGTCGAGATTCTACTGGGTTTTAGAGCTAGAAATAGCAAGTTAAAAT
#2267		GCTTCAAAATTTCTCCAGGGGTTTTAGAGCTAGAAATAGCAAGTTAAAAT
#2270		AAACATTTAGATTTGCAATTCAATTATATA
#2271		CAAGACATCTCGCAATAGGA
#2254	Amplification of T12E12.3 parts for MosSCI	CGCAACTGCTTATACATCAACTATCGAAGGAAC
#2255		CTGGAACAAGAATTGGCGTTGCAAATATTGAAAAG
#2307		GGGGACAACTTTGTATAGAAAAGTTGATTCGCAACTGCTTATACATCAACTATCGA
#2308		GGGGACTGCTTTTTTGTACAAACTTGTTTTTGGACAAAACAAAAAATGAATCCTAAAATTTTCAAAACC
#2309		GGGGACAACTTTGTATAATAAAGTTGCACTTGTTTTTTTTCTATTCTTCCATTCAATTTCTCTCA
#2310		GGGGACAGCTTTCTTGTACAAAGTGGAGTATAACAATTCCAGCTTTTTAAATTCTTAAAAAAATGTATTTGACA
#2311		GGGGACAAGTTTGTACAAAAAAGCAGGCTATTCATTTTCGATATTTCAGCGTTCAAAAAATGTCA
#2312		CTCCTTTACTTCCTGCTCCAGCTCCACAGTTATTGGTTGGCCCAAAATCAAC
#2313		AACCAATAACTGTGGAGCTGGAGCAGGAAGTAAAGGAGAAGAACTTTTCACTGGAGTTG
#2314		GGGGACCACTTTGTACAAGAAAGCTGGGTCATTTGTATAGTTCGTCCATGCCATGTGT
#2275	sequencing Cas9 plasmid	TTACAACGTCGTGACTGGGAAAAC
#2276		GGTGTGAAATACCGCACAGA
#2450	standard plasmid sequencing	GTAATACGACTCACTATAG
#3577		TGT AAA ACG ACG GCC AGT
#2451		CAGGAAACAGCTATGAC
#2294	Cas9 nucleotide sequence sequencing	GTTCAAGGTCCTCGGAAACA
#2295		TGATCAAGCGTTACGACGAG
#2296		ACCGTAAGGTCACCGTCAAG
#2297		CGTATCGAGGAGGGAATCAA
#2298		CCACCGCCAAGTACTTCTTC
#2333	Sequencing of candidate constructs	TGATTTCTTATAGGCTCTTGGATGCGG
#2334		AATGGAGGTAATTTTAACCTGAATTCACTTGGAT
#2473		GCAAGGCCAGTCACTTGTGGATC
#4327		CTG AAC AAT TTT GGG CCG AGC TGC

#2335		CCGCTAGATGTAGAAATCTCCGATTCCTT
#2336		TGTGGTTGCGTGGAAGTTTATCTATGAG
#2337		CGAGATTTCTTCAAGTTTGGTGGATTCTG
#2346		AGTAAAGGAGAAGAACTTTTCACTGGAGTTG
#4299	sequencing Y2H constructs	CGGTATACGGCCTTCCTTCC
#4300		AGAGTTCCTCGGTTTGCCAG
#4301		GGTAGGGGAATTTCGGGCAT
#4302		GGCTCCGAATTCGCCCTT
#4303		TGAATCGGAGATGGTGGACG
#4304		TTGTGATTGGAGCAGCTGGT
#4305		CTTGACGCATGCTCATTCTGA
#4306		TGTGGAGTTTTGAAACAGTATCGA
#4307		TAATTAGACCGGCTGGGGGT
#4308		GTTCTATCACCGGCCTGGAG
#4309		CCGAGTTCCAACAGCCAGAA
#3684	genotyping *C. elegans* genome edited strains (mutants and tagged)	TTTGCGGCCAAATACGATAC
#3685		GCTCGAGGGTTTCAGGATTA
#3686		AGTGGAACGAATTACCCGCA
#3687		GTTCTTGGCCTCCAGGGAAG
#3688		CCGTCAGAACCGTCATTCGA
#3689		ACAAGCCAGCGTGATCATCA
#3690		ATGGTGTCGACTTGAACGCT
#3691		GAGCAGCTTTACGAGTAGTAAGT
#3692		CGTCTCGAGATCCTTGACCG
#3693		AGGCAGAATGTGAACAAGACTCG
#3694		ATCGGGAGGCGAACCTAACTG
#4378		CAG AAG TCC ACA GCG AAG AC
#4379		TGA CTA GGG CGA GGG GTA AG
#4380		GGT GGT GAC GAG GGT TGG
#4381		AGT GAT GCC ATT ACC AAC GC
#4382		GCT TTT GTG ATG AAC GGG AG
#3730		AGTGTGGAGAGGCCGAAAG
MA1019		TGTGCAAATATACTGGAGTGGA
MA1020		GCGCTTCGTCGAAAAATGGA

MA1021		GGATGTCCCTGTGGAACTCC
MA1022		TGGAAGCTGTTACTGACTGTGA
MA1023		AAGAAATGGACGCGGTCTGT
MA1024		GCCCAAGTCTATGCAAGGGA
SJ895		CTC GTG GTG CCT ATG GTA GC
SJ896		GCT ACC ATA GGC ACC ACG AG

sgRNA sequences for CRISPR/Cas9 genome editing (deletion)

Gene	**sgRNA sequence**
R06A4.2	GCATGTCGAGATTCTACTGG
	GCTTCAAAATTTCTCCAGGG
T12E12.3	ACATGAGTCTGTGTTTACGG
	ACGGCTCATAAGAGACTTGG

Protospacer and donor template sequences for CRISPR/Cas9 genome editing (endogenous tag)

Name	**Sequence (5' to 3')**
*dpy-10*_protospacer_1	GCT ACC ATA GGC ACC ACG AG(CGG)
*unc-58*_protospacer_1	ATC CAC GCA CAT GGT CAC TA(CGG)
*R06A4.2*_protospacer_1	GCG CTC ATT GAG GCT GAT TT(TGG)
*T12E12.3*_protospacer_1	CAA GTT CAA CAG TTA TTG GT(TGG)
SJP012_*R06A4.2*_PCR_donor_GFP	GAA GCT TTG ATC GAA GCC GAC TTT GGG CCA ACC AAT GGA TCC GGA GGT GGA GGT AGT AAA GGA GAA GAA TTG TTC ACT GGA GTT GTC CCA ATC CTC GTC GAG CTC GAC GGA GAC GTC AAC GGA CAC AAG TTC TCC GTC TCC GGA GAG GGA GAG GGA GAC GCC ACC TAC GGA AAG CTC ACC CTC AAG TTC ATC TGC ACC ACC GGA AAG CTC CCA GTC CCA TGG CCA ACC CTC GTC ACC ACC TTC TGC TAC GGA GTC CAA TGC TTC TCC CGT TAC CCA GAC CAC ATG AAG CGT CAC GAC TTC TTC AAG TCC GCC ATG CCA GAG GGA TAC GTC CAA GAG CGT ACC ATC TTC TTC AAG GTA AGT TTA AAC ATA TAT ATA CTA ACT ACT GAT TAT TTA AAT TTT CAG GAC GAC GGA AAC TAC AAG ACC CGT GCC GAG GTC AAG TTC GAG GGA GAC ACC CTC GTC AAC CGT ATC GAG CTC AAG GTA AGT TTA AAC AGT TCG GTA CTA ACT AAC CAT ACA TAT TTA AAT TTT CAG GGA ATC GAC TTC AAG GAG GAC GGA AAC ATC CTC GGA CAC AAG CTC GAG TAC AAC TAC AAC TCC CAC AAC GTC TAC ATC ATG GCC GAC AAG CAA AAG AAC GGA ATC AAG GTC AAC TTC AAG GTA AGT TTA AAC ATG ATT TTA CTA ACT AAC TAA TCT GAT TTA AAT TTT CAG ATC CGT CAC AAC ATC GAG GAC GGA TCC GTC CAA CTC GCC GAC CAC TAC CAA CAA AAC ACC CCA ATC GGA GAC GGA CCA GTC CTC CTC CCA GAC AAC CAC TAC CTC TCC ACC CAA TCC GCC CTC TCC AAG GAC CCA AAC GAG AAG CGT GAC CAC ATG GTC CTC CTC GAG TTC GTC ACC GCC GCC GGA ATC ACC CAC

	GGA ATG GAC GAG CTC TAC AAG TAA ATA GAT TTT GAA GTT CTG TTT TTT TCT TTT TCC C
SJP015_*T12E12.3*_PCR_donor_GFP	CTC ATC GAG GTT GAT TTT GGG CCA ACT AAC AAT TGC GGA TCC GGA GGT GGA GGT AGT AAA GGA GAA GAA TTG TTC ACT GGA GTT GTC CCA ATC CTC GTC GAG CTC GAC GGA GAC GTC AAC GGA CAC AAG TTC TCC GTC TCC GGA GAG GGA GAG GGA GAC GCC ACC TAC GGA AAG CTC ACC CTC AAG TTC ATC TGC ACC ACC GGA AAG CTC CCA GTC CCA TGG CCA ACC CTC GTC ACC ACC TTC TGC TAC GGA GTC CAA TGC TTC TCC CGT TAC CCA GAC CAC ATG AAG CGT CAC GAC TTC TTC AAG TCC GCC ATG CCA GAG GGA TAC GTC CAA GAG CGT ACC ATC TTC TTC AAG GTA AGT TTA AAC ATA TAT ATA CTA ACT ACT GAT TAT TTA AAT TTT CAG GAC GAC GGA AAC TAC AAG ACC CGT GCC GAG GTC AAG TTC GAG GGA GAC ACC CTC GTC AAC CGT ATC GAG CTC AAG GTA AGT TTA AAC AGT TCG GTA CTA ACT AAC CAT ACA TAT TTA AAT TTT CAG GGA ATC GAC TTC AAG GAG GAC GGA AAC ATC CTC GGA CAC AAG CTC GAG TAC AAC TAC AAC TCC CAC AAC GTC TAC ATC ATG GCC GAC AAG CAA AAG AAC GGA ATC AAG GTC AAC TTC AAG GTA AGT TTA AAC ATG ATT TTA CTA ACT AAC TAA TCT GAT TTA AAT TTT CAG ATC CGT CAC AAC ATC GAG GAC GGA TCC GTC CAA CTC GCC GAC CAC TAC CAA CAA AAC ACC CCA ATC GGA GAC GGA CCA GTC CTC CTC CCA GAC AAC CAC TAC CTC TCC ACC CAA TCC GCC CTC TCC AAG GAC CCA AAC GAG AAG CGT GAC CAC ATG GTC CTC CTC GAG TTC GTC ACC GCC GCC GGA ATC ACC CAC GGA ATG GAC GAG CTC TAC AAG TGA ACT TGT TTT TTT TCT ATT CTT CCA TTC AAT TTC
SJ665_*dpy-10*_ssODN_donor_*cn64*	CAC TTG AAC TTC AAT ACG GCA AGA TGA GAA TGA CTG GAA ACC GTA CCG CAT GCG GTG CCT ATG GTA GCG GAG CTT CAC ATG GCT TCA GAC CAA CAG CCT AT
SJ763_*unc-58*_ssODN_donor_*e665*	ATT TTG TGG TAT AAA ATA GCC GAG TTA GGA AAC AAA TTT TTC TTT CAG GTT TCT CAG TAG TGA CCA TGT GCG TGG ATC TTG CGT CCA CAC ATC TCA AGG CGT ACT T
SJ985_*R06A4.2*_ssODN_donor_3xFlag	GGG AAA AAG AAA AAA ACA GAA CTT CAA AAT CTA TTT ATC TCT TGT CAT CGT CAT CCT TGT AAT CAC GCT TGT CGT CGT CGT CCT TGT AGT CAC GCT TAT CGT CAT CGT CTT TAT AAT CAC CTC CAC CTC CGG ATC CAT TGG TTG GCC CAA AGT CGG CTT CGA TCA AAG CTT CCC GGA TGG CTT CTG TGC GCA CTT CGA G
SJ1046_*R06A4.2*_ssODN_donor_d10	GGG AAA AAG AAA AAA ACA GAA CTT CAA AAT CTA TTT ACC GCT CGT GGT GCC TAT GGT AGC CAT TGG TTG GCC CAA AGT CGG CTT CGA TCA AAG CTT CCC GGA TGG CTT CTG TGC GCA CTT CGA G
SJ1106_*T12E12.3*_ssODN_donor_d10	GAA ATT GAA TGG AAG AAT AGA AAA AAA ACA AGT TCA CCG CTC GTG GTG CCT ATG GTA GCC GCA ATT GTT AGT TGG CCC AAA ATC AAC CTC GAT GAG CGC TTT TCG

Oligonucleotide combinations for *C. elegans* genotyping

Gene	Chromosome	Allele	Amplicon (bp)	Oligo combination
R06A4.2	II	wild-type	2100	#3691 + #3992
		xf133	607	

		xf134	375	
		wild-type	305	#4378 + #4379
		xf201	404	
		wild-type	305	#4378 + #4379
		xf218	329	
		xf218	231	#4378 + SJ895
		wild-type	305	#4378 + #4379
		xf225	1184	
		xf225	414	#4378 + #4380
T12E12.3	IV	wild-type	901	#3687 + #3688
		xf131	282	
		wild-type	488	#4381 + #4382
		xf234	512	
		xf234	321	SJ896 + #4382
		wild-type	488	#4381 + #4382
		xf235	1366	
		xf235	393	#4381 + #4380
		wild-type	3000	#3693 + #3694
		xfls148	2800	#3693 + #2346
pot-2	II	wild-type	852	#1679 + #1680
		tm1400	524	
		wild-type	712	#3730 + #1680
mrt-1	I	wild-type	855	MA1022 + MA1024
		tm1354	307	
		wild-type	507	MA1023 + MA1024
trt-1	I	wild-type	1650	MA1019 + MA1021
		ok410	207	
		wild-type	507	MA1020 + MA1021
lig-4	III	wild-type	470	#3686 + #3685
		ok716	320	#3684 + #3685

Media

Medium	**Composition**
NGM plates	0.3% (w/v) NaCl
	0.25% (w/v) Peptone

	1.7% (w/v) Agar 5 mg/L Cholesterol 1 mM $CaCl_2$ 1 mM $MgSO_4$ 25 mM Potassium phosphate buffer
LB Luria	1% (w/v) Tryptone 1% (w/v) NaCl 0.5% (w/v) Yeast extract pH 7.0 w NaOH
LB Agar plates	1% (w/v) Tryptone 1% (w/v) NaCl 0.5% (w/v) Yeast extract pH 7.0 w NaOH 1.5% (w/v) Agar supplements dependent on plasmids 100 µg/mL Ampicillin 50 µg/mL Kanamycin 50 µg/mL Spectinomycin
YPD (yeast extract peptone dextrose)- medium	10% (w/v) Peptone 5% (w/v) Yeast extract 2% (w/v) Glucose 0.192% (w/v) Synthetic Dropout medium
YPD plates	10% (w/v) Peptone 5% (w/v) Yeast extract 2% (w/v) Glucose 0.192% (w/v) Synthetic Dropout medium 6.5% (w/v) YPD Agar
Droput Powder (provided by Ulrich Lab, IMB)	20 g each of aminoacid w/o adenine, histidine, leucine, tryptophane or uracil 2 g p-aminobenzoic acid
Synthetic complete powder (provided by Ulrich Lab, IMB)	36.7 g dropout powder 2 g Uracil depending on specific SC needed: 0.5 g adenine 2 g histidine

	4 g leucine 2 g tryptophane
2.5x Synthetic complete (SC-) medium (provided by Ulrich Lab, IMB)	0.425% (w/v) Yeast Nitrogen base 1.25% (w/v) Ammonium sulfate 0.5% (w/v) specific SC powder
1x SC medium	20% (v/v) 2.5x SC medium 1% (w/v) Glucose
SC medium plates	20% (v/v) 2.5x SC medium 1% Glucose 2% Agar
YG medium	2% (w/v) Yeast extract 0.5% (w/v) NaCl 3.5% (v/v) Glycerol
Auto induction medium	2% (w/v) Peptone 3% (w/v) Yeast extract 25 mM Potassium phoshate buffer (from 1 M stock) 0.05% (w/v) Glucose 2.2% (w/v) Lactose 0.5% (v/v) Glycerol 50 mM NH_4Cl 5 mM Na_2SO_4 2 mM $MgSO_4$ 1x TMS

Solutions and Buffers

Buffer/Solution	**Composition**
MS Destaining buffer	50% (v/v) 50 mM ABC 50% (v/v) Ethanol 99.9% p.a
MS Reduction buffer	50 mM ABC 10 mM DTT
MS Alkylation buffer	50 mM ABC 50 mM IAA
MS Digestion buffer	50 mM ABC
MS Trypsin solution	50 mM ABC
	1 µg Trypsin (per sample)

MS Extraction buffer	30% Acetonitrile
MS Digestion buffer (DML)	50 mM TEAB
MS DML light label	4% (v/v) Formaldehyde in H_2O
MS DML medium label	4% (v/v) Formaldehyde -D2 in H_2O
MS DML NaBH3CN solution	0.6 M NaBH3CN in H_2O
MS DML Ammonia solution	1% (v/v) Ammonia solution in H_2O
MS DML Formic Acid solution	10% (v/v) Formic acid in H_2O
MS Buffer A	0.1% (v/v) Formic Acid in HPLC grade H_2O
MS Buffer B	80% (v/v) Acetonitrile 0.1% (v/v) Formic Acid HPLC grade H2O
M9 Buffer w azide	1x M9 Buffer 40 mM Sodium azide
FISH Egg buffer	25 mM Hepes/KOH pH 7.4 118 mM NaCl 48 mM KCl 2 mM EDTA 0.5 mM EGTA 1% (v/v) Tween-20
10x PBS	100 mM Na_2HPO_4 20 mM KH_2PO_4 1.37 M NaCl 27 mM KCl
FISH Permeabilization buffer	20 mM Tris/HCl pH 7.5 50 mM NaCl 3 mM $MgCl_2$ 300 mM Sucrose 0.5% Triton X-100
FISH RNase A solution	1x PBS 0.1% Tween-20 10 µg/ml RNase A
PBS-T (western blot, FISH)	1x PBS 0.1% Tween-20
FISH Hybridization solution	3x SSC 50% (v/v) Formamide

	10% (v/v) Dextran sulfate 50 µg/ml Heparin 100 µg/ml Yeast tRNA 100 µg/ml sheared Salmon sperm DNA
FISH Hybridization wash solution	2x SSC 50% Formamide
TRF Transfer buffer	0.6 M NaCl 0.4 M NaOH
TRF Fixing solution	0.4 M NaOH
20x SSC (pH 7.0)	3 M NaCl 0.3 M Sodium citrate
TRF Hybridization buffer	3.3x SSC 0.1% (w/v) SDS 1 mg/ml Skim Milk powder
TRF Wash buffer 1	2x SSC 0.1% (w/v) SDS
TRF Wash buffer 2	0.2x SSC 0.1% (w/v) SDS
PBS-T (acetone fixation)	1x PBS 0.1% Triton X-100
Single Worm Lysis buffer	50 mM KCl 2.5 mM MgCl2 10 mM Tris/HCl pH 8.3 0.45% (v/v) Igepal CA-630 0.45% (v/v) Tween-20 0.01% (w/v) Fish Skin gelatin 20 µg/ml Proteinase K
10x M9 Buffer	0.22 M KH_2PO_4 0.42 M Na_2HPO4 0.85 M NaCl 10 mM $MgSO_4$
Worm Bleaching solution	1.5% (v/v) Sodium hypochloride 0.625 M NaOH
Nuclear extraction buffer	40 mM NaCl 20 mM Mops pH 7.5

	90 mM KCl 2 mM EDTA 0.5 mM EGTA 10% (v/v) Glycerol 2 mM DTT 1x cOmplete protease inhibitors (Roche)
Buffer C+	0.42 M NaCl 20 mM Hepes/KOH pH 7.9 2 mM $MgCl_2$ 0.2 mM EDTA 20% (v/v) Glycerol 0.1% (v/v) Igepal CA-630 0.5 mM DTT 1x cOmplete protease inhibitors (Roche)
2x Lysis buffer worms	50 mM Tris/HCl pH 7.5 0.3 M NaCl 3 mM $MgCl_2$ 2 mM DTT 0.2% (v/v) Triton X-100 1 tablet cOmplete protease inhibitors (Roche) per 50 ml
1x Lysis buffer worms (embryos)	25 mM Tris/HCl pH 7.5 0.15 M NaCl 1.5 mM $MgCl_2$ 1 mM DTT 0.1% (v/v) Triton X-100 1 tablet cOmplete protease inhibitors (Roche) per 50 ml
Worm Lysis buffer (gDNA/RNA)	0.2 M NaCl 0.1 M Tris/HCl pH 8.5 50 mM EDTA 0.5% (w/v) SDS
Annealing buffer	0.2 M Tris/HCl pH 8.0 0.1 M $MgCl_2$ 1 M KCl
PBB Buffer	50 mM Tris/HCl pH 7.5 0.15 M NaCl

	0.5% (v/v) Igepal CA-630 5 mM $MgCl_2$ before use add: 1 mM DTT
GFP IP wash buffer	10 mM Tris/HCl pH 7.5 0.15/0.3 M NaCl 0.5 mM EDTA 1:1000 Pepstatin A/Leupeptin 1:100 PMSF for Sm nuclease addition: 2 mM $MgCl_2$ 0.05% (v/v) Sm nuclease
FLAG IP wash buffer	25 mM Tris/HCl pH 7.5 0.3 M NaCl 1.5 mM $MgCl_2$ 1 mM DTT 1 tablet cOmplete protease inhibitors (Roche) per 50 ml For Sm nuclease addition: 0.05% (v/v) Sm nuclease
1000 x Trace Metal solution (TMS)	50 mM $FeCl_3$ 20 mM $CaCl_2$ 10 mM $Mn(II)Cl_2$ 10 mM $ZnCl_2$ 2 mM $CoCl_2$ 2 mM $Cu(II)Cl_2$ 2 mM $NiCl_2$ 2 mM $NaMoO_4$ 2 mM Na_2SeO_3
Tris Buffer for *E. coli* harvest (POT-2 protein)	50 mM Tris/HCl pH 7.5 0.1 M NaCl 10 mM MgCl2 1x cOmplete protease inhibitors (Roche)
Lysis buffer for *E. coli* (R06A4.2 and T12E12.3 proteins)	25 mM Tris/HCl pH 7.5 0.3 M NaCl 20 mM Imidazole

	1 mM DTT
Purification binding buffer (FP)	20 mM Tris/HCl pH 7.5 0.5 M NaCl 50 mM Imidazole 1 mM DTT 1x cOmplete protease inhibitors (Roche) For lysis only: 100 µg Dnase I
Purification elution buffer (FP)	20 mM Tris/HCl pH 7.5 0.5 M NaCl 0.5 M Imidazole 1 mM DTT
Purification dialysis buffer (FP)	20 mM Tris/HCl pH 7.5 0.15 M NaCl 1 mM $MgCl_2$ 10% (v/v) Glycerol 1 mM DTT
Fluorescence polarization (FP) buffer	20 mM HEPES/KOH pH 7.0 0.1 M NaCl 5% (v/v) Glycerol
Western blot Transfer buffer	25 mM Tris 192 mM Glycine 20% (v/v) Methanol
10x TBS	0.5 M Tris/HCl pH 7.6 1.5 M NaCl
TBS-T (His-western blot)	1x TBS 0.1% (v/v) Tween-20 0.5% (v/v) Triton X-100
Skim Milk solution (western blot)	1x PBS 0.1% (v/v) Tween-20 5% (w/v) Skim Milk powder
Y2H SORB solution	100 mM LiAc 10 mM Tris/HCl pH 8 1 mM EDTA 1 M Sorbitol
Y2H PEG solution	100 mM LiAc

	10 mM Tris/HCl pH 8 1 mM EDTA 40% (w/v) PEG3350
Y2H NaOH/2-Mercaptoethanol solution	1.85 M NaOH 7.5% (v/v) 2-Mercaptoethanol
Gelfiltration buffer	25 mM Tris/HCl pH 7.5 0.15 M NaCl 2 mM DTT 1 tablet cOmplete protease inhibitors (Roche) per 50 ml
EMSA Binding buffer	20 mM HEPES/KOH pH 7.8 25 mM KCl 1.25 mM $MgCl_2$ 1 mM DTT 10 ng/µl yeast tRNA 10% (v/v) Glycerol
EMSA Loading dye	50% (v/v) Glycerol Bromphenolblue
Purification lysis buffer (EMSA)	50 mM/20 mM Tris/HCl pH 8 (POT-2/R06A4.2) 0.5 M NaCl 20 mM/50 mM Imidazole (POT-2/R06A4.2) 1 mM PMSF 100 µg Dnase I for R06A4.2: 5 mM $MgCl_2$
Purification binding buffer (EMSA)	50 mM/20 mM Tris/HCl pH 8 (POT-2/R06A4.2) 0.5 M NaCl 20 mM/50 mM Imidazole (POT-2/R06A4.2) 1 mM PMSF for R06A4.2: 5 mM $MgCl_2$
Purification elution buffer (EMSA)	50 mM Tris/HCl pH 8 0.5 M NaCl 0.2 M/0.5 M Imidazole (POT-2/R06A4.2) for R06A4.2: 5 mM $MgCl_2$
Purification dialysis buffer (EMSA)	50 mM/20 mM Tris/HCl pH 8 (POT-2/R06A4.2) 0.5 M NaCl 10% (v/v) Glycerol

	for R06A4.2: 5 mM $MgCl_2$ 1 mM DTT

Antibodies and reagents

Antibodies	Supplier	Identifier/Order-No.
Mouse anti-FLAG M2 antibody	Sigma-Aldrich	#F3165; RRID: AB_259529
Mouse anti-GFP antibody	Roche/Sigma-Aldrich	#11814460001; RRID: AB_390913
Rabbit anti-Actin antibody	Sigma-Aldrich	#A2066; RRID: AB_476693
Anti-mouse IgG, HRP-linked antibody	Cell Signaling Technology	#7076; RRID: AB_330924
Anti-rabbit IgG, HRP-linked antibody	GE Healthcare	#NA934; RRID: AB_772206
IRDye 680RD anti-mouse IgG antibody	LI-COR	#926-68072; RRID: AB_10953628
IRDye 800CW anti-rabbit IgG antibody	LI-COR	#926-32213; RRID: AB_621848
GAL4 DBD antibody (RK5C1)	Santa Cruz Biotechnology	#sc-510; RRID: AB_627655
GAL4-TA antibody (C-10)	Santa Cruz Biotechnology	#sc-1663; RRID: AB_669111

Reagent	Supplier	Cat. No
$^{[32]}$P labeled gamma-ATP	Hartmann Analytic	#SRP-301
1 Kb extended DNA marker	New England BioLabs	#N3239
20 gauge needles	Sterican/Roth	#C718.1
2-mercaptoethanol	Roth	#4227.3
2x Gibson Assembly Master Mix	IMB Protein Production CF	-
4-15% Criterion TGX stain-free protein gel	BioRad	#5678085
4x NuPAGE LDS sample buffer	Thermo Fisher Scientific	#NP0008
5x Protein Assay Dye Reagent concentrate	BioRad	#500-0006
Acetone	Roth	#9372.6
Acetonitrile	VWR	#20048.320
Acrylamide/Bis-Acrylamide 30% solution	Sigma-Aldrich	#A3574
Adenosin-triphosphate (ATP)	Sigma-Aldrich	#A2383
Agar	Sigma-Aldrich	#A5306
Agarose	Sigma-Aldrich	#A9539
Amicon Ultra 10kDa centrifugal filter unit	Merck	#UFC5010
Ammonia solution	Sigma-Aldrich	#30501
Ammonium chloride (NH_4Cl)	Roth	#K298.1
Ammonium persulfate (APS)	Sigma-Aldrich	#09913
Ammoniumbicarbonate (ABC, NH_4HCO_3)	Sigma-Aldrich	A6141-500G
Ampicillin		
Biodyne B membrane (telomere southern blot)	Pall	#60207
Biotin-7-dATP	Jena Bioscience	#NU-835-BIO
Biotinylated 5x telomeric/control repeat oligonucleotides	Metabion	-

BP Clonase II enzyme mix	Thermo Fisher Scientific	#11789020
BSA	Sigma-Aldrich	#A3294
C18 MS column	New Objective	#FS360-75-8-N-5-C30
Calcium chloride ($CaCl_2$)	Roth	#5239.1
Chloroform	Roth	#3313.4
Cholesterol	Sigma-Aldrich	#C3045
Cobalt(II) chloride (CoCl2)	Sigma-Aldrich	#232696
cOmplete Mini EDTA-free protease inhibitor tablets	Roche/Sigma-Aldrich	#4693159001
Copper(II) chloride ($Cu(II)Cl_2$)	Sigma-Aldrich	#212946
Cover slips	Langenbrinck	#01-2222/5/get.
Dextran Sulfate	Sigma-Aldrich	#S4030
di-Sodium hydrogen phosphate (Na_2HPO_4)	Roth	#4984.1
Dithiothreitol (DTT)	Sigma-Aldrich	#D0632
DMSO	Sigma-Aldrich	#D2650
DnaseI	New England BioLabs	#M0303
dNTPs (4x 100 mM)	Jena Bioscience	#NU-1005S
DpnI	New England BioLabs	#R0176
Dynabeads MyOne Streptavidin C1	Thermo Fisher Scientific	#65001
Dynabeads ProteinG	Thermo Fisher Scientific	#10004D
EGTA	Sigma-Aldrich	#E3889
Empore C18	3M	#15334911
Ethanol 99.9% p.a	Roth	#9065.3
Fish Skin Gelatin	Sigma-Aldrich	#G7041
FITC-labeled oligonucleotides	Metabion	-
Formaldehyde solution	Sigma-Aldrich	#F8775
Formaldehyde-D2 solution	Sigma-Aldrich	#492620
Formamide	Roth	#6749.1
Formic acid	Merck	#1.00264.1000
Gel filtration size standard	BioRad	#1511901
GeneRuler 1 Kb	Thermo Fisher Scientific	#SM0312
GFPtrap MA, magnetic agarose GFP beads	Chromotek	#gtma-20
Glucose	Sigma-Aldrich	#G7021
Glycerol	Honeywell	#15523-1L-R-D
Heparin	Sigma-Aldrich	#H3393
Hepes	Roth	#HN78.2
Herring testes DNA	Sigma-Aldrich	#D6898
HinfI	New England BioLabs	#R0155
HisTRAP HP column 1 ml	GE Healthcare	#GE17-5247-01
Hydrochloric acid (HCl)	Roth	#4625.1
Igepal CA-630	Sigma-Aldrich	#I8896
Imidazole	Sigma-Aldrich	#56750
Iodoacetamide (IAA)	Sigma-Aldrich	#I6125
IPTG	Roth	#CN08.3
Iron(III) chloride ($FeCl_3$)	Sigma-Aldrich	#157740
Ispopropanol	Roth	#9866.6
Kanamycin		
Klenow fragment -exo	Thermo Fisher Scientific	#EP0422
Lactose	Sigma-Aldrich	#61341

Leupeptin	Serva	#51867.03
Lithium acetate (LiAc)	Sigma-Aldrich	#L4158
LR Clonase II enzyme mix	Thermo Fisher Scientific	#11791020
Magnesium chloride ($MgCl_2$)	Sigma-Aldrich	#M2670
Magnesium sulfate ($MgSO_4$)	Sigma-Aldrich	#M7506
Manganese(II) chloride tetrahydrate ($Mn(II)Cl_2$)	Roth	#0276.2
Methanol (MS grade)	VWR	#20864320
Microspin sephadex G-50 columns	GE Healthcare	#GE27-5330-01
Nickel(II) chloride ($NiCl_2$)	Sigma-Aldrich	#339350
Nitrocellulose Western Blot membrane	BioRad	#1620112
NuPAGE 10% Bis-Tris gel, 10 well	Thermo Fisher Scientific	#NP0301
NuPAGE 20x MOPS running buffer	Thermo Fisher Scientific	#NP0001
NuPAGE 4-12% Bis-Tris gel, 10 well	Thermo Fisher Scientific	#NP0321
OneTaq DNA polymerase	New England BioLabs	#M0480
PD-10 Desalting column	GE Healthcare	#GE17-8051-01
PEG3350	Sigma-Aldrich	#202444
PEG6000	part of Kit Thermo Fisher Scientific	-
Pepstatin A	Serva	#52682.02
Peptone	Sigma-Aldrich	#70173
Pfu Ultra II polymerase	Agilent	#600672
Phenol:Chloroform:isoamyl alcohol (25:24:1)	Invitrogen/Thermo Fisher Scientific	#15593049
Phenylmethylsulfonyl fluoride (PMSF)	Serva	#32395.03
Phosphor storage screen	GE Healthcare	#28956474
PNA telomeric FISH probe	Panagene	
Poly-L slides	Sigma-Aldrich	#P0425
Ponceau S solution	Applichem	#A2935
Potassium chloride (KCl)	Roth	#6781.1
Potassium di-hydrogen phosphate, monobasic (KH_2PO_4)	Roth	#P018.2
Potassium hydroxide (KOH)	Roth	#7986.1
Proteinase K	Sigma-Aldrich	#P2308
Protran Nitrocellulose membrane (Western Blot)	Amersham/VWR	#10600002
Recombinase A	New England BioLabs	#M0249
RNase A	Sigma-Aldrich	#R5503
RsaI	New England BioLabs	#R0167
Salmon sperm	Ambion/Thermo Fisher Scientific	#AM9680
SDS	Roth	#4360.1
Skim Milk powder	Sigma-Aldrich	#70166
Sm nuclease	IMB Protein Production CF	-
Sodium azide	Sigma-Aldrich	#S2002
Sodium chloride (NaCl)	Thermo Fisher Scientific	#15626770
Sodium citrate	Sigma-Aldrich	#25114
Sodium cyanoborohydride ($NaBH_3CN$)	Sigma-Aldrich	#156159
Sodium hydroxide (NaOH)	Roth	#6771.1
Sodium hypochloride solution	Roth	#9062.3
Sodium molybdate ($NaMoO_4$)	Sigma-Aldrich	#243655
Sodium selenite (Na_2SeO_3)	Sigma-Aldrich	#214485
Sodium sulfate (Na_2SO_4)	Sigma-Aldrich	#S9627

Sorbitol	Sigma-Aldrich	#85529
Spectinomycin	Sigma-Aldrich	#S4014
Sucrose	Sigma-Aldrich	#S7903
Superose 6 10/300 GL size exclusion column	GE Healthcare	#17517201
SuperSignal West Pico plus Chemiluminescent Substrate	Thermo Fisher Scientific	#15626144
Sybr Safe DNA stain	Thermo Fisher Scientific	#S33102
T12E12.3 gene block	IDT	-
T4 DNA Ligase	Thermo Fisher Scientific	#EL0011
T4 Polynucleotid Kinase	New England BioLabs	#M0201
Taq polymerase homemade	IMB Protein Production CF	-
TEMED	Sigma-Aldrich	#T9281
Thermo-Fast 24 PCR Plate	Thermo Fisher Scientific	#10542645
Trichloroacteic acid (TCA)	Sigma-Aldrich	#T6399
Triethylammonium bicarbonate buffer (TEAB)	Sigma-Aldrich	#18597
Triton X-100	Sigma-Aldrich	#X100
Trizma Base	Sigma-Aldrich	#T1503
TRIzol LS reagent	Invitrogen/Thermo Fisher Scientific	#10296010
Trypsin (proteomics grade)	Sigma-Aldrich	#T6567
Tween-20	Sigma-Aldrich	#P7949
Vectashield mounting medium with DAPI	Vector Laboratories	#H-1200-10
Whatman paper	GE Healthcare	#WHA10426892
Yeast Extract	Sigma-Aldrich	#70161
yeast tRNA	Thermo Fisher Scientific	#11518736
Zinc chloride ($ZnCl_2$)	Sigma-Aldrich	#96468
Zirkonia beads (0.1 mm)	Roth	#N033.1

Instruments

Instrument	**Supplier**
EASY-nLC 1000 system	Thermo Scientific
QExactive Plus mass spectrometer	Thermo Scientific
Electrospray Ion source (Nanospray flex)	Thermo Scientific
Branson sonifier 450	Branson Ultrasonics Corp.
BioRuptor Plus	Diagenode
Fastprep-24	MP Biomedicals
DM6000	Leica
AF7000 widefield	Leica
SP5 confocal microscope	Leica
SPE STED confocal microscope	Leica
EL6000 Fluorescence lamp	Leica
M80 stereomicroscope	Leica
Ultracentrifuge	Beckmann Coulter

LM10 Microfluidizer	Microfluidics
IPC Microprocessor controlled dispensing pump	Ismatec
Tecan Spark 20M	Tecan
Typhoon FLA 9000	GE Healthcare
Chemidoc XRS+	BioRad
Thermocycler	BioRad/Biometra

Software

Name	**Link/Distributor**
MaxQuant (V. 1.5.2.8)	MaxQuant
R	The R foundation
R-studio	R Studio Inc
Image Lab 5.2	BioRad
Excel 2016	
Word 2016	Microsoft
Powerpoint 2016	
Adobe Illustrator 2020	Adobe
Prism 8	Graph Pad
Image Studio 3.1	LI-COR
ApE plasmid editor	https://jorgensen.biology.utah.edu/wayned/ape/
EMBOSS Needle	https://www.ebi.ac.uk/Tools/psa/emboss_needle/
HHPred	https://toolkit.tuebingen.mpg.de/tools/hhpred
Oasis2	https://sbi.postech.ac.kr/oasis2/surv/#
NEBioCalculator	https://nebiocalculator.neb.com/#!/ligation
LAS X	Leica
Fiji	Image J
Mendeley Desktop	Elsevier

Commercial assays and kits

Assay	**Supplier**	**Cat. No**
QIAprep Spin Miniprep Kit	Qiagen	#27106
QIAquick PCR Purification Kit	Qiagen	#28104
MinElute PCR Purification Kit	Qiagen	#28004
Penta-His HRP Conjugate Kit	Qiagen	#34460
Monarch DNA Gel Extraction Kit	New England BioLabs	#T1020

PureLink HiPure Plasmid Miniprep Kit	Invitrogen/Thermo Fisher Scientific	#K210002
PureLink HiPure Plasmid Midiprep Kit	Invitrogen/Thermo Fisher Scientific	#K210004
First strand cDNA Synthesis Kit	Thermo Fisher Scientific	#K1612
pCR8 GW/TOPO	Fisher Scientific	#10532893

Methods

DNA pulldown for telomeric interactors

Biotinylated telomeric and control DNA for the DNA pulldown for detection of telomeric interactors was prepared as previously published (Kappei et al. 2013; Casas-Vila et al. 2015; Kappei et al. 2017).

Preparation of polymerized telomere/control DNA. 25 µl of 10-mer repeat oligonucleotides of either telomeric or control sequence were mixed 1:1 with 25 µl of their respective reverse complement oligonucleotide and 10 µl Annealing buffer. The mixture was brought to 100 µl final volume with H_2O and heated at 80°C for 5 min in a thermoshaker. After incubation, the oligonucleotides were left to cool down in the switched off thermoshaker. Once at RT, the samples were supplemented with 55 µl H_2O, 20 µl 10x T4 DNA ligase buffer (Thermo Fisher Scientific), 10 µl PEG 6000, 10 µl 100 mM ATP, 2 µl 1M DTT and 5 µl T4 Polynucleotide Kinase (New England BioLabs) and left at 37°C for 2 h to concatenate. Finally, 4 µl of T4 DNA Ligase (Thermo Fisher Scientific) were added and the samples incubated at RT over night for ligation and polymerization. The ligation process was monitored by running 1 µl of the reaction on a 1% agarose gel, checking the length of oligomerization. The samples were cleaned by phenol-chloroform extraction. For this, 1 vol. of H_2O and 200 µl of Phenol/Chloroform/Isoamyl Alcohol (Thermo Fisher Scientific) was added to the mixture, vortexed and centrifuged at 16,000 xg for 2 min. After centrifugation the aqueous phase was transferred to a fresh tube and the DNA precipitated by addition of 1 ml 100% Ethanol and incubation at -20°C for 30 min. To pellet the cleaned DNA the mixture was centrifuged at 16,000 xg for 45 min at 4°C. The resulting DNA pellet was resuspended in 74 µl H_2O and 10 µl 10x Klenow-fragment reaction buffer (Thermo Fisher Scientific), 10 µl 0.4 mM Biotin-7-dATP (Jena Bioscience) as well as 6 µl Klenow-Fragment exo- polymerase (Thermo Fisher Scientific) were added. Biotinylation was carried out by incubation at 37°C over night. The excess biotin and enzymes were removed by size exclusion chromatography using MicroSpin Sephadex G-50 columns (GE Healthcare).

Pulldown. For each pulldown sample 20 µl biotinylated DNA were mixed with 200 µl PBB Buffer and 50 µl of Dynabeads MyOne Streptavidin C1 (Thermo Fisher Scientific) beads. The beads and DNA were incubated at RT for 15 min on a rotating wheel for immobilization. After three washes with 500 µl PBB Buffer, the DNA coupled beads were resuspended in 150 µl PBB buffer. As competitor for unspecific DNA binding 1.5 µl Salmon sperm (Ambion/Thermo Fisher Scientific) were added. Protein extract was added and the samples incubated at 4°C on a rotating wheel for 90 min. Following incubation the beads were washed three times with 500 µl PBB Buffer and resuspended in 25 µl 1x NuPAGE LDS sample buffer (Thermo Fisher Scientific) supplemented with 100 mM DTT. For elution the samples were boiled at 70°C for 10 min and afterwards loaded on a Bis-Tris gel (NuPAGE, 10% for IP-MS; 4-12% for initial LFQ screen and western blot, Thermo Fisher Scientific). For IP-MS experiments these pulldowns were prepared in either technical quadruplicates (LFQ) or technical duplicates (DML) per condition, whereas for IPs followed by western blot all conditions were prepared with one replicate and an input control. For the LFQ and DML telomeric pulldowns as well as the *E. coli* recombinant protein pulldown 200-400 µg of nuclear enriched worm extract or *E. coli* lysate were used, respectively. DNA pulldowns with endogenous *C. elegans* proteins were prepared with 400-700 µg worm lysate of the respective stage.

In gel digest

In-gel digestion for MS was performed as previously described (Shevchenko et al. 2007). Samples were run on a 10% Bis-Tris gel (Thermo Fisher Scientific) for 10 min (IP samples) or on a 4-12% Bis-Tris gel (Thermo Fisher Scientific) for 20 min (LFQ telomere pulldown samples) at 180 V in 1x MOPS buffer (Thermo Fisher Scientific). After running, the gel was placed on a clean glass plate, the respective sample lanes excised with a clean scalpel, cut to small pieces and transferred to 1.5 ml reaction tubes. For the telomeric LFQ screens in *C. elegans* and *C. briggsae*, each sample was cut into four fractions for deeper measurement. The gel pieces were de-stained in MS Destaining buffer at 37°C in a thermoshaker at 1,400 rpm until fully destained or slightly blue. After de-staining the gel pieces incubated in 100% Acetonitrile for 10 min at 25°C shaking at 1,400 rpm until fully dehydrated. The leftover solution was dried off by using a Concentrator Plus (Eppendorf, settings V-AQ) for 5 min. For reduction the gel pieces were incubated in MS Reduction buffer at 56°C for 60 min. Afterwards the gel pieces were incubated in MS Alkylation buffer for 45 min at room temperature in the dark. After reduction and alkylation the gel pieces were washed in MS Digestion buffer for 20 min at 25°C shaking at 1,400 rpm. Following the washing step, the gel pieces were again dehydrated in Acetonitrile and dried as described above. To digest the proteins, the dried gel pieces were rehydrated in MS Trypsin solution and incubated over night at 37°C. The supernatant of trypsin solution was recovered and saved in a fresh reaction tube. Tryptic peptides were extracted from the gel pieces by incubating them in MS Extraction buffer twice for 15 min at 25°C, shaking at 1,400 rpm. The supernatant was recovered each time and combined with the previously recovered trypsin fractions. Finally, the gel pieces were dehydrated by incubation in Acetonitrile until fully dry. The acetonitrile was recovered and combined with the previously collected supernatants. The sample solution containing the tryptic peptides was reduced to 10% original volume in a Concentrator Plus (Eppendorf, settings V-AQ), and purified using the stage tip protocol.

Dimethyl Labeling

Dimethyl labeling of peptides was performed as described (Boersema et al. 2009).
The above described in gel digest was performed but the buffer base exchanged for 50 mM TEAB after the alkylation step. Using a Concentrator Plus (Eppendorf) the peptide volume was reduced to about 100 µl. To ensure proper labeling, the pH of the samples was checked to be between 5 and 8.5. If pH was too low it was adjusted by addition of 100 mM TEAB. For light and medium labeling 4 µl of 4% formaldehyde solution (Sigma-Aldrich) or 4% formaldehyde-D_2 solution (Sigma-Aldrich) were added together with 4 µl 0.6 M $NaBH_3CN$ (Sigma-Aldrich), respectively. Samples were mixed briefly by vortexing, spun down and incubated for 1 h at 20°C in a thermoshaker shaking at 1,000 rpm. The labeling reaction was quenched by addition of 16 µl a 1% ammonia solution. Further quenching and acidification of the samples was achieved by adding 4 µl of a 10% formic acid solution. The respective light and medium samples were mixed 1:1 (light telomere : medium control; medium telomere : light control) and purified by stage tip purification.

Stage tip purification

Stage tip purification was performed as previously described (Rappsilber et al. 2007). Desalting tips were prepared by stacking 2 layers of Empore C18 material (3M) in a 200 µl pipet tip. After activation of the tips with pure methanol, spinning at 500 xg, they were washed two consecutive times with MS Buffer B and MS Buffer A for 5 min at 500 xg. The tryptic peptide samples were added and centrifuged at 500 xg until no liquid was left. After one more wash with Buffer A, the peptides were eluted into a 24-well plate (Thermo Fisher Scientific) with MS Buffer B by centrifugation at 500 xg for 3 min. To evaporate the acetonitrile, the samples were centrifuged in a Concentrator Plus (Eppendorf, setting V-AQ) for 10 min and finally filled up to 14 µl with MS Buffer A. Half the volume of the samples was measured on the MS while the other half was stored at -20°C as backup.

MS measurement and data analysis

From the eluted peptides 5 µl were loaded on an in-house packed C18 column (New Objective, 25 cm long, 75 µm inner diameter) for reverse-phase chromatography. A Q Exactive Plus mass spectrometer (Thermo Fisher Scientific) was coupled to an EASY-nLC 1000 system (Thermo Fisher Scientific). The peptides were eluted from the column in an optimized 2 h gradient from 2 to 40% MS Buffer B (see above) at a flow rate of 225 nL/min. The mass spectrometer was used in a data-dependent acquisition mode with one MS full scan and up to ten MS/MS scans using HCD fragmentation. All raw files obtained in the measurements were processed with MaxQuant (version 1.5.2.8). The *C. elegans* Wormbase protein database (Version WS269), as well as the EnsemblBacteria *E. coli* REL606 database (version from September 2018) were used to detect and identify proteins of the worms and of the feeding strain OP50. Modifications set in the MaxQuant software included Carbamidomethylation (Cys) as fixed modification, as well as oxidation (Met) and protein N-acetylation as variable modifications. Trypsin was selected as the used protease including a maximum of two miscleavages. For all measurements except DML (see below) LFQ quantification was activated without the fast LFQ setting and using at least 2 LFQ ratio counts. In addition, the match between run option was active. Replicates, fractions and experimental conditions were indicated according to each measured experiment. Analysis of the resulting data was performed in R using existing libraries (e.g. reshape2, dplyr, ggplot2, ggrepel) and in-house scripts provided by the Proteomics CF, IMB. The reported protein groups were filtered by removing known contaminants, protein groups only identified by site and those marked as reverse hits. For data visualization purposes missing values were imputed at the lower end of measured LFQ values by using random values from a beta distribution fitted at 0.2-2.5%. P-values were calculated using the Welch's t-test. Enrichment values represent the mean difference of $\log_2$ transformed and imputed LFQ intensities between the telomere and the control enriched proteins. For the gelfiltration samples, mean $\log_2$ transformed LFQ intensities for each fraction and each respective protein were plotted without imputation of missing values.
For analysis of DML samples, the introduced peptide labels were indicated in the MaxQuant software as "N-terminal Dimethyl 0" and "Dimethyl 0" for the light samples as well as "N-terminal Dimethyl 4" and "Dimethyl 4" for the medium labeled samples. Here, the re-quant option was activated instead of the match between runs option. To ensure proper incorporation of the peptide labels over 95%, an incorporation check was run additionally. Protein groups resulting from MaxQuant analysis were filtered like mentioned above. The normalized ratios for each protein were $\log_2$ transformed and plotted in the scatterplot. Filtering and analysis were done in R using existing libraries and an in-house script, provided by the Proteomics CF, IMB.

In vitro single- or double-strand binding of proteins from *C. elegans* extract

Biotinylated oligonucleotides (Metabion) containing a five times repeat of the telomeric G-rich or C-rich sequence or the control sequence were used for this assay. All oligonucleotides contained unique sequences flanking both sides of the repeats to ensure accurate annealing. To anneal oligonucleotides 15 µl of the biotinylated forward oligonucleotide were mixed with 15 µl of the respective non-biotinylated reverse complement oligonucleotide and 10 µl Annealing buffer. After heating the mix at 80°C for 5 min the oligonucleotides were cooled down to RT in the switched-off thermoshaker. Single-stranded oligonucleotides were prepeared the same way, using H_2O instead of the reverse-compliment oligonucleotide. The pulldown itself was performed as described above with 0.5 mg (T12E12.3::GFP) or 0.4 mg (R06A4.2::3xFLAG) total protein extract from *C. elegans* embryos. After elution, the samples were run on a 4-12% Bis-Tris gel (Thermo Fisher Scientific) at 150 V for 120 min and transferred to a membrane. Detection of the tagged proteins was carried out as described below.

Expression of recombinant protein from *E. coli*

(IPTG induction partially performed by Emily Nischwitz, Butter laboratory, IMB)

Auto-induction. His_6-MBP-POT-2 for DNA pulldown and R06A4.2-His_5 for EMSA were expressed using auto-induction (Studier FW, 2005). An over night culture of the expression strain BL21(DE3) was grown at 37°C in 5 ml YG medium supplemented with the respective antibiotic. The next day a 2 ml YG medium pre-culture was prepared by inoculating it 1:50 with over night culture. When an OD_{600} of 0.7 the pre-culture was used to inoculate 100 ml of Auto induction medium to a density of OD_{600} 0.004. The final auto induction culture was grown at 25°C for 24 h and harvested by centrifugation.

IPTG induction. His_6-POT-2 for EMSA was expressed like published before (Raices et al. 2008). In short, LB Luria medium was inoculated 1:200 with an over night culture of BL21(DE3) cells and grown at 37°C until OD_{600} 0.6. The culture was incubated on ice for 30 min prior to induction with 250 µM IPTG and addition of 2% f.c. ethanol. After incubation for 16 h at 18°C the cells were harvested. R06A4.2-His_5 and T12E12.3-His_5 for DNA pulldown were expressed in Rosetta 2 (DE3) pLysS Competent Cells (Novagen). Here, an over night culture was grown in LB containing the respective antibiotic. The growing culture was inoculated with the over night culture and induced with 1 mM IPTG after reaching mid-log growth at 37°C. Cells were then grown at 18°C and harvested after 24 hours.

Purification of recombinant protein from *E. coli*

(IPTG lysis partially performed by Emily Nischwitz, Butter laboratory, IMB)

IPTG and auto-induction cultures were pelleted in 50 ml reaction tubes by centrifugation at 4,000xg after growth and lysed according to the protocol for the respective downstream use.

Lysate preparation for DNA pulldown. His_6-MBP-POT-2 expression pellets were resuspended in 5 ml Tris Buffer for *E. coli* harvest (POT-2 protein) and divided into 2 ml flat lid micro tubes containing ca. 600 µl of 0.1 mm zirconia beads (Roth). Cells were then lysed using the FastPrep -24™ Classic (MP Biomedicals) with 6 m/s for 30 seconds for two rounds. In between the disruption rounds, the samples were centrifuged at 21,000 xg for 2 min to pellet debris, and incubated on ice for 5 min before the second cycle. To pellet cell debis and beads, the suspension was centrifuged at 21,000 xg for 10 min at 4°C after lysis. The cell pellets for R06A4.2-His_5 and T12E12.3-His_5 expression were lysed by sonication with a Branson Sonifier 450 (duty cycle: 50%, output control: 3, duration: 3.5 min, 5 mm tip) in Lysis buffer for *E. coli* (R06A4.2 and T12E12.3 proteins), and protease inhibitor cocktail. Lysates were centrifuged at 4613 xg for 10 minutes at 4°C after sonication. For both preparation methods the supernatant was afterwards transferred to fresh reaction tubes and concentration of the extracts determined by Bradford. The DNA pulldowns were performed as described above.

Lysis and purification for EMSA. Cells expressing His_6-POT-2 and R06A4.2-His_5 for EMSA were resuspended in 20 ml Purification lysis buffer (EMSA) and lysed using a LM10 Microfluidizer at 15,000 psi for two rounds. Lysates were cleared by ultracentrifugation at 25,000 xg for 40 min at 4°C and proteins purified by running the lysates over a Purification binding buffer (EMSA) equilibrated HisTrap HP column (GE Healthcare) attached to a IPC dispensing pump (Ismatec). After loading the lysate, the column was washed with ten column volumes of Purification binding buffer and the proteins eluted with Purification elution buffer (EMSA) in 1.5 ml fractions. The fractions of purified protein were dialyzed over night at 4°C in 1 L Purification dialysis buffer (EMSA) using dialysis tubing (Sigma-Aldrich). Following dialysis, concentration of the fractions was determined by Bradford measurement and the proteins used for EMSA as described below.

Protein expression, purification and Fluorescence polarization assay

(Experiment conducted by Emily Nischwitz, Butter laboratory, IMB)

Protein expression. For expression of R06A4.2-His_5 and T12E12.3-His_5 for fluorescence polarization, *E.coli* ArcticExpress DE3 cells (Agilent) were grown over night in 5 ml LB supplemented with the respective antibiotic for the expression vector. The expression culture was inoculated from the over night culture and induced with 1 mM IPTG upon reaching mid-log growth at 30°C. The induced culture was incubated at 12°C and harvested after 24 hours.

Protein purification. The cell pellet was resuspended in Purification binding buffer (FP) with DNase I (Sigma-Aldrich) and lysed using a Branson Sonifier (duty cycle: 50%, output control: 4, duration: 3 minutes sonication, 3 minutes ice, 3 minutes sonication, 9 mm tip). Lysates were afterwards ultracentrifuged at 27,000 rpm for 30 minutes at 4°C, while equilibrating a HisTap HP column (GE Healthcare) in Purification binding buffer (FP). After loading the lysate, the column was washed with 20 ml of Purification binding buffer (FP), and proteins were eluted in Purification elution buffer (FP) in 250 µL fractions. Proteins were dialyzed with a PD-10 Desalting Column (GE Healthcare) in Purification dialysis buffer (FP), and subsequently concentrated. Concentration of the fractions was determined by Bradford measurement.

Fluorescence polarization. The purified and concentrated protein stocks were two-fold serially diluted from a concentration of 4 µM to 4 nM in ice cold Fluorescence polarization (FP) buffer. FITC labeled oligonucleotides (Metabion) carrying 2.5x repeats of either telomeric (G- and C-rich) or control sequence were used for this assay. Double-stranded oligonucleotides were prepared by mixing the respective reverse complement oligonucleotides followed by an annealing step at 95°C. The oligonucleotides were then cooled at 0.1°C/second until 4°C. The serial diluted proteins were incubated with a final concentration of 20 mM FITC-labeled probe for 10 minutes at room temperature and samples afterwards measured with a Tecan Spark 20M. All experiments were repeated in triplicates, and analyzed with Graph Pad Prism 8.0. Specific binding was calculated by Hill slope fitting.

EMSA

A 6% polyacrylamide (PAA) gel was prepared and pre-run at 5 W for 15 min. 2 µl of the respective oligonucleotides used for the assay were radioactively labeled with 3µl $^{[32]}$P-γ-ATP by adding 1 µl PNK buffer A and 1 µl T4 PNK (New England BioLabs) followed by incubation at 37°C for 1 h. The labeled oligonucleotides were purified using a MicroSpin Sephadex G-50 column (GE Healthcare). For His_6-POT-2 EMSA, a constant amount of 1.25 pmol $^{[32]}$P-labeled oligonucleotide was incubated with increasing amounts of protein (0.5 pmol – 10 pmol) and EMSA Binding buffer, while for EMSA with R06A4.2-His_5, three different oligonucleotides were used: G-rich or C-rich single-stranded oligonucleotides, as well as an annealed double-stranded oligonucleotide (annealing see above). All oligonucleotides used for this assay contained three telomeric repeats. For the second experiment, a constant amount of 5 pmol purified R06A4.2-His_5 was incubated with increasing amounts (0-500 fmol) of $^{[32]}$P-labeled oligonucleotide and EMSA Binding buffer. All samples were brought to a final volume of 10 µl and were incubated for 5 min at 25°C. To load the samples on the gel, 4 µl loading dye (50% Glycerol, Bromphenolblue) were added and the gel was run at 240 V for 3 h. After finishing the run, the glass plates were separated and the gel covered with saran wrap prior to exposure to a phosphor storage screen (GE Healthcare) at 4°C over night. The screens were read out with the Typhoon Scanner (GE Healthcare) at 1000 V PMT with a 200 micron resolution. Obtained tif-files were processed with Fiji.

C. elegans culture

C. elegans was cultured under standard conditions on Nematode Growth Medium (NGM) plates seeded with E. coli OP50 bacteria (Brenner 1974). Unless otherwise noted, worms were grown at 20°C. The

standard wild-type strain used in this study was N2 Bristol. Further strains used and created in this study are listed in the table in the beginning of the chapter.

Creation of mutants using CRISPR-Cas9 technology

(strains prepared by Dr. Miguel Almeida, previously Ketting/Butter laboratory, IMB)

Mutants were created as described, with the following specifications. Single-guide RNA (sgRNA) constructs were cloned as described (Almeida et al. 2018). To create *T12E12.3(xf131)*, N2 animals were injected with a mix of three constructs: 25 ng/µl of co-injection marker pCFJ104 (a gift from Erik Jorgensen, Addgene plasmid #19328; RRID:Addgene_19328); 100 ng/µl of P843 expressing Cas9 and sgRNA1 (derived from pDD162, gift from Bob Goldstein, Addgene plasmid # 47549; RRID:Addgene_47549; (Dickinson et al. 2013)), and 75 ng/µl of P844 expressing sgRNA2 (derived from p46169, gift from John Calarco, Addgene plasmid # 46169; RRID:Addgene_46169). To produce *R06A4.2(xf133)* and *R06A4.2(xf134)*, the following mix was injected into N2 animals: 25 ng/µl of pCFJ104; 150 ng/µl of P841 expressing Cas9 and sgRNA1 (derived from pDD162), and 80 ng/µl of P842 expressing sgRNA2 (derived from p46169). Sequences of the respective sgRNAs for both genes can be found in a table above. After isolation, genotyping and confirmation by Sanger sequencing, mutants were outcrossed four times against the wild-type.

Creation of transgenic worms using MosSCI

(strain prepared by Dr. Miguel Almeida, previously Ketting/Butter laboratory, IMB)

The T12E12.3::GFP fusion transgene *(xfIs148)* was produced as described (Frøkjær-Jensen *et al.*, 2008 and www.wormbuilder.org). To create the MosSCI transgene, promoter, CDS and 3' UTR of T12E12.3 were amplified by PCR. A GFP sequence suitable for use in *C. elegans* was fused to the CDS by fusion PCR. All constructs were amplified with oligonucleotides carrying an attB site for BP recombination. For the BP reaction 1 µl of PCR product and respective pDONR221 vector were mixed with 2 µl H_2O and 1 µl BP Clonase II mix (Thermo Fisher Scientific) and incubated over night at 25°C. The next day the reaction was terminated by addition of 2 µg Proteinase K and subsequent incubation at 37°C for 10 min. The reaction was used to transform DH5alpha competent cells (New England BioLabs). After preparation and sequencing, the three pDONR221 plasmids (P848, P871, P871) were used in a multisite gateway LR reaction with destination vector pCFJ212 (Frøkjær-Jensen et al. 2012) to obtain the final injection plasmid (P1174). For LR recombination entry plasmid and destination vector were mixed 150 ng : 150 ng with 2 µl LR Clonase II enzyme mix (Thermo Fisher Scientific) and TE buffer to a total volume of 10 µl and incubated over night at 25°C. After termination of the reaction by Proteinase K, E. coli DH5alpha chemo-competent cells (New England BioLabs) were transformed with the recombined plasmid and grown on selective LB plates at 37°C. After preparation, the integrity of the plasmids was checked by restriction digest with fitting restriction enzymes and Sanger sequencing. Animals of the strain EG6699 were injected, in order to get insertions in locus ttTi5605 on LGII. The injection mix contained all the injection constructs listed in www.worbuilder.org, including 50 ng/µl of the repair template containing the T12E12.3::gfp sequence (P1174). Selection and genotyping were performed as described (Almeida et al. 2018). Plasmids can be found in the table above.

Creation of tagged strains by CRISPR-Cas9 technology

(strains prepared by Jan Schreier, Ketting laboratory, IMB)

Protospacer sequences were chosen using CRISPOR (http://crispor.tefor.net) (Haeussler et al. 2016), and cloned in pRFK2411 (plasmid expressing Cas9 + sgRNA(F+E) (Chen et al. 2013); derived from pDD162) or pRFK2412 (plasmid expressing sgRNA(F+E) (Chen et al. 2013) with Cas9 deleted; derived from pRFK2411) via site-directed, ligase-independent mutagenesis (SLIM) (Chiu et al. 2004; Chiu et al.

2008). pDD162 (Peft-3::Cas9 + Empty sgRNA) was a gift from Bob Goldstein (Addgene plasmid # 47549; http://n2t.net/addgene:47549; RRID:Addgene_47549) (Dickinson et al. 2013). All plamids were purified using the NucleoSpin Plasmid Kit (Macherey-Nagel), eluted in sterile water and confirmed by enzymatic digestion and sequencing. All Cas9 nuclease induced double-strand breaks (DSBs) were within 20 bp distance to the desired editing site. All CRISPR/Cas9 genome editing was performed using either *dpy-10(cn64)* or *unc-58(e665)* co-conversion strategies (Arribere et al. 2014). Single-stranded oligodeoxynucleotides (ssODN, 4 nmole standard desalted Ultramer DNA oligo from IDT) and PCR products (purified using QIAquick PCR Purification Kit from QIAGEN) served as donor templates for small (3xFLAG epitope tag, protospacer seqences) and big (GFP tag) insertions, respectively. The gfp coding sequence including three introns and flanking homology regions was amplified from pDD282, which was a gift from Bob Goldstein (Addgene plasmid # 66823; http://n2t.net/addgene:66823; RRID:Addgene_66823) (Dickinson et al. 2015). All donor templates contained ~35 bp homology regions (Paix et al. 2014; Paix et al. 2016). Plasmid vectors, ssODN and PCR products were diluted in sterile water and injected at a final concentration of 50 ng/µl, 500 - 1000 nM and 300 ng/µl, respectively. For GFP insertions, the protospacer sequence used for the dpy-10 co conversion was transplanted to the editing site to generate d10-entry strains (El Mouridi et al. 2017), which in turn served as reference strains for further injections. DNA mixes were injected in both gonad arms of ten to 25 1-day old adult hermaphrodites maintained at 20°C. Co-converted F1 progeny were screened for insertions by PCR. Successful editing events were confirmed by Sanger sequencing. All generated mutant strains were out-crossed at least two times prior to any further cross or analysis. CRISPR/Cas9 genome editing reagents are listed above and DNA injection mixes are listed below.

Table **M1**: DNA mixes for injection of *C. elegans*. Injected strains, used plasmids and generated strains are listed.

Injected strain	**DNA mix**	**Approach**	**Total concentration**	**Generated strain**
N2	50 ng/µl pRFK2588 50 ng/µl pRFK3304 500 nM SJ763 1000 nM SJ985	*unc-58* co-conversion	151.69 ng/µl	RFK924; *R06A4.2(xf201[R06A4.2::3xflag]) II.*
N2	50 ng/µl pRFK2588 50 ng/µl pRFK3304 500 nM SJ763 1000 nM SJ1046	*unc-58* co-conversion	154.60 ng/µl	RFK965; *R06A4.2(xf218[R06A4.2::d10]) II.*
RFK965	50 ng/µl pRFK2568 1000 nM SJ665 300 ng/µl SJP012	*dpy-10* co-conversion	381.16 ng/µl	RFK1022; *R06A4.2(xf225[R06A4.2::gfp]) II.*
N2	50 ng/µl pRFK2568 50 ng/µl pRFK3311 750 nM SJ665 750 nM SJ1106	*dpy-10* co-conversion	147.74 ng/µl	RFK1048; *T12E12.3(xf234[T12E12.3::d10]) IV.*
RFK1048	50 ng/µl pRFK2568 1000 nM SJ665 300 ng/µl SJP015	*dpy-10* co-conversion	381.16 ng/µl	RFK1096; *T12E12.3(xf235[T12E12.3::gfp]) IV.*

C. elegans nuclear enriched protein extract preparation

Nuclear extract preparation of gravid adult worms was done as previously described in de Albuquerque *et al.*, 2014. In short, animals were synchronized by bleaching and after re-seeding harvested by washing them off the plate with M9 buffer. After washing the worms in M9 buffer for 4 times by centrifugation at 600 xg for 4 min the buffer was replaced by Nuclear extraction buffer for a last centrifugation step. Worms in Nuclear extraction buffer were dropped into liquid nitrogen by pipetting and the resulting pellets ground to a fine powder in a pre-cooled mortar. The powder was transferred to a pre-cooled glass douncer and the samples were sheared with 30 strokes of piston B. Cell debris was pelleted by centrifugation at 200 xg for 5 min at 4°C for two times after the worm suspension was pipetted to pre-cooled 1.5 ml reaction tubes (1 ml per tube). To separate cytoplasmatic and nuclear fraction, the supernatant of the two previous centrifugation steps was transferred to a fresh tube and spun at 2,000 xg for 5 min at 4°C. The nuclear fraction pellet was washed twice by resuspension in Nuclear extraction buffer and subsequent centrifugation at 2,000 xg for 5 min at 4°C. After washing, the nuclear fraction was resuspended in 200 µl buffer C+ and its concentration determined by Bradford measurement. Between 200 and 400 µg of nuclear extract were used in the subsequent pulldowns.
Nuclear enriched extract of gravid adult worms of *C. briggsae* was prepared as described above.

C. elegans complete protein extract preparation

Worms were harvested at the desired stage and washed in M9 buffer. In the last centrifugation step M9 was replaced with H_2O and the worm suspension divided into 100 µl aliquots. These aliquots were snap frozen in liquid nitrogen and stored at -80°C until extract preparation. For complete extract preparation, the aliquots of worms were mixed 1:1 with 2x Lysis Buffer and sonicated in a Bioruptor 300 (Diagenode) on high level for 10 cycles with 30 sec on/off. After sonication, the samples were centrifuged at 21,000 xg for 10 min to pellet cell debris. The supernatant was transferred to a fresh reaction tube and concentration of the extract was determined by Bradford measurement. For experiments with developmental stages the animals were collected at specific time points after plating synchronized L1s: L1s 7 hours after plating to ensure recovery from starvation; L2s, ~12 hours; L3s, ~28 hours; L4, ~49 hours; YAs were collected ~ 56 hours after plating before showing embryos. With the exception of embryos, extract of all developmental stages of *C. elegans* was prepared as decribed above.

C. elegans complete protein extract preparation from embryos

For extract preparation of embryos, gravid adults were harvested from OP50 high-density plates (Schweinsberg and Grant 2013) by washing them off the plate with M9 buffer. After washing the worm suspension with M9 until the supernatant was clear, the worms were bleached (see below) to obtain mixed stage embryos. To quench the bleaching and remove the bleaching solution the embryos were washed in M9 buffer for three times. After transfer to a new tube they were washed two more times. For the last centrifugation step the embryos were resuspended in 1x Lysis buffer for worms (embryos) and frozen in liquid nitrogen. After freezing, the resulting embryo pellets were ground to a fine powder in a pre-cooled mortar, and transferred to a cold glass douncer. Lastly, the powder was sheared for 40 strokes with piston B. To pellet remaining debris and unsheared embryos, the suspension was transferred to 1.5 ml reaction tubes and centrifuged at 21,000 xg for 15 min at 4°C. After transfer of the supernatant to a new tube the concentration was determined by Bradford measurement.

IPs with *C. elegans* extracts

(supported in parts by Dr. Miguel Almeida, previously Ketting/Butter laboratory, IMB)

IPs with tagged proteins were performed with extract of embryos or young adult animals. For GFP-IPs 10 µl of GFP-binding magnetic agarose beads (Chromotek) were washed in GFP IP wash buffer twice

and mixed with buffer and up to 1 mg of *C. elegans* extract to a total volume of 750 µl. FLAG-IPs were performed with 30 µl Protein-G magnetic beads washed in FLAG IP wash buffer and mixed with up to 1 mg *C. elegans* extract as well as 2 µg FLAG antibody (anti-FLAG M2, Sigma-Aldrich). Both IPs were incubated rotating at 4°C for 2/3 h, respectively. After washing the beads with the respective buffer three times, all samples were resuspended in 1x LDS supplemented with 100 mM DTT and boiled at 70°C for 10 min. For IPs with Sm nuclease (Ball et al. 1987), the buffers were additionally supplemented with 0.05% Sm nuclease. Depending on downstream analysis, the IPs were performed in either quadruplicates for IP-qMS or in single samples with an additional input control for western blot detection. Further downstream processing for MS measurement or western blot is described elsewhere.

Extraction of genomic DNA from C. *elegans*

Mixed stage animals were harvested, washed, resuspended in Worm Lysis buffer and divided in 250 µl samples. For genomic DNA extraction the aliquots were brought to a final volume of 500 µl with WLB and Proteinase K (f.c. 30 µg/ml, Sigma-Aldrich). The samples were incubated at 65°C in a thermoshaker at 1,400 rpm for >2 h until all carcasses were dissolved, then centrifuged at 21,000 xg for 5 min to pellet debris and the supernatant was transferred to a fresh 1.5 ml reaction tube. Next, 500 µl of Phenol:Chloroform:Isoamylalcohol were added, the samples shaken vigorously for 30 sec and spun down at 16,000 xg for 5 min. Afterwards, 500 µl of chloroform were added to the samples and again shaken vigorously for 30 sec and spun at 16,000 xg for 5 min. After centrifugation, the aqueous phase of the samples was transferred to fresh 2 ml reaction tubes. To digest RNA 50 µg RNase A (Sigma-Aldrich) were added, the tubes inverted once and incubated at 37°C for >1 h. After RNA digestion the samples were again purified by Phenol:Chloroform:Isoamylalcohol and chloroform addition as described above. Once more, the aqueous phase was transferred to fresh 1.5 ml reaction tubes. The DNA was precipitated with 350 µl isopropanol for >15 min at -80°C and pelleted by centrifugation at 21,000 xg for 20 min at 4°C. After removing the supernatant carefully, the DNA pellet was washed once with 1 ml of ice-cold 70% ethanol and spun at 21,000xg for 5 min at 4°C. This washing step was repeated if the samples still smelled of phenol. Following washing, the supernatant was taken off and the pellet air dried for ca. 10 min. The pellet was resuspended in 20 µl H_2O. To ensure full resuspension of the DNA, the samples were kept at 4°C over night and mixed again the next day. The integrity of the genomic DNA was tested on a 1% agarose gel and the concentration was determined via nanorop measurement.

RNA extraction from *C. elegans*

For RNA extraction a 100 µl aliquot of harvested mixed stage worms (frozen in Worm Lysis buffer) was thawed on ice and 150 µl of fresh Worm Lysis Buffer and 30 µl of Proteinase K (20 µg/µl) were added. Samples were lysed as described above. After transferring the supernatant, 750 µl of TRIzol LS reagent (Thermo Fisher Scientific) were added to each sample and homogenized by pipetting. The samples were then incubated at RT for 5 min and after addition of 200 µl of chloroform, the tube shaken vigorously for 15 sec. Following incubation at RT for 2-15 min the samples were centrifuged at 12000 xg for 15 min at 4°C to separate the phases. The upper aqueous phase was transferred to a fresh tube. RNA was precipitated by addition of 500 µl isopropanol and incubation at -80°C for 10 min followed by centrifugation at 12000 xg for 10 min at 4°C. The resulting RNA pellet was washed with 1 ml 75% Ethanol by vortexing and centrifuged again at 7500 xg for 5 min at 4°C. The pellet was air dried for 5-10 min after taking off the remaining supernatant and resuspended in 40 µl H_2O. Concentration and integrity of the RNA was controlled via NanoDrop measurement and agarose gel electrophoresis, respectively.

Scoring double mutant crosses with *R06A4.2(xf133)* and *T12E12.3(xf131)*

(experiment in collaboration with Dr. Miguel Almeida, previously Ketting/Butter laboratory, IMB)

Following R06A4.2xT12E12.3 crosses, double homozygous F2 of these double mutant crosses showed a synthetic sterility phenotype. To score fertility, >100 F2 progeny were singled after confirming heterozygosity in the F1 generation. The singled F2 worms were grown to adulthood, allowed to self-propagate and subsequently genotyped. To determine the distribution of fertility phenotypes genotypes of all F2 animals were collected. Progeny of subfertile F2 *R06A4.2(xf133);T12E12.3(xf131)* or *R06A4.2(xf134); T12E12.3(xf131)* mothers were singled to have a look on one more generation of fertility. These F3 animals were genotyped as well and their fertility phenotype collected.

Generation and germline categorization of PGL-1::mTagRFP-T double mutant cross

(experiment in collaboration with Dr. Miguel Almeida, previously Ketting/Butter laboratory, IMB)

Creation of triple mutant strain. The strain *pgl-1::mTagRfp-T* was provided by Jan Schreier, Ketting laboratory, IMB (Schreier *et al.*, in submission). We created the triple mutant strain by crossing *R06A4.2(xf133);pgl-1::mTagRfp-T* males with *T12E12.3(xf131);pgl-1::mTagRfp-T* hermaphrodites. Homo- and heterozygosity of *pgl-1::mTagRfp-T* was determined using a Leica M80 Stereomicroscope with a fluorescence lamp (Leica EL 6000) since RFP-intensity was detectably different between the two genotypes. After confirming heterozygosity of the F1 animals, 300 F2 progeny were singled and left to self-propagate. After genotyping the F2 worms, 20 worms each from three independent *R06A4.2(xf133);T12E12.3(xf131)/+* or *R06A4.2(xf133)/+; T12E12.3(xf131)* mothers as well as 10 worms from two different single mutant siblings as controls were singled. Additionally, all progeny from double-homozygous sub-fertile worms were singled to check their fertility. Germline health as well as growth for all singled worms was determined at day two of adulthood. Germlines were categorized by microscopy with a Leica M80 Stereomicroscope with a fluorescence lamp (Leica EL 6000) as the following 1) wild-type or near wild-type germline, 2) atrophy in one gonad arm, 3) atrophy in both gonad arms. After categorizing germline status, the animals were genotyped. This protocol was repeated until generation F5 to obtain sufficient numbers for all categories and genotypes always singling animals as stated above. After all generations were scored, the germline phenotypes were correlated with the genotypes and plotted using R. Exemplary images for each germline category were taken from F3 and F4 generation animals prior to genotyping.

Imaging of germlines. For more detailed PGL-1::mTagRFP-T images for the scored categories of germline health, adult worms were picked to a droplet of M9 to remove OP50 bacteria, then transferred to a 5 µl drop of Sodium azide/M9 for immobilization on a 2% agarose pad. Animals were immediately imaged with a Leica AF7000 widefield microscope using a 20x objective (NA 0.4) and red fluorescence filters (N3) as well as TL-DIC. Images were processed using Fiji (brightness changes applied only in DIC channel for better visualization).

Mortal Germline Assay

All strains used in the mortal germline assay were outcrossed against the wild-type two times before the experiment. To determine a mortal germline phenotype, six L3 larvae of the chosen strains were picked per plate (n=15 plates) and grown at 25°C. Strains were passaged every five days (= two generations) by transferring six L3 larvae to a fresh plate, allowing them again to propagate further. This protocol was continued until plates were sterile. Plates were considered sterile when the initially transferred six worms failed to produce progeny on two consecutive scheduled transfers.

Fertility assays

(experiment in collaboration with Dr. Miguel Almeida, previously Ketting/Butter laboratory, IMB)

To investigate the broodsize counts of *R06A4.2(xf133)* and *T12E12.3(xf131)* mutants, as well as the *T12E12.3(xfls148)* transgene in mutant background, 75/76 late L3 worms were isolated per strain and assayed at both 20°C and 25°C. When reaching adulthood, animals were passaged to a new plate every day, until egg laying stopped. The viable progeny per strain was assayed about one day after removing the parent. To determine fertility in the double mutants, a cross between *R06A4.2(xf133)* males and *T12E12.3(xf131)* hermaphrodites was performed. The genotypes of the F1 and F2 were confirmed by genotyping and L2/L3 progeny from F2 *R06A4.2(xf133)/+;T12E12.3(xf131)* mothers were isolated and grown at 20°C or 25°C. During the course of reproductive adulthood, the viable brood size was counted as mentioned above. The assayed F3 animals were genotyped two days after egg laying stopped. For all brood size experiments, worms that died before egg laying terminated were excluded from the analysis.

C. elegans life span assay

A longevity assay to determine average life span of the mutant strains was modified after Amrit *et al.*, 2014. To assess life span of the different *C. elegans* mutants in comparison to wild-type, 10 small NGM plates were prepared per strain, each containing 10 L2 worms. The animals were grown at 20°C and day 1 was determined as beginning of egglaying. Animals were moved to new plates every day during their reproductive phase. Afterwards the animals were checked every two/three days until first worms started dying (~day 13). Following first deaths, the plates were checked every day for dead worms and the corpses removed. Worms not dying naturally by drying out, bagging or protruding vulva were censored from the experiment. The resulting numbers were entered into the survival calculation software Oasis2 (Han et al., 2016), thereby calculating a Kaplan-Meyer Survival curve and mean lifespan. The significance between different strains was calculated by log-rank testing and Bonferroni correction implemented in the Oasis2 website.

Male stocks

To create a male stock of worms for crosses, a heatshock of hermaphrodites was prepared. For this, 20 small plates each containing five L4/young adult hermaphrodites of the desired strain were heat shocked at 37°C for 70 min. The plates were then transferred to 20°C and after self-propagation the F1 generation was checked for male worms. Resulting males were either directly used for crosses or mated with hermaphrodites of their respective strain to maintain the male stock via incross.

Crosses

For strain outcrosses or the generation of strains with multiple mutations/tags, male and hermaphrodite L4 or YA of the respective strains were picked to a mating plate (small NGM plate with 1 µl OP50 bacteria) in a ratio of 2(males):1(hermaphrodites). The mating plates were incubated at 20°C over night and the hermaphrodites singled the next day. By checking the F1 progeny for ~50:50 distribution of male worms it was determined if the cross was successful. From the F1 progeny a number of L4 hermaphrodites was singled further and genotyped after self-propagation. Progeny of F2 worms with fitting genotype were singled and genotyped after self-propagation. This protocol was continued until progeny with the desired homozygous genotype could be isolated. Homozygosity was re-confirmed after one more generation.

Genotyping

After self-propagation, cross worms were picked into PCR tubes containing 5 µl Single Worm Lysis Buffer. Lysis was performed in a Thermocycler using the following settings: 65°C for 60 min (worm lysis) and 95°C for 15 min (deactivation of Proteinase K). After lysis, 20 µl H_2O were added and 2 µl worm lysis were used as a template in the PCR reactions. To confirm genotypes, the respective oligonucleotides for each gene were used. Polmyerases used for the PCRs were TAQ polymerase from the IMB Protein Production CF or OneTaq polymerase (New England BioLabs) in 10 µl final reaction volumes. The PCR products were checked on 1%/3% agarose gels respectively, depending on size. Oligonucleotide combinations and PCR product sizes for mutant and tag alleles are listed in the beginning of this chapter.

C. elegans bleaching for synchronization

To obtain a synchronous population of *C. elegans* at a desired life stage, NGM plates were grown until they contained a high number of gravid adults. The worms were washed off the plate with M9 buffer and washed until clean by replacing the buffer after each centrifugation at 600 xg for 4 min. After the last wash, the supernatant was removed until about 5 ml/2 ml (for 50 ml/15 ml tubes respectively) and the worm suspension was mixed 1:1 with Bleaching solution. The tubes were shaken vigorously until mostly embryos could be detected microscopically, then the reaction was quenched by addition of M9 buffer. The embryos were washed 4 times at 600 xg for 4 min, and transferred to a fresh tube. For proper aeriation the tubes were filled to half the volume with M9 buffer and put on a tube roller over night at 20°C for hatching. The hatched and synchronized L1 worms were seeded on standard NGM or high-density plates (Schweinsberg and Grant 2013) the following day and grown until the desired stage.

Telomere Southern Blot

Telomere restriction fragment analysis/telomere Southern blot was performed with 15 µg *C. elegans* genomic DNA digested with 40 U HinfI (New England BioLabs) and RsaI (New England BioLabs) respectively in a total volume of 80 µl. After over night incubation at 37°C, 10 U of each enzyme were added and the samples incubated 1-2 h further. Following digest, samples were evaporated in a Concentrator Plus (Eppendorf, setting V-AQ at 45°C) to reduce the sample volume to 20-30 µl. A 0.6 % agarose gel was prepared (with 1x TBE and Sybr Safe DNA stain) and the samples supplemented with f.c. 2x DNA loading dye and loaded after boiling at 95°C for 10 min. Markers for the gel run were the GeneRuler 1 kb (Thermo Fisher Scientific), as well as the 1 kb extended marker (New England BioLabs). The samples were secured in the gel by running 100 V for 20-30 min then run 16-19 h at 60 V. After the run the DNA was broken by UV crosslinking (crosslinker set to 1 min) and the gel afterwards equilibrated in Sothern blot transfer buffer for 20 min. The DNA was transferred to a positively charged nylon membrane (Pall) via upward alkaline transfer over night. Following transfer, the DNA was fixed on the membrane by incubation in 0.4 M NaOH for 15 min with slight agitation. Afterwards the membrane was neutralized with two washes in 2x SSC for five minutes each and sealed in cling film with 2x SSC until hybridization.
Pre-hybridization of the membrane was performed in 20 ml Southern blot hybridization buffer for at least 1 h at 42°C rotating in a hybridization oven. 2 µl of the $(GCCTAA)_3$ oligonucleotide used for detection were radioactively labeled with 3 µl $^{[32]}$P-gamma-ATP by a polynucleotide Kinase reaction (see EMSA). Before hybridization, the labeled oligonucleotide was denatured at 95°C for 10 min and mixed with 20 ml fresh hybridization buffer. The fresh buffer including the radiolabeled probe was added to the membrane incubated for 3.5 days rotating at 42°C.
Following hybridization the membrane was rinsed twice with Southern blot Wash Buffer 1, then consecutively washed twice in Wash buffer 1 for 5 min and once in Wash buffer 2 for 2 min. Finally, the membrane was rinsed with 2x SSC to re-equilibrate the salt concentration. The membrane was dried on Whatman paper prior to exposure to a phosphoimager screen. After three days the screen was read

out with the Typhoon FLA Scanner with the settings 1000 V PMT and 200 µm pixel size. Contrast and brightness of the resulting tif-file were optimized using Fiji.

Microscopy

DAPI-GFP microscopy. R06A4.2::GFP or T12E12.3::GFP carrying gravid adult animals were picked to a 5 µl drop of M9 buffer and dissected to release gonads and embryos. Worms were fixed on the slides by evaporation of a 10 µl drop of acetone for two times and rehydrated in 10 µl PBS-T for 10 min. Afterwards slides were mounted with DAPI-containing mounting medium and imaged using a AF7000 widefield microscope. Double homozygous escaper animals for chromosome counting in oocytes were prepared the same way.

Colocalization. To localize R06A4.2::GFP and T12E12.3::GFP to telomeres, these strains were crossed with strain YA1197 carrying POT-1::mCherry. Respective progeny of the cross were genotyped and singled until homozygosity was confirmed for both alleles. Adult animals were washed in M9 buffer, immobilized in M9 buffer supplemented with 40 mM sodium azide and mounted on freshly made 2 % agarose pads. For imaging embryos, adult hermaphrodites were washed and dissected in M9 buffer before mounting. Animals were immediately imaged using a TCS SP5 Leica confocal microscope equipped with a HCX PL APO 63x water objective (NA 1.2) and hybrid detectors (HyD). Deconvolution was performed using Huygens Remote Manager and images were further processed using Fiji. (experiment conducted by Jan Schreier, Ketting laboratory, IMB)

qFISH. For telomere length determination, fluorescence in-situ hybridization (FISH) was utilized in a quantitative manner as described in Lansdorp *et al.*, 1996. The staining protocol used here was optimized from Seo and Lee, 2016. Per strain, 100 gravid adults were picked to an unseeded small NGM plate to remove the OP50 bacteria on the outside of the animals. Worms were then picked to a 5 µl drop of Egg buffer on a cover slip and dissected using 20 gauge needles (Sterican, Roth) to release embryos and gonads. Fixing of the worms was achieved by adding 5 µl of 2% Formaldehyde solution and incubating for 5 min. Worms were washed on the cover slip with Egg buffer carefully by pipetting. To permeabilize the worm cuticle, a freeze cracking protocol was used (Duerr, 2013). Poly-lysine coated slides (Sigma Aldrich) were put ontp the cover slips and the slides frozen on an aluminum block in dry ice. Following 15 min freezing, the cover slips were removed by flicking. Further fixation of the slides was achieved by immersion in in ice-cold methanol, then in ice-cold acetone for 5 min, respectively. Afterwards the slides were washed in 1x PBS for 15 min. The samples were then incubated in Permeabilization buffer at 37°C for 30 min followed by a wash in 1x PBS for 5 min at room temperature. Samples were treated with 20 µl RNase A solution at 37°C for 1 h in a humid chamber to avoid unspecific binding of the PNA probe. Following RNA degradation, the slides were washed in 1x PBS-T for 10 min at room temperature and dehydrated by successive 3 min washes in 70%, 85% and 100% ethanol and air dried. The samples were prehybridized by adding 50 µl of Hybridization solution and incubation in a humid chamber for 1 h at 37°C. The FISH probe (PNA-FISH TTAGGC telomeric probe, Panagene, resuspended to 100 µM) was prepared as a 1:500 dilution in Hybridization solution and denatured for 5 min at 70°C prior to hybridization of the sample. The Hybridization solution on the slides was removed as carefully as possible by pipetting and 20 µl of FISH probe were added. For hybridization of the probe the slides were covered with a cover slip and denatured on a heat block at 80°C for 3 min (prepared with wet paper towels for humidity). The samples were hybridized with the FISH probe over night at 37°C in a humidity chamber. To remove the probe, the slides were washed twice in 1x PBS-T for 5 min. FISH staining was completed by incubation in Hybridization wash solution for 30 min at 37°C. After two washes in 1x PBS-T for 15 min at room temperature the samples were mounted by adding 10-20 µl Vectashield mounting medium containing DAPI (Vector laboratories). FISH images were taken with a Leica TCS SP5 confocal microscope with the following settings: pinhole 60.05 µm, 2x zoom, z-stack volume 0.5 µm. The laser and gain settings were adjusted according to the sample with the lowest FISH intensity.
For analysis, images were opened in Image J/Fiji and the color channels split (DAPI and FISH channel). To infer the volume of the imaged object a mask of the image was created. The threshold for the images

was set with the threshold function of the software with activated plugins for identification of round objects (Otsu). After setting the threshold for the image in the histrogram settings, the z-stack was converted to a binary mask and using the 3D OC Options menu volume, mean gray values and integrated density were calculated. Additionally the 3D Object counter menu was used and the filters set to a minimum of 2. The values obtained by this analysis were averaged over several images of either germlines or embryos of the same strain and used for quantitative comparison of telomere length. For comparison all values obtained for the mutant strains were scaled relative to the average of the wild-type values to have the WT set to "1". Standard error of the mean was calculated for all samples and significance tested by a 2-sided t-test. Graphs were plotted using R and R-studio with commonly available packages (ggplot2, dplyr) and in-house scripts. (FISH staining, imaging and analysis performed by Dr. Nikenza Viceconte, previously Butter laboratory, IMB)

Western Blot

Protein samples were boiled at 70°C for 10 min and loaded on a 4-12% Bis-Tris gel (Thermo Fisher Scientific), running at 180 V for 60 min or 150 V for 120 min (depending on the protein size) in 1x MOPS (Thermo Fisher Scientific). Before blotting the gel and a nitrocellulose membrane (VWR) of respective gel size were wet VE H_2O and equilibrated in Western blot transfer buffer. Membrane and gel were stacked with pre-wet Whatman paper (GE Healthcare) and immersed in ice-cold Transfer buffer in a blotting tank (Bio-Rad) additionally cooled with a cooling element. The proteins were transferred at 300 mA for 60-120 min depending on the size. If blotted for over 90 min, the blotting tank was additionally put on ice to keep the temperature. After blotting, the membranes were further prepared according to the respective antibody protocol. Western Blot images were taken with the ChemiDoc XRS+ system (BioRad, Software: Image Lab 5.2.1) when using HRP-coupled secondary antibodies or with the Odyssey CLx (Settings: 700 nm and 800 nm channels, automated intensity, medium quality; Software: Image Studio 3.1) when using LI-COR secondary antibodies, respectively.

His antibody. Membranes were blocked in the kit specific Blocking Solution (PentaHis Kit, Qiagen) for 1 h at room temperature. Following three washes in TBS-T for 5 min each, the membranes were incubated with a 1:1000 dilution of the HRP-coupled penta-His antibody in Blocking Solution for 1 h at room temperature. Afterwards membranes were again washed three times in TBS-T. For detection of His-tagged proteins, the membranes were incubated with ECL Western Blot reagent (Thermo Fisher Scientific).

GFP/FLAG/Actin antibodies. After transfer, membranes were blocked in Skim Milk solution for 1 h at room temperature. The incubation with the respective primary antibody (Roche, Anti-GFP; 1:1000 in Skim Milk solution; Sigma-Aldrich, mouse anti-FLAG M2 antibody,1:5000 in Skim Milk solution; Sigma-Aldrich, rabbit anti-actin, 1:500 in Skim Milk solution) was carried out at 4°C, rotating over night. After the membranes were washed in PBS-T three times for 10 min, they were incubated with the respective secondary antibody (Cell Signaling Technology, Anti-mouse IgG, HRP-linked Antibody,1:10,000 dilution in Skim Milk Solution; GE Healthcare, anti-Rabbit IgG, peroxidase-linked antibody, 1:3000 in Skim Milk solution) for 1 h rotating at room temperature. Following three additional washes in PBS-T the membranes were incubated with ECL solution (Thermo Fisher Scientific) for detection.

LI-COR antibodies. For detection of CoIP, the membranes were first incubated with either anti-GFP or anti-FLAG antibodies as described above. After detection and washing, the membranes were incubated with secondary antibodies compatible with the LI-COR System (FLAG/GFP: Licor IRDye® 680RD Donkey anti-Mouse IgG (H + L); Actin: Licor IRDye® 800CW Donkey anti-Rabbit IgG (H + L); both 1:15000 in Skim Milk solution) for 1 h at room temperature. After additional three washes with PBS-T the membranes were read out with the Odyssey CLx scanner and processed using the Image Studio software (LI-COR, Version 3.1).

Western Blot analysis. For determination of expression differences of R06A4.2::GFP and T12E12.3::GFP in the mutant background of the respective paralog protein 60 and 50 µg embryonic extract were run on western blots as described above. Proteins were detected with LI-COR secondary antibodies with the Odyssee system to enable analysis with the Image Studio software (Version 3.1). Analysis was previously described in Almeida et al., 2018. Within every technical replicate per protein, the signal of the protein of interest was normalized relative to actin. Then the normalized signal of either R06A4.2::GFP, or T12E12.3::GFP in wild-type background were set to 1 for comparison with their expression in the mutant background and averaged over the two biological replicates. (Western Blot analysis performed by Dr. Miguel Almeida, previously Ketting/Butter laboratory, IMB after Almeida *et al.*, 2018)

Yeast two-Hybrid assay

(experiment conducted in collaboration with Dr. Miguel Almeida, previously Ketting/Butter laboratory, IMB, with support from Dr. Christian Renz and Dr. Nicola Zilio (Ulrich laboratory, IMB))

Our yeast two-hybrid assay was performed in the yeast strain PJ69-4α as described before (James et al. 1996; Cordeiro Rodrigues et al. 2019).

Transformation of competent S. cerevisiae cells. To make competent cells of the assay compatible strain *S. cerevisiae* PJ69-4α, an over night culture of 20 ml YPD medium was inoculated with cells and grown at 30°C shaking at 190 rpm. After determination of OD_{600} the next day, a 200 ml growing culture was inoculated with the over night culture to a final OD_{600} of 0.2. The culture was grown at 30°C, shaking at 190 rpm until OD_{600} reached >0.6. Cells were pelleted at 3500 rpm for 7 min at room temperature and washed in 86 ml H_20 followed by 43 ml SORB. After the final wash the cell pellet was resuspended in 1.8 ml SORB, 200 µl carrier ssDNA (herring testes DNA, 10 mg/ml, Sigma-Aldrich) were added and the cells divided into 50 µl aliquots. One aliquot was used per co-transformation with 100 ng of each the respective plasmid from a pair. The cells were supplemented with six volumes of PEG and incubated at room temperature for 30 min. Afterwards 1/9 volume of DMSO was added and the cells heat shocked at 42°C for 15 min. The cells were pelleted by centrifugation at 4000 rpm for 2 min at room temperature and the supernatant was removed. For plating, the cells were resuspended in 500 µl H20 and 200 µl were plated on SC media plates containing the respective selection (-leucine, -tryptophan). The plates were incubated at 30°C until colonies were visible.

Spotting of transformed colonies for two hybrid assay. To determine direct interactions of the candidate proteins, one colony per transformation was resuspended in 200 µl H_2O in a well of a 96-well plate according to the previously determined grid. With a Replica plater (8x6 grid, Sigma-Aldrich) cleaned with ethanol, the cell suspension was spotted onto SC media plates with the respective selections for the assay. As growth control cells were spotted on SC -leu/-trp, while the more restrictive plates for the assay were SC -leu/-trp/-his and SC -leu/-trp/-his/-ade. The spotted plates were grown at 30°C until growth of colonies could be determined.To have a biological replicate, a second grid was spotted per plate, made from cell suspension of a second colony. An additional repetition of the assay was performed starting at transformation to exclude potential pipetting errors during the first preparation and gaining an independent second replicate. Pictures of the respective grid were taken with a ChemiDoc XRS+ system (BioRad, Software: Image Lab 5.2.1).

Control of fusion-construct expression. To control for the proper expression of the fusion constructs, extract from yeast colonies was used for detection by western blot. Colonies expressing both the DBD and the AD construct of the respective candidate proteins were picked from the spotted SC -leu/-trp plate and used to inoculate 3 ml overnight cultures of liquid SC -leu/-trp medium. Cultures were grown at 30°C shaking until the next morning and a growing culture of 3 ml SC -leu/-trp was inoculated 1:20 with the overnight culture. The growing cultures were grown at 30°C shaking until an OD_{600} above 1. A total of 4 x 10^7 cells were harvested and pelleted at 12,000 xg for 15 min at 4°C. The residual medium was removed and the pellet resuspended in 500 µl cold H_2O. The suspension was supplemented with 75 µl NaOH/2-Mercaptoethanol for lysis of the cells, vortexed and incubated on ice for 15 min. Afterwards the proteins were precipitated by addition of 75 µl 55% TCA (trichloroacetic acid

in H_2O), vortexed and incubated on ice for another 10 min. The precipitated proteins were pelleted by centrifugation at full speed for 10 min at 4°C. After taking off the supernatant, proteins were resuspended in 40 µl 1x NuPAGE LDS (supplemented with 100 mM DTT and 50 mM Tris/HCl pH 8, Therme Fisher Scientific) and denatured at 65°C for 10 min. The samples were centrifuged shortly to pellet residual debris and 15 µl of protein solution were loaded per gel, one gel for DBD constructs and AD constructs, respectively. After gel run and transfer of proteins to a nitrocellulose membrane both membranes were stained with Ponceau S solution (Applichem) to control for equal loading. Afterwards the membranes were blocked by incubation in Skim Milk solution for 1 h at RT and incubated with 1:1000 dilutions of the respective primary antibodies (Santa Cruz, GAL4 DBD antibody (RK5C1), #sc-510; GAL4-TA (C-10) antibody, #sc-1663) over night at 4°C. After washes in PBS-T and incubation in secondary antibody (Cell Signaling Technology, Anti-mouse IgG, HRP-linked Antibody; 1:10,000 dilution in Skim Milk Solution) the expression of the fusion constructs was detected by incubation with ECL (Thermo Fisher Scientific).

Size exclusion chromatography

(experiment conducted in collaboration with Dr. Miguel Almeida (previously Ketting/Butter laboratory) and Dr. Christian Renz (Ulrich laboratory), IMB)

Extract of embryos from the double transgenic strain carrying R06A4.2::3xFLAG and T12E12.3::GFP was prepared as described above. For the first size exclusion run, two embryo samples were prepared, combined and concentrated to a final volume of 500 µl using a centrifugal filter with a 10 kDa cutoff (Merck, Amicon Ultra 0.5ML 10K). The NGC Quest system (BioRad) was used with Superose 6 10/300 GL size-exclusion column (GE Healthcare, 17517201) at a flow rate of 0.5 ml/min. A marker run (BioRad) was performed (see table in appendix) to allow for estimation of complex sizes by correlating of elution times. The composition of the used Gelfiltration buffer is described above. After the run several fractions along the size gradient (see table in appendix; bold marked fractions) were concentrated from 500 µl to around 30 µl using the previously mentioned centrifugal filters. For the gel run, the samples were supplemented with 1x LDS (NuPAGE) and 100 mM DTT to a final volume of ~40 µl and boiled at 95°C for 10 min. Half of the sample volume was separated on a 4-15% Criterion TGX Stain-Free Protein Gel (26 wells, BioRad) in 1x SDS running buffer at 200 V for 32 min. Proteins were transferred to a nitrocellulose membrane (BioRad) using the Trans-Blot Turbo Transfer System (BioRad). Detection of the GFP and FLAG-tagged proteins was accomplished as described above. For the second size exclusion run four embryo samples of the double transgenic strain were prepared, combined and concentrated as described. Then the final 1 ml of the sample was split and one half treated with Sm nuclease for 30 min at 4°C. For all runs between 3.6 and 3.8 mg of complete *C. elegans* protein extract were used.
For the preparation of MS samples, the remaining sample of both Sm nuclease untreated runs were loaded on 10% Bis-Tris gels and run at 180 V for 10 min. Downstream treatment was performed as mentioned under in-gel digest. The respective fractions of each run were treated as replicates in the analysis of the MS runs.

Polymerase Chain Reaction (PCR)

PCRs were performed after the guidelines of the respective polymerases with annealing temperatures matching the used oligonucleotides (see table above) and elongation time matching the amplified target. A final reaction volume of 10 µl was used for *C. elegans* genotyping, whereas for other PCRs, depending on the use, the final reaction volume was between 25 and 50 µl. OneTaq polymerase (New England BioLabs) was used for colony PCRs and genotyping PCRs using the POT-2 oligonucleotides. Taq polymerase supplied by the Protein Production Core Facility of IMB was used for standard genotyping reactions using the 10x Reaction buffer supplemented with 5 M Betain and BSA. For long and inverse PCRs Pfu Ultra II (Agilent) was used due to higher fidelity. For colony PCRs, respective colonies from transformations were picked and resuspended in 20 µl TE buffer. 2 µl of the suspension were used in

10 µl PCR reactions run with the respective oligonucleotides and Taq Polymerase from IMB Protein Production CF. PCRs were run in thermocyclers from BioRad (T100) or Biometra (TRIO, TOne).

Preparation of plasmids

For cloning, minipreps of plasmids were done with the QiaPrep Spin miniprep Kit (Qiagen) after the instructions in the manual. For low copy plasmids like pCoofy expression vectors, the column was eluted with 32 µl H_2O and then re-eluted with the same flow-through to increase the yield.
For injection into *C. elegans* the plasmids were purified with the PureLink HiPure Plasmid Mini- or Midiprep Kits (Thermo Fisher Scientific) or the NucleoSpin Plasmid min Kit (Macherey-Nagel) according to manual. All concentrations were measured with a NanoDrop 2000 (Thermo Fisher Scientific). Sequences of all cloned plasmids were confirmed by Sanger sequencing. The integrity of Y2H and worm injection plasmids was additionally checked by restriction digest with fitting restriction enzymes.

SLIC cloning

SLIC cloning was performed as previously described (Scholz et al. 2013). In short, total RNA from *C. elegans* N2 (wild-type) was prepared (see above) and 2 µg used for reverse transcription into cDNA with the First Strand cDNA Synthesis Kit (Thermo Fisher Scientific). The cDNA was used as template for amplification of the respective protein CDSs in a PCR reaction. The plasmids pCoofy1 (N-terminal His_6) and pCoofy4 (N-terminal His_6-MBP) were linearized by PCR with the oligonucleotides mentioned in the table above. In brief, SLIC reactions were prepared in 3:1 (insert:vector) ratio calculated by ng amount of insert and linearized plasmid, respectively. In a total reaction volume of 10 µl 1 µl 10x RecA Buffer and 1 µl Recombinase A dilution (1:1000, New England BioLabs) were added to the reaction and the sample incubated at 37°C for 30 min. After incubation 2.5 µl of the reaction were used to transform 25 µl DH5alpha cells (New England BioLabs). The prepared plasmids were sent for Sanger sequencing to confirm correct sequence of the respective ORF.

TOPO cloning

For holding purposes and LR recombination, PCR products were sub-cloned into the pCR8 GW/TOPO vector (Fisher Scientific). PCR products not amplified with Taq polymerase were incubated with OneTaq (New England BioLabs) for 10 min at 72°C prior to TOPO cloning to create A-overhangs. For the reaction, 0.6 µl of PCR product were mixed with 0.3 µl Salt solution and 0.1 µl pCR8 GW/TOPO vector and incubated at RT for 10 min. Following the incubation, the whole reaction was used for transformation of DH5alpha competent cells (New England BioLabs). The prepared plasmids were sent for Sanger sequencing to confirm correct sequence of the respective ORF.

Inverse PCR and ligation

For creating C-terminally His_5 tagged constructs of R06A4.2 and T12E12.3 in pCoofy1 as well as the sgRNA carrying plasmids for CRISPR/Cas-9 deletions, inverse PCRs of the respective plasmids were performed. The PCRs were run as given by the instructions for Pfu Ultra II polymerase (Agilent), checked for correct size by agarose gel electrophoresis and the product afterwards cleaned by ethanol precipitation. The plasmids were re-ligated by a one-step phosphorylation-ligation-digestion protocol (Almeida et al. 2018), therefore mixing PCR product, 10x T4 ligase buffer, 10 pmol ATP (100 µM), 5 units T4 Polynucleotid-Kinase (New England BioLabs) , 500 units T4 DNA ligase (Thermo Fisher Scientific) and 10 units DpnI (New England BioLabs). The reaction was incubated over night at RT and the ligated product was used to transform *E.coli* DH5alpha (New England BioLabs). The prepared

plasmids were sent for Sanger sequencing to confirm correct sequence of ORF and tag or sgRNA, respectively.

Gibson Cloning

To obtain the full T12E12.3 CDS sequence, which was not possible by PCR, we performed Gibson cloning with a gene block carrying the missing sequence. The reaction was prepared with 100 ng of linearized backbone vector and the respective ng amount of insert to achieve a 2:1 ratio of insert over vector. To calculate the amount of needed insert the tool “NEBioCalculator” was used. The linearized vector produced by PCR was purified with the MinElute PCR Purification Kit (Qiagen) and concentration was determined by NanoDrop measurement. The gene block from IDT to insert the missing part of T12E12.3 was resuspended to a final concentration of 10 ng/µl. Vector and insert were combined with H_2O to a volume of 10 µl, then mixed with 10 µl 2x Gibson Assembly Master Mix (Protein Production CF, IMB) and incubated in a pre-heated thermocycler at 50°C for 60 min. Finally, 5 µl of the reaction were used for transformation of *E. coli* DH5alpha chemo-competent cells (New England BioLabs).

Transformation of chemo-competent *E. coli*

Transformation of chemo-competent *E. coli* strains was performed as described in their respective manuals. In short, for standard transformation of *E. coli* DH5alpha (New England BioLabs) DNA and cells were mixed 1:10 and incubated on ice for 30 min. After incubation on ice, the cells were heat-shocked at 42°C for 45 seconds, put back on ice for 2 min and supplemented with 250 µl room temperature SOC medium. Outgrowth of cells was done in a thermoshaker at 37°C for 1 h at 800 rpm and cells afterwards plated on LB plates containing the respective antibiotic matching the plasmid resistance. The plates were incubated over night at 37°C and checked for colony growth the next day. Additional strains used were One Shot ccdB Survival 2 $T1^R$ Competent Cells (Thermo Fisher Scientific) for empty vector transformations (pCoofy1/4 and Yeast 2 Hybrid), Rosetta 2 (DE3) pLysS Competent Cells (Novagen/Merck), as well as BL21(DE3)-$T1^R$ Competent Cells (Sigma-Aldrich) and ArcticExpress (DE3) Competent Cells (Agilent) for protein expression.

Bradford

To determine protein concentrations of extracts, BSA standards of 0, 0.125, 0.25, 0.5, 0.75 and 1.0 mg/ml BSA in H_2O were prepared for a standard curve. The respective protein extracts were used either undiluted or diluted in a fitting manner. For the standard curve, 30 µl of each BSA standard were pipetted to cuvettes and 1 ml of 1x Bradford Reagent (5x Protein Assay Dye Reagent Concentrate, Biorad, #500-0006) was added. The mixture was incubated for 5 min and measured in a spectrophotometer at 595 nm in duplicates. Respective protein extracts were measured in triplicates. After measurement the values of the BSA samples were plotted in excel and a standard curve was fitted. The slope of the BSA curve was used to calculate the concentration of the protein samples.

Alignments

Alignments of R06A4.2 and T12E12.3 on nucleotide and amino acid level were done using the respective sequences provided by Wormbase (www.wormbase.org) and the pairwise alignment program EMBOSS Needle (Madeira et al. 2019).

Domain prediction

Prediction of potential protein domains by structure homology was done using the HHpred server (Version 3.2.0) (Zimmermann et al. 2018) and the protein sequences of R06A4.2 and T12E12.3 provided by Wormbase (www.wormbase.org).

References

Abad JP, De Pablos B, Osoegawa K, De Jong PJ, Martín-Gallardo A, Villasante A. 2004. Genomic analysis of Drosophila melanogaster telomeres: Full-length copies of HeT-A and TART elements at telomeres. Mol Biol Evol. 21(9):1613–1619. doi:10.1093/molbev/msh174.

Abreu E, Aritonovska E, Reichenbach P, Cristofari G, Culp B, Terns RM, Lingner J, Terns MP. 2010. TIN2-Tethered TPP1 Recruits Human Telomerase to Telomeres In Vivo. Mol Cell Biol. 30(12):2971–2982. doi:10.1128/mcb.00240-10.

Adams JM. 2003. Ways of dying: Multiple pathways to apoptosis. Genes Dev. 17(20):2481–2495. doi:10.1101/gad.1126903.

Ahmed S, Hodgkin J. 2000. MRT-2 checkpoint protein is required for germline immortality and telomere replication in C. elegans. Nature. 403(6766):159–164. doi:10.1038/35003120. http://www.nature.com/articles/35003120.

Ahringer J. 2000. NuRD and SIN3: Histone deacetylase complexes in development. Trends Genet. 16(8):351–356. doi:10.1016/S0168-9525(00)02066-7.

Ai W, Bertram PG, Tsang CK, Chan TF, Zheng XFS. 2002. Regulation of subtelomeric silencing during stress response. Mol Cell. 10(6):1295–1305. doi:10.1016/S1097-2765(02)00695-0.

Albertson DG, Thomson JN. 1993. Segregation of holocentric chromosomes at meiosis in the nematode, *Caenorhabditis elegans*. Chromosom Res. 1(1):15–26. doi:10.1007/BF00710603.

de Albuquerque BFM, Luteijn MJ, Cordeiro Rodrigues RJ, van Bergeijk P, Waaijers S, Kaaij LJT, Klein H, Boxem M, Ketting RF. 2014. PID-1 is a novel factor that operates during 21U-RNA biogenesis in *Caenorhabditis elegans*. Genes Dev. 28(7):683–688. doi:10.1101/gad.238220.114.

Allshire RC, Dempster M, Hastie ND. 1989. Human telomeres contain at least three types of G–rich repeat distributed non-randomly. Nucleic Acids Res. 17(12):4611–4627. doi:10.1093/nar/17.12.4611. https://academic.oup.com/nar/article-lookup/doi/10.1093/nar/17.12.4611.

Almeida MV, Dietz S, Redl S, Karaulanov E, Hildebrandt A, Renz C, Ulrich HD, König J, Butter F, Ketting RF. 2018. GTSF -1 is required for formation of a functional RNA -dependent RNA Polymerase complex in *Caenorhabditis elegans*. EMBO J. 37(12). doi:10.15252/embj.201899325.

Amrit FRG, Ratnappan R, Keith SA, Ghazi A. 2014. The C. elegans lifespan assay toolkit. Methods. 68(3):465–475. doi:10.1016/j.ymeth.2014.04.002. https://linkinghub.elsevier.com/retrieve/pii/S1046202314001467.

Apte MS, Cooper JP. 2017. Life and cancer without telomerase: ALT and other strategies for making sure ends (don't) meet. Crit Rev Biochem Mol Biol. 52(1):57–73. doi:10.1080/10409238.2016.1260090. http://dx.doi.org/10.1080/10409238.2016.1260090.

Armanios M, Blackburn EH. 2012. The telomere syndromes. Nat Rev Genet. 13(10):693–704. doi:10.1038/nrg3246.

Armstrong CA, Moiseeva V, Collopy LC, Pearson SR, Ullah TR, Xi ST, Martin J, Subramaniam S, Marelli S, Amelina H, et al. 2018. Fission yeast Ccq1 is a modulator of telomerase activity. Nucleic Acids Res. 46(2):704–716. doi:10.1093/nar/gkx1223.

Armstrong CA, Pearson SR, Amelina H, Moiseeva V, Tomita K. 2014. Telomerase activation after recruitment in fission yeast. Curr Biol. 24(17):2006–2011. doi:10.1016/j.cub.2014.07.035.

Arnoult N, Van Beneden A, Decottignies A. 2012. Telomere length regulates TERRA levels through increased trimethylation of telomeric H3K9 and HP1α. Nat Struct Mol Biol. 19(9):948–956. doi:10.1038/nsmb.2364.

Arora R, Azzalin CM. 2015. Telomere elongation chooses TERRA ALTernatives. RNA Biol. 12(9):938–941. doi:10.1080/15476286.2015.1065374.

Arora R, Lee Y, Wischnewski H, Brun CM, Schwarz T, Azzalin CM. 2014. RNaseH1 regulates TERRA-telomeric DNA hybrids and telomere maintenance in ALT tumour cells. Nat Commun. 5:1–11. doi:10.1038/ncomms6220.

Arribere JA, Bell RT, Fu BXH, Artiles KL, Hartman PS, Fire AZ. 2014. Efficient Marker-Free Recovery of Custom Genetic Modifications with CRISPR/Cas9 in *Caenorhabditis elegans*. Genetics. 198(3):837–846. doi:10.1534/genetics.114.169730. http://www.genetics.org/lookup/doi/10.1534/genetics.114.169730.

Artandi SE, Chang S, Lee S-L, Alson S, Gottlieb GJ, Chin L, DePinho RA. 2000. Telomere dysfunction promotes non-reciprocal translocations and epithelial cancers in mice. Nature. 406(6796):641–645. doi:10.1038/35020592. http://www.nature.com/articles/35020592.

Awasthi P, Foiani M, Kumar A. 2015. ATM and ATR signaling at a glance. J Cell Sci. 128(23):4255–4262. doi:10.1242/jcs.169730. http://jcs.biologists.org/cgi/doi/10.1242/jcs.169730.

Azvolinsky A, Dunaway S, Torres JZ, Bessler JB, Zakian VA. 2006. The S. cerevisiae Rrm3p DNA helicase moves with the replication fork and affects replication of all yeast chromosomes. Genes Dev. 20(22):3104–3116. doi:10.1101/gad.1478906. http://www.genesdev.org/cgi/doi/10.1101/gad.1478906.

Azzalin CM, Lingner J. 2008. Telomeres: the silence is broken. Cell cycle. 7(9):1161–5. doi:10.4161/cc.7.9.5836. http://www.ncbi.nlm.nih.gov/pubmed/18418035.

Azzalin CM, Reichenbach P, Khoriauli L, Giulotto E, Lingner J. 2007. Telomeric Repeat Containing RNA and RNA Surveillance Factors at Mammalian Chromosome Ends. Science (80-). 318(5851):798–801. doi:10.1126/science.1147182. https://www.sciencemag.org/lookup/doi/10.1126/science.1147182.

Bah A, Wischnewski H, Shchepachev V, Azzalin CM. 2012. The telomeric transcriptome of Schizosaccharomyces pombe. Nucleic Acids Res. 40(7):2995–3005. doi:10.1093/nar/gkr1153.

Balk B, Maicher A, Dees M, Klermund J, Luke-Glaser S, Bender K, Luke B. 2013. Telomeric RNA-DNA hybrids affect telomere-length dynamics and senescence. Nat Struct Mol Biol. 20(10):1199–1206. doi:10.1038/nsmb.2662.

Ball TK, Saurugger PN, Benedik MJ. 1987. The extracellular nuclease gene of Serratia marcescens and its secretion from Escherichia coli. Gene. 57(2–3):183–192. doi:10.1016/0378-1119(87)90121-1.

Barber LJ, Youds JL, Ward JD, McIlwraith MJ, O'Neil NJ, Petalcorin MIR, Martin JS, Collis SJ, Cantor SB, Auclair M, et al. 2008. RTEL1 Maintains Genomic Stability by Suppressing Homologous Recombination. Cell. 135(2):261–271. doi:10.1016/j.cell.2008.08.016. http://dx.doi.org/10.1016/j.cell.2008.08.016.

Barzilai N, Huffman DM, Muzumdar RH, Bartke A. 2012. The critical role of metabolic pathways in aging. Diabetes. 61(6):1315–1322. doi:10.2337/db11-1300.

Baugh LR, Hill AA, Slonim DK, Brown EL, Hunter CP. 2003. Composition and dynamics of the *Caenorhabditis elegans* early embryonic transcriptome. Development. 130(5):889–900. doi:10.1242/dev.00302.

Baumann P, Cech TR. 2000. Protection of telomeres by the Ku protein in fission yeast. Mol Biol Cell. 11(10):3265–3275. doi:10.1091/mbc.11.10.3265.

Baumann P, Cech TR. 2001. Pot1, the putative telomere end-binding protein in fission yeast and humans. Science (80-). 292(5519):1171–1175. doi:10.1126/science.1060036.

Baur JA, Zou Y, Shay JW, Wright WE. 2001. Telomere position effect in human cells. Science (80-). 292(5524):2075–2077. doi:10.1126/science.1062329.

Beernink HTH, Miller K, Deshpande A, Bucher P, Cooper JP. 2003. Telomere Maintenance in Fission Yeast Requires an Est1 Ortholog. Curr Biol. 13(7):575–580. doi:10.1016/S0960-9822(03)00210-0. https://ac.els-cdn.com/S0960982203002471/1-s2.0-S0960982203002471-main.pdf?_tid=9ea29124-fb57-4655-b9bd-2c200a21edf5&acdnat=1527873870_0c24ce83ce3300a7a2530d7fa744e071.

Behrens A, Van Deursen JM, Rudolph KL, Schumacher B. 2014. Impact of genomic damage and ageing on stem cell function. Nat Cell Biol. 16(3):201–207. doi:10.1038/ncb2928.

Beishline K, Vladimirova O, Tutton S, Wang Z, Deng Z, Lieberman PM. 2017. CTCF driven TERRA transcription facilitates completion of telomere DNA replication. Nat Commun. 8(1):1–10. doi:10.1038/s41467-017-02212-w. http://dx.doi.org/10.1038/s41467-017-02212-w.

Bénard C, Hekimi S. 2002. Long-lived mutants, the rate of aging, telomeres and the germline in *Caenorhabditis elegans*. Mech Ageing Dev. 123(8):869–80. doi:10.1016/s0047-6374(02)00024-6. http://www.ncbi.nlm.nih.gov/pubmed/12044935.

Benetti R, García-Cao M, Blasco MA. 2007. Telomere length regulates the epigenetic status of mammalian telomeres and subtelomeres. Nat Genet. 39(2):243–250. doi:10.1038/ng1952.

Bertuch AA, Lundblad V. 2003. Which end: Dissecting Ku's function at telomeres and double-strand breaks. Genes Dev. 17(19):2347–2350. doi:10.1101/gad.1146603.

Bianchi A, Shore D. 2007. Increased association of telomerase with short telomeres in yeast. Genes Dev. 21(14):1726–1730. doi:10.1101/gad.438907.

Bilaud T, Brun C, Ancelin K, Koering CE, Laroche T, Gilson E. 1997. Telomeric localization of TRF2, a novel human telobox protein. Nat Genet. 17(2):239. doi:10.1038/ng1097-236.

Blackburn EH, Gall JG. 1978. A tandemly repeated sequence at the termini of the extrachromosomal ribosomal RNA genes in Tetrahymena. J Mol Biol. 120(1):33–53. doi:10.1016/0022-2836(78)90294-2.

Blasco MA. 2005. Telomeres and human disease: Ageing, cancer and beyond. Nat Rev Genet. 6(8):611–622. doi:10.1038/nrg1656.

Blasco MA. 2007. The epigenetic regulation of mammalian telomeres. Nat Rev Genet. 8(4):299–309. doi:10.1038/nrg2047.

Blazie SM, Geissel HC, Wilky H, Joshi R, Newbern J, Mangone M. 2017. Alternative Polyadenylation Directs Tissue-Specific miRNA Targeting in *Caenorhabditis elegans* Somatic Tissues. Genetics. 206(2):757–774. doi:10.1534/genetics.116.196774. http://www.genetics.org/lookup/doi/10.1534/genetics.116.196774.

Bluhm A, Viceconte N, Li F, Rane G, Ritz S, Wang S, Levin M, Shi Y, Kappei D, Butter F. 2019. ZBTB10 binds the telomeric variant repeat TTGGGG and interacts with TRF2. Nucleic Acids Res. 47(4):1896–1907. doi:10.1093/nar/gky1289.

Boddy MN, Russell P. 1999. DNA replication checkpoint control. Front Biosci. 4:841–848. doi:10.2741/boddy.

Bodnar AG, Ouellette M, Frolkis M, Holt SE, Chiu CP, Morin GB, Harley CB, Shay JW, Lichtsteiner S, Wright WE. 1998. Extension of life-span by introduction of telomerase into normal human cells. Science (80-). 279(5349):349–352. doi:10.1126/science.279.5349.349.

Boerckel J, Walker D, Ahmed S. 2007. The *Caenorhabditis elegans* Rad17 homolog HPR-17 is required for telomere replication. Genetics. 176(1):703–709. doi:10.1534/genetics.106.070201.

Boersema PJ, Raijmakers R, Lemeer S, Mohammed S, Heck AJR. 2009. Multiplex peptide stable isotope dimethyl labeling for quantitative proteomics. Nat Protoc. 4(4):484–494. doi:10.1038/nprot.2009.21.

Bonetti D, Clerici M, Anbalagan S, Martina M, Lucchini G, Longhese MP. 2010. Shelterin-like proteins and Yku inhibit nucleolytic processing of Saccharomyces cerevisiae telomeres. PLoS Genet. 6(5):1. doi:10.1371/journal.pgen.1000966.

Bonetti D, Martina M, Clerici M, Lucchini G, Longhese MP. 2009. Multiple Pathways Regulate 3′ Overhang Generation at S. cerevisiae Telomeres. Mol Cell. 35(1):70–81. doi:10.1016/j.molcel.2009.05.015. http://dx.doi.org/10.1016/j.molcel.2009.05.015.

Brackertz M, Boeke J, Zhang R, Renkawitz R. 2002. Two highly related p66 proteins comprise a new family of potent transcriptional repressors interacting with MBD2 and MBD3. J Biol Chem. 277(43):40958–66. doi:10.1074/jbc.M207467200. http://www.ncbi.nlm.nih.gov/pubmed/12183469.

Brenner AJ, Stampfer MR, Aldaz CM. 1998. Increased p16 expression with first senescence arrest in human mammary epithelial cells and extended growth capacity with p16 inactivation. Oncogene. 17(2):199–205. doi:10.1038/sj.onc.1201919. http://www.nature.com/articles/1201919.

Brenner S. 1974. The Genetics of *Caenorhabditis elegans*. Genetics. 77(1):71–94.

Britanova O, Akopov S, Lukyanov S, Gruss P, Tarabykin V. 2005. Novel transcription factor Satb2 interacts with matrix attachment region DNA elements in a tissue-specific manner and demonstrates cell-type-dependent expression in the developing mouse CNS. Eur J Neurosci. 21(3):658–668. doi:10.1111/j.1460-9568.2005.03897.x.

Broccoli D, Smogorzewska A, Chong L, de Lange T. 1997. Human telomeres contain two distinct Myb-related proteins, TRF1 and TRF2. Nat Genet. 17(2):231–235. doi:10.1038/ng1097-231.

de Bruin D, Kantrow SM, Liberatore RA, Zakian VA. 2000. Telomere Folding Is Required for the Stable Maintenance of Telomere Position Effects in Yeast. Mol Cell Biol. 20(21):7991–8000. doi:10.1128/mcb.20.21.7991-8000.2000.

de Bruin D, Zaman Z, Liberatore RA, Ptashne M. 2001. Telomere looping permits gene activation by a downstream UAS in yeast. Nature. 409(6816):109–113. doi:10.1038/35051119.

Bryan TM, Englezou A, Dalla-Pozza L, Dunham MA, Reddel RR. 1997. Evidence for an alternative mechanism for maintaining telomere length in human tumors and tumor-derived cell lines. Nat Med. 3(11):1271–1274. doi:10.1038/nm1197-1271. http://www.nature.com/articles/nm1197-1271.

Bryan TM, Reddel RR. 1997. Telomere dynamics and telomerase activity in in vitro immortalised human cells. Eur J Cancer Part A. 33(5):767–773. doi:10.1016/S0959-8049(97)00065-8.

Buchman AR, Kimmerly WJ, Rine J, Kornberg RD. 1988. Two DNA-binding factors recognize specific sequences at silencers, upstream activating sequences, autonomously replicating sequences, and telomeres in Saccharomyces cerevisiae. Mol Cell Biol. 8(1):210–225. doi:10.1128/mcb.8.1.210.

Budd ME, Campbell JL. 2013. Dna2 is involved in CA strand resection and nascent lagging strand completion at native yeast telomeres. J Biol Chem. 288(41):29414–29429. doi:10.1074/jbc.M113.472456.

Callegari AJ, Kelly TJ. 2007. Shedding light on the DNA damage checkpoint. Cell Cycle. 6(6):660–666. doi:10.4161/cc.6.6.3984.

Campisi J, D'Adda Di Fagagna F. 2007. Cellular senescence: When bad things happen to good cells. Nat Rev Mol Cell Biol. 8(9):729–740. doi:10.1038/nrm2233.

Capkova Frydrychova R, Biessmann H, Mason JM. 2009. Regulation of telomere length in Drosophila. Cytogenet Genome Res. 122(3–4):356–364. doi:10.1159/000167823.

Casas-Vila N, Scheibe M, Freiwald A, Kappei D, Butter F. 2015. Identification of TTAGGG-binding proteins in Neurospora crassa, a fungus with vertebrate-like telomere repeats. BMC Genomics. 16(1):965. doi:10.1186/s12864-015-2158-0. http://www.pubmedcentral.nih.gov/articlerender.fcgi?artid=4650311&tool=pmcentrez&rendertype=abstract.

Celli GB, Denchi EL, de Lange T. 2006. Ku70 stimulates fusion of dysfunctional telomeres yet protects chromosome ends from homologous recombination. Nat Cell Biol. 8(8):885–890. doi:10.1038/ncb1444.

Celli GB, de Lange T. 2005. DNA processing is not required for ATM-mediated telomere damage response after TRF2 deletion. Nat Cell Biol. 7(7):712–718. doi:10.1038/ncb1275.

Cenci G, Ciapponi L, Gatti M. 2005. The mechanism of telomere protection: A comparison between Drosophila and humans. Chromosoma. 114(3):135–145. doi:10.1007/s00412-005-0005-9.

Cesare AJ, Griffith JD. 2004. Telomeric DNA in ALT Cells Is Characterized by Free Telomeric Circles and Heterogeneous t-Loops. Mol Cell Biol. 24(22):9948–9957. doi:10.1128/mcb.24.22.9948-9957.2004.

Cesare AJ, Reddel RR. 2010. Alternative lengthening of telomeres: Models, mechanisms and implications. Nat Rev Genet. 11(5):319–330. doi:10.1038/nrg2763.

Chan CSM, Tye BK, Herskowitz I. 1983. A family of Saccharomyces cerevisiae repetitive autonomously replicating sequences that have very similar genomic environments. J Mol Biol. 168(3):505–523. doi:10.1016/S0022-2836(83)80299-X.

Chawla R, Redon S, Raftopoulou C, Wischnewski H, Gagos S, Azzalin CM. 2011. Human UPF1 interacts with TPP1 and telomerase and sustains telomere leading-strand replication. EMBO J. 30(19):4047–4058. doi:10.1038/emboj.2011.280. http://dx.doi.org/10.1038/emboj.2011.280.

Chen B, Gilbert LA, Cimini BA, Schnitzbauer J, Zhang W, Li G-W, Park J, Blackburn EH, Weissman JS, Qi LS, et al. 2013. Dynamic Imaging of Genomic Loci in Living Human Cells by an Optimized CRISPR/Cas System. Cell. 155(7):1479–1491. doi:10.1016/j.cell.2013.12.001. http://dx.doi.org/10.1016/j.cell.2013.12.033.

Chen Q, Ijpma A, Greider CW. 2001. Two Survivor Pathways That Allow Growth in the Absence of Telomerase Are Generated by Distinct Telomere Recombination Events. Mol Cell Biol. 21(5):1819–1827. doi:10.1128/mcb.21.5.1819-1827.2001.

Chen Z, Han M. 2001. Role of C. elegans lin-40 MTA in vulval fate specification and morphogenesis. Development. 128(23):4911–4921.

Cheng C, Shtessel L, Brady MM, Ahmed S. 2012. *Caenorhabditis elegans* POT-2 telomere protein represses a mode of alternative lengthening of telomeres with normal telomere lengths. Proc Natl Acad Sci U S A. 109(20):7805–7810. doi:10.1073/pnas.1119191109.

Cheung I. 2004. Strain-specific telomere length revealed by single telomere length analysis in *Caenorhabditis elegans*. Nucleic Acids Res. 32(11):3383–3391. doi:10.1093/nar/gkh661. https://academic.oup.com/nar/article-lookup/doi/10.1093/nar/gkh661.

Cheung I. 2006. High incidence of rapid telomere loss in telomerase-deficient *Caenorhabditis elegans*. Nucleic Acids Res. 34(1):96–103. doi:10.1093/nar/gkj417. https://academic.oup.com/nar/article-lookup/doi/10.1093/nar/gkj417.

Chikashige Y, Ding DQ, Funabiki H, Haraguchi T, Mashiko S, Yanagida M, Hiraoka Y. 1994. Telomere-led premeiotic chromosome movement in fission yeast. Science (80-). 264(5156):270–273. doi:10.1126/science.8146661.

Chikashige Y, Hiraoka Y. 2001. Telomere binding of the Rap1 protein is required for meiosis in fission yeast. Curr Biol. 11(20):1618–1623. doi:10.1016/S0960-9822(01)00457-2. https://linkinghub.elsevier.com/retrieve/pii/S0960982201004572.

Chikashige Y, Tsutsumi C, Yamane M, Okamasa K, Haraguchi T, Hiraoka Y. 2006. Meiotic Proteins Bqt1 and Bqt2 Tether Telomeres to Form the Bouquet Arrangement of Chromosomes. Cell. 125(1):59–69. doi:10.1016/j.cell.2006.01.048.

Childs BG, Durik M, Baker DJ, Van Deursen JM. 2015. Cellular senescence in aging and age-related disease: From mechanisms to therapy. Nat Med. 21(12):1424–1435. doi:10.1038/nm.4000.

Chin GM. 2001. C. elegans mre-11 is required for meiotic recombination and DNA repair but is dispensable for the meiotic G2 DNA damage checkpoint. Genes Dev. 15(5):522–534. doi:10.1101/gad.864101. http://www.genesdev.org/cgi/doi/10.1101/gad.864101.

Chiu J, March PE, Lee R, Tillett D. 2004. Site-directed, Ligase-Independent Mutagenesis (SLIM): a single-tube methodology approaching 100% efficiency in 4 h. Nucleic Acids Res. 32(21):e174–e174. doi:10.1093/nar/gnh172. https://academic.oup.com/nar/article-lookup/doi/10.1093/nar/gnh172.

Chiu J, Tillett D, Dawes IW, March PE. 2008. Site-directed, Ligase-Independent Mutagenesis (SLIM) for highly efficient mutagenesis of plasmids greater than 8kb. J Microbiol Methods. 73(2):195–198. doi:10.1016/j.mimet.2008.02.013. https://linkinghub.elsevier.com/retrieve/pii/S0167701208000407.

Chong L, van Steensel B, Broccoli D, Erdjument-Bromage H, Hanish J, Tempst P, de Lange T. 1995. A Human Telomeric Protein. Science (80-). 270(5242):1663–1667. doi:10.1126/science.270.5242.1663. https://www.sciencemag.org/lookup/doi/10.1126/science.270.5242.1663.

Chu HP, Cifuentes-Rojas C, Kesner B, Aeby E, Lee H goo, Wei C, Oh HJ, Boukhali M, Haas W, Lee JT. 2017. TERRA RNA Antagonizes ATRX and Protects Telomeres. Cell. 170(1):86-101.e16. doi:10.1016/j.cell.2017.06.017. http://dx.doi.org/10.1016/j.cell.2017.06.017.

Cleal K, Baird DM. 2020. Catastrophic Endgames: Emerging Mechanisms of Telomere-Driven Genomic Instability. Trends Genet. 36(5):347–359. doi:10.1016/j.tig.2020.02.001. https://doi.org/10.1016/j.tig.2020.02.001.

Clejan I, Boerckel J, Ahmed S. 2006. Developmental modulation of nonhomologous end joining in *Caenorhabditis elegans*. Genetics. 173(3):1301–1317. doi:10.1534/genetics.106.058628.

Coghlan A, Wolfe KH. 2002. Fourfold faster rate of genome rearrangement in nematodes than in Drosophila. Genome Res. 12(6):857–867. doi:10.1101/gr.172702.

Cohn M, Blackburn EH. 1995. Telomerase in yeast. Science (80-). 269(5222):396–400. doi:10.1126/science.7618104.

Collado M, Blasco MA, Serrano M. 2007. Cellular Senescence in Cancer and Aging. Cell. 130(2):223–233. doi:10.1016/j.cell.2007.07.003.

Conomos D, Reddel RR, Pickett HA. 2014. NuRD-ZNF827 recruitment to telomeres creates a molecular scaffold for homologous recombination. Nat Struct Mol Biol. 21(9):760–770. doi:10.1038/nsmb.2877.

Conomos D, Stutz MD, Hills M, Neumann AA, Bryan TM, Reddel RR, Pickett HA. 2012. Variant repeats are interspersed throughout the telomeres and recruit nuclear receptors in ALT cells. J Cell Biol. 199(6):893–906. doi:10.1083/jcb.201207189.

Conrad MN, Dominguez AM, Dresser ME. 1997. Ndj1p, a meiotic telomere protein required for normal chromosome synapsis and segregation in yeast. Science (80-). 276(5316):1252–1255. doi:10.1126/science.276.5316.1252.

Conrad MN, Lee CY, Wilkerson JL, Dresser ME. 2007. MPS3 mediates meiotic bouquet formation in Saccharomyces cerevisiae. Proc Natl Acad Sci U S A. 104(21):8863–8868. doi:10.1073/pnas.0606165104.

Conrad MN, Wright JH, Wolf AJ, Zakian VA. 1990. RAP1 protein interacts with yeast telomeres in vivo: Overproduction alters telomere structure and decreases chromosome stability. Cell. 63(4):739–750. doi:10.1016/0092-8674(90)90140-A.

Cook DE, Zdraljevic S, Tanny RE, Seo B, Riccardi DD, Noble LM, Rockman M V., Alkema MJ, Braendle C, Kammenga JE, et al. 2016. The Genetic Basis of Natural Variation in *Caenorhabditis elegans* Telomere Length. Genetics. 204(1):371–383. doi:10.1534/genetics.116.191148. http://www.genetics.org/lookup/doi/10.1534/genetics.116.191148.

Cook SJ, Jarrell TA, Brittin CA, Wang Y, Bloniarz AE, Yakovlev MA, Nguyen KCQ, Tang LTH, Bayer EA, Duerr JS, et al. 2019. Whole-animal connectomes of both *Caenorhabditis elegans* sexes. Nature. 571(7763):63–71. doi:10.1038/s41586-019-1352-7. http://dx.doi.org/10.1038/s41586-019-1352-7.

Cooper JP. 2000. Telomere transitions in yeast: The end of the chromosome as we know it. Curr Opin Genet Dev. 10(2):169–177. doi:10.1016/S0959-437X(00)00070-8.

Cooper JP, Nimmo ER, Allshire RC, Cech TR. 1997. Regulation of telomere length and function by a Myb-domain protein in fission yeast. Nature. 385(6618):744–747. doi:10.1038/385744a0.

Cordeiro Rodrigues RJ, De Jesus Domingues AM, Hellmann S, Dietz S, De Albuquerque BFM, Renz C, Ulrich HD, Sarkies P, Butter F, Ketting RF. 2019. PETISCO is a novel protein complex required for 21U RNA biogenesis and embryonic viability. Genes Dev. 33(13–14):857–870. doi:10.1101/gad.322446.118.

Court R, Chapman L, Fairall L, Rhodes D. 2005. How the human telomeric proteins TRF1 and TRF2 recognize telomeric DNA: a view from high-resolution crystal structures. EMBO Rep. 6(1):39–45. doi:10.1038/sj.embor.7400314. http://embor.embopress.org/cgi/doi/10.1038/sj.embor.7400314.

Cox J, Hein MY, Luber CA, Paron I, Nagaraj N, Mann M. 2014. Accurate Proteome-wide Label-free Quantification by Delayed Normalization and Maximal Peptide Ratio Extraction, Termed MaxLFQ. Mol Cell Proteomics. 13(9):2513–2526. doi:10.1074/mcp.M113.031591. http://www.mcponline.org/lookup/doi/10.1074/mcp.M113.031591.

Crabbe L, Cesare AJ, Kasuboski JM, Fitzpatrick JAJ, Karlseder J. 2012. Human Telomeres Are Tethered to the Nuclear Envelope during Postmitotic Nuclear Assembly. Cell Rep. 2(6):1521–1529. doi:10.1016/j.celrep.2012.11.019. http://dx.doi.org/10.1016/j.celrep.2012.11.019.

Creighton HB, McClintock B. 1935. The Correlation of Cytological and Genetical Crossing-Over in Zea Mays. A Corroboration. Proc Natl Acad Sci. 21(3):148–150. doi:10.1073/pnas.21.3.148.

Cristofari G, Lingner J. 2006. Telomere length homeostasis requires that telomerase levels are limiting. EMBO J. 25(3):565–574. doi:10.1038/sj.emboj.7600952.

Crossley MP, Bocek M, Cimprich KA. 2019. R-Loops as Cellular Regulators and Genomic Threats. Mol Cell. 73(3):398–411. doi:10.1016/j.molcel.2019.01.024. https://doi.org/10.1016/j.molcel.2019.01.024.

da Cruz I, Brochier-Armanet C, Benavente R. 2020. The TERB1-TERB2-MAJIN complex of mouse meiotic telomeres dates back to the common ancestor of metazoans. BMC Evol Biol. 20(1):1–11. doi:10.1186/s12862-020-01612-9.

Cusanelli E, Chartrand P. 2014. Telomeric noncoding RNA: Telomeric repeat-containing RNA in telomere biology. Wiley Interdiscip Rev RNA. 5(3):407–419. doi:10.1002/wrna.1220.

Cusanelli E, Romero CAP, Chartrand P. 2013. Telomeric Noncoding RNA TERRA Is Induced by Telomere Shortening to Nucleate Telomerase Molecules at Short Telomeres. Mol Cell. 51(6):780–791. doi:10.1016/j.molcel.2013.08.029. http://dx.doi.org/10.1016/j.molcel.2013.08.029.

D'Adda Di Fagagna F. 2008. Living on a break: Cellular senescence as a DNA-damage response. Nat Rev Cancer. 8(7):512–522. doi:10.1038/nrc2440.

D'Amours D, Desnoyers S, D'Silva I, Poirier GG. 1999. Poly(ADP-ribosyl)ation reactions in the regulation of nuclear functions. Biochem J. 342 (Pt 2:249–68. http://www.ncbi.nlm.nih.gov/pubmed/10455009.

Dahlén M, Olsson T, Kanter-Smoler G, Ramne A, Sunnerhagen P. 1998. Regulation of telomere length by checkpoint genes in Schizosaccharomyces pombe. Mol Biol Cell. 9(3):611–621. doi:10.1091/mbc.9.3.611.

Danial NN, Korsmeyer SJ. 2004. Cell Death: Critical Control Points. Cell. 116(2):205–219. doi:10.1016/S0092-8674(04)00046-7.

Dehé PM, Cooper JP. 2010. Fission yeast telomeres forecast the end of the crisis. FEBS Lett. 584(17):3725–3733. doi:10.1016/j.febslet.2010.07.045.

Dehé PM, Rog O, Ferreira MG, Greenwood J, Cooper JP. 2012. Taz1 Enforces Cell-Cycle Regulation of Telomere Synthesis. Mol Cell. 46(6):797–808. doi:10.1016/j.molcel.2012.04.022.

Déjardin J, Kingston RE. 2009. Purification of Proteins Associated with Specific Genomic Loci. Cell. 136(1):175–186. doi:10.1016/j.cell.2008.11.045.

Denchi EL, De Lange T. 2007. Protection of telomeres through independent control of ATM and ATR by TRF2 and POT1. Nature. 448(7157):1068–1071. doi:10.1038/nature06065.

Deng Z, Norseen J, Wiedmer A, Riethman H, Lieberman PM. 2009. TERRA RNA Binding to TRF2 Facilitates Heterochromatin Formation and ORC Recruitment at Telomeres. Mol Cell. 35(4):403–413. doi:10.1016/j.molcel.2009.06.025. http://dx.doi.org/10.1016/j.molcel.2009.06.025.

Deng Z, Wang Z, Stong N, Plasschaert R, Moczan A, Chen HS, Hu S, Wikramasinghe P, Davuluri R V., Bartolomei MS, et al. 2012. A role for CTCF and cohesin in subtelomere chromatin organization, TERRA transcription, and telomere end protection. EMBO J. 31(21):4165–4178. doi:10.1038/emboj.2012.266. http://dx.doi.org/10.1038/emboj.2012.266.

Denslow SA, Wade PA. 2007. The human Mi-2/NuRD complex and gene regulation. Oncogene. 26(37):5433–5438. doi:10.1038/sj.onc.1210611.

Dickinson DJ, Pani AM, Heppert JK, Higgins CD, Goldstein B. 2015. Streamlined genome engineering with a self-excising drug selection cassette. Genetics. 200(4):1035–1049. doi:10.1534/genetics.115.178335.

Dickinson DJ, Ward JD, Reiner DJ, Goldstein B. 2013. Engineering the *Caenorhabditis elegans* genome using Cas9-triggered homologous recombination. Nat Methods. 10(10):1028–1034. doi:10.1038/nmeth.2641.

Dilova I, Easlon E, Lin SJ. 2007. Calorie restriction and the nutrient sensing signaling pathways. Cell Mol Life Sci. 64(6):752–767. doi:10.1007/s00018-007-6381-y.

Dimri GP, Lee X, Basile G, Acosta M, Scott G, Roskelley C, Medrano EE, Linskens M, Rubelj I, Pereira-Smith O, et al. 1995. A biomarker that identifies senescent human cells in culture and in aging skin in vivo. Proc Natl Acad Sci U S A. 92(20):9363–9367. doi:10.1073/pnas.92.20.9363.

Doksani Y, Wu JY, De Lange T, Zhuang X. 2013. XSuper-resolution fluorescence imaging of telomeres reveals TRF2-dependent T-loop formation. Cell. 155(2):345. doi:10.1016/j.cell.2013.09.048. http://dx.doi.org/10.1016/j.cell.2013.09.048.

Doré AS, Kilkenny ML, Rzechorzek NJ, Pearl LH. 2009. Crystal structure of the rad9-rad1-hus1 DNA damage checkpoint complex--implications for clamp loading and regulation. Mol Cell. 34(6):735–45. doi:10.1016/j.molcel.2009.04.027. http://www.ncbi.nlm.nih.gov/pubmed/19446481.

Ellis HM, Horvitz HR. 1986. Genetic control of programmed cell death in the nematode C. elegans. Cell. 44(6):817–29. doi:10.1016/0092-8674(86)90004-8. http://www.ncbi.nlm.nih.gov/pubmed/3955651.

van Emden TS, Forn M, Forné I, Sarkadi Z, Capella M, Martín Caballero L, Fischer-Burkart S, Brönner C, Simonetta M, Toczyski D, et al. 2019. Shelterin and subtelomeric DNA sequences control nucleosome maintenance and genome stability. EMBO Rep. 20(1). doi:10.15252/embr.201847181. http://www.ncbi.nlm.nih.gov/pubmed/30420521.

Episkopou H, Draskovic I, Van Beneden A, Tilman G, Mattiussi M, Gobin M, Arnoult N, Londoño-Vallejo A, Decottignies A. 2014. Alternative Lengthening of Telomeres is characterized by reduced compaction of telomeric chromatin. Nucleic Acids Res. 42(7):4391–4405. doi:10.1093/nar/gku114.

Ewald CY, Li C. 2010. Understanding the molecular basis of Alzheimer's disease using a *Caenorhabditis elegans* model system. Brain Struct Funct. 214(2–3):263–283. doi:10.1007/s00429-009-0235-3.

Fabrizio P, Longo VD. 2003. The chronological life span of Saccharomyces cerevisiae. Aging Cell. 2(2):73–81. doi:10.1046/j.1474-9728.2003.00033.x. http://doi.wiley.com/10.1046/j.1474-9728.2003.00033.x.

Feng J, Funk WD, Wang SS, Weinrich SL, Avilion AA, Chiu CP, Adams RR, Chang E, Allsopp RC, Yu J, et al. 1995. The RNA component of human telomerase. Science (80-). 269(5228):1236–1241. doi:10.1126/science.7544491.

Feng Q, Cao R, Xia L, Erdjument-Bromage H, Tempst P, Zhang Y. 2002. Identification and Functional Characterization of the p66/p68 Components of the MeCP1 Complex. Mol Cell Biol. 22(2):536–546. doi:10.1128/mcb.22.2.536-546.2002.

Feng Z, Li W, Ward A, Piggott BJ, Larkspur ER, Sternberg PW, Xu XZS. 2006. A C. elegans Model of Nicotine-Dependent Behavior: Regulation by TRP-Family Channels. Cell. 127(3):621–633. doi:10.1016/j.cell.2006.09.035.

Ferreira Helder C., Towbin BD, Jegou T, Gasser SM. 2013. The shelterin protein POT-1 anchors *Caenorhabditis elegans* telomeres through SUN-1 at the nuclear periphery. J Cell Biol. 203(5):727–735. doi:10.1083/jcb.201307181.

Ferreira Helder C, Towbin BD, Jegou T, Gasser SM. 2013. The shelterin protein POT-1 anchors *Caenorhabditis elegans* telomeres through SUN-1 at the nuclear periphery. J Cell Biol. 203(5):727–735. doi:10.1083/jcb.201307181.

Ferreira MG, Cooper JP. 2001. The fission yeast Taz1 protein protects chromosomes from Ku-dependent end-to-end fusions. Mol Cell. 7(1):55–63. doi:10.1016/S1097-2765(01)00154-X.

Fire A, Albertson D, Harrison SW, Moerman DG. 1991. Production of antisense RNA leads to effective and specific inhibition of gene expression in C. elegans muscle. Development. 113(2):503–514.

Fire A, Xu S, Montgomery MK, Kostas SA, Driver SE, Mello CC. 1998. Potent and specific genetic interference by double-stranded RNA in *Caenorhabditis elegans*. Nature. 391(6669):806–811. doi:10.1038/35888. http://www.nature.com/articles/35888.

Fisher TS, Zakian VA. 2005. Ku: A multifunctional protein involved in telomere maintenance. DNA Repair (Amst). 4(11):1215–1226. doi:10.1016/j.dnarep.2005.04.021.

Flynn RL, Centore RC, O'Sullivan RJ, Rai R, Tse A, Songyang Z, Chang S, Karlseder J, Zou L. 2011. TERRA and hnRNPA1 orchestrate an RPA-to-POT1 switch on telomeric single-stranded DNA. Nature. 471(7339):532–538. doi:10.1038/nature09772.

Francia S, Weiss RS, Hande MP, Freire R, d'Adda di Fagagna F. 2006. Telomere and Telomerase Modulation by the Mammalian Rad9/Rad1/Hus1 DNA-Damage-Checkpoint Complex. Curr Biol. 16(15):1551–1558. doi:10.1016/j.cub.2006.06.066.

Frøkjær-Jensen C, Davis MW, Ailion M, Jorgensen EM. 2012. Improved Mos1-mediated transgenesis in C. elegans. Nat Methods. 9(2):117–118. doi:10.1038/nmeth.1865.

Frøkjær-Jensen C, Wayne Davis M, Hopkins CE, Newman BJ, Thummel JM, Olesen SP, Grunnet M, Jorgensen EM. 2008. Single-copy insertion of transgenes in *Caenorhabditis elegans*. Nat Genet. 40(11):1375–1383. doi:10.1038/ng.248.

Fujisawa M, Tanaka H, Tatsumi N, Okada H, Arakawa S, Kamidono S. 1998. Telomerase activity in the testis of infertile patients with selected causes. Hum Reprod. 13(6):1476–1479. doi:10.1093/humrep/13.6.1476.

Funabiki H, Hagan I, Uzawa S, Yanagida M. 1993. Cell cycle-dependent specific positioning and clustering of centromeres and telomeres in fission yeast. J Cell Biol. 121(5):961–976. doi:10.1083/jcb.121.5.961.

Gagnon SN, Hengartner MO, Desnoyers S. 2002. The genes pme-1 and pme-2 encode two poly(ADP-ribose) polymerases in *Caenorhabditis elegans*. Biochem J. 368(1):263–271. doi:10.1042/BJ20020669.

Galbiati A, Beauséjour C, d'Adda di Fagagna F. 2017. A novel single-cell method provides direct evidence of persistent DNA damage in senescent cells and aged mammalian tissues. Aging Cell. 16(2):422–427. doi:10.1111/acel.12573.

García-Cao M, O'Sullivan R, Peters AHFM, Jenuwein T, Blasco MA. 2004. Epigenetic regulation of telomere length in mammalian cells by the Suv39h1 and Suv39h2 histone methyltransferases. Nat Genet. 36(1):94–99. doi:10.1038/ng1278.

Garcia-Muse T, Galindo-Diaz U, Garcia-Rubio M, Martin JS, Polanowska J, O'Reilly N, Aguilera A, Boulton SJ. 2019. A Meiotic Checkpoint Alters Repair Partner Bias to Permit Inter-sister Repair of Persistent DSBs. Cell Rep. 26(3):775-787.e5. doi:10.1016/j.celrep.2018.12.074. https://doi.org/10.1016/j.celrep.2018.12.074.

Gauchier M, Kan S, Barral A, Sauzet S, Agirre E, Bonnell E, Saksouk N, Barth TK, Ide S, Urbach S, et al. 2019. SETDB1-dependent heterochromatin stimulates alternative lengthening of telomeres. Sci Adv. 5(5). doi:10.1126/sciadv.aav3673.

Gems D, Partridge L. 2013. Genetics of Longevity in Model Organisms: Debates and Paradigm Shifts. Annu Rev Physiol. 75(1):621–644. doi:10.1146/annurev-physiol-030212-183712.

Gilson E, Géli V. 2007. How telomeres are replicated. Nat Rev Mol Cell Biol. 8(10):825–838. doi:10.1038/nrm2259.

Gomes NMV, Ryder OA, Houck ML, Charter SJ, Walker W, Forsyth NR, Austad SN, Venditti C, Pagel M, Shay JW, et al. 2011. Comparative biology of mammalian telomeres: Hypotheses on ancestral states and the roles of telomeres in longevity determination. Aging Cell. 10(5):761–768. doi:10.1111/j.1474-9726.2011.00718.x.

Gottschling DE, Aparicio OM, Billington BL, Zakian VA. 1990. Position effect at S. cerevisiae telomeres: Reversible repression of Pol II transcription. Cell. 63(4):751–762. doi:10.1016/0092-8674(90)90141-Z.

Gottschling DE, Zakian VA. 1986. Telomere proteins: Specific recognition and protection of the natural termini of Oxytricha macronuclear DNA. Cell. 47(2):195–205. doi:10.1016/0092-8674(86)90442-3.

Graf M, Bonetti D, Lockhart A, Serhal K, Kellner V, Maicher A, Jolivet P, Teixeira MT, Luke B. 2017. Telomere Length Determines TERRA and R-Loop Regulation through the Cell Cycle. Cell. 170(1):72-85.e14. doi:10.1016/j.cell.2017.06.006.

Grandin N, Damon C, Charbonneau M. 2001. Ten1 functions in telomere end protection and length regulation in association with Stn1 and Cdc13. EMBO J. 20(5):1173–1183. doi:10.1093/emboj/20.5.1173.

Grandin N, Reed SI, Charbonneau M. 1997. Stn1, a new Saccharomyces cerevisiae protein, is implicated in telomere size regulation in association with CDc13. Genes Dev. 11(4):512–527. doi:10.1101/gad.11.4.512.

Gravel S, Larrivée M, Labrecque P, Wellinger RJ. 1998. Yeast Ku as a regulator of chromosomal DNA end structure. Science (80-). 280(5364):741–744. doi:10.1126/science.280.5364.741.

Green DR, Galluzzi L, Kroemer G. 2011. Mitochondria and the Autophagy-Inflammation-Cell Death Axis in Organismal Aging. Science (80-). 333(6046):1109–1112. doi:10.1126/science.1201940. https://www.sciencemag.org/lookup/doi/10.1126/science.1201940.

Greenwood J, Cooper JP. 2012. Non-coding telomeric and subtelomeric transcripts are differentially regulated by telomeric and heterochromatin assembly factors in fission yeast. Nucleic Acids Res. 40(7):2956–2963. doi:10.1093/nar/gkr1155.

Greider CW. 2016. Regulating telomere length from the inside out: The replication fork model. Genes Dev. 30(13):1483–1491. doi:10.1101/gad.280578.116.

Greider CW, Blackburn EH. 1985. Identification of a specific telomere terminal transferase activity in tetrahymena extracts. Cell. 43(2 PART 1):405–413. doi:10.1016/0092-8674(85)90170-9.

Greider CW, Blackburn EH. 1987. The telomere terminal transferase of tetrahymena is a ribonucleoprotein enzyme with two kinds of primer specificity. Cell. 51(6):887–898. doi:10.1016/0092-8674(87)90576-9.

Greider CW, Blackburn EH. 1989. A telomeric sequence in the RNA of Tetrahymena telomerase required for telomere repeat synthesis. Nature. 337(6205):331–337. doi:10.1038/337331a0.

Griffith JD, Comeau L, Rosenfield S, Stansel RM, Bianchi A, Moss H, De Lange T. 1999. Mammalian telomeres end in a large duplex loop. Cell. 97(4):503–514. doi:10.1016/S0092-8674(00)80760-6.

Gyorgy AB, Szemes M, De Juan Romero C, Tarabykin V, Agoston D V. 2008. SATB2 interacts with chromatin-remodeling molecules in differentiating cortical neurons. Eur J Neurosci. 27(4):865–873. doi:10.1111/j.1460-9568.2008.06061.x.

Hackett JA, Feldser DM, Greider CW. 2001. Telomere dysfunction increases mutation rate and genomic instability. Cell. 106(3):275–286. doi:10.1016/S0092-8674(01)00457-3.

Haeussler M, Schönig K, Eckert H, Eschstruth A, Mianné J, Renaud JB, Schneider-Maunoury S, Shkumatava A, Teboul L, Kent J, et al. 2016. Evaluation of off-target and on-target scoring algorithms and integration into the guide RNA selection tool CRISPOR. Genome Biol. 17(1):1–12. doi:10.1186/s13059-016-1012-2. http://dx.doi.org/10.1186/s13059-016-1012-2.

Harley CB, Futcher AB, Greider CW. 1990. Telomeres shorten during ageing of human fibroblasts. Nature. 345(6274):458–460. doi:10.1038/345458a0. http://www.nature.com/articles/246170a0.

Hayflick L. 1965. The limited in vitro lifetime of human diploid cell strains. Exp Cell Res. 37(3):614–636. doi:10.1016/0014-4827(65)90211-9.

Hayflick L, Moorhead PS. 1961. The serial cultivation of human diploid cell strains. Exp Cell Res. 25:585–621. doi:10.1016/0014-4827(61)90192-6. http://www.ncbi.nlm.nih.gov/pubmed/13905658.

Haynes CM, Petrova K, Benedetti C, Yang Y, Ron D. 2007. ClpP Mediates Activation of a Mitochondrial Unfolded Protein Response in C. elegans. Dev Cell. 13(4):467–480. doi:10.1016/j.devcel.2007.07.016.

He H, Multani AS, Cosme-Blanco W, Tahara H, Ma J, Pathak S, Deng Y, Chang S. 2006. POT1b protects telomeres from end-to-end chromosomal fusions and aberrant homologous recombination. EMBO J. 25(21):5180–5190. doi:10.1038/sj.emboj.7601294.

Hector RE, Shtofman RL, Ray A, Chen BR, Nyun T, Berkner KL, Runge KW. 2007. Tel1p Preferentially Associates with Short Telomeres to Stimulate Their Elongation. Mol Cell. 27(5):851–858. doi:10.1016/j.molcel.2007.08.007.

Hedgecock EM, Sulston JE, Thomson JN. 1983. Mutations affecting programmed cell deaths in the nematode *Caenorhabditis elegans*. Science (80-). 220(4603):1277–9. doi:10.1126/science.6857247. http://www.ncbi.nlm.nih.gov/pubmed/6857247.

Henson JD, Cao Y, Huschtscha LI, Chang AC, Au AYM, Pickett HA, Reddel RR. 2009. DNA C-circles are specific and quantifiable markers of alternative-lengthening-of-telomeres activity. Nat Biotechnol. 27(12):1181–1185. doi:10.1038/nbt.1587. http://www.nature.com/articles/nbt.1587.

Herbig U, Jobling WA, Chen BPC, Chen DJ, Sedivy JM. 2004. Telomere shortening triggers senescence of human cells through a pathway involving ATM, p53, and p21CIP1, but not p16INK4a. Mol Cell. 14(4):501–513. doi:10.1016/S1097-2765(04)00256-4.

Herman RK, Kari CK, Hartman PS. 1982. Dominant X-chromosome nondisjunction mutants of *Caenorhabditis elegans*. Genetics. 102(3):379–400.

Hill AA, Hunter CP, Tsung BT, Tucker-Kellogg G, Brown EL. 2000. Genomic Analysis of Gene Expression in C. elegans. Science (80-). 290(5492):809–812. doi:10.1126/science.290.5492.809. https://www.sciencemag.org/lookup/doi/10.1126/science.290.5492.809.

Hiraoka Y, Dernburg AF. 2009. The SUN Rises on Meiotic Chromosome Dynamics. Dev Cell. 17(5):598–605. doi:10.1016/j.devcel.2009.10.014. http://dx.doi.org/10.1016/j.devcel.2009.10.014.

Hockemeyer D, Daniels JP, Takai H, de Lange T. 2006. Recent Expansion of the Telomeric Complex in Rodents: Two Distinct POT1 Proteins Protect Mouse Telomeres. Cell. 126(1):63–77. doi:10.1016/j.cell.2006.04.044.

Hodgkin J, Horvitz HR, Brenner S. 1979. Nondisjunction Mutants of the Nematode *Caenorhabditis elegans*. Genetics. 91(1):67–94. http://www.ncbi.nlm.nih.gov/pubmed/17248881.

Hofmann ER, Milstein S, Boulton SJ, Ye M, Hofmann JJ, Stergiou L, Gartner A, Vidal M, Hengartner MO. 2002. *Caenorhabditis elegans* HUS-1 is a DNA damage checkpoint protein required for genome stability and EGL-1-mediated apoptosis. Curr Biol. 12(22):1908–18. doi:10.1016/s0960-9822(02)01262-9. http://www.ncbi.nlm.nih.gov/pubmed/12445383.

Holmes GE, Bernstein C, Bernstein H. 1992. Oxidative and other DNA damages as the basis of aging: a review. Mutat Res DNAging. 275(3–6):305–315. doi:10.1016/0921-8734(92)90034-M.

Holohan B, Wright WE, Shay JW. 2014. Cell biology of disease: Telomeropathies: an emerging spectrum disorder. J Cell Biol. 205(3):289–99. doi:10.1083/jcb.201401012. http://www.ncbi.nlm.nih.gov/pubmed/24821837.

Holstein EM, Ngo G, Lawless C, Banks P, Greetham M, Wilkinson D, Lydall D. 2017. Systematic analysis of the DNA damage response network in telomere defective budding yeast. G3 Genes, Genomes, Genet. 7(7):2375–2389. doi:10.1534/g3.117.042283.

Honda S, Ishii N, Suzuki K, Matsuo M. 1993. Oxygen-dependent perturbation of life span and aging rate in the nematode. Journals Gerontol. 48(2):57–61. doi:10.1093/geronj/48.2.B57.

Hsu HL, Gilley D, Galande SA, Prakash Hande M, Allen B, Kim SH, Li GC, Campisi J, Kohwi-Shigematsu T, Chen DJ. 2000. Ku acts in a unique way at the mammalian telomere to prevent end joining. Genes Dev. 14(22):2807–2812. doi:10.1101/gad.844000.

Hsu JL, Huang SY, Chow NH, Chen SH. 2003. Stable-Isotope Dimethyl Labeling for Quantitative Proteomics. Anal Chem. 75(24):6843–6852. doi:10.1021/ac0348625.

Hu Y, Bennett HW, Liu N, Moravec M, Williams JF, Azzalin CM, King MC. 2019. RNA-DNA hybrids support recombination-based telomere maintenance in fission yeast. Genetics. 213(2):431–437. doi:10.1534/genetics.119.302606.

Hubbard EJA, Greenstein D. 2005. Introduction to the germ line. WormBook.:1–4. doi:10.1895/wormbook.1.18.1.

Hug N, Lingner J. 2006. Telomere length homeostasis. Chromosoma. 115(6):413–425. doi:10.1007/s00412-006-0067-3.

Iglesias N, Redon S, Pfeiffer V, Dees M, Lingner J, Luke B. 2011. Subtelomeric repetitive elements determine TERRA regulation by Rap1/Rif and Rap1/Sir complexes in yeast. EMBO Rep. 12(6):587–593. doi:10.1038/embor.2011.73. http://dx.doi.org/10.1038/embor.2011.73.

Im SH, Lee J. 2003. Identification of HMG-5 as a double-stranded telomeric DNA-binding protein in the nematode *Caenorhabditis elegans*. FEBS Lett. 554(3):455–461. doi:10.1016/S0014-5793(03)01191-8.

Im SH, Lee J. 2005. PLP-1 binds nematode double-stranded telomeric DNA. Mol Cells. 20(2):297–302.

Jahn A, Rane G, Paszkowski-Rogacz M, Sayols S, Bluhm A, Han Chung-ting, Draškovič I, Londoño-Vallejo JA, Kumar AP, Buchholz F, et al. 2017. ZBTB48 is both a vertebrate telomere-binding protein and a transcriptional activator. EMBO Rep. 18(6):929–946. doi:10.15252/embr.201744095. https://onlinelibrary.wiley.com/doi/abs/10.15252/embr.201744095.

Jahn A, Rane G, Paszkowski-Rogacz M, Sayols S, Bluhm A, Han Chung-Ting, Draškovič I, Londoño-Vallejo JA, Kumar AP, Buchholz F, et al. 2017. ZBTB48 is both a vertebrate telomere-binding protein and a transcriptional activator. EMBO Rep. 18(6):929–946. doi:10.15252/embr.201744095. http://embor.embopress.org/lookup/doi/10.15252/embr.201744095.

Jain D, Hebden AK, Nakamura TM, Miller KM, Cooper JP. 2010. HAATI survivors replace canonical telomeres with blocks of generic heterochromatin. Nature. 467(7312):223–227. doi:10.1038/nature09374.

James P, Halladay J, Craig EA. 1996. Genomic libraries and a host strain designed for highly efficient two-hybrid selection in yeast. Genetics. 144(4):1425–36. http://www.ncbi.nlm.nih.gov/pubmed/8978031.

Joeng KS, Song EJ, Lee K-J, Lee J. 2004. Long lifespan in worms with long telomeric DNA. Nat Genet. 36(6):607–611. doi:10.1038/ng1356. http://www.nature.com/doifinder/10.1038/ng1356.

Johnson TE, Friedman DB. 1988. A Mutation in the age-1 Gene in *Caenorhabditis elegans* Lengthens Life and Reduces Hermaphrodite Fertility. Genetics. 118(Martin 1978):75–86. doi:10.1128/MCB.25.18.8064. https://www.genetics.org/content/genetics/118/1/75.full.pdf.

Kaletta T, Hengartner MO. 2006. Finding function in novel targets: C. elegans as a model organism. Nat Rev Drug Discov. 5(5):387–399. doi:10.1038/nrd2031.

Kalmbach KH, Fontes Antunes DM, Dracxler RC, Knier TW, Seth-Smith ML, Wang F, Liu L, Keefe DL. 2013. Telomeres and human reproduction. Fertil Steril. 99(1):23–29. doi:10.1016/j.fertnstert.2012.11.039. http://dx.doi.org/10.1016/j.fertnstert.2012.11.039.

Kanoh J, Sadaie M, Urano T, Ishikawa F. 2005. Telomere binding protein Taz1 establishes Swi6 heterochromatin independently of RNAi at telomeres. Curr Biol. 15(20):1808–1819. doi:10.1016/j.cub.2005.09.041.

Kappei D, Butter F, Benda C, Scheibe M, Draškovič I, Stevense M, Novo CL, Basquin C, Araki M, Araki K, et al. 2013. HOT1 is a mammalian direct telomere repeat-binding protein contributing to telomerase recruitment. EMBO J. 32(12):1681–1701. doi:10.1038/emboj.2013.105.

Kappei D, Scheibe M, Paszkowski-Rogacz M, Bluhm A, Gossmann TI, Dietz S, Dejung M, Herlyn H, Buchholz F, Mann M, et al. 2017. Phylointeractomics reconstructs functional evolution of protein binding. Nat Commun. 8:14334. doi:10.1038/ncomms14334. http://dx.doi.org/10.1038/ncomms14334.

Karlseder J, Hoke K, Mirzoeva OK, Bakkenist C, Kastan MB, Petrini JHJ, De Lange T. 2004. The telomeric protein TRF2 binds the ATM Kinase and Can Inhibit the ATM-dependent DNA damage response. PLoS Biol. 2(8). doi:10.1371/journal.pbio.0020240.

Kasap M, Rajani V, Rajani J, Dwyer DS. 2018. Surprising conservation of schizophrenia risk genes in lower organisms reflects their essential function and the evolution of genetic liability. Schizophr Res. 202:120–128. doi:10.1016/j.schres.2018.07.017. http://www.ncbi.nlm.nih.gov/pubmed/30017463.

Kawasaki I, Shim YH, Kirchner J, Kaminker J, Wood WB, Strome S. 1998. PGL-1, a predicted RNA-binding component of germ granules, is essential for fertility in C. elegans. Cell. 94(5):635–645. doi:10.1016/S0092-8674(00)81605-0.

Kenyon C. 1988. The nematode *Caenorhabditis elegans*. Science (80-). 240(4858):1448–53. doi:10.1126/science.3287621. http://www.ncbi.nlm.nih.gov/pubmed/3287621.

Kenyon C. 2001. A conserved regulatory system for aging. Cell. 105(2):165–168. doi:10.1016/S0092-8674(01)00306-3.

Khair L, Subramanian L, Moser BA, Nakamura TM. 2010. Roles of heterochromatin and telomere proteins in regulation of fission yeast telomere recombination and telomerase recruitment. J Biol Chem. 285(8):5327–5337. doi:10.1074/jbc.M109.078840.

Kibe T, Osawa GA, Keegan CE, de Lange T. 2010. Telomere Protection by TPP1 Is Mediated by POT1a and POT1b. Mol Cell Biol. 30(4):1059–1066. doi:10.1128/mcb.01498-09.

Kim NW, Piatyszek MA, Prowse KR, Harley CB, West MD, Ho PLC, Coviello GM, Wright WE, Weinrich SL, Shay JW. 1994. Specific association of human telomerase activity with immortal cells and cancer. Science (80-). 266(5193):2011–2015. doi:10.1126/science.7605428.

Kim S, Kaminker P, Campisi J. 1999. TIN2, a new regulator of telomere length in human cells. Nat Genet. 23(4):405–412. doi:10.1038/70508. http://www.nature.com/articles/ng1299_405.

Kim SH, Hwang SB, Chung IK, Lee J. 2003. Sequence-specific binding to telomeric DNA by CEH-37, a homeodomain protein in the nematode *Caenorhabditis elegans*. J Biol Chem. 278(30):28038–28044. doi:10.1074/jbc.M302192200.

Kim SM, Huberman JA. 2001. Regulation of replication timing in fission yeast. EMBO J. 20(21):6115–6126. doi:10.1093/emboj/20.21.6115.

Kim W, Shay JW. 2018. Long-range telomere regulation of gene expression: Telomere looping and telomere position effect over long distances (TPE-OLD). Differentiation. 99:1–9. doi:10.1016/j.diff.2017.11.005. https://doi.org/10.1016/j.diff.2017.11.005.

Kimble J, Hirsh D. 1979. The postembryonic cell lineages of the hermaphrodite and male gonads in *Caenorhabditis elegans*. Dev Biol. 70(2):396–417. doi:10.1016/0012-1606(79)90035-6.

Kimble JE, White JG. 1981. On the control of germ cell development in *Caenorhabditis elegans*. Dev Biol. 81(2):208–19. doi:10.1016/0012-1606(81)90284-0. http://www.ncbi.nlm.nih.gov/pubmed/7202837.

Klass MR. 1977. Aging in the nematode *Caenorhabditis elegans*: major biological and environmental factors influencing life span. Mech Ageing Dev. 6(6):413–29. doi:10.1016/0047-6374(77)90043-4. http://www.ncbi.nlm.nih.gov/pubmed/926867.

Klass MR. 1983. A method for the isolation of longevity mutants in the nematode *Caenorhabditis elegans* and initial results. Mech Ageing Dev. 22(3–4):279–286. doi:10.1016/0047-6374(83)90082-9.

König P, Giraldo R, Chapman L, Rhodes D. 1996. The crystal structure of the DNA-binding domain of yeast RAP1 in complex with telomeric DNA. Cell. 85(1):125–136. doi:10.1016/S0092-8674(00)81088-0.

Koreth J, Van Den Heuvel S. 2005. Cell-cycle control in *Caenorhabditis elegans*: How the worm moves from G1 to S. Oncogene. 24(17):2756–2764. doi:10.1038/sj.onc.1208607.

Koury E, Harrell K, Smolikove S. 2018. Differential RPA-1 and RAD-51 recruitment in vivo throughout the C. Elegans germline, as revealed by laser microirradiation. Nucleic Acids Res. 46(2):748–764. doi:10.1093/nar/gkx1243.

Krauskopf A, Blackburn EH. 1996. Control of telomere growth by interactions of RAP1 with the most distal telomeric repeats. Nature. 383(6598):354–357. doi:10.1038/383354a0.

Kretzschmar K, Watt FM. 2012. Lineage tracing. Cell. 148(1–2):33–45. doi:10.1016/j.cell.2012.01.002. http://dx.doi.org/10.1016/j.cell.2012.01.002.

Kuilman T, Michaloglou C, Mooi WJ, Peeper DS. 2010. The essence of senescence. Genes Dev. 24(22):2463–2479. doi:10.1101/gad.1971610. http://genesdev.cshlp.org/cgi/doi/10.1101/gad.1971610.

Lackner DH, Raices M, Maruyama H, Haggblom C, Karlseder J. 2012. Organismal propagation in the absence of a functional telomerase pathway in *Caenorhabditis elegans*. EMBO J. 31(8):2024–2033. doi:10.1038/emboj.2012.61. http://emboj.embopress.org/cgi/doi/10.1038/emboj.2012.61.

Lai AY, Wade PA. 2011. NuRD: A multi-faceted chromatin remodeling complex in regulating cancer biology. Nat Rev Cancer. 11(8):588–596. doi:10.1038/nrc3091.NuRD.

Lakowski B, Hekimi S. 1996. Determination of life-span in *Caenorhabditis elegans* by four clock genes. Science (80-). 272(5264):1010–1013. doi:10.1126/science.272.5264.1010.

Lam YC, Akhter S, Gu P, Ye J, Poulet A, Giraud-Panis MJ, Bailey SM, Gilson E, Legerski RJ, Chang S. 2010. SNMIB/Apollo protects leading-strand telomeres against NHEJ-mediated repair. EMBO J. 29(13):2230–2241. doi:10.1038/emboj.2010.58.

Lambie EJ. 2002. Cell proliferation and growth in C. elegans. BioEssays. 24(1):38–53. doi:10.1002/bies.10019. http://www.ncbi.nlm.nih.gov/pubmed/11782949.

de Lange T. 2005. Shelterin: The protein complex that shapes and safeguards human telomeres. Genes Dev. 19(18):2100–2110. doi:10.1101/gad.1346005.

de Lange T. 2009. How telomeres solve the end-protection problem. Science (80-). 326(5955):948–952. doi:10.1126/science.1170633.

de Lange T. 2018. Shelterin-Mediated Telomere Protection. Annu Rev Genet. 52(1):annurev-genet-032918-021921. doi:10.1146/annurev-genet-032918-021921. https://www.annualreviews.org/doi/10.1146/annurev-genet-032918-021921.

Lansdorp PM, Verwoerd NP, Van De Rijke FM, Dragowska V, Little MT, Dirks RW, Raap AK, Tanke HJ. 1996. Heterogeneity in telomere length of human chromosomes. Hum Mol Genet. 5(5):685–691. doi:10.1093/hmg/5.5.685.

Le S, Moore JK, Haber JE, Greider CW. 1999. RAD50 and RAD51 define two pathways that collaborate to maintain telomeres in the absence of telomerase. Genetics. 152(1):143–152.

Lee CY, Conrad MN, Dresser ME. 2012. Meiotic chromosome pairing is promoted by telomere-led chromosome movements independent of bouquet formation. PLoS Genet. 8(5). doi:10.1371/journal.pgen.1002730.

Lee SS, Bohrson C, Pike AM, Wheelan SJ, Greider CW. 2015. ATM Kinase Is Required for Telomere Elongation in Mouse and Human Cells. Cell Rep. 13(8):1623–1632. doi:10.1016/j.celrep.2015.10.035. http://dx.doi.org/10.1016/j.celrep.2015.10.035.

Leman AR, Dheekollu J, Deng Z, Lee SW, Das MM, Lieberman PM, Noguchi E. 2012. Timeless preserves telomere length by promoting efficient DNA replication through human telomeres. Cell Cycle. 11(12):2337–2347. doi:10.4161/cc.20810.

Leman AR, Noguchi E. 2012. Local and global functions of Timeless and Tipin in replication fork protection. Cell Cycle. 11(21):3945–3955. doi:10.4161/cc.21989.

Lendvay TS, Morris DK, Sah J, Balasubramanian B, Lundblad V. 1996. Senescence mutants of Saccharomyces cerevisiae with a defect in telomere replication identify three additional EST genes. Genetics. 144(4):1399–1412.

Levi-Ferber M, Salzberg Y, Safra M, Haviv-Chesner A, Bülow HE, Henis-Korenblit S. 2014. It's All in Your Mind: Determining Germ Cell Fate by Neuronal IRE-1 in C. elegans. PLoS Genet. 10(10):1–14. doi:10.1371/journal.pgen.1004747.

Levy DL, Blackburn EH. 2004. Counting of Rif1p and Rif2p on Saccharomyces cerevisiae telomeres regulates telomere length. Mol Cell Biol. 24(24):10857–67. doi:10.1128/MCB.24.24.10857-10867.2004. http://www.ncbi.nlm.nih.gov/pubmed/15572688.

Li B, Oestreich S, De Lange T. 2000. Identification of human Rap1: Implications for telomere evolution. Cell. 101(5):471–483. doi:10.1016/S0092-8674(00)80858-2.

Li JSZ, Fusté JM, Simavorian T, Bartocci C, Tsai J, Karlseder J, Denchi EL. 2017. TZAP: A telomere-associated protein involved in telomere length control. Science (80-). 355(6325):638–641. doi:10.1126/science.aah6752.

Lim CS, Mian IS, Dernburg AF, Campisi J. 2001. C. elegans clk-2, a gene that limits life span, encodes a telomere length regulator similar to yeast telomere binding protein Tel2p. Curr Biol. 11(21):1706–1710. doi:10.1016/S0960-9822(01)00526-7.

Lin SJ, Austriaco N. 2014. Aging and cell death in the other yeasts, Schizosaccharomyces pombe and Candida albicans. FEMS Yeast Res. 14(1):119–135. doi:10.1111/1567-1364.12113.

Linger BR, Morin GB, Price CM. 2011. The Pot1a-associated proteins Tpt1 and Pat1 coordinate telomere protection and length regulation in Tetrahymena. Mol Biol Cell. 22(21):4161–4170. doi:10.1091/mbc.E11-06-0551.

Lingner J, Cech TR, Hughes TR, Lundblad V. 1997. Three ever shorter telomere (EST) genes are dispensable for in vitro yeast telomerase activity. Proc Natl Acad Sci U S A. 94(21):11190–11195. doi:10.1073/pnas.94.21.11190.

Lingner J, Cooper JP, Cech TR. 1995. Telomerase and DNA End Replication: No Longer a Lagging Strand Problem? Science (80-). 269(September):533–535.

Link J, Jahn D, Alsheimer M. 2015. Structural and functional adaptations of the mammalian nuclear envelope to meet the meiotic requirements. Nucleus. 6(2):93–101. doi:10.1080/19491034.2015.1004941.

Liu D, O'Connor MS, Qin J, Songyang Z. 2004. Telosome, a mammalian telomere-associated complex formed by multiple telomeric proteins. J Biol Chem. 279(49):51338–51342. doi:10.1074/jbc.M409293200.

Liu D, Safari A, O'Connor MS, Chan DW, Laegeler A, Qin J, Songyang Z. 2004. PTOP interacts with POT1 and regulates its localization to telomeres. Nat Cell Biol. 6(7):673–680. doi:10.1038/ncb1142.

Liu W. 2019. The structure of the checkpoint clamp 9-1-1 complex and clamp loader Rad24-RFC in Saccharomyces cerevisiae. Biochem Biophys Res Commun. 515(4):688–692. doi:10.1016/j.bbrc.2019.05.138. https://doi.org/10.1016/j.bbrc.2019.05.138.

Loe TK, Li JSZ, Zhang Y, Azeroglu B, Boddy MN, Denchi EL. 2020. Telomere length heterogeneity in ALT cells is maintained by PML-dependent localization of the BTR complex to telomeres. Genes Dev.:1–13. doi:10.1101/gad.333963.119.

Londoño-Vallejo JA, Der-Sarkissian H, Cazes L, Bacchetti S, Reddel RR. 2004. Alternative Lengthening of Telomeres Is Characterized by High Rates of Telomeric Exchange. Cancer Res. 64(7):2324–2327. doi:10.1158/0008-5472.CAN-03-4035.

Long J, Huang C, Chen Y, Zhang Y, Shi S, Wu L, Liu Y, Liu C, Wu J, Lei M. 2017. Telomeric TERB1–TRF1 interaction is crucial for male meiosis. Nat Struct Mol Biol. 24(12):1073–1080. doi:10.1038/nsmb.3496. http://www.nature.com/articles/nsmb.3496.

Longhese MP, Bonetti D, Manfrini N, Clerici M. 2010. Mechanisms and regulation of DNA end resection. EMBO J. 29(17):2864–2874. doi:10.1038/emboj.2010.165. http://dx.doi.org/10.1038/emboj.2010.165.

Longhese MP, Paciotti V, Neecke H, Lucchini G. 2000. Checkpoint proteins influence telomeric silencing and length maintenance in budding yeast. Genetics. 155(4):1577–1591.

Longo VD, Shadel GS, Kaeberlein M, Kennedy B. 2012. Replicative and chronological aging in saccharomyces cerevisiae. Cell Metab. 16(1):18–31. doi:10.1016/j.cmet.2012.06.002. http://dx.doi.org/10.1016/j.cmet.2012.06.002.

Lopes AC, Oliveira PF, Sousa M. 2019. Shedding light into the relevance of telomeres in human reproduction and male factor infertility. Biol Reprod. 100(2):318–330. doi:10.1093/biolre/ioy215.

López-Otín C, Blasco MA, Partridge L, Serrano M, Kroemer G. 2013. The hallmarks of aging. Cell. 153(6):1194–217. doi:10.1016/j.cell.2013.05.039. http://www.ncbi.nlm.nih.gov/pubmed/23746838.

Louis EJ, Haber JE. 1992. The structure and evolution of subtelomeric Y' repeats in Saccharomyces cerevisiae. Genetics. 131(3):559–574.

Lovejoy CA, Li W, Reisenweber S, Thongthip S, Bruno J, de Lange T, De S, Petrini JHJ, Sung PA, Jasin M, et al. 2012. Loss of ATRX, genome instability, and an altered DNA damage response are hallmarks of the alternative lengthening of Telomeres pathway. PLoS Genet. 8(7):12–15. doi:10.1371/journal.pgen.1002772.

Lowden MR, Meier B, Lee TWS, Hall J, Ahmed S. 2008. End joining at *Caenorhabditis elegans* telomeres. Genetics. 180(2):741–754. doi:10.1534/genetics.108.089920.

Luciano P, Coulon S, Faure V, Corda Y, Bos J, Brill SJ, Gilson E, Simon MN, Géli V. 2012. RPA facilitates telomerase activity at chromosome ends in budding and fission yeasts. EMBO J. 31(8):2034–2046. doi:10.1038/emboj.2012.40.

Luke B, Panza A, Redon S, Iglesias N, Li Z, Lingner J. 2008. The Rat1p 5′ to 3′ Exonuclease Degrades Telomeric Repeat-Containing RNA and Promotes Telomere Elongation in Saccharomyces cerevisiae. Mol Cell. 32(4):465–477. doi:10.1016/j.molcel.2008.10.019. http://dx.doi.org/10.1016/j.molcel.2008.10.019.

Lundblad V, Blackburn EH. 1993. An alternative pathway for yeast telomere maintenance rescues est1- senescence. Cell. 73(2):347–360. doi:10.1016/0092-8674(93)90234-H.

Lundblad V, Szostak JW. 1989. A mutant with a defect in telomere elongation leads to senescence in yeast. Cell. 57(4):633–643. doi:10.1016/0092-8674(89)90132-3.

Lustig AJ, Kurtz S, Shore D. 1990. Involvement of the silencer and UAS binding protein RAP1 in regulation of telomere length. Science (80-). 250(4980):549–553. doi:10.1126/science.2237406.

Lydeard JR, Jain S, Yamaguchi M, Haber JE. 2007. Break-induced replication and telomerase-independent telomere maintenance require Pol32. Nature. 448(7155):820–823. doi:10.1038/nature06047.

Lynch M, Conery JS. 2000. The evolutionary fate and consequences of duplicate genes. Science (80-). 290(5494):1151–1155. doi:10.1126/science.290.5494.1151.

Ma C, Lowenthal BM, Pai RK. 2018. SATB2 Is Superior to CDX2 in Distinguishing Signet Ring Cell Carcinoma of the Upper Gastrointestinal Tract and Lower Gastrointestinal Tract. Am J Surg Pathol. 42(12):1715–1722. doi:10.1097/PAS.0000000000001159. http://www.ncbi.nlm.nih.gov/pubmed/30212392.

Ma C, Olevian D, Miller C, Herbst C, Jayachandran P, Kozak MM, Chang DT, Pai RK. 2019. SATB2 and CDX2 are prognostic biomarkers in DNA mismatch repair protein deficient colon cancer. Mod Pathol. 32(8):1217–1231. doi:10.1038/s41379-019-0265-1. http://dx.doi.org/10.1038/s41379-019-0265-1.

Maciejowski J, De Lange T. 2017. Telomeres in cancer: Tumour suppression and genome instability. Nat Rev Mol Cell Biol. 18(3):175–186. doi:10.1038/nrm.2016.171.

Maciejowski J, Li Y, Bosco N, Campbell PJ, De Lange T. 2015. Chromothripsis and Kataegis Induced by Telomere Crisis. Cell. 163(7):1641–1654. doi:10.1016/j.cell.2015.11.054. http://dx.doi.org/10.1016/j.cell.2015.11.054.

MacQueen AJ, Phillips CM, Bhalla N, Weiser P, Villeneuve AM, Dernburg AF. 2005. Chromosome sites play dual roles to establish homologous synapsis during meiosis in C. elegans. Cell. 123(6):1037–1050. doi:10.1016/j.cell.2005.09.034.

Madeira F, Park YM, Lee J, Buso N, Gur T, Madhusoodanan N, Basutkar P, Tivey ARN, Potter SC, Finn RD, et al. 2019. The EMBL-EBI search and sequence analysis tools APIs in 2019. Nucleic Acids Res. 47(W1):W636–W641. doi:10.1093/nar/gkz268.

Maestroni L, Matmati S, Coulon S. 2017. Solving the telomere replication problem. Genes (Basel). 8(2):1–16. doi:10.3390/genes8020055.

Maicher A, Kastner L, Dees M, Luke B. 2012. Deregulated telomere transcription causes replication-dependent telomere shortening and promotes cellular senescence. Nucleic Acids Res. 40(14):6649–6659. doi:10.1093/nar/gks358.

Malik HS, Burke WD, Eickbush TH. 2000. Putative telomerase catalytic subunits from Giardia lamblia and *Caenorhabditis elegans*. Gene. 251(2):101–108. doi:10.1016/S0378-1119(00)00207-9.

Marcand S, Brevet V, Mann C, Gilson E. 2000. Cell cycle restriction of telomere elongation. Curr Biol. 10(8):487–490. doi:10.1016/S0960-9822(00)00450-4.

Marcand S, Gilson E, Shore D. 1997. A protein-counting mechanism for telomere length regulation in yeast. Science (80-). 275(5302):986–990. doi:10.1126/science.275.5302.986.

Marcand S, Pardo B, Gratias A, Cahun S, Callebaut I. 2008. Multiple pathways inhibit NHEJ at telomeres. Genes Dev. 22(9):1153–1158. doi:10.1101/gad.455108.

Markaki M, Tavernarakis N. 2010. Modeling human diseases in *Caenorhabditis elegans*. Biotechnol J. 5(12):1261–1276. doi:10.1002/biot.201000183.

Marshall WF, Dernburg AF, Harmon B, Agard DA, Sedat JW. 1996. Specific interactions of chromatin with the nuclear envelope: Positional determination within the nucleus in Drosophila melanogaster. Mol Biol Cell. 7(5):825–842. doi:10.1091/mbc.7.5.825.

Martin JS, Winkelmann N, Petalcorin MIR, McIlwraith MJ, Boulton SJ. 2005. RAD-51-Dependent and -Independent Roles of a *Caenorhabditis elegans* BRCA2-Related Protein during DNA Double-Strand Break Repair. Mol Cell Biol. 25(8):3127–3139. doi:10.1128/MCB.25.8.3127-3139.2005. https://mcb.asm.org/content/25/8/3127.

Maser RS, Wong K-K, Sahin E, Xia H, Naylor M, Hedberg HM, Artandi SE, DePinho RA. 2007. DNA-Dependent Protein Kinase Catalytic Subunit Is Not Required for Dysfunctional Telomere Fusion and Checkpoint Response in the Telomerase-Deficient Mouse. Mol Cell Biol. 27(6):2253–2265. doi:10.1128/mcb.01354-06.

Mason JM, Biessmann H. 1995. The unusual telomeres of Drosophila. Trends Genet. 11(2):58–62. doi:10.1016/S0168-9525(00)88998-2.

Matsuda A, Chikashige Y, Ding DQ, Ohtsuki C, Mori C, Asakawa H, Kimura H, Haraguchi T, Hiraoka Y. 2015. Highly condensed chromatins are formed adjacent to subtelomeric and decondensed silent chromatin in fission yeast. Nat Commun. 6:1–3. doi:10.1038/ncomms8753.

Maupas E. 1900. Modes et formes de reproduction des nematodes. Arch Zool expérimentale générale.

McClintock B. 1941. The Stability of Broken Ends of Chromosomes in Zea Mays. Genetics. 26(2):234–82. http://www.pubmedcentral.nih.gov/articlerender.fcgi?artid=PMC1209127.

McDonald KR, Sabouri N, Webb CJ, Zakian VA. 2014. The Pif1 family helicase Pfh1 facilitates telomere replication and has an RPA-dependent role during telomere lengthening. DNA Repair (Amst). 24:80–86. doi:10.1016/j.dnarep.2014.09.008. http://dx.doi.org/10.1016/j.dnarep.2014.09.008.

McGee JS, Phillips JA, Chan A, Sabourin M, Paeschke K, Zakian VA. 2010. Reduced Rif2 and lack of Mec1 target short telomeres for elongation rather than double-strand break repair. Nat Struct Mol Biol. 17(12):1438–1445. doi:10.1038/nsmb.1947.

Meier B, Barber LJ, Liu Y, Shtessel L, Boulton SJ, Gartner A, Ahmed S. 2009. The MRT-1 nuclease is required for DNA crosslink repair and telomerase activity in vivo in *Caenorhabditis elegans*. EMBO J. 1(22):1–15. doi:10.1038/emboj.2009.278. http://www.ncbi.nlm.nih.gov/pubmed/19779462.

Meier B, Clejan I, Liu Y, Lowden M, Gartner A, Hodgkin J, Ahmed S. 2006. trt-1 is the *Caenorhabditis elegans* catalytic subunit of telomerase. PLoS Genet. 2(2):187–197. doi:10.1371/journal.pgen.0020018.

Meyne J, Ratliff RL, Moyzis RK. 1989. Conservation of the human telomere sequence (TTAGGG)(n) among vertebrates. Proc Natl Acad Sci U S A. 86(18):7049–7053. doi:10.1073/pnas.86.18.7049.

Miller KM, Ferreira MG, Cooper JP. 2005. Taz1, Rap1 and Rif1 act both interdependently and independently to maintain telomeres. EMBO J. 24(17):3128–3135. doi:10.1038/sj.emboj.7600779.

Miller KM, Rog O, Cooper JP. 2006. Semi-conservative DNA replication through telomeres requires Taz1. Nature. 440(7085):824–828. doi:10.1038/nature04638.

Min J, Wright WE, Shay JW. 2019. Clustered telomeres in phase-separated nuclear condensates engage mitotic DNA synthesis through BLM and RAD52. Genes Dev. 33(13–14):814–827. doi:10.1101/gad.324905.119.

Miyake Y, Nakamura M, Nabetani A, Shimamura S, Tamura M, Yonehara S, Saito M, Ishikawa F. 2009. RPA-like Mammalian Ctc1-Stn1-Ten1 Complex Binds to Single-Stranded DNA and Protects Telomeres Independently of the Pot1 Pathway. Mol Cell. 36(2):193–206. doi:10.1016/j.molcel.2009.08.009. http://dx.doi.org/10.1016/j.molcel.2009.08.009.

Miyoshi T, Kanoh J, Saito M, Ishikawa F. 2008. Fission yeast pot1-Tpp1 protects telomeres and regulates telomere length. Science (80-). 320(5881):1341–1344. doi:10.1126/science.1154819.

Moiseeva V, Amelina H, Collopy LC, Armstrong CA, Pearson SR, Tomita K. 2017. The telomere bouquet facilitates meiotic prophase progression and exit in fission yeast. Cell Discov. 3:1–19. doi:10.1038/celldisc.2017.41. http://dx.doi.org/10.1038/celldisc.2017.41.

Montero JJ, López-Silanes I, Megías D, F. Fraga M, Castells-García Á, Blasco MA. 2018. TERRA recruitment of polycomb to telomeres is essential for histone trymethylation marks at telomeric heterochromatin. Nat Commun. 9(1):1548. doi:10.1038/s41467-018-03916-3. http://www.nature.com/articles/s41467-018-03916-3.

Moravec M, Wischnewski H, Bah A, Hu Y, Liu N, Lafranchi L, King MC, Azzalin CM. 2016. TERRA promotes telomerase-mediated telomere elongation in Schizosaccharomyces pombe . EMBO Rep. 17(7):999–1012. doi:10.15252/embr.201541708.

Moretti P, Freeman K, Coodly L, Shore D. 1994. Evidence that a complex of SIR proteins interacts with the silencer and telomere-binding protein RAP1. Genes Dev. 8(19):2257–2269. doi:10.1101/gad.8.19.2257.

Morin GB. 1989. The human telomere terminal transferase enzyme is a ribonucleoprotein that synthesizes TTAGGG repeats. Cell. 59(3):521–529. doi:10.1016/0092-8674(89)90035-4.

Morton J, Davis MW, Jorgensen EM, Carroll D. 2006. Induction and repair of zinc-finger nuclease-targeted double-strand breaks in *Caenorhabditis elegans* somatic cells. Proc Natl Acad Sci U S A. 103(44):16370–5. doi:10.1073/pnas.0605633103. http://www.ncbi.nlm.nih.gov/pubmed/17060623.

Moser BA, Nakamura TM. 2009. Protection and replication of telomeres in fission yeast. Biochem Cell Biol. 87(5):747–758. doi:10.1139/O09-037.

Moser BA, Subramanian L, Khair L, Chang YT, Nakamura TM. 2009. Fission yeast Tel1ATM and Rad3ATR promote telomere protection and telomerase recruitment. PLoS Genet. 5(8):1–11. doi:10.1371/journal.pgen.1000622.

Moskalev AA, Shaposhnikov M V., Plyusnina EN, Zhavoronkov A, Budovsky A, Yanai H, Fraifeld VE. 2013. The role of DNA damage and repair in aging through the prism of Koch-like criteria. Ageing Res Rev. 12(2):661–684. doi:10.1016/j.arr.2012.02.001. http://dx.doi.org/10.1016/j.arr.2012.02.001.

El Mouridi S, Lecroisey C, Tardy P, Mercier M, Leclercq-Blondel A, Zariohi N, Boulin T. 2017. Reliable CRISPR/Cas9 genome engineering in *Caenorhabditis elegans* using a single efficient sgRNA and an easily recognizable phenotype. G3 Genes, Genomes, Genet. 7(5):1429–1437. doi:10.1534/g3.117.040824.

Moyzis RK, Buckingham JM, Cram LS, Dani M, Deaven LL, Jones MD, Meyne J, Ratliff RL, Wu JR. 1988. A highly conserved repetitive DNA sequence, (TTAGGG)(n), present at the telomeres of human chromosomes. Proc Natl Acad Sci U S A. 85(18):6622–6626. doi:10.1073/pnas.85.18.6622.

Muller HJ. 1938. The Remaking of Chromosomes. Collect Net. 8:182–198.

Murnane JP, Sabatier L, Marder BA, Morgan WF. 1994. Telomere dynamics in an immortal human cell line. EMBO J. 13(20):4953–4962. doi:10.1002/j.1460-2075.1994.tb06822.x.

Nabetani A, Ishikawa F. 2009. Unusual Telomeric DNAs in Human Telomerase-Negative Immortalized Cells. Mol Cell Biol. 29(3):703–713. doi:10.1128/mcb.00603-08.

Nakamura TM, Cooper JP, Cech TR. 1998. Two modes of survival of fission yeast without telomerase. Science (80-). 282(5388):493–496. doi:10.1126/science.282.5388.493.

Nakamura TM, Morin GB, Chapman KB, Weinrich SL, Andrews WH, Lingner J, Harley CB, Cech TR. 1997. Telomerase catalytic subunit homologs from fission yeast and human. Science (80-). 277(5328):955–959. doi:10.1126/science.277.5328.955.

Nanbu T, Takahashi K, Murray JM, Hirata N, Ukimori S, Kanke M, Masukata H, Yukawa M, Tsuchiya E, Ueno M. 2013. Fission Yeast RecQ Helicase Rqh1 Is Required for the Maintenance of Circular Chromosomes. Mol Cell Biol. 33(6):1175–1187. doi:10.1128/mcb.01713-12.

Ng LJ, Cropley JE, Pickett HA, Reddel RR, Suter CM. 2009. Telomerase activity is associated with an increase in DNA methylation at the proximal subtelomere and a reduction in telomeric transcription. Nucleic Acids Res. 37(4):1152–1159. doi:10.1093/nar/gkn1030.

Nimmo ER, Pidoux AL, Perry PE, Allshire RC. 1998. Defective meiosis in telomere-silencing mutants of Schizosaccharomyces pombe. Nature. 392(6678):825–828. doi:10.1038/33941.

O'Sullivan RJ, Almouzni G. 2014. Assembly of telomeric chromatin to create ALTernative endings. Trends Cell Biol. 24(11):675–85. doi:10.1016/j.tcb.2014.07.007. http://www.ncbi.nlm.nih.gov/pubmed/25172551.

Oganesian L, Karlseder J. 2011. Mammalian 5′ C-Rich Telomeric Overhangs Are a Mark of Recombination-Dependent Telomere Maintenance. Mol Cell. 42(2):224–236. doi:10.1016/j.molcel.2011.03.015. http://dx.doi.org/10.1016/j.molcel.2011.03.015.

Okamoto K, Bartocci C, Ouzounov I, Diedrich JK, Yates JR, Denchi EL. 2013. A two-step mechanism for TRF2-mediated chromosome-end protection. Nature. 494(7438):502–505. doi:10.1038/nature11873.

Olovnikov AM. 1973. A theory of marginotomy. The incomplete copying of template margin in enzymic synthesis of polynucleotides and biological significance of the phenomenon. J Theor Biol. 41(1):181–190. doi:10.1016/0022-5193(73)90198-7.

Opresko PL, Mason PA, Podell ER, Lei M, Hickson ID, Cech TR, Bohr VA. 2005. POT1 stimulates RecQ helicases WRN and BLM to unwind telomeric DNA substrates. J Biol Chem. 280(37):32069–32080. doi:10.1074/jbc.M505211200.

Opresko PL, Shay JW. 2017. Telomere-associated aging disorders. Ageing Res Rev. 33:52–66. doi:10.1016/j.arr.2016.05.009. http://dx.doi.org/10.1016/j.arr.2016.05.009.

van Overbeek M, de Lange T. 2006. Apollo, an Artemis-Related Nuclease, Interacts with TRF2 and Protects Human Telomeres in S Phase. Curr Biol. 16(13):1295–1302. doi:10.1016/j.cub.2006.05.022.

Paeschke K, Capra JA, Zakian VA. 2011. DNA Replication through G-Quadruplex Motifs Is Promoted by the Saccharomyces cerevisiae Pif1 DNA Helicase. Cell. 145(5):678–691. doi:10.1016/j.cell.2011.04.015. http://dx.doi.org/10.1016/j.cell.2011.04.015.

Paix A, Schmidt H, Seydoux G. 2016. Cas9-assisted recombineering in C. elegans: Genome editing using in vivo assembly of linear DNAs. Nucleic Acids Res. 44(15):e128. doi:10.1093/nar/gkw502.

Paix A, Wang Y, Smith HE, Lee CYS, Calidas D, Lu T, Smith J, Schmidt H, Krause MW, Seydoux G. 2014. Scalable and versatile genome editing using linear DNAs with microhomology to Cas9 sites in *Caenorhabditis elegans*. Genetics. 198(4):1347–1356. doi:10.1534/genetics.114.170423.

Palladino F, Laroche T, Gilson E, Axelrod A, Pillus L, Gasser SM. 1993. SIR3 and SIR4 proteins are required for the positioning and integrity of yeast telomeres. Cell. 75(3):543–55. doi:10.1016/0092-8674(93)90388-7. http://www.ncbi.nlm.nih.gov/pubmed/8221893.

Palm W, de Lange T. 2008. How Shelterin Protects Mammalian Telomeres. Annu Rev Genet. 42(1):301–334. doi:10.1146/annurev.genet.41.110306.130350. http://www.annualreviews.org/doi/10.1146/annurev.genet.41.110306.130350.

Pardo B, Marcand S. 2005. Rap1 prevents telomere fusions by nonhomologous end joining. EMBO J. 24(17):3117–3127. doi:10.1038/sj.emboj.7600778.

Pardue M Lou, Debaryshe PG. 2008. Drosophila telomeres: A variation on the telomerase theme. Fly (Austin). 2(3):101–110. doi:10.4161/fly.6393.

Passannante M, Marti CO, Pfefferli C, Moroni PS, Kaeser-Pebernard S, Puoti A, Hunziker P, Wicky C, Müller F. 2010. Different Mi-2 complexes for various developmental functions in *caenorhabditis elegans*. PLoS One. 5(10). doi:10.1371/journal.pone.0013681.

Pendlebury DF, Fujiwara Y, Tesmer VM, Smith EM, Shibuya H, Watanabe Y, Nandakumar J. 2017. Dissecting the telomere-inner nuclear membrane interface formed in meiosis. Nat Struct Mol Biol. 24(12):1064–1072. doi:10.1038/nsmb.3493.

Penkner A, Tang L, Novatchkova M, Ladurner M, Fridkin A, Gruenbaum Y, Schweizer D, Loidl J, Jantsch V. 2007. The Nuclear Envelope Protein Matefin/SUN-1 Is Required for Homologous Pairing in C. elegans Meiosis. Dev Cell. 12(6):873–885. doi:10.1016/j.devcel.2007.05.004.

Pérez-Martínez L, Öztürk M, Butter F, Luke B. 2020. Npl3 stabilizes R-loops at telomeres to prevent accelerated replicative senescence. EMBO Rep. 21(3):1–12. doi:10.15252/embr.201949087.

Phillips CM, Dernburg AF. 2006. A Family of Zinc-Finger Proteins Is Required for Chromosome-Specific Pairing and Synapsis during Meiosis in C. elegans. Dev Cell. 11(6):817–829. doi:10.1016/j.devcel.2006.09.020.

Polotnianka RM, Li J, Lustig AJ. 1998. The yeast ku heterodimer is essential for protection of the telomere against nucleolytic and recombinational activities. Curr Biol. 8(14):831–835. doi:10.1016/s0960-9822(98)70325-2.

Porro A, Feuerhahn S, Reichenbach P, Lingner J. 2010. Molecular Dissection of Telomeric Repeat-Containing RNA Biogenesis Unveils the Presence of Distinct and Multiple Regulatory Pathways. Mol Cell Biol. 30(20):4808–4817. doi:10.1128/mcb.00460-10.

Poschke H, Dees M, Chang M, Amberkar S, Kaderali L, Rothstein R, Luke B. 2012. Rif2 Promotes a Telomere Fold-Back Structure through Rpd3L Recruitment in Budding Yeast. PLoS Genet. 8(9). doi:10.1371/journal.pgen.1002960.

Poulin G, Dong Y, Fraser AG, Hopper NA, Ahringer J. 2005. Chromatin regulation and sumoylation in the inhibition of Ras-induced vulval development in *Caenorhabditis elegans*. EMBO J. 24(14):2613–2623. doi:10.1038/sj.emboj.7600726. http://emboj.embopress.org/cgi/doi/10.1038/sj.emboj.7600726.

Powers ET, Morimoto RI, Dillin A, Kelly JW, Balch WE. 2009. Biological and Chemical Approaches to Diseases of Proteostasis Deficiency. Annu Rev Biochem. 78(1):959–991. doi:10.1146/annurev.biochem.052308.114844.

Procházková Schrumpfová P, Vychodilová I, Dvořáčková M, Majerská J, Dokládal L, Schořová Š, Fajkus J. 2014. Telomere repeat binding proteins are functional components of Arabidopsis telomeres and interact with telomerase. Plant J. 77(5):770–781. doi:10.1111/tpj.12428. http://doi.wiley.com/10.1111/tpj.12428.

Qi H, Zakian VA. 2000. The Saccharomyces telomere-binding protein Cdc13p interacts with both the catalytic subunit of DNA polymerase α and the telomerase-associated Est1 protein. Genes Dev. 14(14):1777–1788. doi:10.1101/gad.14.14.1777.

Raffa GD, Cenci G, Ciapponi L, Gatti M. 2013. Organization and evolution of Drosophila terminin: Similarities and differences between Drosophila and human telomeres. Front Oncol. 3 MAY(May):1–7. doi:10.3389/fonc.2013.00112.

Raghuraman MK, Winzeler E a, Collingwood D, Hunt S, Wodicka L, Conway A, Lockhart DJ, Davis RW, Brewer BJ, Fangman WL. 2001. Replication dynamics of the yeast genome. Science (80-). 294(5540):115–21. doi:10.1126/science.294.5540.115. http://www.ncbi.nlm.nih.gov/pubmed/11588253.

Rai R, Chen Y, Lei M, Chang S. 2016. TRF2-RAP1 is required to protect telomeres from engaging in homologous recombination-mediated deletions and fusions. Nat Commun. 7. doi:10.1038/ncomms10881.

Raices M, Maruyama H, Dillin A, Kariseder J. 2005. Uncoupling of longevity and telomere length in C, elegans. PLoS Genet. 1(3):295–301. doi:10.1371/journal.pgen.0010030.

Raices M, Verdun RE, Compton SA, Haggblom CI, Griffith JD, Dillin A, Karlseder J. 2008. C. elegans Telomeres Contain G-Strand and C-Strand Overhangs that Are Bound by Distinct Proteins. Cell. 132(5):745–757. doi:10.1016/j.cell.2007.12.039.

Rappsilber J, Mann M, Ishihama Y. 2007. Protocol for micro-purification, enrichment, pre-fractionation and storage of peptides for proteomics using StageTips. Nat Protoc. 2(8):1896–1906. doi:10.1038/nprot.2007.261. http://www.nature.com/doifinder/10.1038/nprot.2007.261.

Redon S, Reichenbach P, Lingner J. 2010. The non-coding RNA TERRA is a natural ligand and direct inhibitor of human telomerase. Nucleic Acids Res. 38(17):5797–5806. doi:10.1093/nar/gkq296.

Redon S, Zemp I, Lingner J. 2013. A three-state model for the regulation of telomerase by TERRA and hnRNPA1. Nucleic Acids Res. 41(19):9117–9128. doi:10.1093/nar/gkt695.

Reichenbach P, Höss M, Azzalin CM, Nabholz M, Bucher P, Lingner J. 2003. A Human Homolog of Yeast Est1 Associates with Telomerase and Uncaps Chromosome Ends When Overexpressed. Curr Biol. 13(7):568–574. doi:10.1016/S0960-9822(03)00173-8. https://ac.els-cdn.com/S0960982203002471/1-s2.0-S0960982203002471-main.pdf?_tid=9ea29124-fb57-4655-b9bd-2c200a21edf5&acdnat=1527873870_0c24ce83ce3300a7a2530d7fa744e071.

Rhie BH, Song YH, Ryu HY, Ahn SH. 2013. Cellular aging is associated with increased ubiquitylation of histone H2B in yeast telomeric heterochromatin. Biochem Biophys Res Commun. 439(4):570–575. doi:10.1016/j.bbrc.2013.09.017. http://dx.doi.org/10.1016/j.bbrc.2013.09.017.

Riha K, Heacock ML, Shippen DE. 2006. The Role of the Nonhomologous End-Joining DNA Double-Strand Break Repair Pathway in Telomere Biology. Annu Rev Genet. 40(1):237–277. doi:10.1146/annurev.genet.39.110304.095755.

Rippe K, Luke B. 2015. TERRA and the state of the telomere. Nat Struct Mol Biol. 22(11):853–858. doi:10.1038/nsmb.3078.

Robert V, Bessereau J-L. 2007. Targeted engineering of the *Caenorhabditis elegans* genome following Mos1-triggered chromosomal breaks. EMBO J. 26(1):170–183. doi:10.1038/sj.emboj.7601463. http://emboj.embopress.org/cgi/doi/10.1038/sj.emboj.7601463.

Robin JD, Ludlow AT, Batten K, Magdinier F, Stadler G, Wagner KR, Shay JW, Wright WE. 2014. Telomere position effect: Regulation of gene expression with progressive telomere shortening over long distances. Genes Dev. 28(22):2464–2476. doi:10.1101/gad.251041.114.

Rockmill B, Roeder GS. 1998. Telomere-mediated chromosome pairing during meiosis in budding yeast. Genes Dev. 12(16):2574–2586. doi:10.1101/gad.12.16.2574.

Rossi ML, Ghosh AK, Bohr VA. 2010. Roles of Werner syndrome protein in protection of genome integrity. DNA Repair (Amst). 9(3):331–344. doi:10.1016/j.dnarep.2009.12.011. http://dx.doi.org/10.1016/j.dnarep.2009.12.011.

Roux AE, Chartrand P, Ferbeyre G, Rokeach LA. 2010. Fission yeast and other yeasts as emergent models to unravel cellular aging in eukaryotes. Journals Gerontol - Ser A Biol Sci Med Sci. 65(1):1–8. doi:10.1093/gerona/glp152.

Ryu JS, Koo HS. 2017. The *Caenorhabditis elegans* WRN helicase promotes double-strand DNA break repair by mediating end resection and checkpoint activation. FEBS Lett. 591(14):2155–2166. doi:10.1002/1873-3468.12724.

Sabourin M, Tuzon CT, Zakian VA. 2007. Telomerase and Tel1p Preferentially Associate with Short Telomeres in S. cerevisiae. Mol Cell. 27(4):550–561. doi:10.1016/j.molcel.2007.07.016.

Sagie S, Toubiana S, Hartono SR, Katzir H, Tzur-Gilat A, Havazelet S, Francastel C, Velasco G, Chédin F, Selig S. 2017. Telomeres in ICF syndrome cells are vulnerable to DNA damage due to elevated DNA:RNA hybrids. Nat Commun. 8(1):14015. doi:10.1038/ncomms14015. http://www.nature.com/articles/ncomms14015.

Salas TR, Petruseva I, Lavrik O, Bourdoncle A, Mergny JL, Favre A, Saintomé C. 2006. Human replication protein A unfolds telomeric G-quadruplexes. Nucleic Acids Res. 34(17):4857–4865. doi:10.1093/nar/gkl564.

Schafer WR. 2005. Deciphering the neural and molecular mechanisms of C. elegans behavior. Curr Biol. 15(17):723–729. doi:10.1016/j.cub.2005.08.020.

Scheibe M, Arnoult N, Kappei D, Buchholz F, Decottignies A, Butter F, Mann M. 2013. Quantitative interaction screen of telomeric repeatcontaining RNA reveals novel TERRA regulators. Genome Res. 23(12):2149–2157. doi:10.1101/gr.151878.112.

Scherthan H. 2007. Telomere attachment and clustering during meiosis. Cell Mol Life Sci. 64(2):117–124. doi:10.1007/s00018-006-6463-2.

Schmutz I, De Lange T. 2016. Shelterin. Curr Biol. 26(10):R397–R399. doi:10.1016/j.cub.2016.01.056.

Schoeftner S, Blasco MA. 2008. Developmentally regulated transcription of mammalian telomeres by DNA-dependent RNA polymerase II. Nat Cell Biol. 10(2):228–236. doi:10.1038/ncb1685.

Schoeftner S, Blasco MA. 2010. Chromatin regulation and non-coding RNAs at mammalian telomeres. Semin Cell Dev Biol. 21(2):186–193. doi:10.1016/j.semcdb.2009.09.015. http://dx.doi.org/10.1016/j.semcdb.2009.09.015.

Scholz J, Besir H, Strasser C, Suppmann S. 2013. A new method to customize protein expression vectors for fast, efficient and background free parallel cloning. BMC Biotechnol. 13:1–11. doi:10.1186/1472-6750-13-12.

Schramke V, Luciano P, Brevet V, Guillot S, Corda Y, Longhese MP, Gilson E, Géli V. 2004. RPA regulates telomerase action by providing Est1p access to chromosome ends. Nat Genet. 36(1):46–54. doi:10.1038/ng1284.

Schreier J, Dietz S, De Jesus Domingues AM, Seistrup A-S, Nguyen DA, Gleason EJ, Ling H, L'Hernault SW, Phillips CM, Butter F, et al. 2020. A membrane-associated condensate ensures paternal epigenetic inheritance in C. elegans. Submiss.

Schumacher B, Hanazawa M, Lee MH, Nayak S, Volkmann K, Hofmann R, Hengartner M, Schedl T, Gartner A. 2005. Translational repression of C. elegans p53 by GLD-1 regulates DNA damage-induced apoptosis. Cell. 120(3):357–368. doi:10.1016/j.cell.2004.12.009.

Schweinsberg PJ, Grant BD. 2013. C. elegans gene transformation by microparticle bombardment. WormBook.:1–10. doi:10.1895/wormbook.1.166.1.

Sen N, Gui B, Kumar R. 2014. Physiological functions of MTA family of proteins. Cancer Metastasis Rev. 33(4):869–877. doi:10.1007/s10555-014-9514-4. https://www.ncbi.nlm.nih.gov/pmc/articles/PMC3624763/pdf/nihms412728.pdf.

Seo B, Kim C, Hills M, Sung S, Kim H, Kim E, Lim DS, Oh HS, Choi RMJ, Chun J, et al. 2015. Telomere maintenance through recruitment of internal genomic regions. Nat Commun. 6:1–10. doi:10.1038/ncomms9189. http://dx.doi.org/10.1038/ncomms9189.

Seo B, Lee J. 2016. Observation and quantification of telomere and repetitive sequences using fluorescence in Situ hybridization (FISH) with PNA probes in *Caenorhabditis elegans*. J Vis Exp. doi:10.3791/54224.

Sfeir A, Kosiyatrakul ST, Hockemeyer D, MacRae SL, Karlseder J, Schildkraut CL, de Lange T. 2009. Mammalian Telomeres Resemble Fragile Sites and Require TRF1 for Efficient Replication. Cell. 138(1):90–103. doi:10.1016/j.cell.2009.06.021. http://dx.doi.org/10.1016/j.cell.2009.06.021.

Sfeir A, de Lange T. 2012. Removal of shelterin reveals the telomere end-protection problem. Science (80-). 336(6081):593–597. doi:10.1126/science.1218498.

Shamim HM, Minami Y, Tanaka D, Ukimori S, Murray JM, Ueno M. 2017. Fission yeast strains with circular chromosomes require the 9-1-1 checkpoint complex for the viability in response to the anti-cancer drug 5-fluorodeoxyuridine. PLoS One. 12(11):1–16. doi:10.1371/journal.pone.0187775.

Shay JW, Bacchetti S. 1997. A survey of telomerase activity in human cancer. Eur J Cancer Part A. 33(5):787–791. doi:10.1016/S0959-8049(97)00062-2.

Shevchenko A, Tomas H, Havliš J, Olsen J V, Mann M. 2007. In-gel digestion for mass spectrometric characterization of proteins and proteomes. Nat Protoc. 1(6):2856–2860. doi:10.1038/nprot.2006.468.

Shibuya H, Hernández-Hernández A, Morimoto A, Negishi L, Höög C, Watanabe Y. 2015. MAJIN Links Telomeric DNA to the Nuclear Membrane by Exchanging Telomere Cap. Cell. 163(5):1252–1266. doi:10.1016/j.cell.2015.10.030.

Shibuya H, Ishiguro KI, Watanabe Y. 2014. The TRF1-binding protein TERB1 promotes chromosome movement and telomere rigidity in meiosis. Nat Cell Biol. 16(2):145–156. doi:10.1038/ncb2896. http://dx.doi.org/10.1038/ncb2896.

Shtessel L, Lowden MR, Cheng C, Simon M, Wang K, Ahmed S. 2013. *Caenorhabditis elegans* POT-1 and POT-2 Repress Telomere Maintenance Pathways. G3 Genes | Genomes | Genet. 3(2):305–313. doi:10.1534/g3.112.004440. http://g3journal.org/lookup/doi/10.1534/g3.112.004440.

Singer M, Gottschling D. 1994. TLC1: template RNA component of Saccharomyces cerevisiae telomerase. Science (80-). 266(5184):404–409. doi:10.1126/science.7545955. https://www.sciencemag.org/lookup/doi/10.1126/science.7545955.

Školáková P, Foldynová-Trantírková S, Bednářová K, Fiala R, Vorlíčková M, Trantírek L. 2015. Unique C. elegans telomeric overhang structures reveal the evolutionarily conserved properties of telomeric DNA. Nucleic Acids Res. 43(9):4733–4745. doi:10.1093/nar/gkv296.

Smith JS, Chen Q, Yatsunyk LA, Nicoludis JM, Garcia MS, Kranaster R, Balasubramanian S, Monchaud D, Teulade-Fichou MP, Abramowitz L, et al. 2011. Rudimentary G-quadruplex-based telomere capping in Saccharomyces cerevisiae. Nat Struct Mol Biol. 18(4):478–486. doi:10.1038/nsmb.2033.

Smith S, Giriat I, Schmitt A, De Lange T. 1998. Tankyrase, a poly(ADP-ribose) polymerase at human telomeres. Science (80-). 282(5393):1484–1487. doi:10.1126/science.282.5393.1484.

Smith S, De Lange T. 2000. Tankyrase promotes telomere elongation in human cells. Curr Biol. 10(20):1299–1302. doi:10.1016/S0960-9822(00)00752-1.

Smogorzewska A, Karlseder J, Holtgreve-Grez H, Jauch A, De Lange T. 2002. DNA ligase IV-dependent NHEJ of deprotected mammalian telomeres in G1 and G2. Curr Biol. 12(19):1635–1644. doi:10.1016/S0960-9822(02)01179-X.

Smogorzewska A, van Steensel B, Bianchi A, Oelmann S, Schaefer MR, Schnapp G, de Lange T. 2000. Control of Human Telomere Length by TRF1 and TRF2. Mol Cell Biol. 20(5):1659–1668. doi:10.1128/mcb.20.5.1659-1668.2000.

Snow BE, Erdmann N, Cruickshank J, Goldman H, Gill RM, Robinson MO, Harrington L. 2003. Functional Conservation of the Telomerase Protein Est1p in Humans. Curr Biol. 13(8):698–704. doi:10.1016/S0960-9822(03)00210-0. https://linkinghub.elsevier.com/retrieve/pii/S0960982203002100.

Solari F, Bateman A, Ahringer J. 1999. The *Caenorhabditis elegans* genes egl-27 and egr-1 are similar to MTA1, a member of a chromatin regulatory complex, and are redundantly required for embryonic patterning. Development. 126(11):2483–2494.

Soudet J, Jolivet P, Teixeira MT. 2014. Elucidation of the DNA end-replication problem in saccharomyces cerevisiae. Mol Cell. 53(6):954–964. doi:10.1016/j.molcel.2014.02.030. http://dx.doi.org/10.1016/j.molcel.2014.02.030.

Starr DA. 2009. A nuclear-envelope bridge positions nuclei and moves chromosomes. J Cell Sci. 122(5):577–586. doi:10.1242/jcs.037622.

van Steensel B, de Lange T. 1997. Control of telomere length by the human telomeric protein TRF1. Nature. 385(6618):740–3. doi:10.1038/385740a0. http://www.nature.com/articles/385740a0.

Van Steensel B, Smogorzewska A, De Lange T. 1998. TRF2 protects human telomeres from end-to-end fusions. Cell. 92(3):401–413. doi:10.1016/S0092-8674(00)80932-0.

Strome S, Updike D. 2015. Specifying and protecting germ cell fate. Nat Rev Mol Cell Biol. 16(7):406–416. doi:10.1038/nrm4009.

Subramanian L, Moser BA, Nakamura TM. 2008. Recombination-Based Telomere Maintenance Is Dependent on Tel1-MRN and Rap1 and Inhibited by Telomerase, Taz1, and Ku in Fission Yeast. Mol Cell Biol. 28(5):1443–1455. doi:10.1128/mcb.01614-07.

Suetomi K, Mereiter S, Mori C, Takanami T, Higashitani A. 2013. *Caenorhabditis elegans* ATR checkpoint kinase ATL-1 influences life span through mitochondrial maintenance. Mitochondrion. 13(6):729–735. doi:10.1016/j.mito.2013.02.004. http://dx.doi.org/10.1016/j.mito.2013.02.004.

Sulston JE, Horvitz HR. 1977. Post-embryonic cell lineages of the nematode, *Caenorhabditis elegans*. Dev Biol. 56(1):110–156. doi:10.1016/0012-1606(77)90158-0.

Sulston JE, Schierenberg E, White JG, Thomson JN. 1983. The embryonic cell lineage of the nematode *Caenorhabditis elegans*. Dev Biol. 100(1):64–119. doi:10.1016/0012-1606(83)90201-4.

Szemes M, Gyorgy A, Paweletz C, Dobi A, Agoston D V. 2006. Isolation and characterization of SATB2, a novel AT-rich DNA binding protein expressed in development- and cell-specific manner in the rat brain. Neurochem Res. 31(2):237–246. doi:10.1007/s11064-005-9012-8.

Szostak JW, Blackburn EH. 1982. Cloning yeast telomeres on linear plasmid vectors. Cell. 29(1):245–255. doi:10.1016/0092-8674(82)90109-X.

Taggart AKP, Teng SC, Zakian VA. 2002. Est1p as a cell cycle-regulated activator of telomere-bound telomerase. Science (80-). 297(5583):1023–1026. doi:10.1126/science.1074968.

Takai H, Smogorzewska A, de Lange T. 2003. DNA Damage Foci at Dysfunctional Telomeres. Curr Biol. 13(17):1549–1556. doi:10.1016/S0960-9822(03)00542-6. https://ac.els-cdn.com/S0960982203002471/1-s2.0-S0960982203002471-main.pdf?_tid=9ea29124-fb57-4655-b9bd-2c200a21edf5&acdnat=1527873870_0c24ce83ce3300a7a2530d7fa744e071.

Takai KK, Kibe T, Donigian JR, Frescas D, de Lange T. 2011. Telomere Protection by TPP1/POT1 Requires Tethering to TIN2. Mol Cell. 44(4):647–659. doi:10.1016/j.molcel.2011.08.043. http://dx.doi.org/10.1016/j.molcel.2011.08.043.

Takanami T, Sato S, Ishihara T, Katsura I, Takahashi H, Higashitani A. 1998. Characterization of a *Caenorhabditis elegans* recA-like gene Ce-rdh-1 involved in meiotic recombination. DNA Res. 5(6):373–377. doi:10.1093/dnares/5.6.373.

Takubo K, Izumiyama-Shimomura N, Honma N, Sawabe M, Arai T, Kato M, Oshimura M, Nakamura KI. 2002. Telomere lengths are characteristic in each human individual. Exp Gerontol. 37(4):523–531. doi:10.1016/S0531-5565(01)00218-2.

Talens RP, Christensen K, Putter H, Willemsen G, Christiansen L, Kremer D, Suchiman HED, Slagboom PE, Boomsma DI, Heijmans BT. 2012. Epigenetic variation during the adult lifespan: Cross-sectional and longitudinal data on monozygotic twin pairs. Aging Cell. 11(4):694–703. doi:10.1111/j.1474-9726.2012.00835.x.

Tashiro S, Nishihara Y, Kugou K, Ohta K, Kanoh J. 2017. NAR breakthrough article: Subtelomeres constitute a safeguard for gene expression and chromosome homeostasis. Nucleic Acids Res. 45(18):10333–10349. doi:10.1093/nar/gkx780.

Teixeira MT. 2013. Saccharomyces cerevisiae as a model to study replicative senescence triggered by telomere shortening. Front Oncol. 3 APR(April):1–16. doi:10.3389/fonc.2013.00101.

Teixeira MT, Arneric M, Sperisen P, Lingner J. 2004. Telomere length homeostasis is achieved via a switch between telomerase- extendible and -nonextendible states. Cell. 117(3):323–335. doi:10.1016/S0092-8674(04)00334-4.

Teng S-C, Zakian VA. 1999. Telomere-Telomere Recombination Is an Efficient Bypass Pathway for Telomere Maintenance in Saccharomyces cerevisiae . Mol Cell Biol. 19(12):8083–8093. doi:10.1128/mcb.19.12.8083.

Teng SC, Chang J, McCowan B, Zakian VA. 2000. Telomerase-independent lengthening of yeast telomeres occurs by an abrupt Rad50p-dependent, Rif-inhibited recombinational process. Mol Cell. 6(4):947–952. doi:10.1016/S1097-2765(05)00094-8.

The C. elegans Sequencing Consortium. 1998. Genome Sequence of the Nematode C. elegans: A Platform for Investigating Biology. Science (80-). 282(5396):2012–2018. doi:10.1126/science.282.5396.2012. https://www.sciencemag.org/lookup/doi/10.1126/science.282.5396.2012.

Tian Y, Garcia G, Bian Q, Steffen KK, Joe L, Wolff S, Meyer BJ, Dillin A. 2016. Mitochondrial Stress Induces Chromatin Reorganization to Promote Longevity and UPRmt. Cell. 165(5):1197–1208. doi:10.1016/j.cell.2016.04.011. http://dx.doi.org/10.1016/j.cell.2016.04.011.

Tomaska L, Willcox S, Slezakova J, Nosek J, Griffith JD. 2004. Taz1 binding to a fission yeast model telomere: Formation of telomeric loops and higher order structures. J Biol Chem. 279(49):50764–50772. doi:10.1074/jbc.M409790200.

Tomita K, Cooper JP. 2008. Fission yeast Ccq1 is telomerase recruiter and local checkpoint controller. Genes Dev. 22(24):3461–3474. doi:10.1101/gad.498608.

Tomita K, Kibe T, Kang H-Y, Seo Y-S, Uritani M, Ushimaru T, Ueno M. 2004. Fission Yeast Dna2 Is Required for Generation of the Telomeric Single-Strand Overhang. Mol Cell Biol. 24(21):9557–9567. doi:10.1128/mcb.24.21.9557-9567.2004.

Tomlinson RL, Ziegler TD, Supakorndej T, Terns RM, Terns MP. 2006. Cell cycle-regulated trafficking of human telomerase to telomeres. Mol Biol Cell. 17(2):955–65. doi:10.1091/mbc.e05-09-0903. http://www.ncbi.nlm.nih.gov/pubmed/16339074.

Tong AS, Stern JL, Sfeir A, Kartawinata M, de Lange T, Zhu XD, Bryan TM. 2015. ATM and ATR Signaling Regulate the Recruitment of Human Telomerase to Telomeres. Cell Rep. 13(8):1633–1646. doi:10.1016/j.celrep.2015.10.041. http://dx.doi.org/10.1016/j.celrep.2015.10.041.

Ueno M. 2010. Roles of DNA repair proteins in telomere maintenance. Biosci Biotechnol Biochem. 74(1):1–6. doi:10.1271/bbb.90682.

Vannier JB, Pavicic-Kaltenbrunner V, Petalcorin MIR, Ding H, Boulton SJ. 2012. RTEL1 dismantles T loops and counteracts telomeric G4-DNA to maintain telomere integrity. Cell. 149(4):795–806. doi:10.1016/j.cell.2012.03.030. http://dx.doi.org/10.1016/j.cell.2012.03.030.

Vasilopoulos E, Fragkiadaki P, Kalliora C, Fragou D, Docea AO, Vakonaki E, Tsoukalas D, Calina D, Buga AM, Georgiadis G, et al. 2019. The association of female and male infertility with telomere length (Review). Int J Mol Med. 44(2):375–389. doi:10.3892/ijmm.2019.4225.

Verdun RE, Karlseder J. 2006. The DNA Damage Machinery and Homologous Recombination Pathway Act Consecutively to Protect Human Telomeres. Cell. 127(4):709–720. doi:10.1016/j.cell.2006.09.034.

Vermezovic J, Stergiou L, Hengartner MO, D'Adda Di Fagagna F. 2012. Differential regulation of DNA damage response activation between somatic and germline cells in *Caenorhabditis elegans*. Cell Death Differ. 19(11):1847–1855. doi:10.1038/cdd.2012.69.

Vodenicharov MD, Laterreur N, Wellinger RJ. 2010. Telomere capping in non-dividing yeast cells requires Yku and Rap1. EMBO J. 29(17):3007–3019. doi:10.1038/emboj.2010.155. http://dx.doi.org/10.1038/emboj.2010.155.

Vodenicharov MD, Wellinger RJ. 2006. DNA Degradation at Unprotected Telomeres in Yeast Is Regulated by the CDK1 (Cdc28/Clb) Cell-Cycle Kinase. Mol Cell. 24(1):127–137. doi:10.1016/j.molcel.2006.07.035.

Volkmer E, Karnitz LM. 1999. Human Homologs of Schizosaccharomyces pombe Rad1, Hus1, and Rad9 Form a DNA Damage-responsive Protein Complex. J Biol Chem. 274(2):567–570. doi:10.1074/jbc.274.2.567. http://www.jbc.org/lookup/doi/10.1074/jbc.274.2.567.

Wagner T, Perez-Martinez L, Schellhaas R, Barrientos-Moreno M, Öztürk M, Prado F, Butter F, Luke B. 2020. Chromatin modifiers and recombination factors promote a telomere fold-back structure, that is lost during replicative senescence. bioRxiv.:2020.01.13.904086. doi:10.1101/2020.01.13.904086.

Wallgren M, Mohammad JB, Yan KP, Pourbozorgi-Langroudi P, Ebrahimi M, Sabouri N. 2016. G-rich telomeric and ribosomal DNA sequences from the fission yeast genome form stable G-quadruplex DNA structures in vitro and are unwound by the Pfh1 DNA helicase. Nucleic Acids Res. 44(13):6213–6231. doi:10.1093/nar/gkw349.

Wanat JJ, Kim KP, Koszul R, Zanders S, Weiner B, Kleckner N, Alani E. 2008. Csm4, in collaboration with Ndj1, mediates telomere-led chromosome dynamics and recombination during yeast meiosis. PLoS Genet. 4(9). doi:10.1371/journal.pgen.1000188.

Wang F, Podell ER, Zaug AJ, Yang Y, Baciu P, Cech TR, Lei M. 2007. The POT1-TPP1 telomere complex is a telomerase processivity factor. Nature. 445(7127):506–510. doi:10.1038/nature05454.

Wang X, Baumann P. 2008. Chromosome Fusions following Telomere Loss Are Mediated by Single-Strand Annealing. Mol Cell. 31(4):463–473. doi:10.1016/j.molcel.2008.05.028.

Wang Y, Chen Y, Chen J, Wang L, Nie L, Long J, Chang H, Wu J, Huang C, Lei M. 2019. The meiotic TERB1-TERB2-MAJIN complex tethers telomeres to the nuclear envelope. Nat Commun. 10(1):1–19. doi:10.1038/s41467-019-08437-1. http://dx.doi.org/10.1038/s41467-019-08437-1.

Wang Y, Ghosh G, Hendrickson EA. 2009. Ku86 represses lethal telomere deletion events in human somatic cells. Proc Natl Acad Sci U S A. 106(30):12430–12435. doi:10.1073/pnas.0903362106.

Watson JD. 1972. Origin of concatemeric T7 DNA. Nat New Biol. 239(94):197–201. doi:10.1038/newbio239197a0. http://www.nature.com/articles/newbio239197a0.

Webb CJ, Zakian VA. 2008. Identification and characterization of the Schizosaccharomyces pombe TER1 telomerase RNA. Nat Struct Mol Biol. 15(1):34–42. doi:10.1038/nsmb1354.

Webb CJ, Zakian VA. 2012. Schizosaccharomyces pombe Ccq1 and TER1 bind the 14-3-3-like domain of Est1, which promotes and stabilizes telomerase-telomere association. Genes Dev. 26(1):82–91. doi:10.1101/gad.181826.111.

Wei H, Yu X. 2016. Functions of PARylation in DNA Damage Repair Pathways. Genomics Proteomics Bioinformatics. 14(3):131–139. doi:10.1016/j.gpb.2016.05.001. http://www.ncbi.nlm.nih.gov/pubmed/27240471.

Weinert TA, Hartwell LH. 1988. The RAD9 gene controls the cell cycle response to DNA damage in saccharomyces cerevisiae. Science (80-). 241(4863):317–322. doi:10.1126/science.3291120.

Wellinger RJ, Ethier K, Labrecque P, Zakian VA. 1996. Evidence for a new step in telomere maintenance. Cell. 85(3):423–433. doi:10.1016/S0092-8674(00)81120-4.

Wellinger RJ, Zakian VA. 2012. Everything you ever wanted to know about Saccharomyces cerevisiae telomeres: Beginning to end. Genetics. 191(4):1073–1105. doi:10.1534/genetics.111.137851.

White C, Gagnon SN, St-Laurent J-F, Gravel C, Proulx L-I, Desnoyers S. 2009. The DNA damage-inducible C. elegans tankyrase is a nuclear protein closely linked to chromosomes. Mol Cell Biochem. 324(1–2):73–83. doi:10.1007/s11010-008-9986-z. http://link.springer.com/10.1007/s11010-008-9986-z.

White JG, Southgate E, Thomson JN, Brenner S. 1986. The structure of the nervous system of the nematode *Caenorhabditis elegans*. Philos Trans R Soc London. 314(1165):1–340. doi:10.1098/rstb.1986.0056. http://www.ncbi.nlm.nih.gov/pubmed/22462104.

Wicky C, Villeneuve a M, Lauper N, Codourey L, Tobler H, Müller F. 1996. Telomeric repeats (TTAGGC)n are sufficient for chromosome capping function in *Caenorhabditis elegans*. Proc Natl Acad Sci U S A. 93(August):8983–8988. doi:10.1073/pnas.93.17.8983.

Wright D., Gibbons W., Lanzendorf S. 2000. Characterization of Telomerase Activity in the Human Oocyte and Preimplantation Embryo. Fertil Steril. 74(3):S67. doi:10.1016/s0015-0282(00)00902-x.

Wright JH, Gottschling DE, Zakian VA. 1992. Saccharomyces telomeres assume a non-nucleosomal chromatin structure. Genes Dev. 6(2):197–210. doi:10.1101/gad.6.2.197.

Wright WE, Piatyszek MA, Rainey WE, Byrd W, Shay JW. 1996. Telomerase activity in human germline and embryonic tissues and cells. Dev Genet. 18(2):173–9. doi:10.1002/(SICI)1520-6408(1996)18:2<173::AID-DVG10>3.0.CO;2-3. http://www.ncbi.nlm.nih.gov/pubmed/8934879.

Wright WE, Tesmer VM, Liao ML, Shay JW. 1999. Normal human telomeres are not late replicating. Exp Cell Res. 251(2):492–499. doi:10.1006/excr.1999.4602.

Wu P, van Overbeek M, Rooney S, de Lange T. 2010. Apollo Contributes to G Overhang Maintenance and Protects Leading-End Telomeres. Mol Cell. 39(4):606–617. doi:10.1016/j.molcel.2010.06.031. http://dx.doi.org/10.1016/j.molcel.2010.06.031.

Wu P, Takai H, De Lange T. 2012. Telomeric 3′ overhangs derive from resection by Exo1 and apollo and fill-in by POT1b-associated CST. Cell. 150(1):39–52. doi:10.1016/j.cell.2012.05.026. http://dx.doi.org/10.1016/j.cell.2012.05.026.

Wu RA, Upton HE, Vogan JM, Collins K. 2017. Telomerase Mechanism of Telomere Synthesis. Annu Rev Biochem. 86(1):439–460. doi:10.1146/annurev-biochem-061516-045019.

Wu Y, Zakian VA. 2011. The telomeric Cdc13 protein interacts directly with the telomerase subunit Est1 to bring it to telomeric DNA ends in vitro. Proc Natl Acad Sci U S A. 108(51):20362–20369. doi:10.1073/pnas.1100281108.

Wu Z, He MH, Zhang L li, Liu J, Zhang Q Di, Zhou JQ. 2018. Rad6-Bre1 mediated histone H2Bub1 protects uncapped telomeres from exonuclease Exo1 in Saccharomyces cerevisiae. DNA Repair (Amst). 72:64–76. doi:10.1016/j.dnarep.2018.09.007. https://doi.org/10.1016/j.dnarep.2018.09.007.

Xue Y, Wong J, Moreno GT, Young MK, Côté J, Wang W. 1998. NURD, a novel complex with both ATP-dependent chromatin-remodeling and histone deacetylase activities. Mol Cell. 2(6):851–861. doi:10.1016/S1097-2765(00)80299-3.

Yasaei H, Slijepcevic P. 2010. Defective Artemis causes mild telomere dysfunction. Genome Integr. 1:1–12. doi:10.1186/2041-9414-1-3.

Yeager TR, Neumann AA, Englezou A, Huschtscha LI, Noble JR, Reddel RR. 1999. Telomerase-negative immortalized human cells contain a novel type of promyelocytic leukemia (PML) body. Cancer Res. 59(17):4175–4179.

Yuan J. 1993. The C. elegans cell death gene ced-3 encodes a protein similar to mammalian interleukin-1β-converting enzyme. Cell. 75(4):641–652. doi:10.1016/0092-8674(93)90485-9. https://linkinghub.elsevier.com/retrieve/pii/0092867493904859.

Yuan J, Horvitz HR. 1992. The *Caenorhabditis elegans* cell death gene ced-4 encodes a novel protein and is expressed during the period of extensive programmed cell death. Development. 116(2):309–320.

Zhang JM, Yadav T, Ouyang J, Lan L, Zou L. 2019. Alternative Lengthening of Telomeres through Two Distinct Break-Induced Replication Pathways. Cell Rep. 26(4):955-968.e3. doi:10.1016/j.celrep.2018.12.102. https://doi.org/10.1016/j.celrep.2018.12.102.

Zhang QS, Manche L, Xu RM, Krainer AR. 2006. hnRNP A1 associates with telomere ends and stimulates telomerase activity. Rna. 12(6):1116–1128. doi:10.1261/rna.58806.

Zhang Y-J, Chen J-W, He X-S, Zhang H-Z, Ling Y-H, Wen J-H, Deng W-H, Li P, Yun J-P, Xie D, et al. 2018. SATB2 is a Promising Biomarker for Identifying a Colorectal Origin for Liver Metastatic Adenocarcinomas. EBioMedicine. 28:62–69. doi:10.1016/j.ebiom.2018.01.001. http://www.ncbi.nlm.nih.gov/pubmed/29396302.

Zhao Z, Fang L, Chen N, Johnsen RC, Stein L, Baillie DL. 2005. Distinct regulatory elements mediate similar expression patterns in the excretory cell of *Caenorhabditis elegans*. J Biol Chem. 280(46):38787–38794. doi:10.1074/jbc.M505701200.

Zhong FL, Batista LFZ, Freund A, Pech MF, Venteicher AS, Artandi SE. 2012. TPP1 OB-fold domain controls telomere maintenance by recruiting telomerase to chromosome ends. Cell. 150(3):481–494. doi:10.1016/j.cell.2012.07.012.

Zhong Z, Shiue L, Kaplan S, de Lange T. 1992. A mammalian factor that binds telomeric TTAGGG repeats in vitro. Mol Cell Biol. 12(11):4834–4843. doi:10.1128/mcb.12.11.4834.

Zimmermann L, Stephens A, Nam SZ, Rau D, Kübler J, Lozajic M, Gabler F, Söding J, Lupas AN, Alva V. 2018. A Completely Reimplemented MPI Bioinformatics Toolkit with a New HHpred Server at its Core. J Mol Biol. 430(15):2237–2243. doi:10.1016/j.jmb.2017.12.007. https://doi.org/10.1016/j.jmb.2017.12.007.